Stability Analysis of Magnetised Neutron Stars

a Semi-Analytic Approach

Dissertation
der Mathematisch-Naturwissenschaftlichen Fakultät
der Eberhard Karls Universität Tübingen
zur Erlangung des Grades eines
Doktors der Naturwissenschaften
(Dr. rer. nat.)

vorgelegt von
Marlene Herbrik
aus Göppingen

Tübingen
2017

Gedruckt mit Genehmigung der Mathematisch-Naturwissenschaftlichen Fakultät der Eberhard Karls Universität Tübingen.

Tag der mündlichen Prüfung:	20.12.2017
Dekan:	Prof. Dr. Wolfgang Rosenstiel
1. Berichterstatter:	Prof. Dr. Kostas Kokkotas
2. Berichterstatter:	Prof. Dr. Wilhelm Kley

Thy phyſick iſ theoretical, but thy fun iſ real.

Sheldon Lee Cooper (Lorre & Aronsohn, 2009)

Contents

Abstract

In this work, the stability problem of magnetised neutron stars will be addressed, by applying a new semi-analytic method for stability analysis.

The durability and long-lasting stability of magnetised neutron stars, inferred from numerous pulsar observations, is not explicable with the current state of research. This key issue of neutron star physics implies that the interior neutron star magnetic field structure is widely unknown. This situation is highly undesirable since neutron stars, showing the most extreme densities and field strengths of extended objects in the universe, represent highly interesting objects for investigations on fundamental physics.

The semi-analytic method presented here is based on the energy variational principle, where the stability of an equilibrium system is tested towards perturbations of the equilibrium state. An increase in the system energy for all perturbation modes represents stability, an energy decrease for at least one mode indicates instability. The innovative idea of the semi-analytic method is to set up the energy variation density of the parametrised system analytically, and to perform the required volume integration numerically. With this approach, the investigated model systems can be kept more complex than in previous analytical studies. The generality of the model system compared to numerical studies allows for conclusions on realistic magnetic field and composition structures inside the star.

The functionality of the implemented computation code is verified by re-detections of the known Tayler instabilities in the purely toroidally and purely poloidally magnetised neutron star. The stabilising impact of stratification, i.e. deviations from barotropicity, and the interplay of both magnetic field components found in analytic studies is confirmed.

New physical insights are gained by removing the Cowling approximation that has commonly been used in all stability studies on magnetised neutron stars so far. This simplification neglects the change in the gravitational potential caused by the perturbation. This approximation is tested here on its validity in modern studies. Even though the Cowling approximation is justified for instability detections in toy models, it might distort the results of stability proofs in more realistic systems.

It is shown that the semi-analytic method represents a valuable tool for future stability investigations. It provides essential advantages for a straightforward stability analysis compared to previous approaches, and it is a promising method to achieve progress in the field of magnetised neutron stars.

Zusammenfassung

Die vorliegende Arbeit befasst sich mit dem Stabilitätsproblem magnetisierter Neutronensterne, unter Verwendung einer neuen semi-analytischen Untersuchungsmethode zur Stabilitätsanalyse.

Die in Pulsarbeobachtungen vielfach detektierte hohe Lebensdauer und anhaltende Stabilität magnetisierter Neutronensterne kann bei derzeitigem Forschungsstand nicht erklärt werden. Dieses zentrale Problem der Neutronensternphysik hat zur Folge, dass die innere Magnetfeldstruktur von Neutronensternen weitgehend unbekannt ist. Dieser Zustand ist höchst problematisch, da Neutronensterne die höchsten Dichten und Feldstärken unter allen ausgedehnten Objekten des Universums aufweisen und somit hochinteressante Untersuchungsobjekte für die physikalische Grundlagenforschung darstellen.

Die hier vorgestellte semi-analytische Methode beruht auf dem Energievariationsprinzip, nach dem die Stabilität eines Systems auf Störungen seines Gleichgewichtszustands hin untersucht wird. Beim Anstieg der Systemenergie gegenüber allen Störungsmoden liegt Stabilität vor, ein Energieabfall für mindestens eine Mode zeigt Instabilität an. Die neuartige Idee der semi-analytischen Methode ist es, die Energievariationsdichte des parametrisierten Systems analytisch aufzustellen, die erforderliche Volumenintegration aber numerisch auszuführen. Mit diesem Ansatz kann das untersuchte System komplexer gehalten werden als es in bisherigen analytischen Studien möglich war. Verglichen mit numerischen Studien ist bei der Konstruktion des Modellsystems ein höheres Maß an Allgemeingültigkeit möglich, welches Rückschlüsse auf realistische Konfigurationen des Magnetfelds und der stellaren Zusammensetzung erlaubt.

Die Funktionalität des aufgesetzten numerischen Codes wird anhand von Instabilitätsnachweisen der bekannten Taylerinstabilitäten in rein toroidal und rein poloidal magnetisierten Neutronensternen bewiesen. Der in analytischen Untersuchungen gefundene stabilisierende Einfluss von Stratifikation, d. h. Abweichungen von der barotropen Zusammensetzung des Sterns, und dem Wechselspiel beider Magnetfeldkomponenten wird bestätigt.

Neue physikalische Erkenntnisse werden erzielt, indem die Cowlingnäherung aufgehoben wird, die üblicherweise für alle Stabilitätsuntersuchungen an magnetisierten Neutronensternen bislang angenommen wurde. Diese Näherung vernachlässigt die durch die Störung entstehende Änderung des Gravitationspotentials. Diese Näherung wird hier auf ihre Gültigkeit in aktuellen Studien hin untersucht. Obwohl die Verwendung der Cowlingnäherung zur Detektion von Instabilitäten in vereinfachten Systemen gerechtfertigt ist, verfälscht sie möglicherweise die Ergebnisse von Stabilitätsnachweisen in realistischeren Systemen.

Es wird gezeigt, dass die semi-analytische Methode ein nützliches Hilfsmittel für zukünftige Stabilitätsuntersuchungen darstellt. Verglichen mit früheren Herangehensweisen bietet sie entscheidende Vorteile bezüglich einer unkomplizierten Stabilitätsanalyse und stellt eine vielversprechende Methode dar, mit der Fortschritte auf dem Gebiet der magnetisierten Neutronensterne zu erwarten sind.

1. Motivation

Neutron stars have been known as enormously interesting objects with high densities and strong magnetic fields for decades. They attract attention by observations of their pulsar characteristics, giant flare activities, partially enormously fast rotation or their characteristic cooling curves. However, they are of interest to modern research not only because they are fascinating objects, but predominantly because they provide essential insights for up-to-date fundamental physics.

Relevance of neutron stars

Neutron stars are the most compact extended objects in the universe, representing unique laboratories for identifying the fundamental characteristics of matter under extreme conditions.

Investigating these kinds of systems is a crucial step towards finding the equation of state for matter at high densities. This relation describes the composition of matter for pressure levels occurring in ordinary atomic nuclei as well as in the innermost parts of neutron stars. Even though this relation represents a basic component of our understanding of physics itself, it is still unknown for high pressure values.

This fact is owed to the extreme conditions that are necessary to test matter in this regime and that cannot be realised in experimental setups. Neutron stars, in contrast, naturally provide these extreme environments and might bring us closer to a solution.

In the course of finding the equation of state, we expect insights about atomic nuclei and about the actual existence of potential particles, lightening our entire understanding of matter. Due to this potential, finding the equation of state for high densities is often referred to as the Holy Grail of neutron star physics.

Relevance of neutron star magnetic fields

For the purpose of enhancing our physical understanding based on neutron stars, they need to be understood sufficiently.

One essential component are the commonly strong magnetic fields typical neutron stars possess. Aside from the equation of state, the magnetic field determines how neutron star matter behaves. From observations it is known that neutron star magnetic fields are strong enough to crucially impact all kinds of neutron star processes.

Typical surface field strengths of neutron stars are of the order of $10^8\,\mathrm{G}$ to $10^{13}\,\mathrm{G}$, while the interior field strength is expected to exceed $10^{15}\,\mathrm{G}$ (Manchester et al., 2005; Pulsar Catalogue, 2017). The neutron star subclass of so-called magnetars shows surface fields of more than $10^{14}\,\mathrm{G}$ and is expected to have accordingly even stronger interior fields (Olausen & Kaspi, 2014; Magnetar Catalog, 2016). Thus, the evolution of magnetars is in fact dominated by their magnetic field.

For an adequate description of neutron stars, it is essential to take into account their magnetic field. Beyond this fundamental requirement, the neutron star magnetic field

represents a highly interesting field itself. It is unique, artificially not reproducible and highly topical, since it converts neutron stars into sources of gravitational waves, whose first direct detection succeeded recently.

Key issue of magnetised neutron star physics

However, despite its importance there is no theoretical model describing magnetised neutron stars sufficiently until today. This issue leads to the fact that studies on neutron stars are based on assumptions and estimates for the magnetic field. Considering the massive impact magnetic fields exert on neutron stars, this situation is unacceptable.

The problem in particular is that simplified theoretical models cannot support stable magnetised neutron stars. This implies that magnetised neutron stars could not persist and would thus not be observable. This obvious contradiction between theory and observations indicates that an essential feature must be missing in the model. Unfortunately, it is extremely difficult to make the model more realistic. Analytical studies rely on oversimplifications to keep the system treatable. Numerical simulations on the other hand cannot provide the universal conclusions which are necessary for a conceptual understanding. Therefore, the structure of interior neutron star magnetic fields is still widely unknown.

Fundamental idea of this work

In this work, a semi-analytic approach combining the advantages of both pure analytic and pure numerical attempts will be developed and implemented for the first time. It is designed as a method of semi-analytic stability analysis to find the stellar configurations that are most likely to be stable. The method is expected to constrain which composition and magnetic field structures are possibly present in actual neutron stars.

The semi-analytic method will be based on the variational principle. It states that an equilibrium state is stable if the total system energy increases towards every possible perturbation mode. The system is unstable as soon as at least one perturbation mode lowers the total system energy.

In analogy to an analytical treatment, the energy variation density of the star towards an arbitrary perturbation will be set up analytically in the semi-analytic approach. From that, the energy variation follows by an integration over the stellar volume. The sign of the energy variation indicates whether the system is stable or not. In contrast to the analytical approach where simplifications in the model are necessary to perform the integration, the semi-analytic method will make use of a numerical Simpson integration.

Compared to numerical simulations, the semi-analytic method will not require specific initial conditions. Due to parametrisation, classes of systems can be investigated at once. That way, the semi-analytic approach allows for a preservation of the system's complexity, yet providing universal conclusions. It is expected to improve the analytical approach allowing for a description of more realistic stars.

Outline of this work

The structure of this work is as follows.

Before the fundamental idea of the semi-analytic method explained above can be framed in a detailed and mathematical way, theoretical foundations need to be presented. Chapter 2 summarises the astrophysical foundations. Section 2.1 gives a global scientific overview

on neutron stars. Section 2.2 presents the equations of magnetohydrodynamics required for a mathematical description of neutron stars. In section 2.3, the essentials of stability analysis are explained, applying either the variational principle or a normal mode analysis. The analytical expressions for the energy variation the semi-analytic method is based on are derived.

Afterwards, the central underlying problem of this work is discussed in chapter 3. The current state of research is outlined and the idea of the semi-analytic approach is explicitly motivated.

Chapter 4 describes the development of the semi-analytic method with the necessary analytical and numerical steps that have been implemented so far. The analytical steps in sections 4.1 and 4.2 particularly involve the derivation of additional terms in the energy variation that need to be considered when stratified stars are investigated and the Cowling approximation is removed. The numerical implementation of the method is shown in section 4.3.

The implemented method is applied to different systems in chapter 5 in order to prove its functionality and to gain first new insights about more complex systems. Sections 5.1 and 5.2 cover the field of stability analysis of magnetised neutron stars in simple model systems. Section 5.3 addresses systems with more realistic magnetic field and composition structures. Section 5.4 demonstrates the generality of the method through applications on further issues such as the calculation of system eigenfrequencies and eigenfunctions.

The conclusions are drawn in chapter 6. The technical functionality of the method is discussed in section 6.1, and the physical achievements are discussed in section 6.2. Chapter 7 gives an outlook on the upcoming follow-up projects.

2. Theoretical foundations and system setup

Before the main idea of this work can be brought into an astrophysical and mathematical context, the required theoretical foundations need to be outlined.

Section 2.1 will give an overview of today's state of neutron star research, providing the basis for the magnetised neutron stars investigated in this work. Part 2.2 covers the mathematical treatment of these systems applying magnetohydrodynamics (MHD). Section 2.3 introduces the mathematical concept of stability analysis which will be extended and applied in this work to study neutron stars.

2.1. Research state on neutron stars

As briefly touched in the previous chapter 1, the understanding of neutron stars in general and their magnetic fields in particular is of exceptional relevance to modern research. For an illustration of this fact, this chapter presents the most important characteristics of neutron stars and their magnetic fields.

Neutron stars are among the most extreme objects known to exist in the universe. Showing masses on the order of $1.5\,\mathrm{M}_\odot$ and radii of approximately 12 km, they represent the densest objects with finite extents. Providing densities, gravitational potentials and magnetic field strengths that are not reproducible artificially by far, they are unique laboratories for investigations of matter under extreme conditions. These studies are about to reveal the most fundamental characteristics of matter, promoting today's progress of our understanding of physics itself.

2.1.1. Neutron star formation

Neutron stars as compact objects represent one of the final stages of stellar evolution. They originally evolve from stars with an initial mass of 8 to $29\,\mathrm{M}_\odot$ after their supergiant phase in a core collapse supernova.

Lighter stars do not reach the stage where neutron stars can be built because their temperature stays too low to start the required fusion processes. They end up as brown dwarfs or helium, or respectively CO (carbonate and oxygen), white dwarfs. Heavier stars undergo an unstoppable core collapse creating a black hole.

The evolution of a potential neutron star forming candidate is as follows (Wessel, 2009).

Stars with initial masses of 8 to $29\,\mathrm{M}_\odot$ fuse hydrogen, helium and heavier elements in their interior during their evolution. Finally, their core consists of the iron isotope ^{56}Fe. For this isotope, no further energy-providing fusion processes exist.

The nuclear power produced in the core drops, the total energy E decreases locally. According to the virial theorem of classical and degenerated gases in hydrostatic equilibrium,

$$E = \frac{1}{2} E_{\mathrm{grav}} = -E_{\mathrm{int}} < 0 \tag{2.1}$$

holds, which leads to an increase in the internal energy E_{int} supplied by the gravitational energy E_{grav}. The stellar core collapses.

The increasing temperature enables inverse β-decays and photo disintegration, both being endothermic processes that further accelerate the collapse. With increasing density, electrons are first pressed into the nuclei and also neutronise free protons eventually. Thus, the electron degeneracy pressure drops, accelerating the core collapse even more. Simultaneously, the existing nuclei are disintegrated. Finally, the stellar core consists of a fluid of mostly free neutrons, protons and electrons.

Once temperature and density rise high enough, the neutrons degenerate. Their degeneracy pressure has the ability to stop the collapse and create a stiff stellar core. The material still infalling from outer layers is repelled in a shock wave creating an explosive ejection of matter. The former outer layers of the star form supernova remnants, while the original compact stellar core remains as a proto neutron star. Discharging its energy mainly by neutrino emission, the proto neutron star cools down from initially 10^{11} to $10^{12}\,\mathrm{K}$ to approximately $10^{8}\,\mathrm{K}$ in about 100 years, eventually forming a neutron star.

Apart from core collapses of old stars, highly massive neutron stars can also be formed as the end product of a stellar binary merger (Schwenzer, 2015; Baiotti & Rezzolla, 2017).

Due to their original formation via fragmentation in interstellar clouds, stars are often arranged in groups. In the course of their development, heavy stars thus commonly capture other main sequence or compact stars and form a binary system. Both objects rotate around their common centre of mass, while emitting gravitational waves, and merge into each other eventually.

The fast rotating emerging object can be described as a hypermassive neutron star. Its mass exceeds the critical upper limit for neutron stars, while it is stabilised by its rotation. If the material loss during its spin-down phase is high enough, the hypermassive neutron star will not collapse to a black hole, but transform into a new massive neutron star instead.

2.1.2. Neutron star composition

The developmental history of neutron stars explains their high masses at small radii. The internal neutron star structure is well understood in the outer parts and widely unknown for the core (Lattimer & Prakash, 2004).

The outermost parts of the neutron star are its thin atmosphere and envelope, followed by the crust underneath with a thickness of 1 to 2 km.

At relatively low densities, the outer crust consists of nuclei arranged in a Coulomb lattice, starting from ^{56}Fe at the surface towards neutron-richer nuclei in deeper layers, as well as free electrons. At densities above $4 \times 10^{11}\,\mathrm{g\,cm^{-3}}$, neutrons start to drip out of the nuclei, creating a fluid of free neutrons around the nuclei within the inner crust.

After a possible transition area between crust and core, where structures of different dimensions might appear, the neutron star core starts at a density of $2 \times 10^{14}\,\mathrm{g\,cm^{-3}}$. The stellar core contains 99% of the neutron star mass. The outer core consists of a fluid containing neutrons, protons, electrons and muons. The free neutrons are stabilised by the proton and electron Fermi seas that prevent the β-decay of neutrons, holding no free states for the emerging particles. The ratio of protons to neutrons is in β-equilibrium.

Considering the temperature and density inside the core, the neutrons are expected to be in a superfluid state, while the protons form a superconductor.

At densities exceeding $10^{15}\,\mathrm{g\,cm^{-3}}$, there might be an unknown state of matter forming an inner core. In this density regime exceeding nuclear densities, strong interactions are relevant. The associated theory of quantum chromo dynamics (QCD) can neither be solved numerically or be tested experimentally for the required density levels. It relies on assumptions for hadronic interactions and quantum many body effects. Therefore, there is a full variety of theoretically possible scenarios for the neutron star interior. For example, different fluids containing strangeness-carrying hyperons might appear, the possible existence of a quark fluid is still under discussion, colour superconduction might arise or mixed phases of hadronic and deconfined matter might emerge.

Neutron stars provide a unique opportunity to test these theories which are difficult to access otherwise. The interior neutron star structure is indirectly revealed by observational data being affected by the stellar composition (Özel & Freire, 2016).

2.1.3. Neutron star features and observational data

According to their formation and composition, neutron stars show characteristic features that allow for a connection between observables and the underlying theory of internal processes.

Neutron stars are usually classified by type according to their dominant energy source. Emission processes in *pulsars* are driven by their rotational energy, the evolution of *magnetars* is determined by their strong magnetic field, and binary neutron stars are predominantly *accretion powered*. There are common features basically applying to all neutron stars, as well as characteristics which are typical only for one of these subclasses.

The subsequent paragraphs briefly list the fundamental properties and characteristics of neutron stars.

Mass limit Despite their compactness, neutron stars underlie the Tolman-Oppenheimer-Volkoff limit, an upper limit for the neutron star mass (Wessel, 2009). It follows from the fact that an ultra relativistic degenerate gas in hydrostatic equilibrium is on the boundary between its bound and unbound state, according to the virial theorem $E_{\mathrm{int}} = -E_{\mathrm{grav}}$, i.e. $E = E_{\mathrm{int}} + E_{\mathrm{grav}} = 0$.

In a series of neutron stars with increasing masses, their average density increases, while their radius decreases, different from main sequence stars. Heavy neutron stars would thus eventually reach the critical density where the mean free path meets the neutron Compton wave length $\lambda_C = h_P/(m_n\,c)$. The neutron mass is denoted by m_n, h_P and c denote the Planck constant and the speed of light. At this point, the star would be dominated by the relativistic degenerate neutron gas.

In the ultra relativistic regime where the neutron rest mass is negligible compared to its kinetic energy, $m_n\,c^2 \ll |\boldsymbol{p}_n|$, i.e. $E = |\boldsymbol{p}_n|\,c$ with the neutron momentum $\boldsymbol{p}_n$, the stars could not be bound any more.

Due to the unknown equation of state for high densities, the mass limit for neutron stars is rather inaccurately predicted between $1.4\,\mathrm{M}_\odot$ and $3\,\mathrm{M}_\odot$. The masses of the neutron

stars detected so far observationally constrain the lower bound (Lattimer & Prakash, 2005; Lattimer, 2016). The causality limit, stating that the speed of light must exceed the speed of sound, constrains the upper bound.

Rotation Typically, neutron stars show fast rotation with periods of 10^{-3} to 1 s (Wessel, 2009; Schwenzer, 2015).

This observation can be explained based on the conservation of angular momentum during the neutron star formation collapse if the coupling between the core and the ejected envelope is assumed to be weak.

If the initial amount of pre-collapse angular momentum is concentrated mainly onto the proto neutron star, millisecond periods can arise. In contrast to other stellar objects, neutron stars are compact enough to keep these high rotation rates without reaching the mass shedding limit, where the centrifugal force would overcome the gravitational force leading to mass loss. So called millisecond pulsars show periods of less than 10^{-2} s. They are believed to form in recycling processes where an old neutron star gains angular momentum via accretion from its companion star in a low mass X-ray binary.

Magnetic field Neutron stars stand out for their magnetic fields reaching strengths that are not achieved in other objects by far.

The surface field strength of a typical pulsar is on the order of 10^8 to 10^{13} G, and exceeds 10^{14} G in magnetars (Goldreich & Reisenegger, 1992; Manchester et al., 2005; Pulsar Catalogue, 2017; Olausen & Kaspi, 2014; Magnetar Catalog, 2016). The internal field strength is expected to reach above 10^{15} G (Tayler, 1973; Akgün et al., 2013).

The reason for the long-lasting and strong magnetic fields is still an open question of astrophysics.

Commonly, the field origin in neutron stars is explained by flux freezing during the star formation process. Weak initial galactic fields are frozen into the collapsing material when stars are formed. During this process, the magnetic field strength increases according to flux conservation when the cross section traversed by the magnetic field lines decreases to stellar scales. Taking into account ambipolar diffusion, which describes the relative movement of charged particles to neutral particles caused by the stronger coupling of charged material to the magnetic field compared to the neutral material, the flux is not completely preserved. During the neutron star formation core collapse afterwards, extremely strong magnetic fields are created in the transition from the original main sequence stellar dimensions to the final extremely small neutron star radii.

Ohmic magnetic field decay, on the other hand, is not expected to be relevant on a neutron star life timescale. This estimate is a necessary condition for the observed durability of the fields. Nevertheless, this durability cannot be explained sufficiently until today. There is a number of instabilities that are expected to affect the magnetic field, preventing a persistent development.

However, works as Thompson & Duncan (1993) show that the theory of flux freezing can most likely not explain the eventual field strengths observed for neutron stars and suggest a dynamo process producing the magnetic field instead. Beyond the theory of flux freezing, there is a number of theories aiming on the explanation of the neutron star magnetic field strengths and related features. Magnetic field amplification caused by the magneto-rotational instability seems to be active both during the core collapse process, as

well as in the neutron star binary merger (Friedman et al., 2017). This effect might explain the extraordinarily high magnetar field strengths (Rembiasz et al., 2017). According to currents in the stellar magnetosphere, the dipole momentum assigned to magnetars might appear stronger than it actually is (Akgün et al., 2016).

Besides the ongoing search for an explanation for the extreme field strengths, the neutron star magnetic field is highly interesting itself.

Neutron stars, respectively magnetars, show flares and superflares, highly energetic radiation outbursts in the frequency range of X-rays and γ-rays. They are associated with possibly global scale rearrangements of the magnetic field and possible crust breaking after the occurrence of a magnetic field instability (Thompson & Duncan, 1995).

The magnetic field induced global deformation of neutron stars as well as possible magnetically confined mountains transform neutron stars into gravitational wave sources (Melatos & Payne, 2005; Mastrano et al., 2011). With the first direct detection of gravitational waves recently, this opens up an entirely new detection channel for neutron star data. It is highly desired to prepare the underlying theory before first detections of gravitational waves induced by isolated neutron stars will be possible.

Pulsar emission Neutron stars posses a generally weak omnidirectional luminosity, but a characteristic directional pulsar emission by what they were first detected (Hewish et al., 1968; Gold, 1968). According to this effect, they are called "pulsars" even though their luminosity is not variable as it is the case for actual pulsating stars. Instead, the lighthouse model explains their periodic luminosity (Wessel, 2009).

Pulsars emit electromagnetic radiation particularly from their magnetic pole areas, creating two light cones. If the symmetry axis of the mainly dipole structured magnetic field is not aligned with the stellar rotation axis, the light cone periodically hits an observer that is located in the emission plane. This periodicity with typical pulse durations of 5% of the pulse period is greatly precise for the pulsars observed so far.

Due to the short pulse durations indicating a compact source and the short periods indicating a fast rotating source, the observed pulsars could be identified as neutron stars. The pulse period allows a straightforward determination of the neutron star rotation rate. The frequency of the directional electromagnetic emission usually lies in the radio band and for some pulsars it is in the optical, X-ray or γ-band.

Despite the universality of the pulsar behaviour, the reason for the directional emission is not completely understood yet.

The common model by Goldreich & Julian (1969) states that the strong electromagnetic fields at the neutron star surface drag charged particles out of the surface. Within the light cylinder, i.e. the region around the star where the rotation speed is still less than the speed of light, the neutron star magnetic field corotates with the star, see figure 2.1. The charged particles are forced on spiral trajectories around the field lines and create a corotating magnetosphere. Field lines that do not close inside the light cylinder are open and charged particles can stream out along them.

It is still uncertain, however, whether the emitted photons are created right above the neutron star polar caps due to synchrotron radiation and inverse Compton radiation or whether the charged particles are accelerated to outer vacuum gaps where they induce γ-γ

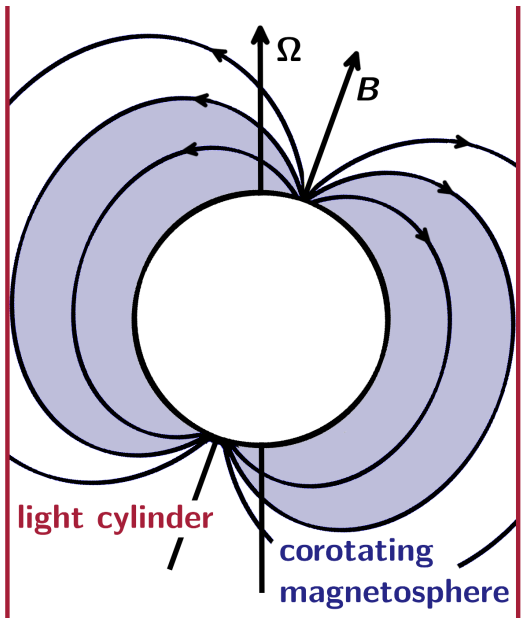

Figure 2.1.: Schematic illustration of the pulsar model by Goldreich & Julian (1969).

pair production. Independently of the model, the light cones develop eventually because the magnetic fields lines are most dense and open at the polar regions.

Spin-down Despite their very accurate periodic behaviour, pulsars show a well-defined spin-down in rotation during their evolution, detectable by a systematic increase in the pulsar emission period.

The energy loss can be caused by different effects such as electromagnetic dipole radiation, emission of gravitational waves due to magnetically induced distortions from rotational symmetry or the excitation of r-modes. The spin-down process type is characterised by the braking index

$$n_{\mathrm{br}} = \Omega\,\ddot{\Omega}/\dot{\Omega}^2, \tag{2.2}$$

which describes the decrease in the angular velocity Ω via $\dot{\Omega} = -k_{\mathrm{br}}\,\Omega^{n_{\mathrm{br}}}$, where the dots denote time derivatives and k_{br} is a proportionality constant (Alpar & Baykal, 2006).

The evaluation of spin-down curves is essential for the categorisation of neutron stars, the identification of energy providing processes, a better understanding of pulsar emission and thus a more detailed knowledge about neutron star magnetic fields.

Glitches Another characteristic feature in the observed pulsar spin-down curves are sudden spin-ups, so-called glitches.

A suitable explanation for the unexpected and unpredictable spin-up events is provided by superfluidity (Ruderman et al., 1998). Assuming that the neutrons form a superfluid in the outer core, the rotational energy of the star is quantised in vortices that are pinned to the crust. During the regular continuous crust spin-down, the superfluid vortices keep

their velocity until the velocity difference becomes large enough to unpin the vortices from the crust. In a glitch event, the released rotational energy is transferred from the vortices to the crust which is observed as a sudden increase in the stellar rotation.

Luminosity The omnidirectional electromagnetic radiation of neutron stars can be explained by the dipole emission of the generally aligned rotator mentioned above, cf. figure 2.1 (Wessel, 2009).

According to the stellar rotation rate, the omnidirectional emission frequency is very low. The directional emission is thus clearly distinguishable from the dipole radiation.

The visual luminosity L of neutron stars is very weak as can be seen by the radiation law of a black body,

$$L = 4\pi R^2 \, \sigma_{\mathrm{SB}} \, T_{\mathrm{eff}}^4, \tag{2.3}$$

where σ_{SB} denotes the Stefan-Boltzmann constant and T_{eff} the effective temperature of the star. Neutron stars do not run fusion processes anymore and they posses extremely small radii R.

In contrast to main sequence stars and white dwarfs with surface temperatures of 10^3 to 10^4 K, the neutron star surface temperature is on the order of 10^5 K. Neutron stars are thus not bright enough and too hot to appear in the Hertzsprung-Russel diagramme.

The interpretation of neutron star cooling curves, where the thermal luminosity is connected to the age of the star, is an important tool for understanding the early neutron star evolution.

Besides dipole emission, neutron stars in binary systems provide another electromagnetic observation channel via accretion powered X-ray emission. When matter is transferred from the companion to the neutron star, its gravitational potential energy is released in an accretion luminosity which lays in the X-ray band.

Beyond that, bursts and superbursts are detectable if the accreted matter causes unstable hydrogen or helium burning at the surface of the neutron star or carbon burning in deeper layers.

Present-day neutron star research fields Summarising the previous paragraphs, neutron stars show features which are extremely interesting on one hand and still not fully understood yet on the other hand.

All four fundamental forces come into play, which makes the system unique and complicates its description at the same time (Lattimer & Prakash, 2004). Gravity is relevant during the whole evolution of the neutron star due to its compactness; electromagnetism is needed for the description of the stellar magnetic field, its charged fluids and emission; weak forces determine the composition of the outer stellar core, i.e. the main part of the neutron star; strong forces are relevant for the density levels occurring in the inner stellar core, and they are related to observational features via the equation of state. Therefore, there is a broad variety of current neutron star studies, where the question of the equation of state for matter under high pressure is the central subject.

The collection of observational data for neutron star masses and radii is supposed to constrain the potential equation of state (Lattimer & Prakash, 2004; Lattimer, 2016; Özel & Freire, 2016).

Many equations of state calculated from nuclear physics or QCD provide a rather steep curve in the mass-radius diagramme, see figure 2.2. A precise measurement of neutron star radii could thus rule out many possible theories. These radius measurements, however, are very difficult. The scattering behaviour and the composition of the stellar atmosphere strongly impact the determined radii, while they are poorly known at the same time.

The underlying theory is not complex enough to yield reliable radius measurements currently, which is why this is an active research field.

Cooling curves of nearby neutron stars showing detectable optical thermal emission are studied to connect the neutron star age to their internal β-decay reactions, envelope compositions and potential superfluid phases (Potekhin et al., 2016).

Pulsar spin-down rates connect neutron star ages to their magnetic field strengths (Scholz et al., 2017). Glitches are analysed to elaborate the interaction of a superfluid core with a solid crust, which is also influenced by the internal composition (Pizzochero et al., 2017).

In the aftermath of giant flares, quasiperiodic oscillations in the emission spectra have been detected. These oscillations can be related to stellar oscillation modes (Passamonti & Lander, 2014). The identification of these modes in the spectra that are directly related to the stellar composition, is expected to be another approach to constrain the equation of state. Beyond that, unstable eigenmodes could be responsible for crust breaking or major magnetic field rearrangements (Lander et al., 2015).

Another possible source for crust breaking are strong magnetic fields which might become noticeable in flares, giant flares or bursts (Perna & Pons, 2011). The origin of giant flares is still under discussion currently. The interpretation of quasiperiodic oscillations detected in the aftermath of flare events might shed light on these questions.

Binary systems including neutron stars are excellent test objects for gravitational wave emission which represents a new investigation channel for equation of state related observables. Beyond that, binaries are possible sources of neutron star formation and can provide information about the early state of recycled neutron stars (Bose et al., 2017; Tauris et al., 2017).

2.2. Mathematical description of magnetised neutron stars

After gaining a global understanding of magnetised neutron stars in the previous section, the mathematical framework for a description of these systems must be constructed.

The modelling process will be explained in section 2.2.1. Mathematical conventions will be defined in section 2.2.2, the required system equations will be listed in section 2.2.3.

2.2.1. Modelling

Due to the fact that the stability problem of magnetised neutron stars is a globally unresolved issue and that this work is a first attempt to build a semi-analytic investigation method for this problem, the mathematical framework will be kept fairly simple. Once the

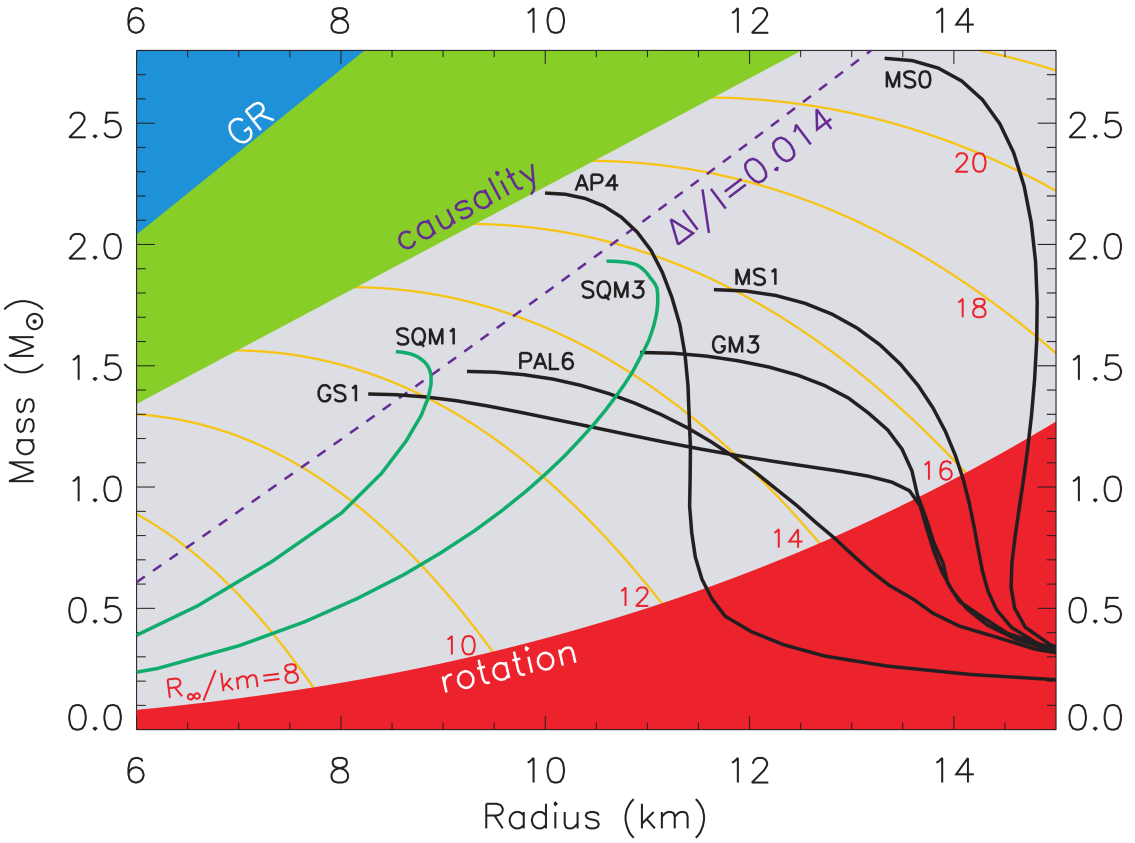

Figure 2.2.: Mass-radius diagramme for neutron stars from Lattimer & Prakash (2004). Mass-radius relations based on different choices for the equation of state are shown, black curves correspond to normal matter, green curves to strange quark matter models. The orange contours represent radiation radii $R_\infty \equiv R/\sqrt{1-\frac{2GM}{Rc^2}}$. The dashed line shows the radius limit deduced from Vela pulsar glitches, cf. Lattimer & Prakash (2001). The blue region (GR) excludes radii equal to or smaller than the Schwarzschild radius $R_S = 2GM/c^2$ for which the object would be a black hole. The green region excludes radii $R \leq 3GM/c^2$ for which the speed of sound inside the star would exceed the speed of light, causing causality problems. The red region excludes radii equal to or above the mass shedding limit, where particles are not bound to the stellar surface anymore.

method proved itself by providing results on this simple system, the system complexity will be enhanced in subsequent steps.

The mathematical framework set up here is derived from magnetohydrodynamics and the theory of mass distributions.

Perturbative approach The semi-analytic stability analysis method set up here will be based on the energy variational principle.

This principle is a perturbative approach, which offers the opportunity to keep the model complexity quite low. We can distinguish between one model for the unperturbed equilibrium system and reasonable conditions for its perturbations, rather than constructing one complete complex system.

The perturbation theory will be discussed in detail in section 2.3. In section 2.2, it is sufficient to know that we need to construct one model system for the hydrostatic equilibrium state of the star and one perturbed model system for deviations from equilibrium which cause slight changes in all system quantities.

Simplifications The model equilibrium system describes the mass, density and pressure distribution of the star, which is assumed to be barotropic. The magnetic field as well as possible deviations from barotropicity will be superimposed on the background model as perturbations.

This procedure is a simplification, particularly because the so constructed magnetised neutron star does in general not correspond to an actual equilibrium state fulfilling the Grad-Shafranov equation. However, this approach is justified for a first attempt as it has been shown in equation (21) in Sotani et al. (2007) that the equilibrium density and pressure distribution are only slightly influenced by the magnetic field. Later on, this step can be skipped by using an accurate magnetic equilibrium as an initial state instead. The semi-analytic method is just as well compatible with an actual magnetic equilibrium.

Furthermore, the neutron star rotation will be neglected for now in both the background system and the perturbed state. This assumption is justified as long as the rotational energy is exceeded by other relevant energy contributions, such as magnetic and gravitational energy. Beyond that, Pitts & Tayler (1985) found that rotation is not stringently required to explain the stability behaviour of magnetised neutron stars, while it considerably complicates the description of the system dynamics.

2.2.2. Mathematical Definitions

Coordinate system In this work, different types of coordinate systems will be used, adjusted to the respective geometry of the system under investigation (Bronstein et al., 2008).

The spherically symmetric background equilibrium system is best described in spherical

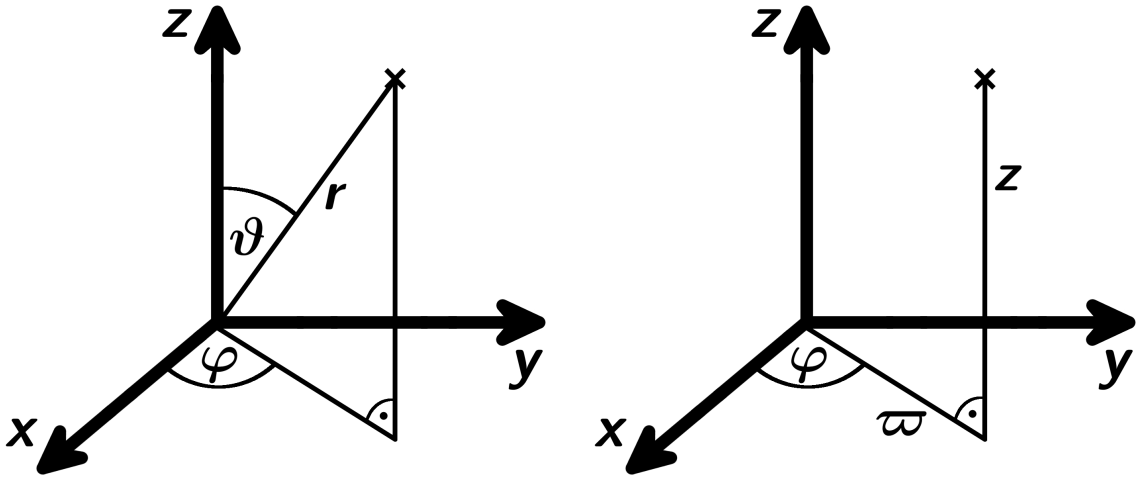

(a) Spherical coordinates. (b) Cylindrical coordinates.

Figure 2.3.: Coordinate systems utilised in this work.

coordinates $\{r, \vartheta, \varphi\}$, where

$$\begin{aligned} x &= r \sin\vartheta \cos\varphi & r &= \sqrt{x^2 + y^2 + z^2} \\ y &= r \sin\vartheta \sin\varphi & \vartheta &= \arccos\frac{z}{r} \\ z &= r \cos\vartheta & \varphi &= \arctan\frac{y}{x} \end{aligned} \tag{2.4}$$

describes the transformation to cartesian coordinates $\{x, y, z\}$. The volume element is

$$\mathrm{d}V = r^2 \sin\vartheta \,\mathrm{d}r \,\mathrm{d}\vartheta \,\mathrm{d}\varphi. \tag{2.5}$$

Due to its spherical symmetry, the background system is basically one-dimensional in coordinate system (2.4). The coordinates are the radial distance r from the stellar centre, the poloidal angle ϑ and the azimuthal angle φ. For an illustration of the coordinate system, see figure 2.3a.

According to the lack of magnetic field symmetry in a mixed field system and for the sake of comparability with the work by Akgün et al. (2013), we are going to apply spherical coordinates also for neutron stars with mixed magnetic fields.

Neutron stars with a simple purely toroidal magnetic field structure will be described in cylindrical coordinates $\{\varpi, \varphi, z\}$:

$$\begin{aligned} x &= \varpi \cos\varphi & \varpi &= \sqrt{x^2 + y^2} \\ y &= \varpi \sin\varphi & \varphi &= \arctan\frac{y}{x} \\ z &= z & z &= z \end{aligned} \tag{2.6}$$

with the volume element

$$\mathrm{d}V = \varpi \,\mathrm{d}\varpi \,\mathrm{d}\varphi \,\mathrm{d}z. \tag{2.7}$$

According to the axisymmetry we assume for the magnetised equilibrium star, the un-

perturbed system is two-dimensional in cylindrical coordinates. The cylindrical radius ϖ measures the distance of a point from the stellar symmetry axis in the (ϖ, φ)-plane, cf. figure 2.3b. The azimuthal angle φ is identically defined as in spherical coordinates, while z describes the cartesian height with respect to the equatorial plane.

Finally, the system with a purely poloidal magnetic field requires toroidal coordinates $\{\psi, \varphi, \chi\}$ to optimally fit the magnetic field geometry. In accordance with Markey & Tayler (1973), the transformation relations between cylindrical and toroidal coordinates are

$$\begin{aligned} \psi &= -\frac{B_{\mathrm{pol}}\,\bar{r}^2}{2} & \varpi &= R_{\mathrm{tor}} - \bar{r}\cos\chi \\ \varphi &= \varphi & \varphi &= \varphi \\ \chi &= \arctan\frac{z}{R_{\mathrm{tor}} - \varpi} & z &= \bar{r}\sin\chi. \end{aligned} \tag{2.8}$$

with

$$\bar{r} = \sqrt{(R_{\mathrm{tor}} - \varpi)^2 + z^2} = \sqrt{-\frac{2\psi}{B_{\mathrm{pol}}}} \tag{2.9}$$

and the volume element

$$\mathrm{d}V = J\,\mathrm{d}\psi\,\mathrm{d}\varphi\,\mathrm{d}\chi = \frac{\varpi}{B_{\mathrm{pol}}}\,\mathrm{d}\psi\,\mathrm{d}\varphi\,\mathrm{d}\chi. \tag{2.10}$$

The Jacobi determinant is denoted by J. The toroidal coordinates span a torus with radius $\bar{r}$, centred around the origin, as can be seen in figure 2.4. The torus centre lies in the equatorial plane and its distance to the stellar centre is given by R_{tor}. The azimuthal angle φ remains unchanged compared to the previously defined coordinate systems. The other coordinates ψ and χ represent polar coordinates in the (ϖ, z)-plane.

Note that for the specific choice of toroidal coordinates (2.8) used in this work, the unit vector $\boldsymbol{e}_\psi$ points towards the torus centre. The coordinate $\psi \leq 0$ takes negative values everywhere besides the torus centre, where $\psi = 0$. According to that, the backtransformation to relation (2.9) is

$$\psi = -\frac{\bar{r}^2\,B_{\mathrm{pol}}}{2}, \tag{2.11}$$

where out of the two square root solutions, the negative sign is compatible with $\psi \leq 0$.

Beyond that, ψ represents a stream function defining the poloidal magnetic field. The poloidal field amplitude is denoted by the constant B_{pol}. The connection between the toroidal coordinate system and the magnetic field structure will be explained in section 2.2.3.

Unit system In this work, cgs-units, and more precisely Gaussian units, will be used. For an overview on the unit systems utilised in this work and related works, see appendix section A.8.

The derivations in this work will be presented in non-geometrised non-rationalised Gaussian units (A.63). That way, we keep track of the appearance of prefactors, i.e. the speed of light c, the gravitational constant G and the factor $4\,\pi$ in the equations related to the Maxwell equations as well as the Poisson equation.

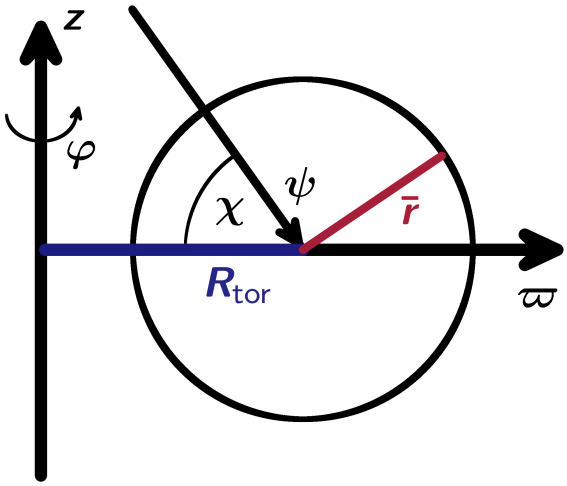

Figure 2.4.: Toroidal coordinate system utilised in this work.

For the explicit derivations and calculations performed in sections 5.1 and 5.2, geometrised rationalised Gaussian cgs units (A.64) will be applied, i.e. $c = 1$ and $G = 1$. That way, the expressions and results are directly comparable to the works by Tayler (1973) and Markey & Tayler (1973) which are based on geometrised rationalised Gaussian cgs units.

The formulas and computations in section 5.3 are based on non-rationalised Gaussian units instead, in order to allow for a quantitative comparison with Akgün et al. (2013). In the end, the difference between both approaches will manifest in an additional factor of $1/(4\pi)$ in the magnetic field related terms of the energy variation in the non-rationalised expression compared to the rationalised one.

For all numerical calculations, dimensionless quantities will be defined. The dimensionless system is based on the solar mass $\mathrm{M}_\odot$, the speed of light c and the gravitational constant G.

Partial and material derivatives In fluid dynamics, system quantities depend on position variables that are in general time-dependent as well due to fluid movements. Therefore, two kinds of derivatives are defined, distinguished by their reference frame (Thompson, 2006).

The partial time derivative $\partial_t Q$ describes the change in a system quantity Q at a fixed position. The material time derivative $\mathrm{D}_t Q$ describes the change in Q within a generally moving fluid element. The fluid motion at a velocity $\boldsymbol{v}$ provides an extra term in the material derivative:

$$\mathrm{D}_t Q = \partial_t Q + \boldsymbol{v} \cdot \nabla Q, \tag{2.12}$$

where ∇ denotes the nabla operator. The derivation of this expression and further remarks are shown in the appendix B.1.

2.2.3. System equations

This section presents all basic equations the neutron star description in this work is based on, structured by the general setup, the background system and the perturbed system (Bernstein et al., 1958; Shapiro & Teukolsky, 1983; Mestel, 1999).

General system setup

In this first attempt of building a semi-analytic stability analysis method, we will focus on the outer core of the star and neglect the thin crust as well as a potential inner core in the model. This is obviously a strong simplification but a necessary step at the same time to include more realistic features later on.

The investigated system is a fluid consisting of neutrons, protons and electrons. Being a fluid of charged particles, its time evolution is described by magnetohydrodynamics.

Electromagnetic field The neutron star fluid is assumed to be electromagnetically force-free. Assuming an infinitely high conductivity, the charged particles can arrange their position in such a way that they take the energetically lowest state where Lorentz force and electric forces on the particles are vanishing:

$$\boldsymbol{E} + \frac{\boldsymbol{v} \times \boldsymbol{B}}{c} = 0. \tag{2.13}$$

The electric and magnetic field vectors are denoted by $\boldsymbol{E}$ and $\boldsymbol{B}$, the fluid velocity by $\boldsymbol{v}$.

The Maxwell equations describe the connection between electric and magnetic fields, electric charge densities ρ_e and electromagnetic currents $\boldsymbol{j}$:

$$\nabla \cdot \boldsymbol{E} = 4\pi \rho_e \tag{2.14a}$$

$$\nabla \times \boldsymbol{E} = -\frac{\partial_t \boldsymbol{B}}{c} \tag{2.14b}$$

$$\nabla \cdot \boldsymbol{B} = 0 \tag{2.14c}$$

$$\nabla \times \boldsymbol{B} = \frac{4\pi}{c} \boldsymbol{j}. \tag{2.14d}$$

Charge densities represent sources of the electric field according to Gauß's law (2.14a). The Maxwell-Faraday equation (2.14b) describes the electric eddy current field created by changes in the magnetic field. The magnetic field is divergence free as shown by equation (2.14c). Ampère's law (2.14d) is based on the assumption of a negligible displacement current $\partial_t \boldsymbol{D} = \partial_t \boldsymbol{E} = 0$.

Applying the force-free condition (2.13) to Faraday's law (2.14b), the basic equation of magnetokinematics follows:

$$\partial_t \boldsymbol{B} = \nabla \times (\boldsymbol{v} \times \boldsymbol{B}). \tag{2.15}$$

Equation of motion The evolution of each stellar fluid element is described by the Euler equation of motion. It is the equation of motion of an ideally conducting magnetisable self-gravitating fluid:

$$\rho \, \mathrm{D}_t \boldsymbol{v} = -\nabla p \pm \rho \nabla \Phi + \frac{\boldsymbol{j} \times \boldsymbol{B}}{c}. \tag{2.16}$$

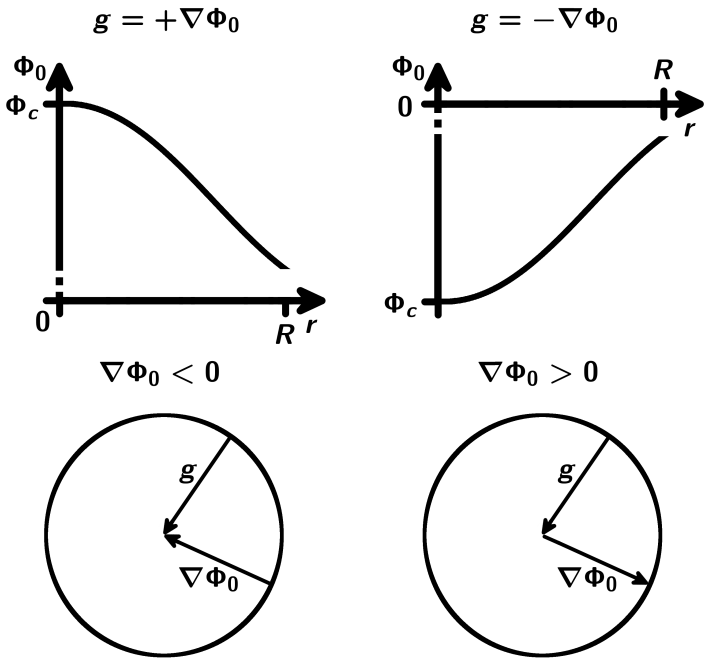

Figure 2.5.: Geometrical consideration for both sign conventions for the gravitational field, given in equation (2.17). The equilibrium gravitational potential is denoted by Φ_0, its value at the stellar centre by $\Phi_c = \Phi_0(r = 0)$.

Fluid pressure, mass density and gravitational potential are denoted by p, ρ and Φ. On the right hand side of (2.16), all relevant force densities are considered, being the fluid pressure gradient, the gravitational force and the Lorentz force.

Upper and lower sign correspond to different conventions of defining the gravitational field via

$$\boldsymbol{g} = \pm\nabla\Phi. \tag{2.17}$$

In both cases, the gravitational field vector is oriented towards the stellar centre. Upper and lower sign convention correspond to $\nabla\Phi \lessgtr 0$. For an illustration, see figure 2.5.

Both sign conventions are commonly used in studies strongly related to this work. Therefore, the equations formulated here are all compatible with both conventions in order to avoid confusion and to allow for a direct comparison with these studies. The upper sign is used in Chandrasekhar & Lebovitz (1964); Tayler (1973); Markey & Tayler (1973) etc., the lower sign convention in Akgün et al. (2013); Bernstein et al. (1958) etc. For an overview, cf. table E.3 in the appendix.

Mass conservation The stellar fluid obeys the continuity equation of mass conservation

$$\partial_t\rho = -\nabla\cdot(\rho\,\boldsymbol{v})\,. \tag{2.18}$$

Or, with the definition of the material derivative (2.12) and relation (A.1),

$$\mathrm{D}_t\rho = -\rho\,\nabla\boldsymbol{v}. \tag{2.19}$$

Poisson equation The gravitational potential of the neutron star mass distribution is described by the Poisson equation

$$\nabla^2\Phi = \mp 4\,\pi\,G\,\rho, \tag{2.20}$$

with sign convention (2.17). It is formally solved by

$$\Phi = \pm G \iiint \frac{\rho(\boldsymbol{r}')}{|\boldsymbol{r}-\boldsymbol{r}'|}\,\mathrm{d}V'. \tag{2.21}$$

Background equilibrium state

In the absence of magnetic fields and rotation, the background system is not subject to deformations and the stellar fluid takes on the energetically most favourable, i.e. spherical, shape.

Equation of state The equilibrium composition of the fluid can be described by a barotropic equation of state $p_0 = p_0(\rho_0)$, where the fluid pressure depends on the mass density only. The index 0 indicates an unperturbed equilibrium quantity.

More precisely, we assume a polytropic equation of state of the form

$$p_0(\rho_0) = \kappa\,\rho_0^{\Gamma_0}, \tag{2.22}$$

with the time-invariant constant κ and the equilibrium polytropic index

$$\Gamma_0 = \frac{\mathrm{d}\ln p_0}{\mathrm{d}\ln\rho_0} = \frac{\partial\ln p_0}{\partial\ln\rho_0}. \tag{2.23}$$

In the barotropic model, the total and partial derivatives of $\ln p_0$, denoted by operators d and ∂, are equivalent.

In the context of phase transitions in general, the polytropic equation of state (2.22) is equivalent to an adiabatic process with

$$\mathrm{D}_t\left(p\,\rho^{-\Gamma_0}\right) = \left(\partial_t + \boldsymbol{v}\cdot\nabla\right)\left(p\,\rho^{-\Gamma_0}\right) = 0, \tag{2.24}$$

where $\Gamma_0 = c_p/c_V$ is the ratio of isobaric and isochoric specific heat capacities.

Barotropicity further implies that the individual proton and neutron densities ρ_0^p and ρ_0^n, contributing to $\rho_0 = \rho_0^p + \rho_0^n$, both show the same radial dependency. That means, the proton fraction

$$x^p = \frac{\rho^p(r)}{\rho^n(r)} \tag{2.25}$$

is spatially homogeneous inside the star.

System equations for mass distribution According to the spherical symmetry of the background system, the equilibrium stellar mass distribution can be described by the

one-dimensional Newtonian system equations

$$\mathrm{d}_r m_0 = \quad 4\pi r^2 \rho_0(r) \tag{2.26a}$$

$$\mathrm{d}_r p_0 = -\frac{\rho_0(r)\, m_0(r)}{r^2} \tag{2.26b}$$

$$\mathrm{d}_r \Phi_0 = \pm \frac{\mathrm{d}_r p_0(r)}{\rho_0(r)}, \tag{2.26c}$$

where $m_0(r)$ denotes the mass enclosed inside a sphere with radius r and $\Phi_0(r)$ is its gravitational potential. The sign convention is defined in equation (2.17).

In this work, we apply Newtonian system equations (2.26) despite the fact that a relativistic treatment seems advisable when dealing with objects as compact as neutron stars. The reason is that this work is focussed on magnetic field and stability effects that do not involve extensive mass movements. Compared to studies on compact objects in binaries for example, the isolated magnetised neutron star description is only weakly influenced by relativistic corrections. A fully relativistic treatment would thus be an unnecessary complication for the first test applications presented here.

An alternative is the consideration of relativistic corrections in the system equations. The Newtonian system equations (2.26) can easily be replaced by the relativistic Tolman-Oppenheimer-Volkoff (TOV) equations

$$\mathrm{d}_r m_0 = \quad 4\pi r^2 \rho_0(r) \tag{2.27a}$$

$$\mathrm{d}_r p_0 = -\frac{\rho_0(r)\, m_0(r)}{r^2} \left(1 + \frac{p_0(r)}{\rho_0(r)}\right) \left(1 + \frac{4\pi\, p_0(r)\, r^3}{m_0(r)}\right) \left(1 - \frac{2\, m_0(r)}{r}\right)^{-1} \tag{2.27b}$$

$$\mathrm{d}_r \Phi_0 = \pm \frac{\mathrm{d}_r p_0(r)}{\rho_0(r)} \left(1 + \frac{p_0(r)}{\rho_0(r)}\right)^{-1}. \tag{2.27c}$$

However, in order to apply equations (2.27) consistently, an equivalent relativistic or at least post-Newtonian description for the magnetic field must be derived. The effort associated with this is too big for the first test setup of the semi-analytic method.

Therefore, the fully consistent relativistic treatment of the problem represents a task for future projects.

Hydrostatic equilibrium In equilibrium, the Euler equation (2.16) reads

$$-\nabla p_0 \pm \rho_0 \nabla \Phi_0 + \frac{\boldsymbol{j}_0 \times \boldsymbol{B}_0}{c} = 0, \tag{2.28}$$

as $\mathrm{d}_t \boldsymbol{v} = 0$.

The special case of an unmagnetised stationary fluid with $\boldsymbol{B}_0 = 0$ we assume in equilibrium is described by the hydrostatic equilibrium equation

$$\nabla p_0 = \pm \rho_0 \nabla \Phi_0. \tag{2.29}$$

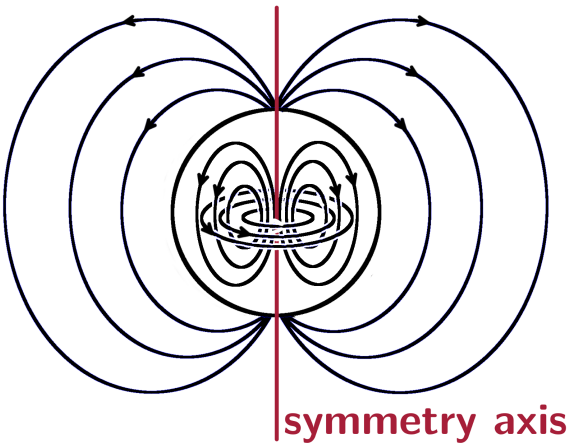

Figure 2.6.: Geometry of an arbitrarily magnetised neutron star, with toroidal and poloidal field components. The symmetry axis of the toroidal field forms the stellar symmetry axis. The interior magnetic field is schematically illustrated as the superposition of both field components. The actual interior magnetic field structure is still widely unknown. The exterior field is purely poloidal.

Perturbed state

Magnetic field In the perturbed state, the global magnetic field structure is superimposed to the background system, violating the spherical symmetry of the star. In the absence of rotation, the magnetised system is axisymmetric to the symmetry axis of the magnetic field. Therefore, the total magnetic field symmetry axis will be called stellar symmetry axis henceforth. Cf. figure 2.6.

Note that any arbitrary magnetic field structure can be decomposed into toroidal and poloidal parts:

$$\boldsymbol{B} = \boldsymbol{B}_{\mathrm{tor}} + \boldsymbol{B}_{\mathrm{pol}}, \tag{2.30}$$

cf. Grad & Rubin (1958).

In the vacuum exterior model system applied here, the toroidal magnetic field component cannot be sustained outside the star, as illustrated in figure 2.7. The poloidal field component pervades the stellar interior and exterior.

It is worth mentioning that the magnetic field has been neglected in the equilibrium state constructed above, but the magnetic field vector $\boldsymbol{B}$ will be treated as an ordinary and generally perturbed system quantity in the subsequent sections. That means, it consists of an equilibrium part and a part caused by the perturbation. This circumstance can be understood as follows. The unmagnetised background state has above been assumed in order to construct a mass, pressure and density profile. Now, the magnetic field is superimposed to this background state, creating an approximated magnetised equilibrium state which will be perturbed in the following consideration.

Depending on the system under investigation, we will choose different parametrisations for the magnetic field structure in this work. In particular, we will describe neutron stars with purely toroidal magnetic fields, purely poloidal magnetic fields and a special case

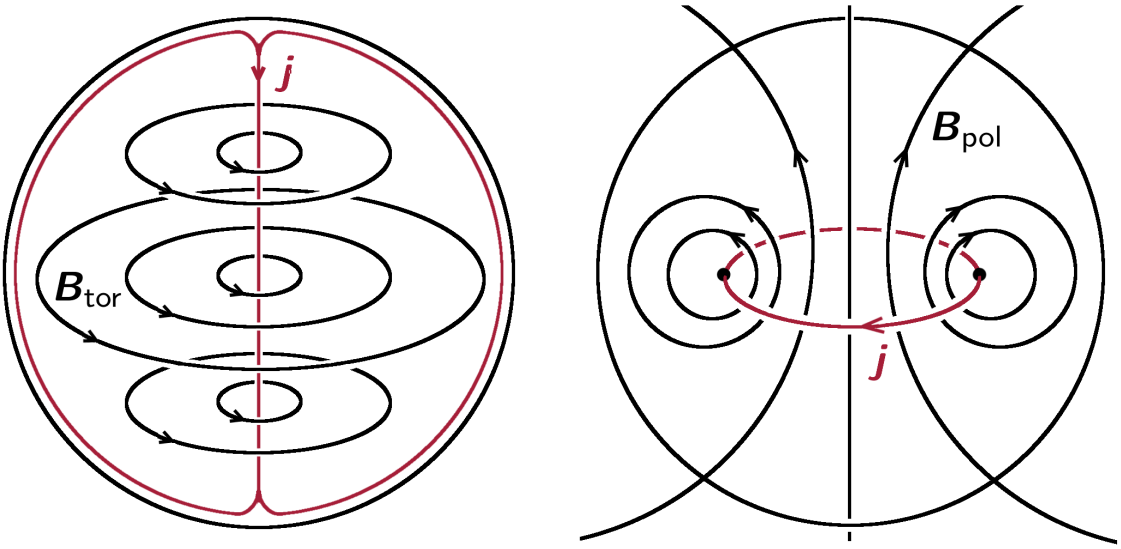

(a) Toroidal field induced by poloidal currents. (b) Poloidal field induced by toroidal currents.

Figure 2.7.: Magnetic field components and their schematically generating current densities. In the case of a vacuum exterior, a toroidal magnetic field cannot be sustained outside the neutron star as it would require electrical currents extending to the stellar exterior. In contrast, a poloidal magnetic field produced by a toroidal current density inside the star extends beyond the stellar surface to infinity.

of mixed magnetic fields, where a weak poloidal part is superimposed to the toroidal field component. These choices are reasonable assumptions to gradually approach more complex systems and they allow for a direct comparison with works by Tayler (1973); Markey & Tayler (1973) and Akgün et al. (2013).

The purely toroidal magnetic field will be parametrised by

$$\begin{aligned} B_\varpi &= 0 \\ B_\varphi &= \varpi\, \rho_0\, B_{\mathrm{tor}} \\ B_z &= 0, \end{aligned} \tag{2.31}$$

depicted in cylindrical coordinates and in accordance with Tayler (1973).

The radial form of B_φ ensures that the magnetic field is physically reasonable, as can be seen in figure 2.8: The toroidal field $B_\varphi \sim \rho_0$ drops to zero at the stellar surface, guaranteeing that the vacuum exterior is field free. As mentioned above, this is demanded because electromagnetic currents cannot exist in the vacuum exterior to maintain the toroidal field component.

The magnetic field strength $B_\varphi \sim \varpi$ further vanishes at the symmetry axis in order to stay consistent with the assumption of axisymmetry at $\varpi = 0$.

The field strength can be arbitrarily adjusted by the constant amplitude parameter B_{tor}.

For the purely poloidal magnetic field, we draw on the fact that an axisymmetric mag-

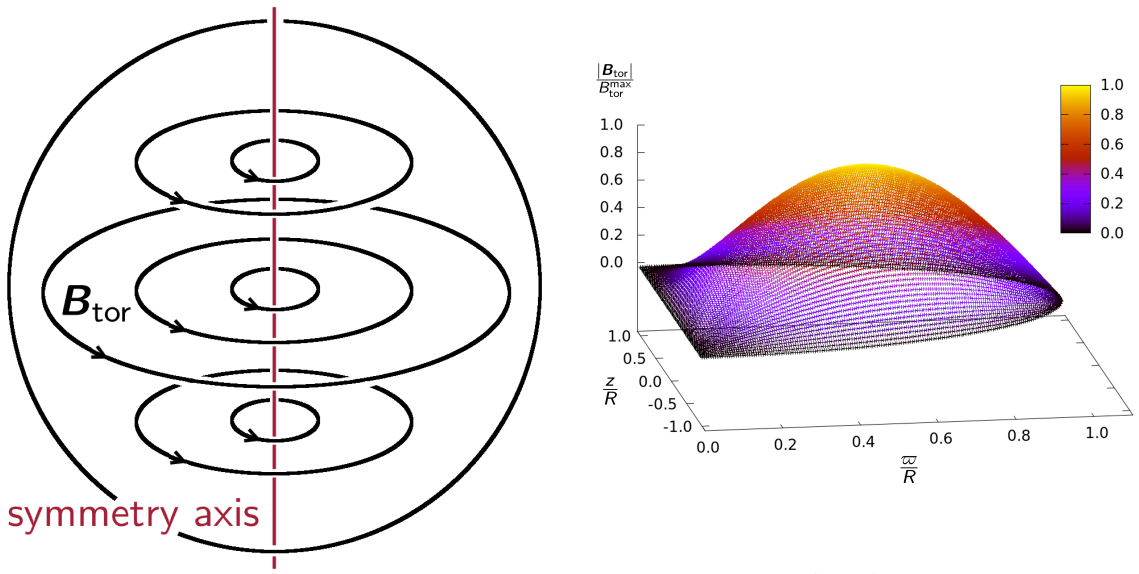

(a) Geometry.

(b) Field strength $|\boldsymbol{B}_{\mathrm{tor}}|$, where $B_{\mathrm{tor}}^{\mathrm{max}}$ denotes the maximum field strength of $|\boldsymbol{B}_{\mathrm{tor}}| = B_\varphi$.

Figure 2.8.: Purely toroidal magnetic field structure according to assumption (2.31).

netic field can be expressed by a stream function $\psi = \psi(\varpi, z)$, as demonstrated in Grad & Rubin (1958); Lander & Jones (2009) and illustrated in the appendix section B.2. The poloidal field assumed in this work is

$$\begin{aligned} B_\varpi &= -\frac{1}{\varpi}\,\partial_z\psi & B_\psi &= 0 \\ B_\varphi &= 0 & B_\varphi &= 0 \\ B_z &= \frac{1}{\varpi}\,\partial_\varpi\psi & B_\chi &= B_{\mathrm{pol}}\,\frac{\bar{r}}{\varpi}, \end{aligned} \tag{2.32}$$

represented in cylindrical coordinates (left hand side) and toroidal coordinates (right hand side). The specific choice (2.8) for toroidal coordinates has been applied to transform the expressions from cylindrical to toroidal coordinates. In toroidal coordinates, the purely poloidal magnetic field structure is more obvious since B_χ is the only non-vanishing component of $\boldsymbol{B}_{\mathrm{pol}}$.

The amplitude of the field can be adjusted by the constant factor B_{pol}, measured in cm^{-2}. Note that in toroidal coordinates, the magnetic field dependency on the stream function is comprised by the proportionality $B_\chi \sim \bar{r}(\psi)/\varpi$, according to equation (2.9).

The structure of the poloidal field is illustrated in figure 2.9a. The symmetry axis of the poloidal field, called neutral line, lies in the equatorial plane. It is a closed circle of radius R_{tor} around the stellar symmetry axis. The poloidal field chosen in equation (2.32) vanishes at the neutral line.

Beyond that, choice (2.32) is connected to the toroidal coordinates chosen in equation (2.8) in the following way. The torus spanned by the toroidal coordinates (ψ, φ, χ) confines an area around the symmetry axis in the equatorial plane. The magnetic flux flowing through this area along z is given by $2\,\pi\,\psi$, as illustrated in figure 2.9b.

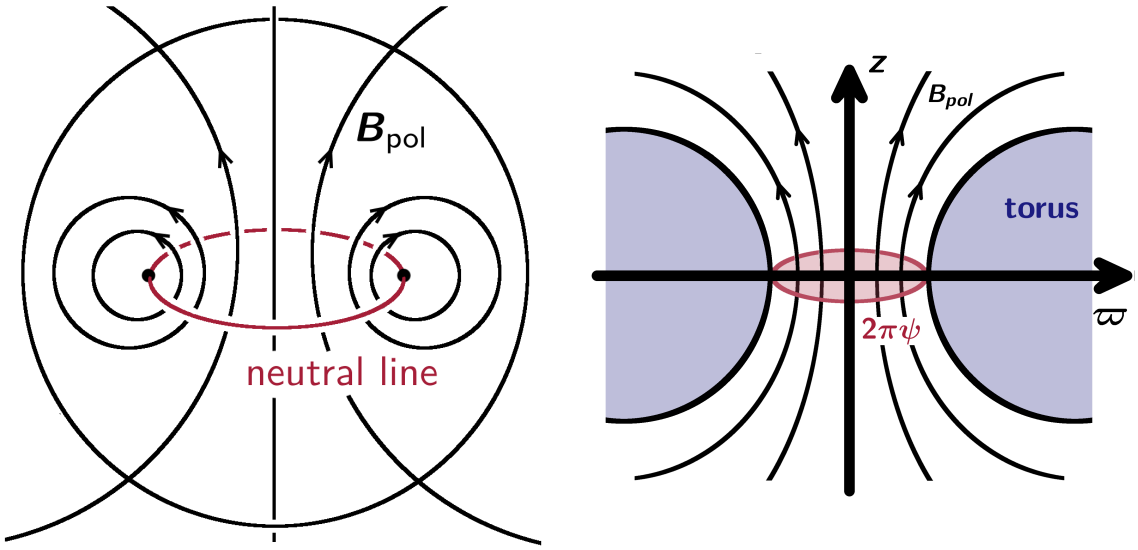

(a) Geometry. (b) Magnetic Flux.

Figure 2.9.: Purely poloidal magnetic field structure according to assumption (2.32). The magnetic flux along z through the area enclosed by symmetry axis and torus surface is $2\,\pi\,\psi$.

In accordance with Akgün et al. (2013), the magnetic field structure chosen for the mixed field case investigated in this work is

$$\begin{aligned} \boldsymbol{B}_{\mathrm{tor}} &= B_0\,\eta_{\mathrm{tor}}\,R\,\hat{\beta}(r,\vartheta)\,\nabla_r\varphi \\ \boldsymbol{B}_{\mathrm{pol}} &= B_0\,\eta_{\mathrm{pol}}\,R^2\,\nabla_r\hat{\alpha}(r,\vartheta)\times\nabla_r\varphi, \end{aligned} \tag{2.33}$$

depicted in spherical coordinates. The $\boldsymbol{B}$-defining functions are

$$\hat{\alpha}(r,\vartheta) = f(x)\,\sin^2\vartheta \qquad \hat{\beta}(r,\vartheta) = \begin{cases} (\hat{\alpha}-1)^2 & \text{for } \hat{\alpha}\geq 1 \\ 0 & \text{for } \hat{\alpha}<1, \end{cases} \tag{2.34}$$

with $x \equiv r/R$ and

$$f(x) = \frac{35}{8}\,x^2 - \frac{21}{4}\,x^4 + \frac{15}{8}\,x^6 \qquad \text{for } x\leq 1 \tag{2.35}$$

inside the star. The gradient index r indicates that derivatives are taken with respect to r as opposed to x.

Applying choices (2.34) and (2.35), the magnetic field fulfils the boundary condition at the stellar surface that enables the exterior field to have the observed dipole structure. Beyond that, the magnetic field and its generating current density are assured to be finite by boundary conditions at the stellar centre.

The amplitudes of toroidal and poloidal field components can be adjusted by appropriate choices for η_{tor} and η_{pol}. They measure the maximum field strengths $B_{\mathrm{tor}}^{\mathrm{max}}$ and $B_{\mathrm{pol}}^{\mathrm{max}}$ that

are achieved by the separate field components inside the star:

$$B_{\mathrm{tor}}^{\mathrm{max}} = B_{\mathrm{tor}}\left(x \approx 0.782\,, \vartheta = \frac{\pi}{2}\right) \approx 0.0254\ \eta_{\mathrm{tor}}\, B_0 \tag{2.36a}$$

$$B_{\mathrm{pol}}^{\mathrm{max}} = B_{\mathrm{pol}}\Big(r = 0,\ \vartheta = 0\Big) = \frac{35}{4}\,\eta_{\mathrm{pol}}\, B_0. \tag{2.36b}$$

The overall amplitude of the field is given by the constant prefactor B_0, measured in cm^{-2}. In this work, for the sake of comparison with Akgün et al. (2013), we will investigate mixed magnetic fields that posses a strong toroidal field, superimposed by a weak poloidal component.

For an illustration of the field geometry chosen by assumption (2.33), see Akgün et al. (2013). The toroidal field is localised to the region inside the outermost poloidal field line that closes inside the star. Outside this region, the toroidal field vanishes.

Stratification In order to allow for a treatment of non-barotropic stars, the perturbed star is assumed to be generally stratified. Stratification means that neutron and proton densities can be distributed differently inside the star, the proton fraction $x^p = x^p(r)$ varies with depth. In retrospection to the current knowledge about neutron star composition in section 2.1.2, this picture is by far more realistic than the barotropic description (Passamonti et al., 2009; Passamonti, 2009; Lander et al., 2011).

Mathematically, there are two ways to realise the treatment of stratified stars. For one thing, the star can be considered as a multifluid where neutrons and protons are described separately with individual equations of state and density distributions.

Alternatively, the established description of the one-component fluid is maintained, while the former barotropic equation of state is replaced by a non-barotropic one depending on an additional parameter.

In this work, the second possibility will be utilised, as it allows for a continued application of the standard frame for stability analysis that has been developed for magnetised neutron stars over the past decades. However, we will assume stratification in the perturbed system only, for the purpose of keeping the model as simple as possible in this first investigation step. In addition to the equilibrium polytropic index Γ_0, a new polytropic index Γ_1 for the perturbations will be introduced.

The concrete realisation is as follows.

In this work, the polytropic equation of state (2.22) will be applied to describe the equilibrium model neutron star, while the generally perturbed system is stratified. That means, proton and neutron densities take on the most favourable value at every position $\boldsymbol{r}$ inside the star, according to the β-equilibrium:

$$n \longrightarrow p^+ + e^- + \bar{\nu}_e \tag{2.37a}$$

$$p^+ + e^- \longrightarrow n + \nu_e. \tag{2.37b}$$

Here, n, p^+ and e^- denote neutrons, protons and electrons, ν_e and $\bar{\nu}_e$ are electron neutrino and antineutrino.

The weak force determining the conversion between neutrons and protons according to β^-- and inverse β^--decay reactions (2.37), sets the proton fraction $x^p(r)$ at every position.

The individual proton and neutron densities ρ^p and ρ^n can be distributed differently with r. Thus, x^p is not spatially homogeneous in general.

The perturbed system obeys

$$p = p(\rho, x^p). \tag{2.38}$$

With mass density $\rho(r)$ and proton fraction $x^p(r)$ being independent quantities now, the neutron star pressure depends on both quantities. Relation (2.38) represents a special case of non-barotropic equations of state in general, where the pressure depends on density and entropy.

The polytropic index Γ_1 describing the perturbations is defined in analogy to the background polytropic index Γ_0 in (2.23):

$$\Gamma_1 = \left(\frac{\partial \ln p}{\partial \ln \rho}\right)_{x^p}. \tag{2.39}$$

The polytropic index of the perturbations represents the change in $\ln p$ with $\ln \rho$ for a fixed proton fraction, as indicated by the index x^p.

Note that in general, both polytropic indices are different. This can be seen by applying the chain rule to the total differential of the logarithm of $p = p(\rho, x^p(\rho))$:

$$\Gamma_0 = \frac{\mathrm{d} \ln p_0}{\mathrm{d} \ln \rho_0} = \left(\frac{\partial \ln p_0}{\partial \ln \rho_0}\right)_{x^p} + \left(\frac{\partial \ln p_0}{\partial \ln x_0^p}\right)_{\rho} \frac{\mathrm{d} \ln x_0^p}{\mathrm{d} \ln \rho_0} = \Gamma_1 + \left(\frac{\partial \ln p_0}{\partial \ln x_0^p}\right)_{\rho} \frac{\mathrm{d} \ln x_0^p}{\mathrm{d} \ln \rho_0} \neq \Gamma_1. \tag{2.40}$$

The special case of $\Gamma_1 = \Gamma_0$ represents an actual barotropic star, where $p = p(\rho)$ describes the equilibrium state as well as the perturbed state. Any deviation from barotropicity

$$\Delta\Gamma \equiv \Gamma_1 - \Gamma_0 \gtrless 0 \tag{2.41}$$

indicates whether the star is stably or unstably stratified.

The meaning of stable and unstable stratification will be explained here by the example of a g-mode type displacement. G-modes are stellar fluid eigenmodes where gravity acts as a restoring force. They will be discussed in section 2.3.1.

We consider a fluid element in a stratified star that is displaced outwards radially. According to the decrease in the ambient pressure, its volume increases. The pressure p_{fe} inside the fluid element adjusts quickly to the pressure level of the surroundings, $p_{\mathrm{fe}} = p_{\mathrm{sur}}$. The proton fraction x^p_{fe}, however, stays unchanged, because the displacement happens on a time-scale short compared to nuclear reaction time-scales. There is not enough time to adjust the proton and neutron densities via β-decay reactions (2.37).

According to the equation of state $p = p(\rho, x^p)$, we can deduce information about the density inside the fluid element. The displaced fluid element shows the same pressure and a different entropy, i.e. proton fraction, than its surroundings. For $x^p_{\mathrm{sur}} \gtrless x^p_{\mathrm{fe}}$, the density inside the fluid element obeys $\rho_{\mathrm{fe}} \gtrless \rho_{\mathrm{sur}}$. This can easily be understood in the analogy where temperature plays the role of the entropy. A higher ambient temperature can achieve the same pressure level that is present inside the fluid element with a lower density than ρ_{fe} due to the faster particle movement at higher temperatures. Analogously, a higher proton fraction x^p implies more charged particles, who achieve the given pressure level at a lower density than a neutron-richer fluid.

Therefore, the density of the displaced fluid element is higher/lower than the equilibrium fluid density would be at this position if x^p increases/decreases with r. The gravitational force directed at the stellar centre acts stronger/less strong on the fluid element compared to its surroundings. In consequence, the fluid element moves inwards towards its initial position/further outwards. The perturbation corresponds to a stable oscillation/unstable exponential growth.

The same consideration can be done for an inward radial displacement. Again, the g-mode type displacement is stable/unstable if the entropy, respectively proton fraction, increases/decreases with r. The star is "stably"/"unstably" stratified.

The implication of stable and unstable stratification on the model system via $\Delta\Gamma \gtrless 0$ will become clear in sections 4.1 and 5.3.

2.3. Stability analysis

The goal of this work is to develop a semi-analytic method for the perturbative stability analysis of magnetised neutron stars. Therefore, section 2.3.1 explains the general concept of stability analysis and illustrates the meaning of stability, which mainly motivates this work. The mathematical framework applied for the specific stability analysis of magnetised neutron stars is outlined in section 2.3.2.

2.3.1. Concept of stability analysis

According to perturbation theory, the stability of an equilibrium state can be tested by imposing a small perturbation on a system situated in this equilibrium state and investigating its reaction towards the disturbance. The initial equilibrium state is stable if the system relaxes back to the initial state after the perturbation. It is unstable if the system further diverges from the equilibrium state (Bernstein et al., 1958; Mestel, 1999).

The perturbation is represented by an infinitesimal spatial displacement of generally all system points to new positions:

$$\boldsymbol{r}(t) = \boldsymbol{r}_0 + \boldsymbol{\xi}(\boldsymbol{r}, t), \tag{2.42}$$

where $\boldsymbol{r}$ denotes the position vector, in general in the perturbed state, while $\boldsymbol{r}_0$ is the position vector in equilibrium. The time variable is denoted by t. The displacement field $\boldsymbol{\xi}$ characterises the perturbation. It will be written in an exponential ansatz

$$\boldsymbol{\xi}^n(\boldsymbol{r}, t) = \boldsymbol{\xi}(\boldsymbol{r})\, \mathrm{e}^{\mathrm{i}\omega_n t} \tag{2.43}$$

with a time-independent amplitude $\boldsymbol{\xi}(\boldsymbol{r})$, the complex quantity ω characterising its time-evolution and the temporal mode index n.

Based on this, the stability test can be mathematically performed in two different ways. The normal mode analysis is based on the time-dependent study of the perturbation mode $\boldsymbol{\xi}(\boldsymbol{r}, t)$. In contrast, the energy variational principle makes use of the fact that the system's perturbative behaviour also affects its energy. The variational principle studies the change in the total energy during the displacement in a stationary picture.

Here, both approaches will be outlined for the purpose of a better understanding and in view of future applications of the semi-analytic method. This work, however, is predominantly based on the energy variational principle which is better suited for the aims pursued here.

The energy principle is based on purely stationary considerations and can be adopted in a straightforward way. The application of the normal mode analysis as a time-dependent procedure is more complex. As a consequence, normal mode analysis provides more information, i.e. eigenmodes and eigenfrequencies, than the energy variation principle. Until today, magnetised neutron stars cannot be modelled to a sufficiently realistic extent explaining their stability. A simple method providing predictions about stability only is thus most suitable at the present time. The time evolution of the system might be studied in a later step using normal mode analysis once a stable equilibrium state has been found.

Normal mode analysis

The method of normal mode analysis tests whether the perturbation imposed on a system corresponds to one of the system's eigenmodes.

The displacement field $\boldsymbol{\xi}^n(\boldsymbol{r},t)$ corresponds to a stable oscillation around the equilibrium state with the real frequency ω_n if $\omega_n^2 > 0$. In contrast, the amplitude of $\boldsymbol{\xi}^n(\boldsymbol{r},t)$ evolves exponentially, i.e. in an unstable way, if ω_n describes an imaginary damping coefficient: $\omega_n^2 < 0$.

An equilibrium state is stable if all possible perturbations evolve stably. As soon as there exists at least one unstable perturbation, the equilibrium is unstable. Mathematically formulated this reads

$$\left\{ \begin{array}{ll} \omega_n^2 > 0 & \forall \quad n \\ \omega_n^2 < 0 & \text{for at least one } n \end{array} \right\} \Leftrightarrow \left\{ \begin{array}{c} \text{stability} \\ \text{instability.} \end{array} \right\} \tag{2.44}$$

Stability criterion in normal mode analysis towards $\boldsymbol{\xi}^n(\boldsymbol{r},t) = \boldsymbol{\xi}(\boldsymbol{r})\,\mathrm{e}^{\mathrm{i}\omega_n t}$

For $\omega_n^2 = 0$, the system is metastable. It might remain in the equilibrium state for an extended period of time, possibly due to an inhibited transition, but it will finally decay into an energetically more favourable state.

For unstable modes, $-\omega_n$ corresponds to the growth rate of the mode n. The faster an instability grows, the less likely it is to be damped out.

Modes that grow slowly on the time-scale of typical system processes can transfer energy to other modes and achieve a saturation state as for example the rotationally driven CFS-instability (Chandrasekhar, Friedman, Schutz) in neutron stars.

If the growth rate of an unstable mode is short compared to the system time-scale, the instability cannot be stopped by any other process and will become active. The occurrence of such a so-called dynamical instability therefore leads to the instability of the entire star. Examples for this type of instability are the Tayler-instabilities of magnetised fluids occurring in neutron star models. Therefore, all unstable modes relevant for this work can be looked at as dynamical ones.

The eigenmodes of the spherically symmetric background neutron star are divided into three categories distinguished by their restoring forces Finn (1987); Aerts et al. (2010).

All mode types can posses an imaginary frequency part describing damping mechanisms. Apart from that, the existence of a potential real frequency part determines according to condition (2.44) whether the mode can be stable or not.

Pressure modes / p-modes The fluid pressure gradient acts as a restoring force towards pressure modes. They generate acoustical waves because the fluid pressure gradient implies a spatially varying sound speed. P-modes are always stable for their frequencies posses a non-vanishing real part.

Gravity modes / g-modes Gravity acts as a restoring force towards gravity modes. They generate gravity waves, because gravity implies an entropy gradient or, more specifically, stratification. G-modes can be stable, marginally stable or unstable for their frequencies can be arbitrary combinations of real and imaginary parts.

Fundamental mode / f-mode There is only one fundamental mode per star. It generates surface gravity waves. The fundamental mode does not involve compressive displacements, i.e. there is no change in sign in $\boldsymbol{\xi}$ throughout the star. The f-mode is always stable in non-rotating stars for its frequency possesses a non-vanishing real part. In rotating stars, the f-mode can become CFS-unstable.

Energy variational principle

A physical system aims for minimising its total energy, which enables the possibility to formulate the stability criterion as an energy statement.

A displacement mode is stable if it increases the total energy W of the system for the transition from its equilibrium state to the perturbed state. The displacement mode is unstable if it decreases the system energy. In the first case, the displaced system will try to return to the energetically more favourable initial state. In the second case it will develop into a new even more favourable state, see figure 2.10.

Mathematically spoken, the first variation of the system energy $\delta W^{(1)} = 0$ vanishes. The total energy is extremal as the system is assumed to be in equilibrium. The second variation $\delta W^{(2)} \equiv \delta W$ provides the stability information. It indicates whether the extremum is a minimum, corresponding to a stable perturbation, or a maximum, corresponding to an unstable one.

The entire equilibrium state is stable if the total energy increases for all possible displacement fields and it is unstable as soon as the energy decreases for at least one perturbation:

$$\left\{ \begin{array}{ll} \delta W > 0 & \forall \quad n \\ \delta W < 0 & \text{for at least one } n \end{array} \right\} \Leftrightarrow \left\{ \begin{array}{c} \text{stability} \\ \text{instability.} \end{array} \right\} \tag{2.45}$$

Stability criterion according to the energy variational principle for $\boldsymbol{\xi}^n(\boldsymbol{r},t) = \boldsymbol{\xi}(\boldsymbol{r})\,\mathrm{e}^{\mathrm{i}\omega_n t}$

It can be shown that both stability criteria (2.44) and (2.45) of normal mode analysis and energy variational principle are equivalent (Shapiro & Teukolsky, 1983).

The metastable state with $\delta W = 0$ corresponds to the situation where the perturbation does not impact the system energy. Usually, this scenario is highly improbable due to the high complexity of real systems.

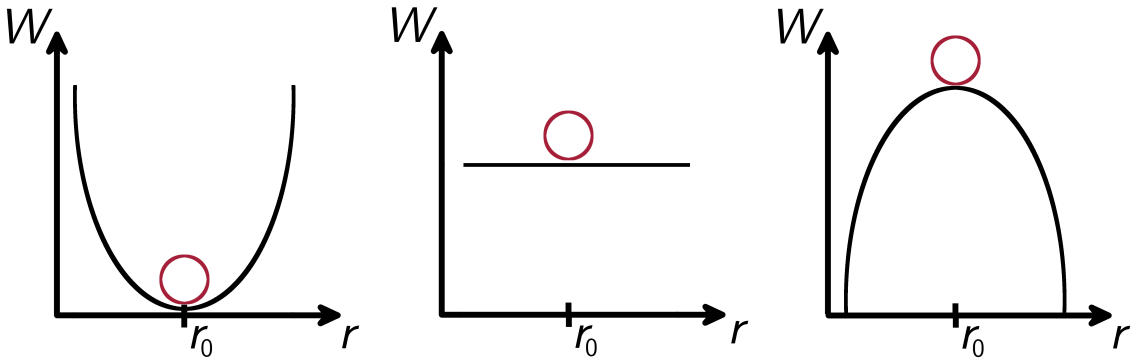

(a) Stable equilibrium. (b) Metastable equilibrium. (c) Unstable equilibrium.

Figure 2.10.: Schematic stability behaviour of a system in equilibrium. The equilibrium state is stable if a deflection from equilibrium increases the system energy (a), unstable if it decreases the system energy (c) and metastable if the deflection does not influence the total energy (b).

Meaning of stability

From an observational point of view, the stability behaviour of a system is of particular interest.

In real systems, small perturbations of an equilibrium state occur constantly, caused by external influences, variations, uncertainty and quantum fluctuations. Even isolated systems are subject to some of these causes.

This discovery has a decisive consequence on observations.

> A system in an unstable state cannot persist long enough to be detectable. Therefore, it is expected that all neutron stars we observe must be in a stable equilibrium state.
>
> **Observationally inferred requirement for theoretical neutron star models**

Although a long-term "metastable" state with inhibited transitions might explain the observed durability of neutron stars as well, metastability in the proper sense is not expected in the context of neutron stars, due to the high complexity of the system and the dynamical type of the potential instabilities.

2.3.2. Energy variation for magnetised neutron stars

For the purpose of applying the energy variational principle to the systems discussed in this work, the energy variation of magnetised neutron stars needs to be calculated. In this section, we will define the required notations and present the derivation of an expression for δW. Subsequently, the expression will be made explicit by applying the Euler equation of motion (2.16) for the system under consideration.

Note that in this chapter, the foundations on neutron star stability analysis will be summed up. That means, the energy variation will be derived in the common way of previous works, i.e. for a barotropic star in Cowling approximation. Therefore, the polytropic equation of state (2.22) will be used here and it is assumed that the gravitational

potential does not change due to the perturbation. Both simplifications will be removed in chapters 4 and 5, where the innovations of this work are presented.

Eulerian and Lagrangian perturbations

Definitions The infinitesimal displacement field imposed on the position vector in equation (2.42) causes all system quantities Q to change as well (Bernstein et al., 1958; Shapiro & Teukolsky, 1983; Mestel, 1999). The variable Q can represent an arbitrary system quantity, for example $Q \in \{\rho, p, \Phi, \boldsymbol{B}, \boldsymbol{j}, ...\}$.

The perturbed quantities Q^{E} or Q^{L} can be expressed in an Eulerian or Lagrangian framework via

$$Q^{\mathrm{E}}(\boldsymbol{r}_0, t) = Q_0(\boldsymbol{r}_0)\Big|_t + \delta Q(\boldsymbol{r}_0, t) \tag{2.46a}$$

$$Q^{\mathrm{L}}(\boldsymbol{r}, t) = Q_0(\boldsymbol{r}_0)\Big|_t + \Delta Q(\boldsymbol{r}, t) = Q_0(\boldsymbol{r}_0)\Big|_t + \delta Q(\boldsymbol{r}_0, t) + \boldsymbol{\xi} \cdot \nabla Q, \tag{2.46b}$$

where $Q_0(\boldsymbol{r}_0)|_t$ denotes the equilibrium quantity Q_0 at the unperturbed position $\boldsymbol{r}_0$, evaluated at time t. The notation indicates that Q_0 does not depend on t.

Also note that

$$\boldsymbol{r}(t) = \boldsymbol{r}_0|_t + \boldsymbol{\xi}(\boldsymbol{r}, t) \tag{2.47}$$

from equation (2.42).

The Eulerian perturbation δQ represents the change in Q at the fixed position $\boldsymbol{r}_0$. The Lagrangian perturbation ΔQ represents the change in Q inside the fluid element that was located at $\boldsymbol{r}_0$ in the unperturbed state and that was displaced to the position $\boldsymbol{r}$ by the perturbation. Compare figure 2.11. Note that δQ and ΔQ are caused by an instantaneous deflection $\boldsymbol{\xi}$, as opposed to an actual temporally finite shift. Both layers in the illustration thus correspond to the time t.

The deflection of the fluid element itself causes a contribution $\boldsymbol{\xi} \cdot \nabla Q$ which connects both perturbations via

$$\Delta Q = \delta Q + \boldsymbol{\xi} \cdot \nabla Q. \tag{2.48a}$$

Note that relations (2.46) and (2.48a) hold for scalar quantities Q. In the case of a vector quantity $\boldsymbol{Q} = (Q_1, Q_2, Q_3)$, these relations are equally valid for the individual components, i. e.:

$$\Delta \boldsymbol{Q} = \delta \boldsymbol{Q} + (\boldsymbol{\xi} \cdot \nabla)\, \boldsymbol{Q} = \begin{pmatrix} \delta Q_1 \\ \delta Q_2 \\ \delta Q_3 \end{pmatrix} + \begin{pmatrix} (\xi_1 \partial_1 + \xi_2 \partial_2 + \xi_3 \partial_3)\, Q_1 \\ (\xi_1 \partial_1 + \xi_2 \partial_2 + \xi_3 \partial_3)\, Q_2 \\ (\xi_1 \partial_1 + \xi_2 \partial_2 + \xi_3 \partial_3)\, Q_3 \end{pmatrix}. \tag{2.48b}$$

Eulerian and Lagrangian perturbations are defined analogously to partial and material derivatives ∂_t and D_t which are taken at a fixed position, respectively fixed fluid element, and which are connected via relation (2.12).

However, note that δQ and ΔQ are differentials rather than derivatives and that they refer to the infinitesimal displacement $\boldsymbol{\xi}$ rather than an arbitrary fluid movement $\boldsymbol{v}$. Further remarks are made in the appendix B.3.

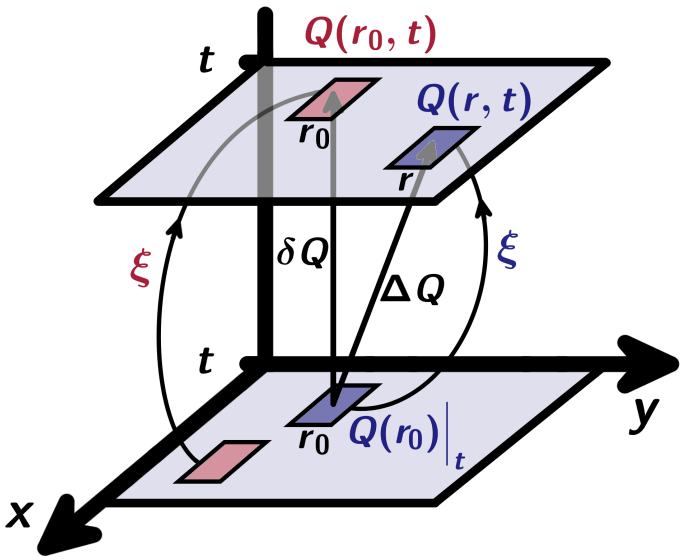

Figure 2.11.: Illustration of Euler and Lagrange perturbations. The Euler perturbation δQ describes the change from the blue coloured fluid element at r_0, t to the red coloured fluid element at r_0, t. The Lagrange perturbation describes the change from the blue coloured fluid element at r_0, t to the blue coloured fluid element at r, t.

Below, the system quantities will be expanded in terms of different powers of $\boldsymbol{\xi}$:

$$Q = Q_0 + \delta Q^{(1)} + \mathcal{O}(\boldsymbol{\xi}^2) \tag{2.49}$$

$$W = W_0 + \delta W^{(1)} + \delta W^{(2)} + \mathcal{O}(\boldsymbol{\xi}^3), \tag{2.50}$$

where $\mathcal{O}(\boldsymbol{\xi}^k)$ denotes terms of the order $\boldsymbol{\xi}^k$ and higher.

An analogous expansion can be made in the Lagrangian framework:

$$Q = Q_0 + \Delta Q^{(1)} + \mathcal{O}(\boldsymbol{\xi}^2) \tag{2.51}$$

$$W = W_0 + \Delta W^{(1)} + \Delta W^{(2)} + \mathcal{O}(\boldsymbol{\xi}^3). \tag{2.52}$$

Since the perturbative approach used in this work will be based on a second order consideration in the energy variation δW, it involves first order approximations in δQ $\forall Q \neq \{W, E\}$. Thus, the notations

$$\delta Q \equiv \delta Q^{(1)} \qquad \forall \quad Q \neq \{W, E\} \tag{2.53}$$

$$\Delta Q \equiv \Delta Q^{(1)} \qquad \forall \quad Q \neq \{W, E\} \text{ and} \tag{2.54}$$

$$\delta W \equiv \delta W^{(2)} \tag{2.55}$$

will be convenient.

In the linearised framework, relation (2.48) becomes

$$\Delta Q = \delta Q + \boldsymbol{\xi} \cdot \nabla Q_0 + \mathcal{O}(\boldsymbol{\xi}^2). \tag{2.56}$$

Relations for position and velocity From figure 2.11, the special cases of the positional Euler and Lagrange differentials can be identified as

$$\delta \boldsymbol{r} = 0 \tag{2.57}$$

$$\Delta \boldsymbol{r} = \delta \boldsymbol{r} + (\boldsymbol{\xi} \cdot \nabla)\, \boldsymbol{r} = \begin{pmatrix} (\xi_1 \partial_1 + \xi_2 \partial_2 + \xi_3 \partial_3)\, r_1 \\ (\xi_1 \partial_1 + \xi_2 \partial_2 + \xi_3 \partial_3)\, r_2 \\ (\xi_1 \partial_1 + \xi_2 \partial_2 + \xi_3 \partial_3)\, r_3 \end{pmatrix} = \boldsymbol{\xi}. \tag{2.58}$$

Note that $\partial_i r_j = \delta_{ij}$, with the Kronecker delta δ_{ij}.

Furthermore, the time derivatives of the position vector are

$$\partial_t \boldsymbol{r}|_{\boldsymbol{r}} = 0 \tag{2.59}$$

$$\mathrm{D}_t \boldsymbol{r}|_{\boldsymbol{r}} = \underbrace{\partial_t \boldsymbol{r}|_{\boldsymbol{r}}}_{0} + (\boldsymbol{v}|_{\boldsymbol{r}} \cdot \nabla)\, \boldsymbol{r} = \begin{pmatrix} (v_1 \partial_1 + v_2 \partial_2 + v_3 \partial_3)\, r_1 \\ (v_1 \partial_1 + v_2 \partial_2 + v_3 \partial_3)\, r_2 \\ (v_1 \partial_1 + v_2 \partial_2 + v_3 \partial_3)\, r_3 \end{pmatrix} = \boldsymbol{v}|_{\boldsymbol{r}}\,, \tag{2.60}$$

Equation (2.59) states that the change in $\boldsymbol{r}$ at a fixed position always vanishes, whereas the change in $\boldsymbol{r}$ within a fluid element represents the fluid velocity, as shown by equation (2.60). Thus, the fluid velocity $\boldsymbol{v}$ is given by the material derivative.

The Euler and Lagrange differentials of the fluid velocity are

$$\delta \boldsymbol{v} = \boldsymbol{v}(\boldsymbol{r}_0, t) - \boldsymbol{v}_0(\boldsymbol{r}_0)|_t = \mathrm{D}_t \boldsymbol{r}|_{\boldsymbol{r}_0} - \mathrm{D}_t \boldsymbol{r}_0|_{\boldsymbol{r}_0} = \mathrm{D}_t\, (\boldsymbol{r}_0 + \boldsymbol{\xi})|_{\boldsymbol{r}_0} - \mathrm{D}_t \boldsymbol{r}_0|_{\boldsymbol{r}_0} = \mathrm{D}_t \boldsymbol{\xi}|_{\boldsymbol{r}_0} = \partial_t \boldsymbol{\xi} \tag{2.61}$$

$$\Delta \boldsymbol{v} = \boldsymbol{v}(\boldsymbol{r}\ , t) - \boldsymbol{v}_0(\boldsymbol{r}_0)|_t = \mathrm{D}_t \boldsymbol{r}|_{\boldsymbol{r}}\ - \mathrm{D}_t \boldsymbol{r}_0|_{\boldsymbol{r}_0} = \mathrm{D}_t\, (\boldsymbol{r}_0 + \boldsymbol{\xi})|_{\boldsymbol{r}}\ - \mathrm{D}_t \boldsymbol{r}_0|_{\boldsymbol{r}_0} = \mathrm{D}_t \boldsymbol{\xi}. \tag{2.62}$$

Equations (2.61) and (2.62) follow from the definition of the Euler respectively Lagrange perturbations (2.46), according to which

$$\boldsymbol{v}(\boldsymbol{r}_0, t) = \boldsymbol{v}_0(\boldsymbol{r}_0)|_t + \delta \boldsymbol{v}(\boldsymbol{r}, t) \tag{2.63a}$$

$$\boldsymbol{v}(\boldsymbol{r}, t) = \boldsymbol{v}_0(\boldsymbol{r}_0)|_t + \Delta \boldsymbol{v}(\boldsymbol{r}, t), \tag{2.63b}$$

and from the relation for the fluid velocity (2.60). The last step in relation (2.61) is based on the fact that the material derivative of any quantity at a fixed position involves no movement of the respective fluid element, i. e. $\boldsymbol{v}_0 = 0$. Therefore, material and partial derivative are identical, $\mathrm{D}_t Q|_{\boldsymbol{r}_0} = \partial_t Q$. Based on that, $\mathrm{D}_t \boldsymbol{r}_0|_{\boldsymbol{r}} = \mathrm{D}_t \boldsymbol{r}_0|_{\boldsymbol{r}_0}$ holds as well, applied in the last step of relation (2.62).

The interpretation of expressions (2.61) and (2.62) is as follows. The Euler variation $\delta \boldsymbol{v}$ describes the change of $\boldsymbol{v}$ at a fixed position $\boldsymbol{r}_0$. According to equation (2.61), it is equivalent to the partial derivative of the displacement field. The Lagrange variation $\Delta \boldsymbol{v}$ describes the change of $\boldsymbol{v}$ within a fluid element that is displaced from $\boldsymbol{r}_0$ to $\boldsymbol{r} = \boldsymbol{r}_0 + \boldsymbol{\xi}$.

According to equation (2.62), it is equivalent to the material derivative of the displacement field.

Furthermore, we will assume a stationary equilibrium fluid below, with

$$\boldsymbol{v}_0 = \mathrm{D}_t \boldsymbol{r}_0 = 0. \tag{2.64}$$

This assumption allows for non-stationary equilibria as well as long as the equilibrium flow is generally spoken slow compared to the perturbative flow:

$$\boldsymbol{v}_0 = \mathrm{D}_t \boldsymbol{r}_0 \ll \begin{cases} \delta\boldsymbol{v} = \partial_t \boldsymbol{\xi} \\ \Delta\boldsymbol{v} = \mathrm{D}_t \boldsymbol{\xi}. \end{cases} \tag{2.65}$$

Note that according to assumption (2.64) or (2.65), the linearisation in $\boldsymbol{\xi}$ yields the relations

$$\Delta\boldsymbol{v} = \delta\boldsymbol{v} + (\boldsymbol{\xi}\cdot\nabla)\,\boldsymbol{v} = \delta\boldsymbol{v} + (\boldsymbol{\xi}\cdot\nabla)\,\boldsymbol{v}_0 + \mathcal{O}\left(\boldsymbol{\xi}^2\right) = \delta\boldsymbol{v} + \mathcal{O}(\boldsymbol{\xi}^2) \tag{2.66}$$

$$\mathrm{D}_t\boldsymbol{\xi} = \partial_t\boldsymbol{\xi} + (\boldsymbol{v}\cdot\nabla)\,\boldsymbol{\xi} = \partial_t\boldsymbol{\xi} + (\boldsymbol{v}_0\cdot\nabla)\,\boldsymbol{\xi} + \mathcal{O}\left(\boldsymbol{\xi}^2\right) = \partial_t\boldsymbol{\xi} + \mathcal{O}(\boldsymbol{\xi}^2) \tag{2.67}$$

$$\boldsymbol{v} = \delta\boldsymbol{v} = \Delta\boldsymbol{v} = \partial_t\boldsymbol{\xi} = \mathrm{D}_t\boldsymbol{\xi}. \tag{2.68}$$

Implicit form for the energy variation δW

In this paragraph, we outline the derivation of an expression for the energy variation during the perturbation of a magnetised fluid. The derivation is shown in Bernstein et al. (1958); Mestel (1999).

The first step is to set up the work W done by the displacement $\boldsymbol{\xi}$. This can be achieved by multiplying the force densities appearing in the Euler equation (2.16) with $\boldsymbol{\xi}$ and integrating over the system volume. The Euler equation includes all relevant force density contributions. After the multiplication with a length and the volume integration, it provides an energy:

$$\rho\,\mathrm{D}_t\boldsymbol{v} = -\nabla p \pm \rho\,\nabla\Phi + \frac{\boldsymbol{j}\times\boldsymbol{B}}{c} \tag{2.69}$$

$$\iiint \rho\,\boldsymbol{\xi}\cdot\mathrm{D}_t\boldsymbol{v}\;\mathrm{d}V = \iiint \left\{-\boldsymbol{\xi}\cdot\nabla p \pm \rho\,\boldsymbol{\xi}\cdot\nabla\Phi + \boldsymbol{\xi}\cdot\frac{\boldsymbol{j}\times\boldsymbol{B}}{c}\right\}\mathrm{d}V, \tag{2.70}$$

where $\mathrm{d}V$ denotes the integration over the stellar volume. In the simplified model neglecting rotation and magnetic deformations, the stellar volume is represented by a sphere.

The left hand side LHS can be expanded with respect to $\boldsymbol{\xi}$ using Lagrange expansions (2.51) and a negligible equilibrium flow with (2.68), yielding

$$\mathrm{LHS} = \iiint \left(\rho_0 + \Delta\rho + \mathcal{O}\left(\boldsymbol{\xi}^2\right)\right)\boldsymbol{\xi}\cdot\mathrm{D}_t\left(\mathrm{D}_t\boldsymbol{\xi}\right)\;\mathrm{d}V = \iiint \rho_0\,\boldsymbol{\xi}\cdot\mathrm{D}_t^2\boldsymbol{\xi}\;\mathrm{d}V + \mathcal{O}(\boldsymbol{\xi}^3). \tag{2.71}$$

Applying relation (2.68) and the exponential ansatz (2.43), $\boldsymbol{\xi} = \boldsymbol{\xi}(\boldsymbol{r})\,\mathrm{e}^{\mathrm{i}\omega t}$, for the displacement field, we receive

$$\boldsymbol{\xi}\cdot D_t^2\boldsymbol{\xi} = \boldsymbol{\xi}\cdot\partial_t^2\boldsymbol{\xi} = -\omega^2\boldsymbol{\xi}(\boldsymbol{r})\cdot\boldsymbol{\xi}(\boldsymbol{r})\,\mathrm{e}^{2i\omega t} = |\partial_t\boldsymbol{\xi}|^2\,. \tag{2.72}$$

This time derivative can be identified as the fluid velocity by relation (2.68). Then,

$$\text{LHS} = \iiint \rho_0 \left|\partial_t \boldsymbol{\xi}\right|^2 \,\mathrm{d}V + \mathcal{O}(\boldsymbol{\xi}^3) = \iiint \rho_0 \left|\boldsymbol{v}\right|^2 \,\mathrm{d}V + \mathcal{O}(\boldsymbol{\xi}^3). \tag{2.73}$$

Inferred from that, equation (2.70) provides the kinetic energy E_{kin} on the left hand side if it is multiplied by 1/2:

$$\frac{1}{2} \iiint \rho_0 \left|\partial_t \boldsymbol{\xi}\right|^2 \,\mathrm{d}V + \mathcal{O}(\boldsymbol{\xi}^3) = \frac{1}{2} \iiint \left\{ -\boldsymbol{\xi} \cdot \nabla p \pm \rho \boldsymbol{\xi} \cdot \nabla \Phi + \boldsymbol{\xi} \cdot \frac{\boldsymbol{j} \times \boldsymbol{B}}{c} \right\} \mathrm{d}V. \tag{2.74}$$

From the energy conservation law, $E_{\text{kin}} = -W$, the negative work $-W$ can be identified on the right hand side. This work represents the potential energy W which is converted during the perturbation. Thus, up to second order:

$$W + \mathcal{O}(\boldsymbol{\xi}^3) = \frac{1}{2} \iiint \left\{ \boldsymbol{\xi} \cdot \nabla p \mp \rho \boldsymbol{\xi} \cdot \nabla \Phi - \boldsymbol{\xi} \cdot \frac{\boldsymbol{j} \times \boldsymbol{B}}{c} \right\} \mathrm{d}V. \tag{2.75}$$

The potential energy can next be expanded with respect to $\boldsymbol{\xi}$ as well, yielding

$$\begin{aligned} W_0 + \delta W^{(1)} + \delta W^{(2)} + \mathcal{O}(\boldsymbol{\xi}^3) = \frac{1}{2} \iiint \Big\{ & \boldsymbol{\xi} \cdot \nabla \left(p_0 + \delta p\right) \mp \left(\rho_0 + \delta\rho\right) \boldsymbol{\xi} \cdot \nabla \left(\Phi_0 + \delta\Phi\right) \\ & - \frac{\boldsymbol{\xi}}{c} \cdot \left[\left(\boldsymbol{j}_0 + \delta \boldsymbol{j}\right) \times \left(\boldsymbol{B}_0 + \delta \boldsymbol{B}\right) \right] \Big\} \,\mathrm{d}V + \mathcal{O}(\boldsymbol{\xi}^3). \end{aligned} \tag{2.76}$$

Terms of different order in $\boldsymbol{\xi}$ can now be identified as

$$W_0 = 0 \tag{2.77a}$$

$$\delta W^{(1)} = \frac{1}{2} \iiint \boldsymbol{\xi} \cdot \left\{ \nabla p_0 \mp \rho_0 \nabla \Phi_0 - \frac{\boldsymbol{j}_0 \times \boldsymbol{B}_0}{c} \right\} \mathrm{d}V = 0 \tag{2.77b}$$

$$\delta W^{(2)} = \frac{1}{2} \iiint \left\{ \boldsymbol{\xi} \cdot \nabla \delta p \mp \rho_0 \boldsymbol{\xi} \cdot \nabla \delta\Phi \mp \delta\rho \boldsymbol{\xi} \cdot \nabla \Phi_0 - \boldsymbol{\xi} \cdot \frac{\boldsymbol{j}_0 \times \delta \boldsymbol{B}}{c} - \boldsymbol{\xi} \cdot \frac{\delta \boldsymbol{j} \times \boldsymbol{B}_0}{c} \right\} \mathrm{d}V. \tag{2.77c}$$

The equilibrium quantity W_0 vanishes since W is the work done by the displacement field $\boldsymbol{\xi}$. There are no contributions to W not depending on $\boldsymbol{\xi}$.

The first variation $\delta W^{(1)}$ vanishes since it includes the equilibrium Euler equation (2.28). Physically spoken, the first energy variation indicates whether the system is in equilibrium. The kinetic energy contribution given by equation (2.74) is quadratic in $\boldsymbol{\xi}$, i. e. $E_{\text{kin}\,0} = 0$ and $\delta E^{(1)}_{\text{kin}} = 0$. Thus, up to first order the potential energy represents the total system energy. Since we assume the initial state to be an equilibrium, $\delta E^{(1)} = \delta W^{(1)} = 0$ follows.

The second variation of the energy $\delta W \equiv \delta W^{(2)}$ given by equation (2.77c) provides information about the system's stability behaviour. It needs to be calculated for the stability analysing purpose of this work. Expression (2.77c) is the form Bernstein et al. (1958) derived for the energy variation.

Note that we implicitly assumed a real function $\boldsymbol{\xi}$ for the foregoing derivation. In the subsequent part of this work, the displacement field will be chosen as a generally complex function. In this case, the energy variation will obtain an additional factor of 1/2 that

is still missing in equation (2.77c). The detailed explanation of this circumstance will be given in the following section.

Preserving the physical meaning of the energy variation

Before the energy variation will be expressed explicitly, we need to make a remark on the generally complex nature of the displacement field $\boldsymbol{\xi}$.

The energy variation given by equation (2.77c) depends on the displacement field $\boldsymbol{\xi}$ as well as the Euler perturbations. They can also be expressed in terms of $\boldsymbol{\xi}$, $\delta Q = \delta Q(\boldsymbol{\xi})$, as will be seen below in relations (2.101).

The displacement field will be assumed to be complex in this work in general. Particularly the description of a spatially periodic displacement field involves imaginary parts.

The energy variation δW, however, needs to be a real number in order to represent a meaningful physical quantity with the dimension of an energy. This requirement is fulfilled in this work by taking the real part of the integrand $\mathcal{E}$ before integrating. In doing so, an additional prefactor of $1/2$ occurs in the expression for the energy variation.

Note that Tayler (1973) and Markey & Tayler (1973) we follow in the application sections 5.1 and 5.2, use a different approach to guarantee the physical meaningfulness of the energy variation. In these works, the real part of $\boldsymbol{\xi}$ is taken before it is inserted into the energy variation integral in order to keep δW real.

Consequently, the energy variation formulas given by Tayler et al. are missing the factor $1/2$ compared to their analogues presented in this work. The mathematical proof for that is given in the appendix section A.5.4, where the connection between both procedures is discussed in detail. That way, the equations in this work are directly comparable to Tayler (1973) and Markey & Tayler (1973).

The approach we use shows several advantages for this work compared to the one utilised by Tayler et al.

First, the derivation of the explicit form of δW required in the application chapter 5 is simplified.

Beyond that, constraints regarding the choice of the $\boldsymbol{\xi}$-defining functions are removed in the poloidal field application shown in section 5.2.

Finally, our procedure allows for a consistent approach for all applications, the ones based on the work by Tayler et al. as well as the one based on the work by Akgün et al. (2013), shown in section 5.3.

Explicit form for the energy variation δW

In order to practise stability analysis on magnetised neutron stars, the energy variation set up in equation (2.77c) needs to be expressed in an explicit form. For this purpose, the Eulerian perturbations δQ of the system quantities will be calculated.

For convenience, the energy variation will be split into three parts hereafter, stemming from magnetic field, fluid pressure gradient and gravity:

$$\delta W = \delta W_{\text{magn}} + \delta W_{\text{fluid}} + \delta W_{\text{grav}} \tag{2.78a}$$
$$= \iiint \left\{ \mathcal{E}_{\text{magn}} + \mathcal{E}_{\text{fluid}} + \mathcal{E}_{\text{grav}} \right\} \mathrm{d}V \tag{2.78b}$$

with the energy variation densities

$$\mathcal{E}_{\text{magn}} = -\frac{1}{4} \Re \left\{ \boldsymbol{\xi}^* \cdot \frac{\boldsymbol{j}_0 \times \delta \boldsymbol{B}}{c} + \boldsymbol{\xi}^* \cdot \frac{\delta \boldsymbol{j} \times \boldsymbol{B}_0}{c} \right\} \tag{2.79a}$$
$$\mathcal{E}_{\text{fluid}} = \frac{1}{4} \Re \left\{ \boldsymbol{\xi}^* \cdot \nabla \delta p \right\} \tag{2.79b}$$
$$\mathcal{E}_{\text{grav}} = \mp \frac{1}{4} \Re \left\{ \rho_0 \left(\boldsymbol{\xi}^* \cdot \nabla \delta \Phi \right) + \delta \rho \left(\boldsymbol{\xi}^* \cdot \nabla \Phi_0 \right) \right\}. \tag{2.79c}$$

Implicit energy variation for an arbitrary equation of state, in full description

In this notation, we took into account that the energy variation depends on the generally complex displacement field $\boldsymbol{\xi}$. As explained in the previous section, the additional prefactor of 1/2 occurs in equation (2.78) with (2.79) compared to expression (2.77c) when the real part is taken over the integrand $\mathcal{E}$. The explanation is given in the appendix section A.5.4. Expressions (2.79) can be simplified by removing the real part if the displacement field is fully real. This special case is discussed in the appendix section A.5.2.

Further note that not all terms included in the above form of the energy variation need to be considered in this work. Bernstein et al. (1958) showed that the energy variation given by (2.78) and (2.79) can be split into terms that are expressible by surface integrals δW_{surf} over the stellar surface, terms that are expressible by volume integrals δW_{vac} over the exterior of the star, and actual volume integrals δW_{star} over the stellar volume.

Hereafter, we will only consider contributions of δW_{star} as the other terms vanish for the explicit choices we will make for the displacement field below. The mathematical proof is given in the appendix B.4.

Calculation of the Eulerian perturbations For an explicit expression of δW, the Eulerian perturbations $\delta\rho$, δp, $\delta\Phi$, $\delta \boldsymbol{B}$ and $\delta \boldsymbol{j}$ need to be expressed in terms of equilibrium quantities Q_0 and the displacement field $\boldsymbol{\xi}$ only. This can be achieved by perturbing all relevant system equations presented in section 2.2.3. In order to perturb the equations, all appearing quantities are expressed by expansions (2.49) in linear order of $\boldsymbol{\xi}$.

The Euler perturbation $\delta\rho$ of the mass density can be calculated by perturbing the continuity equation of mass conservation (2.18):

$$\partial_t \left(\rho_0 + \delta\rho \right) = -\nabla \cdot \left(\rho_0 \, \boldsymbol{v}_0 \right) - \nabla \cdot \left(\rho_0 \, \delta \boldsymbol{v} \right) - \nabla \cdot \left(\delta\rho \, \boldsymbol{v}_0 \right) + \mathcal{O}(\boldsymbol{\xi}^2). \tag{2.80}$$

Here, the equilibrium equation $\partial_t \rho_0 = -\nabla \cdot \left(\rho_0 \, \boldsymbol{v}_0 \right)$ can be identified. The derivative with respect to $\boldsymbol{r}$ is equivalent to the derivative with respect to $\boldsymbol{r}_0$ in first order in $\boldsymbol{\xi}$, since $\nabla_{\boldsymbol{r}} = \nabla_{\boldsymbol{r}_0} + \mathcal{O}(\boldsymbol{\xi})$, as discussed by Bernstein et al. (1958). Therefore, we will interchange

the spatial derivatives with respect to $\boldsymbol{r}$ and $\boldsymbol{r}_0$ in this section in a way that is most favourable for the demonstrated derivations.

The term including $\boldsymbol{v}_0$ will be neglected according to assumption (2.65) and $\delta\boldsymbol{v} = \partial_t\boldsymbol{\xi}$ holds according to relation (2.61). Considering $\partial_t\rho_0 = 0$ for equilibrium quantities, the Euler density perturbation follows:

$$\partial_t\delta\rho = -\nabla\cdot(\rho_0\,\delta\boldsymbol{v}) + \mathcal{O}\left(\boldsymbol{\xi}^2\right) = -\nabla\cdot(\rho_0\,\partial_t\boldsymbol{\xi}) + \mathcal{O}(\boldsymbol{\xi}^2) \tag{2.81}$$

$$\delta\rho = -\nabla\cdot(\rho_0\,\boldsymbol{\xi}) + \mathcal{O}(\boldsymbol{\xi}^2). \tag{2.82}$$

The Lagrange density perturbation follows with connection (2.48) and vector identity (A.1):

$$\Delta\rho = \delta\rho + \boldsymbol{\xi}\cdot\nabla\rho_0 + \mathcal{O}\left(\boldsymbol{\xi}^2\right) = -\nabla\cdot(\rho_0\,\boldsymbol{\xi}) + \boldsymbol{\xi}\cdot\nabla\rho_0 + \mathcal{O}\left(\boldsymbol{\xi}^2\right) = -\rho_0\,\nabla\cdot\boldsymbol{\xi} + \mathcal{O}\left(\boldsymbol{\xi}^2\right). \tag{2.83}$$

The Euler and Lagrange perturbations δp and Δp of the fluid pressure follow from the density perturbations (2.82) and (2.83) with the use of the equation of state (2.22). The assumption of a polytropic equilibrium $p_0 = p_0(\rho_0) = \kappa\,\rho_0^{\Gamma_0}$ yields

$$\frac{dp_0}{d\rho_0} = \frac{\partial p_0}{\partial\rho_0} = \Gamma_0\,\kappa\,\rho_0^{\Gamma_0-1} = \frac{\Gamma_0\,p_0}{\rho_0}, \tag{2.84}$$

and thus

$$\Delta p^{\mathrm{poly}} = \frac{\partial p_0}{\partial\rho_0}\,\Delta\rho = \frac{dp_0}{d\rho_0}\,\Delta\rho = \frac{\Gamma_0\,p_0}{\rho_0}\,\Delta\rho. \tag{2.85}$$

The superscript poly indicates the polytropic star we consider here. Making use of the density perturbation (2.83), the Lagrange pressure perturbation reads

$$\Delta p^{\mathrm{poly}} = -\Gamma_0\,p_0\nabla\cdot\boldsymbol{\xi} + \mathcal{O}(\boldsymbol{\xi}^2). \tag{2.86}$$

From that, the Euler pressure perturbation follows with connection (2.48):

$$\delta p^{\mathrm{poly}} = \Delta p^{\mathrm{poly}} - \boldsymbol{\xi}\cdot\nabla p_0 + \mathcal{O}\left(\boldsymbol{\xi}^2\right) = -\Gamma_0\,p_0\nabla\cdot\boldsymbol{\xi} - \boldsymbol{\xi}\cdot\nabla p_0 + \mathcal{O}(\boldsymbol{\xi}^2). \tag{2.87}$$

The Euler perturbation $\delta\Phi$ of the gravitational potential can be calculated by perturbing the Poisson equation (2.20):

$$\nabla^2\left(\Phi_0 + \delta\Phi\right) = \mp 4\,\pi\,G\left(\rho_0 + \delta\rho\right). \tag{2.88}$$

Here, the equilibrium equation $\nabla^2\Phi_0 = \mp 4\,\pi\,G\,\rho_0$ can be identified. The perturbation is thus determined by a Poisson equation itself:

$$\nabla^2\delta\Phi = \mp 4\,\pi\,G\,\delta\rho. \tag{2.89}$$

The Poisson equation for the Euler perturbation is formally solved by

$$\delta\Phi = \pm G \iiint \frac{\delta\rho(\boldsymbol{r}')}{|\boldsymbol{r}-\boldsymbol{r}'|}\,\mathrm{d}V' = \mp G \iiint \frac{\nabla_{\boldsymbol{r}'}\left[\rho_0(\boldsymbol{r}')\,\boldsymbol{\xi}(\boldsymbol{r}')\right]}{|\boldsymbol{r}-\boldsymbol{r}'|}\,\mathrm{d}V' + \mathcal{O}(\boldsymbol{\xi}^2), \tag{2.90}$$

where the Euler density perturbation (2.82) has been inserted. Equation (2.90) can be further transformed by 3D-partial integration (A.9) with $a = \frac{1}{|\boldsymbol{r}-\boldsymbol{r}'|}$ and $\boldsymbol{b} = \rho_0(\boldsymbol{r}')\boldsymbol{\xi}(\boldsymbol{r}')$ to yield

$$\delta\Phi = \mp G \underbrace{\oiint_{\partial V} \frac{\rho_0(\boldsymbol{r}')\,\boldsymbol{\xi}(\boldsymbol{r}')}{|\boldsymbol{r}-\boldsymbol{r}'|}\,\mathrm{d}\boldsymbol{S}'}_{=0} \pm G \iiint \rho_0(\boldsymbol{r}')\,\boldsymbol{\xi}(\boldsymbol{r}')\cdot\nabla_{\boldsymbol{r}'}\frac{1}{|\boldsymbol{r}-\boldsymbol{r}'|}\,\mathrm{d}V' + \mathcal{O}(\boldsymbol{\xi}^2). \tag{2.91}$$

The surface integral in relation (2.91) vanishes because the polytropic density distribution given by system equations (2.26) vanishes at the stellar surface, $\rho_0(R) = 0$.

The Lagrange perturbation of the gravitational potential follows with connection (2.48), respectively from equation (2.83) in analogy to (2.90):

$$\Delta\Phi = \pm G \iiint \rho_0(\boldsymbol{r}')\,\boldsymbol{\xi}(\boldsymbol{r}')\cdot\nabla_{\boldsymbol{r}'}\frac{1}{|\boldsymbol{r}-\boldsymbol{r}'|}\,\mathrm{d}V' + \boldsymbol{\xi}\cdot\nabla\Phi_0 + \mathcal{O}(\boldsymbol{\xi}^2) \tag{2.92}$$

$$= \mp G \iiint \frac{\rho_0(\boldsymbol{r}')\,\left[\nabla_{\boldsymbol{r}'}\cdot\boldsymbol{\xi}(\boldsymbol{r}')\right]}{|\boldsymbol{r}-\boldsymbol{r}'|}\,\mathrm{d}V' + \mathcal{O}\left(\boldsymbol{\xi}^2\right). \tag{2.93}$$

The Euler perturbation $\delta\boldsymbol{B}$ of the magnetic field can be calculated by perturbing the basic equation of magnetokinematics (2.15):

$$\partial_t\left(\boldsymbol{B}_0 + \delta\boldsymbol{B}\right) = \nabla\times\left(\boldsymbol{v}_0\times\boldsymbol{B}_0\right) + \nabla\times\left(\boldsymbol{v}_0\times\delta\boldsymbol{B}\right) + \nabla\times\left(\delta\boldsymbol{v}\times\boldsymbol{B}_0\right) + \mathcal{O}\left(\boldsymbol{\xi}^2\right). \tag{2.94}$$

Here, the equilibrium equation $\partial_t\boldsymbol{B}_0 = \nabla\times(\boldsymbol{v}_0\times\boldsymbol{B}_0)$ can be identified. The term including $\boldsymbol{v}_0$ will be neglected according to assumption (2.65) and $\delta\boldsymbol{v} = \partial_t\boldsymbol{\xi}$ holds according to relation (2.61). Considering $\partial_t\boldsymbol{B}_0 = 0$ for equilibrium quantities, the Euler perturbation of the magnetic field reads

$$\partial_t\delta\boldsymbol{B} = \nabla\times\left(\delta\boldsymbol{v}\times\boldsymbol{B}_0\right) + \mathcal{O}\left(\boldsymbol{\xi}^2\right) = \nabla\times\left(\partial_t\boldsymbol{\xi}\times\boldsymbol{B}_0\right) + \mathcal{O}(\boldsymbol{\xi}^2) \tag{2.95}$$

$$\delta\boldsymbol{B} = \nabla\times\left(\boldsymbol{\xi}\times\boldsymbol{B}_0\right) + \mathcal{O}(\boldsymbol{\xi}^2). \tag{2.96}$$

The Lagrange perturbation of the magnetic field follows with connection (2.48) and vector identity (A.2):

$$\Delta\boldsymbol{B} = \delta\boldsymbol{B} + \left(\boldsymbol{\xi}\cdot\nabla\right)\boldsymbol{B}_0 + \mathcal{O}\left(\boldsymbol{\xi}^2\right) = \boldsymbol{\xi}\left(\nabla\cdot\boldsymbol{B}_0\right) - \boldsymbol{B}_0\left(\nabla\cdot\boldsymbol{\xi}\right) + \left(\boldsymbol{B}_0\cdot\nabla\right)\boldsymbol{\xi} + \mathcal{O}(\boldsymbol{\xi}^2). \tag{2.97}$$

Note that for the derivation shown above, the magnetic field vector is treated in the same way as the other system quantities. It is assumed to consist of an equilibrium part $\boldsymbol{B}_0$ and an Eulerian, respectively Lagrangian, perturbation $\delta\boldsymbol{B}$ or $\Delta\boldsymbol{B}$. As explained in the magnetic field paragraph of section 2.2.3, this approach is a simplified treatment which

does not conflict with the assumption of an unmagnetised equilibrium system we applied for the hydrostatic system setup.

The Euler perturbation $\delta\boldsymbol{j}$ of the current density can be calculated perturbing Ampère's law (2.14d):

$$(\boldsymbol{j}_0 + \delta\boldsymbol{j}) = \frac{c}{4\pi}\left(\nabla \times \boldsymbol{B}_0 + \nabla \times \delta\boldsymbol{B}\right). \tag{2.98}$$

Here, the equilibrium equation $\boldsymbol{j}_0 = \frac{c}{4\pi}\nabla \times \boldsymbol{B}_0$ can be identified. Applying the magnetic field perturbation (2.96), the Euler perturbation of the electric current density reads

$$\delta\boldsymbol{j} = \frac{c}{4\pi}\nabla \times \delta\boldsymbol{B} = \frac{c}{4\pi}\nabla \times \left[\nabla \times (\boldsymbol{\xi} \times \boldsymbol{B}_0)\right] + \mathcal{O}(\boldsymbol{\xi}^2). \tag{2.99}$$

The Lagrange perturbation of the electric current density follows with connection (2.48):

$$\Delta\boldsymbol{j} = \delta\boldsymbol{j} + (\boldsymbol{\xi}\cdot\nabla)\,\boldsymbol{j}_0 + \mathcal{O}(\boldsymbol{\xi}^2). \tag{2.100}$$

To sum up, the Euler perturbations (2.82), (2.87), (2.91), (2.96) and (2.99) calculated in this paragraph are

$$\delta\rho = -\nabla\cdot(\rho_0\,\boldsymbol{\xi}) + \mathcal{O}(\boldsymbol{\xi}^2) \tag{2.101a}$$

$$\delta p^{\mathrm{poly}} = -\Gamma_0\, p_0\,(\nabla\cdot\boldsymbol{\xi}) - \boldsymbol{\xi}\cdot\nabla p_0 + \mathcal{O}(\boldsymbol{\xi}^2) \tag{2.101b}$$

$$\delta\Phi = \pm G \iiint \rho_0(\boldsymbol{r}')\,\boldsymbol{\xi}(\boldsymbol{r}')\cdot\nabla_{\boldsymbol{r}'}\frac{1}{|\boldsymbol{r}-\boldsymbol{r}'|}\,\mathrm{d}V' + \mathcal{O}(\boldsymbol{\xi}^2) \tag{2.101c}$$

$$\delta\boldsymbol{B} = \nabla \times (\boldsymbol{\xi} \times \boldsymbol{B}_0) + \mathcal{O}(\boldsymbol{\xi}^2) \tag{2.101d}$$

$$\delta\boldsymbol{j} = \frac{c}{4\pi}\nabla \times \left[\nabla \times (\boldsymbol{\xi} \times \boldsymbol{B}_0)\right] + \mathcal{O}(\boldsymbol{\xi}^2). \tag{2.101e}$$

Explicit Euler perturbations of all system quantities for polytropes, in full description

According to the fact that in general the displacement field is a complex function, the Euler perturbations of all system quantities given by equations (2.101) are complex functions as well.

Magnetic contribution to the energy variation The energy variation density caused by the magnetic field can be calculated substituting $\delta\boldsymbol{B}$ and $\delta\boldsymbol{j}$ from (2.101d) and (2.101e) into the implicit expression (2.79a):

$$\mathcal{E}_{\mathrm{magn}} = -\frac{1}{4}\,\Re\left\{\boldsymbol{\xi}^*\cdot\frac{\boldsymbol{j}_0\times\delta\boldsymbol{B}}{c} + \boldsymbol{\xi}^*\cdot\frac{(\nabla\times\delta\boldsymbol{B})\times\boldsymbol{B}_0}{4\pi}\right\} \tag{2.102}$$

$$= \frac{1}{4}\,\Re\left\{-\boldsymbol{j}_0\cdot\frac{\delta\boldsymbol{B}\times\boldsymbol{\xi}^*}{c} + \frac{1}{4\pi}\,(\nabla\times\delta\boldsymbol{B})\cdot(\boldsymbol{\xi}^*\times\boldsymbol{B}_0)\right\}. \tag{2.103}$$

Here, cyclic commutation of the scalar triple product has been used according to identities (A.3) and (A.4).

Remember that δW has been defined in equation (2.77c) to be of second order in $\boldsymbol{\xi}$. The energy variation densities derived here thus are of first order in $\boldsymbol{\xi}$.

Further, identity (A.6) for divergences of cross products can be applied to the second term, yielding

$$\mathcal{E}_{\text{magn}} = \frac{1}{4}\,\Re\left\{-\boldsymbol{j}_0\cdot\frac{\delta\boldsymbol{B}\times\boldsymbol{\xi}^*}{c}+\frac{\delta\boldsymbol{B}}{4\,\pi}\cdot\left[\nabla\times\left(\boldsymbol{\xi}^*\times\boldsymbol{B}_0\right)\right]-\frac{1}{4\,\pi}\,\nabla\cdot\left[\left(\boldsymbol{\xi}^*\times\boldsymbol{B}_0\right)\times\delta\boldsymbol{B}\right]\right\} \tag{2.104}$$

$$= \frac{1}{4}\,\Re\left\{-\boldsymbol{j}_0\cdot\frac{\delta\boldsymbol{B}\times\boldsymbol{\xi}^*}{c}+\frac{\delta\boldsymbol{B}^*\cdot\delta\boldsymbol{B}}{4\,\pi}-\frac{1}{4\,\pi}\,\nabla\cdot\left[\left(\boldsymbol{\xi}^*\times\boldsymbol{B}_0\right)\times\delta\boldsymbol{B}\right]\right\}, \tag{2.105}$$

where the Euler perturbation of the magnetic field (2.101d) has been identified. Writing (2.105) in the integral form (2.78), the last term being a divergence term can be expressed by a surface integral applying Gauß' theorem (A.8):

$$\delta W_{\text{magn}} = \frac{1}{4}\iiint\Re\left\{\frac{\delta\boldsymbol{B}^*\cdot\delta\boldsymbol{B}}{4\,\pi}-\boldsymbol{j}_0\cdot\frac{\delta\boldsymbol{B}\times\boldsymbol{\xi}^*}{c}\right\}\mathrm{d}V \tag{2.106}$$

$$-\frac{1}{16\,\pi}\iiint\Re\left\{\nabla\cdot\left[\left(\boldsymbol{\xi}^*\times\boldsymbol{B}_0\right)\times\delta\boldsymbol{B}\right]\right\}\mathrm{d}V$$

$$= \frac{1}{4}\iiint\Re\left\{\frac{\delta\boldsymbol{B}^*\cdot\delta\boldsymbol{B}}{4\,\pi}-\boldsymbol{j}_0\cdot\frac{\delta\boldsymbol{B}\times\boldsymbol{\xi}^*}{c}\right\}\mathrm{d}V \tag{2.107}$$

$$-\frac{1}{16\,\pi}\underbrace{\oiint\Re\left\{\left(\boldsymbol{\xi}^*\times\boldsymbol{B}_0\right)\times\delta\boldsymbol{B}\right\}\cdot\boldsymbol{n}\,\mathrm{d}\boldsymbol{S}}_{0}.$$

The surface integral contribution vanishes for the displacement field assumptions we will use below, as shown in the appendix B.4.

The magnetic contribution to the energy variation is thus given by

$$\mathcal{E}_{\text{magn}} = \frac{1}{4}\,\Re\left\{\frac{\delta\boldsymbol{B}^*\cdot\delta\boldsymbol{B}}{4\pi}-\boldsymbol{j}_0\cdot\frac{\delta\boldsymbol{B}\times\boldsymbol{\xi}^*}{c}\right\}, \tag{2.108}$$

with $\delta\boldsymbol{B} = \nabla\times(\boldsymbol{\xi}\times\boldsymbol{B}_0)$ according to equation (2.101d).

Note that for fully real displacement fields, the complex scalar product in expression (2.108) simplifies to $\delta\boldsymbol{B}^*\cdot\delta\boldsymbol{B} = \delta\boldsymbol{B}^2$.

Fluid pressure contribution to the energy variation The energy variation density caused by the fluid pressure gradient can be calculated substituting δp^{poly} from (2.101b) into the implicit expression (2.79b):

$$\mathcal{E}^{\text{poly}}_{\text{fluid}} = -\frac{1}{4}\,\Re\left\{\boldsymbol{\xi}^*\cdot\nabla\cdot\left[\Gamma_0\,p_0\,\left(\nabla\cdot\boldsymbol{\xi}\right)\right]+\boldsymbol{\xi}^*\cdot\nabla\cdot\left[\boldsymbol{\xi}\cdot\nabla p_0\right]\right\} \tag{2.109}$$

$$= -\frac{1}{4}\,\Re\left\{\boldsymbol{\xi}^*\cdot\nabla\cdot\left[\Gamma_0\,p_0\,\left(\nabla\cdot\boldsymbol{\xi}\right)+\boldsymbol{\xi}\cdot\nabla p_0\right]\right\} \tag{2.110}$$

Next, identity (A.1) for divergences of scalar-vector products can be applied with $a = \Gamma_0 p_0 (\nabla \cdot \boldsymbol{\xi}) + \boldsymbol{\xi} \cdot \nabla p_0$ and $\boldsymbol{b} = \boldsymbol{\xi}^*$, yielding

$$\mathcal{E}_{\text{fluid}}^{\text{poly}} = \frac{1}{4} \Re \left\{ \Gamma_0 p_0 (\nabla \cdot \xi^*) (\nabla \cdot \xi) + \boldsymbol{\xi} \cdot \nabla p_0 (\nabla \cdot \boldsymbol{\xi}^*) - \nabla \cdot \left[\Gamma_0 p_0 \boldsymbol{\xi}^* (\nabla \cdot \boldsymbol{\xi}) + \boldsymbol{\xi} \cdot \nabla p_0 \boldsymbol{\xi}^* \right] \right\}. \tag{2.111}$$

Writing (2.111) in the integral form (2.78), the pure divergence term can be expressed by a surface integral applying Gauß' theorem (A.8):

$$\begin{aligned} \delta W_{\text{fluid}}^{\text{poly}} = & \frac{1}{4} \iiint \Re \left\{ \Gamma_0 p_0 (\nabla \cdot \boldsymbol{\xi}^*) (\nabla \cdot \boldsymbol{\xi}) + \boldsymbol{\xi} \cdot \nabla p_0 (\nabla \cdot \boldsymbol{\xi}^*) \right\} \mathrm{d}V \qquad (2.112) \\ & - \frac{1}{4} \iiint \Re \left\{ \nabla \cdot \left[\Gamma_0 p_0 \boldsymbol{\xi}^* (\nabla \cdot \boldsymbol{\xi}) + \boldsymbol{\xi}^* (\boldsymbol{\xi} \cdot \nabla) p_0 \right] \right\} \mathrm{d}V \\ = & \frac{1}{4} \iiint \Re \left\{ \Gamma_0 p_0 (\nabla \cdot \boldsymbol{\xi}^*) (\nabla \cdot \boldsymbol{\xi}) + \boldsymbol{\xi} \cdot \nabla p_0 (\nabla \cdot \boldsymbol{\xi}^*) \right\} \mathrm{d}V \qquad (2.113) \\ & - \frac{1}{4} \underbrace{\oiint \Re \left\{ \Gamma_0 p_0 \boldsymbol{\xi}^* (\nabla \cdot \boldsymbol{\xi}) + \boldsymbol{\xi}^* (\boldsymbol{\xi} \cdot \nabla) p_0 \right\} \cdot \boldsymbol{n} \, \mathrm{d}\boldsymbol{S}}_{0}. \end{aligned}$$

The surface integral contribution vanishes for the displacement field assumptions we will use below, as shown in the appendix B.4.

The fluid pressure gradient contribution to the energy variation is thus given by

$$\mathcal{E}_{\text{fluid}}^{\text{poly}} = \frac{1}{4} \Re \left\{ \Gamma_0 p_0 (\nabla \cdot \boldsymbol{\xi}^*) (\nabla \cdot \boldsymbol{\xi}) + \boldsymbol{\xi} \cdot \nabla p_0 (\nabla \cdot \boldsymbol{\xi}^*) \right\}. \tag{2.114}$$

Gravitational contribution to the energy variation Typically, in previous works the change in the gravitational potential caused by the perturbation has been neglected. The so-called Cowling approximation $\delta\Phi = 0$ has been applied in order to avoid the integration for the calculation of the actual Euler perturbation given by (2.91).

The energy variation density caused by gravity can then be calculated substituting $\delta\rho$ from (2.101a) into the implicit expression (2.79c):

$$\mathcal{E}_{\text{grav}}^{\text{Cowl}} = \pm \frac{1}{4} \Re \left\{ \boldsymbol{\xi} \cdot \nabla \Phi_0 (\nabla \cdot (\rho_0 \boldsymbol{\xi}^*)) \right\}. \tag{2.115}$$

Note that according to relation (A.29), it is irrelevant which of the two displacement field vectors in this expression is complex conjugated.

According to equations (2.78), (2.108), (2.114), (2.115) and (2.101d), the total volume integral contribution to the energy variation of a polytropic star in Cowling approximation is

$$\delta W = \iiint \left\{ \mathcal{E}_{\text{magn}} + \mathcal{E}_{\text{fluid}}^{\text{poly}} + \mathcal{E}_{\text{grav}}^{\text{Cowl}} \right\} \mathrm{d}V, \tag{2.116}$$

with

$$\mathcal{E}_{\text{magn}} = \frac{1}{4} \Re \left\{ \frac{\delta \boldsymbol{B}^* \cdot \delta \boldsymbol{B}}{4\pi} - \boldsymbol{j}_0 \cdot \frac{\delta \boldsymbol{B} \times \boldsymbol{\xi}^*}{c} \right\} \tag{2.117a}$$

$$\mathcal{E}_{\text{fluid}}^{\text{poly}} = \frac{1}{4} \Re \left\{ \Gamma_0 \, p_0 \, (\nabla \cdot \boldsymbol{\xi}^*) \, (\nabla \cdot \boldsymbol{\xi}) + \boldsymbol{\xi} \cdot \nabla p_0 \, (\nabla \cdot \boldsymbol{\xi}^*) \right\} \tag{2.117b}$$

$$\mathcal{E}_{\text{grav}}^{\text{Cowl}} = \pm \frac{1}{4} \Re \left\{ \boldsymbol{\xi} \cdot \nabla \Phi_0 \, (\nabla \cdot (\rho_0 \, \boldsymbol{\xi}^*)) \right\} \tag{2.117c}$$

and $\delta \boldsymbol{B} = \nabla \times (\boldsymbol{\xi} \times \boldsymbol{B}_0) + \mathcal{O}(\boldsymbol{\xi}^2)$.

Explicit energy variation for polytropes, in Cowling approximation

This expression is identical to the energy variation derived in Bernstein et al. (1958) or applied in Tayler (1973).

2.3.3. Displacement field for stability tests

As stated in the previous sections, we are going to investigate the stability of magnetised neutron stars by subjecting the system to a perturbation $\boldsymbol{\xi}(\boldsymbol{r}, t)$ and observing its reaction in the form of the energy variation given by equations (2.116) and (2.117). The final component needed for this task is an appropriate choice for the displacement field.

Remember the assumption we made for its time-dependence in equation (2.43),

$$\boldsymbol{\xi}^n(\boldsymbol{r}, t) = \boldsymbol{\xi}(\boldsymbol{r}) \, \mathrm{e}^{\mathrm{i}\omega_n t}, \tag{2.118}$$

with the temporal mode index n. In this section, we make choices for the generally complex spatial part $\boldsymbol{\xi}(\boldsymbol{r})$.

Required displacement field properties

Most prominent unstable modes Stability criterion (2.45) suggests that a system must be subject to all possible kinds of perturbations in order to test its overall stability behaviour and especially to conduct a stability proof.

This task would be exceptionally time-consuming if not impossible. However, since we are going to address a system comprising established instabilities known from previous works, we will focus on these instabilities first and keep the framework as simple as possible.

It is convenient to first study the particular unstable modes that have the most crucial impact on the system. These modes are the fastest growing ones. The chances for them to be damped away are low and they probably become global modes instead. That means, they show high amplitudes and eventually affect the entire star.

In the variational approach, the most violent modes are the ones producing the lowest energy variation and thus causing the "strongest instability". However, these modes can generally differ from the fastest growing modes and might not be the dominating instabilities.

Later on, less violent instabilities and overtones should be investigated as well. The question is whether stability can be sustained against all locally unstable modes without any of them gaining influence over the whole star. The excitation of unstable high-order modes can for instance be suppressed by dissipative mechanisms, such as viscosity or resistivity. Not every mathematical instability must therefore lead to an astrophysically unstable system.

Currently, however, it is sufficient to study the most dominant modes first, since we cannot even explain the stellar stability against these violent modes yet. In the end, weaker and higher modes might be suppressed by the same effect that also stabilises the star against the strongest modes.

In our specific case, we will examine whether the instabilities unexpectedly occurring in the simple model neutron star are still present in the more realistic system, or whether they dissolve or lose relevance when additional features are taken into account.

Predominantly, the instabilities we need to focus on are the dynamical Tayler instabilities occurring in purely toroidally and purely poloidally magnetised neutron stars shown in figure 2.12.

Displacement field geometry The most relevant types of instabilities occurring in a system depend on the system's particular magnetic field structure. For the purpose of concentrating on these specific modes, the utilised perturbation will be adjusted to the system geometry.

With respect to the magnetic field lines, the displacement field needs to be oriented in such a way that the induced inflection is able to excite possibly unstable eigenmodes of the magnetised fluid.

In magnetised neutron stars, the fastest growing pinch instabilities are localised close to the symmetry axes of the toroidal and poloidal magnetic field components, cf. figures 2.8a and 2.9a (Tayler, 1973; Markey & Tayler, 1973).

In this work, neutron stars with purely toroidal, purely poloidal and mixed magnetic fields will be investigated. In the mixed field case, the instability under consideration is the toroidal field instability in the presence of a weak poloidal component. The geometry required for its displacement field is thus analogous to the toroidal field case.

In all cases, the system is axisymmetric and $\boldsymbol{\xi}$ is the only quantity entering the energy variation (2.116) that generally depends on the azimuthal angle φ. It is therefore convenient to use an exponential ansatz for the φ-dependence of $\boldsymbol{\xi}$:

$$\boldsymbol{\xi}(\boldsymbol{r}) \sim \mathrm{e}^{\mathrm{i}m\varphi}, \tag{2.119}$$

with the angular mode index m. This notation allows us to pull the φ-dependency out of the energy variation integrand $\mathcal{E}$, and carry out the φ-integration analytically. That way, the number of integrations that are necessary for the calculation of δW is reduced by one, exploiting the axisymmetry of the system.

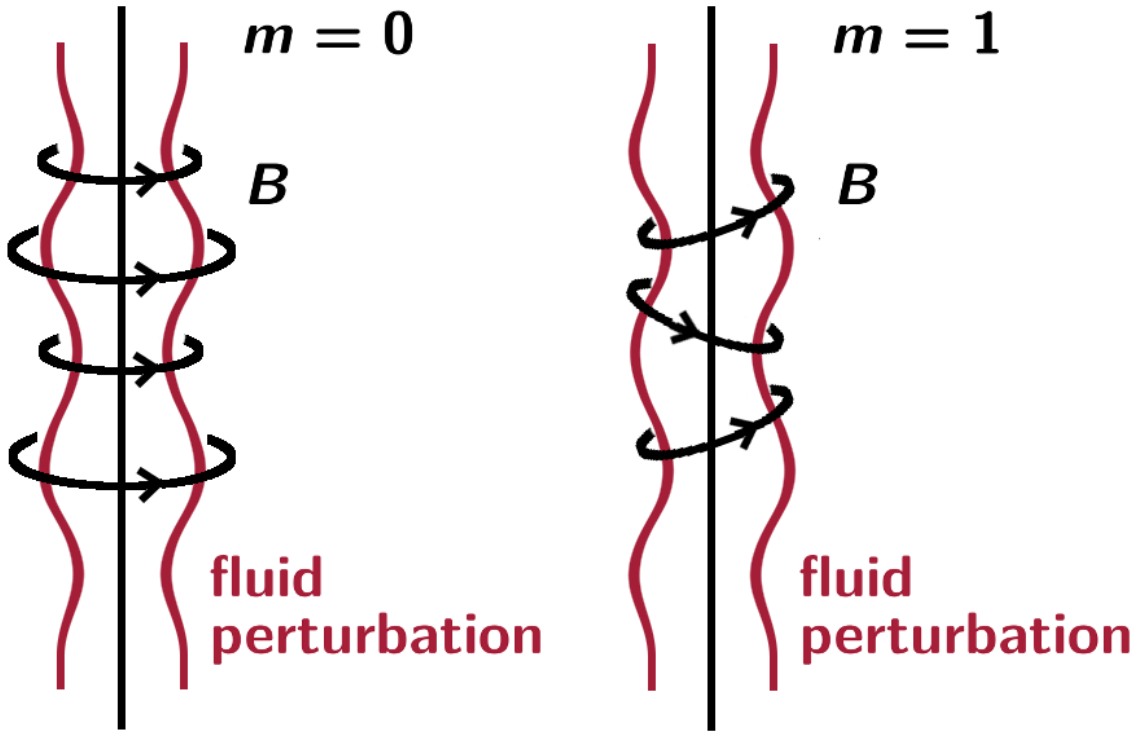

(a) Axisymmetric "sausage" mode with $m = 0$. (b) Non-axisymmetric "kink" mode with $m = 1$.

Figure 2.12.: Tayler instabilities in a cylindrical fluid discharge.

Localised displacement fields Beyond their general geometry, instabilities might be localised in a closed region inside the star. Modes that dominate in a strongly constrained region occur if their amplitude spatially decays rapidly.

Based on that, we will draw on the option of localising the displacement field to a region A inside the star, where $\boldsymbol{\xi} \neq 0$, while $\boldsymbol{\xi} = 0$ elsewhere. That way, we only observe a certain area inside the star and prevent possible instabilities located there from staying undetected. Their negative contribution to the energy variation cannot be covered by possibly strong positive contributions stemming from other parts of the star.

One further advantage of localised displacement fields is that with their use, surface terms in the energy variation can be neglected for any particular choice of $\boldsymbol{\xi}(\boldsymbol{r})$. Condition (B.23), determining whether the surface integral can be neglected, can always be fulfilled.

This is the case if $\boldsymbol{\xi}$ is localised to A and vanishes at its boundary ∂A, as explained in the appendix B.4. If the energy variation integrand vanishes in a defined connected region, the surface integral over the stellar volume V can be replaced by a surface integral over the localisation region A, where the integrand is finite. The surface integral over A vanishes itself if the integrand vanishes at its boundary ∂A:

$$\oiint_{\partial V} \mathcal{E}\,\mathrm{d}S = \oiint_{\partial A} \mathcal{E}\,\mathrm{d}S = 0. \tag{2.120}$$

The localisation of a displacement field is not highly realistic, since in a real star, per-

turbations spread due to coupling mechanisms. Still, this assumption is a valid approach for a first attempt in a semi-analytic stability analysis. We assume that the couplings in the fluid are weak and that other regions do not strongly contribute to the system's stability behaviour if the localisation area includes the strongest instabilities.

According to these considerations, the surface contributions to the energy variation can be neglected for all applications shown in this work. The displacement fields will be chosen appropriately. However, for future applications it is worth mentioning that the semi-analytic method in general is capable of treating the surface and vacuum integral contributions as well.

In this work, five different choices for the displacement field will be used. They are shown in the subsequent paragraphs.

As explained in section 2.3.2, the displacement field will be a complex function according to the assumptions we make, while the physical meaningfulness of δW will be guaranteed by taking the real part over the energy variation integrand.

Displacement field choice for investigations of purely toroidal magnetic fields

In a toroidally magnetised non-rotating neutron star, the instability region is expected to be close to the stellar symmetry axis. The area around the symmetry axis is equivalent to a pinched cylindrical fluid discharge creating the toroidal field, as can be seen in figure 2.13. In comparison to the fluid discharge, the star is additionally subject to gravity.

According to Tayler (1973), a convenient perturbation to investigate this system is

$$\xi_\varpi = X(\varpi, z)\, \mathrm{e}^{\mathrm{i}m\varphi} \tag{2.121a}$$

$$\xi_\varphi = \frac{\mathrm{i}Y(\varpi, z)}{m}\, \mathrm{e}^{\mathrm{i}m\varphi} \tag{2.121b}$$

$$\xi_z = Z(\varpi, z)\, \mathrm{e}^{\mathrm{i}m\varphi}\,. \tag{2.121c}$$

Displacement field choice $\boldsymbol{\xi}(\boldsymbol{r})$ for stars with purely toroidal magnetic fields

Here, $X(\varpi, z)$, $Y(\varpi, z)$ and $Z(\varpi, z)$ are generally complex $\boldsymbol{\xi}$-defining functions. However, as shown by Tayler, their real and imaginary parts contribute structurally equivalent terms to the energy variation. Therefore, X, Y and Z can be assumed to be real without restriction. A proof of that will be given in the appendix section C.1.5.

The displacement field is expressed in cylindrical coordinates, according to the axisymmetry of the system. The structure of the field components is illustrated in figure 2.14.

The axisymmetric $m = 0$ mode, which is unstable in the fluid discharge, is likely to be suppressed in the star by gravity, cf. figure 2.12.

The $m = 1$ mode, in contrast, mainly involves motion along surfaces of constant gravity. This mode is expected to be unstable in the fluid discharge as well as in the presence of gravity. Causing the lowest energy variation under the non-axisymmetric modes, the $m = 1$ mode is the strongest instability in the toroidally magnetised neutron star.

According to Tayler, the specific choice we use for the $\boldsymbol{\xi}$-defining functions is given by

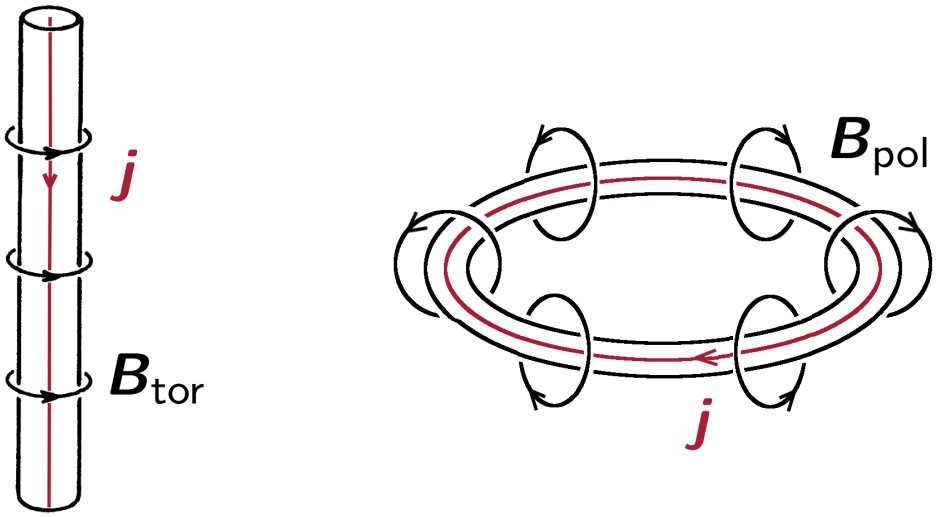

(a) Toroidal magnetic field.

(b) Poloidal magnetic field.

Figure 2.13.: Analogy between the cylindrical fluid discharge and magnetised neutron stars. While the toroidal field system is described by the fluid discharge with the geometry of a straight cylinder (a), the poloidal field can be represented by a toroidally closed cylinder, i.e. a torus (b).

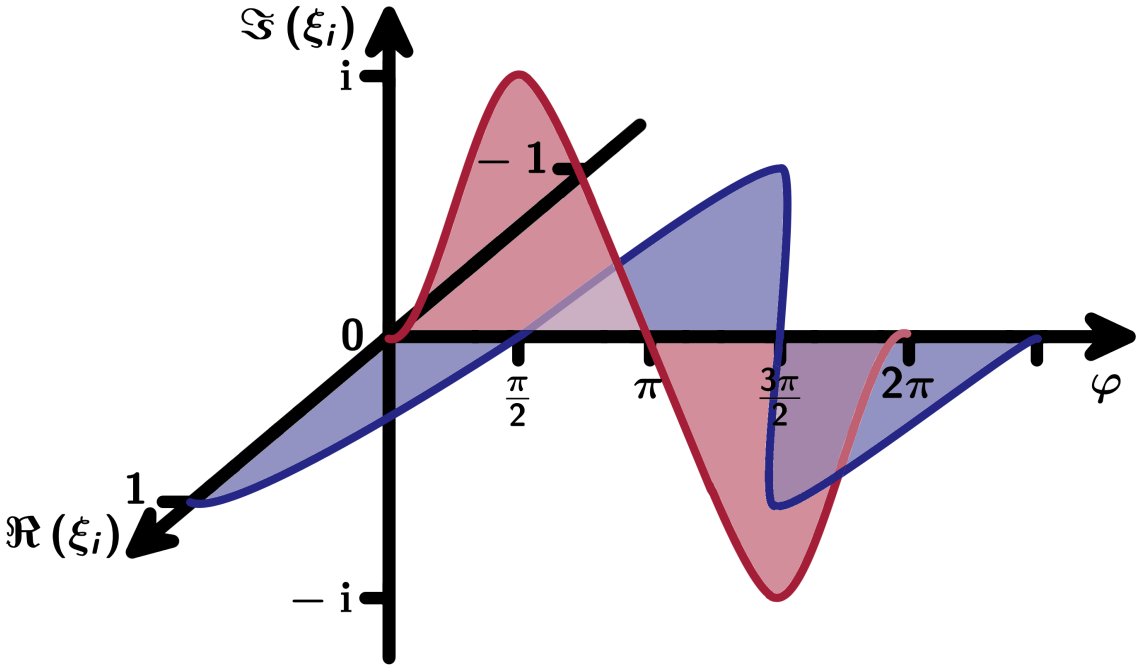

Figure 2.14.: Illustration of the displacement field components $\xi_i = \{\xi_\varpi, \xi_\varphi, \xi_z\}$ for the toroidal field choice (2.121), $\xi_i = \{\xi_\psi, \xi_\varphi, \xi_\chi\}$ for the poloidal field choice (2.125) and $\xi_i = \{\xi_r, \xi_\vartheta, \xi_\varphi\}$ for the mixed field choice (2.130). Imaginary and real parts of $\boldsymbol{\xi}$ oscillate with the azimuthal angle φ.

$$\left.\begin{aligned} X(\varpi,z) &= X_0\,\varpi\,\sin(k_A\,(\varpi-\epsilon_A))\,\cos(l_A\,z) \\ Z(\varpi,z) &= Z_0\,\varpi\,\cos(k_A\,(\varpi-\epsilon_A))\,\sin(l_A\,z) \end{aligned}\right\} \text{ in } A, \qquad \left.\begin{aligned} X(\varpi,z) &= 0 \\ Z(\varpi,z) &= 0 \end{aligned}\right\} \text{ else,} \tag{2.122}$$

and

$$\begin{aligned} Y(\varpi,z) = Y_{\min} \equiv & \partial_\varpi(\varpi X) + \varpi\,\partial_z Z \pm \frac{\varpi\,\rho_0}{\Gamma_0\,p_0}\left(g_\varpi X + g_z Z\right) \\ & + \frac{\varpi B_\varphi}{2\,\Gamma_0\,p_0}\left(\frac{\partial_\varpi\,(\varpi B_\varphi)}{\varpi} X + \partial_z B_\varphi Z\right) \end{aligned}$$

with

$$k_A\,X_0 + l_A\,Z_0 = 0 \qquad |l_A| \gg |k_A| \gg \frac{1}{h} \qquad \epsilon_A > \frac{\pi}{k_A}. \tag{2.123}$$

Explicit choice of the $\boldsymbol{\xi}$-defining functions for stars with purely toroidal magnetic fields

Here, $X_0, Z_0 \neq 0$ are numerical constants representing constant amplitudes. Further, ϵ_A denotes a distance from the symmetry axis in ϖ-direction, determining the position of the localisation area, while the numerical constants k_A and l_A determine the extent of the localisation area. Their absolute values are constrained by the typical scale height h of the physical system quantities.

The details concerning this choice will be motivated in the application chapter 5.1. Altogether, the localisation region is defined as

$$A = \left\{\varpi \in \mathbb{R}\,\middle|\,\epsilon_A - \frac{\pi}{k_A} < \varpi < \epsilon_A + \frac{\pi}{k_A}\,,\; z \in \mathbb{R}\,\middle|\,-\frac{\pi}{l_A} < z < \frac{\pi}{l_A}\right\}. \tag{2.124}$$

The intersection of the localisation area with the (ϖ, z)-plane is a rectangle close to the symmetry axis, see figure 2.15.

Note that X, Y and Z vanish everywhere outside A, fulfilling the localisation condition for $\boldsymbol{\xi}$.

The ξ_φ-defining function $Y(\varpi, z)$ has been chosen as $Y_{\min}$, the value which minimises the energy variation density $\mathcal{E}$ with respect to Y. This procedure will be explained in section 5.1, illustrating the applications of the semi-analytic method on the toroidally magnetised star.

Displacement field choice for investigations of purely poloidal magnetic fields

In the purely poloidally magnetised star, the instability region is close to the magnetic field symmetry axis which is the neutral line. The system is equivalent to the previous one, under the conception that the cylindrical discharge is closed here. It forms a torus that includes the neutral line, cf. figure 2.13. The displacement field has an analogous structure to the toroidal field case, as explained in the appendix section C.2.2. However, the impact of gravity on the modes is different now as the geometry of $\boldsymbol{\xi}$, $\boldsymbol{B}$ and $\boldsymbol{g}$ has changed.

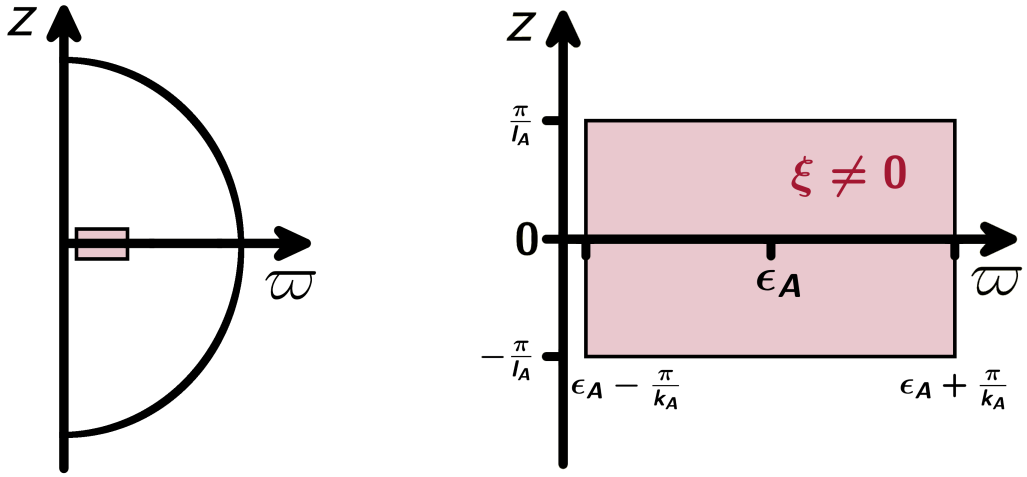

Figure 2.15.: Displacement field localisation area A for the purely toroidally magnetised neutron star, cf. relation (2.124). The two-dimensional integration area for the Simpson integration will be chosen as one half of the stellar cross section. The sketch is not true to scale.

According to Markey & Tayler (1973), we will use the following displacement field, expressed in toroidal coordinates:

$$\xi_\psi = \frac{X(\psi,\chi)}{\varpi B_\chi}\, \mathrm{e}^{\mathrm{i}m\varphi} \tag{2.125a}$$

$$\xi_\varphi = \frac{\mathrm{i}\varpi Y(\psi,\chi)}{m}\, \mathrm{e}^{\mathrm{i}m\varphi} \tag{2.125b}$$

$$\xi_\chi = B_\chi\, Z(\psi,\chi)\, \mathrm{e}^{\mathrm{i}m\varphi}\,. \tag{2.125c}$$

Displacement field choice $\boldsymbol{\xi}(r)$ for stars with purely poloidal magnetic fields

The $\boldsymbol{\xi}$-defining functions $X(\psi,\chi)$, $Y(\psi,\chi)$ and $Z(\psi,\chi)$ are complex in general, but they can be assumed to be real without restriction based on the same argument as in the toroidal field case.

Due to the definition of the toroidal coordinate system in (2.8), the magnetic field enters $\boldsymbol{\xi}$ in the form of B_χ.

The localisation of the displacement field inside the star is different from the toroidal field case. We will thus vary the mode index m in the application section 5.2 in order to find the strongest instability in the gravity subjected star for the poloidal field case.

Our specific choice for the $\boldsymbol{\xi}$-defining functions is

$$\left.\begin{aligned} X(\psi,\chi) &= f(\psi,\chi)\,(\psi-\psi_{\mathrm{tor}})^2 \\ Y(\psi,\chi) &= \tfrac{1}{J}\left(X\,\partial_\psi J + \partial_\chi Z\right) + \partial_\psi X \\ Z(\psi,\chi) &= -X\,\frac{(R_{\mathrm{tor}}\cos\chi-\bar{r})\,(R_{\mathrm{tor}}-\bar{r}\cos\chi)}{B_{\mathrm{pol}}^2\,R_{\mathrm{tor}}\,\bar{r}^2\sin\chi} \end{aligned}\right\} \quad \text{in } A, \qquad \left.\begin{aligned} X(\psi,\chi) &= 0 \\ Y(\psi,\chi) &= 0 \\ Z(\psi,\chi) &= 0 \end{aligned}\right\} \quad \text{else,} \tag{2.126}$$

with

$$\partial_\chi Z = \frac{1}{B_{\mathrm{pol}}^2\,R_{\mathrm{tor}}\,\bar{r}^2}\left[\left(\frac{X\cos\chi}{\sin^2\chi}-\frac{\partial_\chi X}{\sin\chi}\right)(R_{\mathrm{tor}}\cos\chi-\bar{r})\,(R_{\mathrm{tor}}-\bar{r}\cos\chi)\right. \tag{2.127}$$
$$\left. + X\left(\bar{r}^2 - R_{\mathrm{tor}}\,(\bar{r}\cos\chi-\varpi)\right)\right].$$

Explicit choice of the $\boldsymbol{\xi}$-defining functions for stars with purely poloidal magnetic fields

The Jacobi determinant $J = \varpi/B_{\mathrm{pol}}$ was defined in equation (2.10).

The function $f(\psi,\chi)$ describes the remaining dependence of X on ψ and χ besides its prespecified proportionality to $(\psi-\psi_{\mathrm{tor}})^2$. The role and structure of $f(\psi,\chi)$ will be discussed in detail in the application section 5.2. The explicit choice we use for the application here is

$$f(\psi,\chi) = \frac{X_0\sin\chi}{B_{\mathrm{pol}}^2}, \tag{2.128}$$

with a numerical constant $X_0 \neq 0$ which plays the role of a displacement field amplitude.

Further, R_{tor} is the distance between neutral line and stellar symmetry axis, defining the position of the localisation area, while the radius ψ_{tor} of the torus cross section determines the extent of the localisation area.

Altogether, the localisation region is a torus around the symmetry axis of the star that includes the neutral line and is defined by

$$A = \left\{\psi \in \mathbb{R}^- \,\middle|\, |\psi| \leq |\psi_{\mathrm{tor}}|\right\}. \tag{2.129}$$

For an illustration of the localisation area geometry see figure 2.16.

Note that X, Y and Z vanish everywhere outside A, fulfilling the localisation condition for $\boldsymbol{\xi}$.

Displacement field choice for investigations of mixed magnetic fields

In the case of mixed magnetic field investigations, we consider the toroidal field instability in the presence of a weak poloidal component. Therefore, the utilised displacement field is equivalent to the one applied in the purely toroidal field case (2.121).

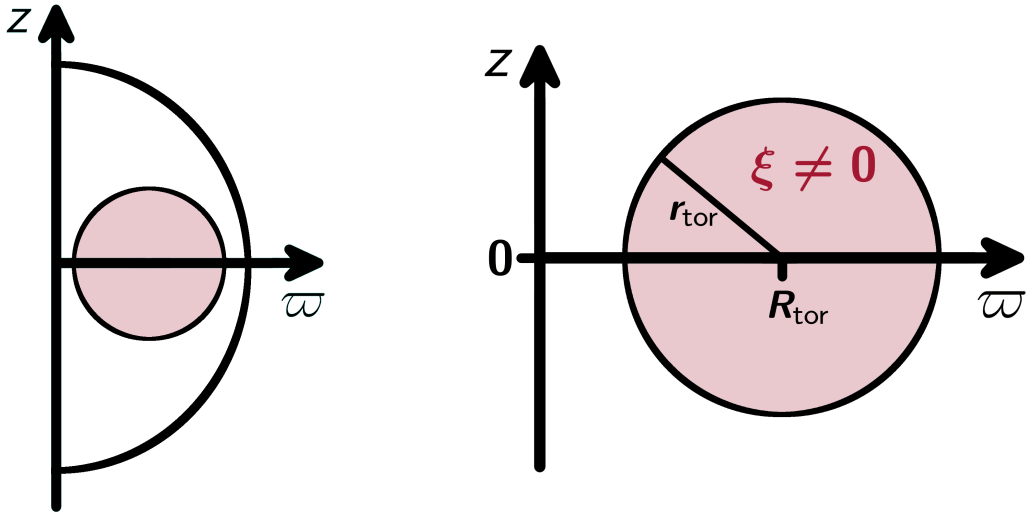

Figure 2.16.: Displacement field localisation area A for the purely poloidally magnetised neutron star, cf. relation (2.129). The 2D-integration area that will be chosen coincides with the localisation area. The sketch is not true to scale.

However, in order to keep this work comparable to Akgün et al. (2013) in a straightforward way, their notation will be used here:

$$\xi_r = \tilde{R}(r,\vartheta)\, r \sin\vartheta\, \mathrm{e}^{\mathrm{i}m\varphi} \tag{2.130a}$$
$$\xi_\vartheta = \tilde{S}(r,\vartheta)\, r \sin\vartheta\, \mathrm{e}^{\mathrm{i}m\varphi} \tag{2.130b}$$
$$\xi_\varphi = \mathrm{i}\tilde{T}(r,\vartheta)\, r \sin\vartheta\, \mathrm{e}^{\mathrm{i}m\varphi}\,. \tag{2.130c}$$

Displacement field choice $\boldsymbol{\xi}(r)$ for stars with mixed magnetic fields

The generally complex $\boldsymbol{\xi}$-defining functions $\tilde{R}(r,\vartheta)$, $\tilde{S}(r,\vartheta)$ and $\tilde{T}(r,\vartheta)$ are dimensionless. Just like in the previous cases, we will assume that $\tilde{R}$, $\tilde{S}$ and $\tilde{T}$ are real without restriction.

Note that choice (2.130) is structurally equivalent to choice (2.121) if the generating functions fulfil

$$X = \left(\varpi\,\tilde{R} + z\,\tilde{S}\right)\frac{\varpi}{r} \tag{2.131a}$$
$$Y = m\,\varpi\,\tilde{T} \tag{2.131b}$$
$$Z = \left(z\,\tilde{R} - \varpi\,\tilde{S}\right)\frac{\varpi}{r}, \tag{2.131c}$$

as shown in the appendix section C.3.1.

Due to the presence of both toroidal and poloidal field components, neither the cylindrical nor the toroidal coordinate system fit perfectly to the system geometry. For the sake of comparison with Akgün et al., spherical coordinates are used.

The $\boldsymbol{\xi}$-defining functions will be used in the specific form chosen by Akgün et al.:

$$\left.\begin{aligned} \tilde{R}(r,\vartheta) &= -\frac{\xi_0}{r}\,\sigma\left(1-\bar{\chi}^2\right)^{\sigma-1}\,\partial_\vartheta\bar{\chi}^2 \\ \tilde{S}(r,\vartheta) &= \frac{\xi_0}{R}\,\sigma\left(1-\bar{\chi}^2\right)^{\sigma-1}\,\partial_x\bar{\chi}^2 \end{aligned}\right\} \quad \text{in } A, \qquad \left.\begin{aligned} \tilde{R}(r,\vartheta) &= 0 \\ \tilde{S}(r,\vartheta) &= 0 \end{aligned}\right\} \quad \text{else,} \tag{2.132}$$

with

$$\tilde{T}(r,\vartheta) = \tilde{T}_{\min} \equiv -\frac{E_1(r,\vartheta)}{2\,m\,E_2(r,\vartheta)} \tag{2.133}$$

Explicit choice of the $\boldsymbol{\xi}$-defining functions for stars with mixed magnetic fields

The abbreviatory notation

$$\bar{\chi}^2 = \left(\frac{x-x_0}{\delta_r}\right)^2 + \left(\frac{\vartheta-\vartheta_0}{\delta_\vartheta}\right)^2 \tag{2.134}$$

has been used. Further, $\xi_0 \neq 0$ is a numerical constant, representing a constant amplitude. The constant σ can be chosen as $\sigma \geq 2$. The energy terms $E_1(r,\vartheta)$ and $E_2(r,\vartheta)$ can be expressed by analytical relations of system quantities. Their exact form and its derivation will be shown in the application section 5.3. The dimensionless radial variable x is defined as $x \equiv r/R$. Further, r_0 and ϑ_0 determine the position of the localisation area, while δ_r and δ_ϑ set its extent.

Altogether, the localisation region is defined as

$$A = \left\{\bar{\chi}^2 \in \mathbb{R}^+ \,\middle|\, \bar{\chi}^2 < 1\right\}. \tag{2.135}$$

The intersection of A with the (r,ϑ)-plane has an ellipse-like shape, as shown by figure 2.17.

Note that $\tilde{R}$, $\tilde{S}$ and $\tilde{T}$ vanish everywhere outside A, fulfilling the localisation condition for $\boldsymbol{\xi}$. The ξ_φ-defining function $\tilde{T}(r,\vartheta)$ has been chosen as $\tilde{T}_{\min}$, the value which minimises the energy variation density $\mathcal{E}$ with respect to $\tilde{T}$. This procedure will be explained in section 5.3.

Displacement field expressed by spherical harmonics

Besides the specific choices made above for the displacement field, we will apply a universal notation for $\boldsymbol{\xi}$.

One way of systematically describing all possible perturbations is to express them by spherical harmonics. This form will become useful in the course of dropping the Cowling approximation.

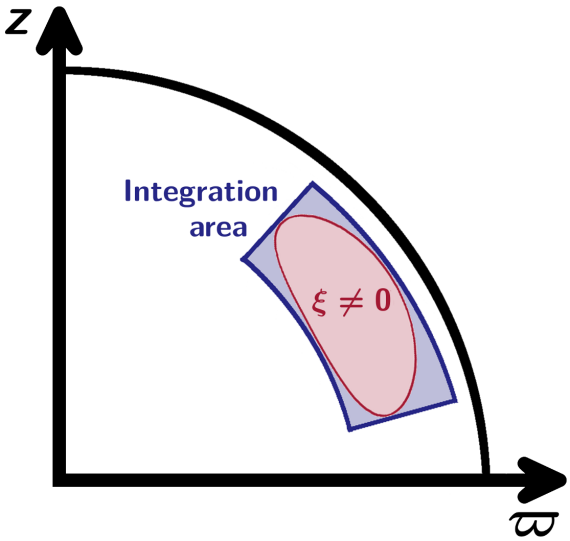

Figure 2.17.: Displacement field localisation area A and corresponding 2D-integration area for neutron stars with mixed magnetic fields, cf. relation (2.135). The integration area for J and K in the non-Cowling treatment will be discussed below in section 4.3.4.

Following Chandrasekhar (1964), we write

$$\xi_r = \frac{g(r)\, Y_l^m(\vartheta,\varphi)}{r^2} \tag{2.136a}$$

$$\xi_\vartheta = \frac{d_r h(r)\, \partial_\vartheta Y_l^m(\vartheta,\varphi)}{l(l+1)\, r} \tag{2.136b}$$

$$\xi_\varphi = \frac{d_r h(r)\, \partial_\varphi Y_l^m(\vartheta,\varphi)}{l(l+1)\, r \sin\vartheta}, \tag{2.136c}$$

with radial functions $g(r)$ and $h(r)$.

Displacement field choice $\boldsymbol{\xi}(r)$ expressed by spherical harmonics

The spherical harmonics with mode indices l and m are given by

$$Y_l^m(\vartheta,\varphi) = N_{lm}\, P_{lm}(\cos\vartheta)\, \mathrm{e}^{\mathrm{i}m\varphi} \tag{2.137}$$

with the normalisation constant

$$N_{lm} = \sqrt{\frac{2l+1}{4\pi}\,\frac{(l-m)!}{(l+m)!}} \tag{2.138}$$

and the associated Legendre polynomials

$$P_{lm}(\cos\vartheta) = \frac{(-1)^m}{2^l\, l!} \left(1-\cos^2\vartheta\right)^{\frac{m}{2}} \frac{d^{l+m}\left(\cos^2\vartheta - 1\right)^l}{d^{l+m}\cos\vartheta}. \tag{2.139}$$

The expression $\frac{d^{l+m}}{d^{l+m}\cos\vartheta}$ denotes the $(l+m)$-th derivative with respect to $\cos\vartheta$.

Displacement field expressed by stellar eigenfunctions

Another systematic way of describing a universal displacement field is to express it by stellar eigenfunctions.

This approach is most closely related to the system's geometry and oscillation properties. It will become useful for the idea of one day actually testing the system towards stability instead of scanning it for instabilities. Given that a stability proof requires the usage of all possible perturbations according to criterion (2.45), this systematic notation is a very first step approaching this goal.

According to Unno et al. (1989), the displacement field can be expressed by

$$\boldsymbol{\xi} = \sum_{n,l,m} c_{n,l,m}\, \boldsymbol{u}_{n,l,m}, \tag{2.140}$$

with the expansion coefficients $c_{n,l,m}$ and the stellar eigenfunctions

$$u_r = u_r(r)\, Y_l^m(\vartheta,\varphi) \tag{2.141a}$$
$$u_\vartheta = u_h(r)\, \partial_\vartheta Y_l^m(\vartheta,\varphi) \tag{2.141b}$$
$$u_\varphi = u_h(r)\, \frac{\partial_\varphi Y_l^m(\vartheta,\varphi)}{\sin\vartheta}, \tag{2.141c}$$

where $u_r(r)$ and $u_h(r)$ denote the radial parts.

Displacement field choice $\boldsymbol{\xi}(r)$ expressed by stellar eigenfunctions

The angular parts of the eigenfunctions are expressed by spherical harmonics. Therefore, in the simplest case of $\boldsymbol{\xi} = \boldsymbol{u}$, the notation of $\boldsymbol{\xi}$ using spherical harmonics (2.136) and the notation of $\boldsymbol{\xi}$ using eigenfunctions (2.141) are related via

$$g(r) = r^2\, u_r(r) \tag{2.142}$$
$$\partial_r h(r) = l(l+1)\, r\, u_h(r). \tag{2.143}$$

The radial functions $u_r(r)$ and $u_h(r)$ can further be expressed (Flügge, 1958; Smeyers & van Hoolst, 2010) in the form

$$u_r(r) = r\, y_1 \qquad\qquad u_h(r) = \frac{r\, y_2}{c_1\, \omega^2}, \tag{2.144}$$

where

$$c_1 \equiv \frac{r^3}{R^3}\, \frac{M}{m}. \tag{2.145}$$

The explicit form of the stellar eigenfunctions is defined by the functions y_1 and y_2.

The eigenfunctions of a homogeneous incompressible star can be expressed by analytical relations for y_1 and y_2, for given eigenfrequencies. These relations are shown in the appendix section A.7.

3. Basic idea of the semi-analytic method for stability analysis

After the theoretical foundations on neutron stars have been set, this chapter explains the key problem of neutron star research and motivates the solution approach proposed in this work.

3.1. Central problem of present neutron star research

In section 2.1 it was shown that strong magnetic fields are a characteristic feature of neutron stars. They strongly influence the stellar evolution and the observational properties. The magnetic fields led to the discovery of neutron stars by pulsar observations in the first place. In general, the magnetic field is essential for the explanation of basically all neutron star processes.

Surprisingly, the nature of neutron star magnetic fields still is an unresolved question. In contrast to the external neutron star magnetic fields, whose existence is proved by observations, the interior field structure is widely unknown. The origin of the enormous magnetic field strength is still a matter of debate. No general model is able to describe the reality sufficiently at the moment. The reason is that all models that currently exist are too simplified to produce stable realistic configurations. At the same time, it is mathematically difficult to make the models more realistic, as the following section will show.

3.1.1. Stability problem of magnetised neutron stars

As explained in section 2.3.1, a physical equilibrium state is globally stable if the system eventually relaxes back to the equilibrium state after any displacement $\boldsymbol{\xi}$ from equilibrium. If at least one possible perturbation causes the system to further diverge from the initial equilibrium state, the equilibrium state is unstable.

In reality, small deviations from equilibrium are unavoidable. The growth rate of the potential unstable modes in neutron stars is short on a typical neutron star timescale.

Any state existing long enough to be observed, must be in a stable state. This stable state apparently does not strongly depend on the specific conditions of the individual neutron star, since all observed neutron stars show a broadly universal behaviour.

So far, no theoretical model system could produce universally stable stars for a broad range of parameters, i.e. conditions. That means, according to the current theory, magnetised neutron stars could not exist. The model used for the description of this problem is obviously oversimplified. This issue could neither be solved with an analytical approach nor a numerical approach so far.

3.1.2. Analytical treatment of the stability problem

The established analytical stability analysis of magnetised neutron stars is based on the variational principle.

According to criterion (2.45), the total energy of a system increases/decreases during its displacement from equilibrium if the applied perturbation mode $\boldsymbol{\xi}$ is stable/unstable. As a consequence, the equilibrium state is stable if the energy variation δW caused by any possible perturbation $\boldsymbol{\xi}$ is positive and unstable if δW is negative for at least one displacement field $\boldsymbol{\xi}$.

In order to calculate the energy variation and analyse the stability behaviour of the neutron star, the contributions to the variational density need to be integrated over the stellar volume. In the analytical treatment, this is only possible for a model system that is noticeably simplified compared to the real system.

The first investigations on simple models by Tayler (1973); Markey & Tayler (1973, 1974); Wright (1973) showed that polytropic stars with a purely toroidal or a purely poloidal magnetic field display generic instabilities. The so-called Tayler instabilities of the cylindrical fluid discharge are illustrated in figure 2.12.

Over the following decades, many neutron star aspects that have been neglected in the first studies were tested for their impact on stability.

One first study of mixed magnetic fields with toroidal and poloidal components showed indications that stable mixed field models might exist (Tayler, 1980). Due to the strong simplifications in this work, it was rather based on estimations drawn from particular cases than a universal stability study. One supposedly stable mode was identified but the capabilities were far from creating a general mathematical proof.

Beyond this, it was investigated how Ohmic decay might influence the stability behaviour of an initially stable configuration during the main sequence phase of the star (Tayler, 1981). This is important in order to understand the origin of neutron star magnetic fields. However, the question whether the theory of flux freezing is convenient could not be clarified at that time.

Stellar rotation was expected to have a stabilising impact on the system, as discussed in Pitts & Tayler (1985). Nevertheless, rotation at realistic frequencies is probably not capable of removing all instabilities of the non-rotating star.

Overall, no universal solution of the stability problem, nor any concrete suggestions for realistic field configurations could be found. The underlying fundamental problem is that, contrary to an instability verification where only one unstable mode must be detected, a stability proof requires the consideration of all possible perturbations.

Recently, another refined mathematical approach was eventually done by Akgün et al. (2013). The stability of a stratified star with a toroidal field in the presence of a weak poloidal component was studied. This work showed that stratification and a mixed magnetic field seem to be decisive factors for the explanation of neutron star stability. However, owed to the analytical nature of the study, this consideration still relied on simplifications. The equation of state for example was approximated to make it analytically treatable. The Cowling approximation has been used. Furthermore, the stability analysis Akgün et al. performed did not investigate the reaction of an actual mixed field towards perturbations. It rather considered the isolated toroidal field stability in the presence of a poloidal field component. This means, the final conclusions are confirmed for a very specific class of

models and perturbation modes only. Although this work represented an important step for the field, the generalised conclusions drawn from this work are still based on estimates.

Altogether, analytical approaches experience difficulties in producing universal findings while keeping the system complexity sufficiently high.

3.1.3. Numerical treatment of the stability problem

As an alternative to the analytical investigation, a numerical stability analysis can be performed by tracing the evolution of a model system in numerical simulations. The system may either show a stable behaviour during the calculation period or underlie unstable exponential growth over time.

The advantage of the numerical approach is to make quite realistic systems treatable, without a need for excessive simplifications.

On the other hand, numerical simulations can never distinguish between a metastable state that decays after the computation ends and an actually stable state. Another disadvantage all numerical studies have in common, is that they can not address slightly different models at the same time. It is not possible to parametrise the system or the perturbation. The simulation requires explicit initial conditions and cannot produce universal results. This issue can be particularly inconvenient if a minor change in the model parameters or the displacement field changes the structure of the energy variation density significantly. In this case, every set of parameters requires a separate simulation.

The constriction of potential realistic field configurations requires a global picture of the star under different conditions. The eventually intended stability proof even requires the consideration of all possible perturbations. Regarding both facts, it is desirable to investigate the impact of numerous perturbations onto different systems at once. A numerical approach cannot offer this.

Simulations that have been performed so far reproduce the Tayler instabilities (Braithwaite, 2004, 2006b; Colaiuda et al., 2008; Ciolfi et al., 2009; Lander & Jones, 2011, 2010; Lasky et al., 2011).

Furthermore, mixed magnetic fields and stratification were considered as well (Braithwaite, 2006a; Lander & Jones, 2012).

Some simulations feature the so-called twisted-torus field, a quasi-stable state where the system remains for time-scales long compared to the Alfvén time, the typical time a magnetohydrodynamic wave takes to cross the star (Braithwaite, 2006a; Lander & Jones, 2012). The twisted field structure emerges from the superposition of poloidal and toroidal components, see figure 3.1. This configuration might be a candidate for the stable magnetic field in neutron stars.

However, numerical studies are not able to prove that no instability will occur later or would occur for slightly different conditions. It is a tedious or impossible task to scan the entire parameter space using numerical methods.

In conclusion, simulations are not suited best to constrain neutron star magnetic field configurations for a start.

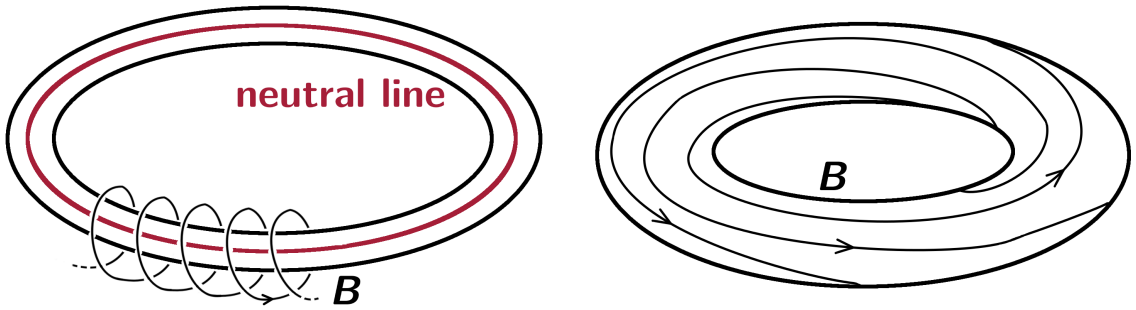

(a) $|\boldsymbol{B}_{\mathrm{pol}}| \gg |\boldsymbol{B}_{\mathrm{tor}}|$ (b) $|\boldsymbol{B}_{\mathrm{tor}}| \gg |\boldsymbol{B}_{\mathrm{pol}}|$

Figure 3.1.: 'Twisted-torus' fields, i.e. mixed magnetic fields with toroidal and poloidal components. The field geometry differs whether a strong poloidal component is disturbed by a toroidal part (a) or a strong toroidal component is disturbed by a poloidal part (b). In principle, all intermediate stages are possible. The neutral line is still defined as the axis where the poloidal field component vanishes.

3.1.4. The impact of the unknown magnetic field structure on modern research

Theory and observations imply that the behaviour of pulsars and especially magnetars is crucially influenced by their magnetic field due to its strength. Since the magnetic field structure is broadly unknown, all studies on neutron stars rely on assumptions and estimates for the magnetic field. The unresolved question of the magnetic field configuration complicates neutron star research in basically all areas.

In order to clarify the severity of the neutron star magnetic field problem, this section lists some of the many present studies that suffer from the unknown field structure.

Starting with the neutron star formation and proto neutron star phase, the mechanisms of neutrino cooling and neutrino driven winds are influenced by the unknown factor magnetic field (Perego et al., 2014). For neutron stars formed in binary mergers, the interaction of the original companion magnetic fields cannot be described sufficiently. Accretion, inspiral, merger and the creation of the new proto neutron star cannot be simulated reliably (Kawamura et al., 2016).

The interpretation of cooling curves is strongly affected by the magnetic field, especially for high field strengths $B \geq 10^{14}\,\mathrm{G}$ (Lazzati et al., 2008). On one hand, the magnetic field creates heat by joule heating. Inferred from the high magnetar temperatures, this seems to be a relevant effect (Kargaltsev et al., 2012). On the other hand, the magnetic field creates an anisotropy in the conductivity because charged particles cannot move across the magnetic field lines. Quantisation effects might be relevant if the field is enclosed in flux tubes. Although the magnetic field cannot be neglected, its consideration brings too many free parameters into play because it is too poorly understood (Pons et al., 2007).

The investigation of spin-down curves is essential not only for a better understanding of the pulsar evolution, but also to learn about the magnetic field itself. However, the stellar braking process itself depends on the unknown magnetic field, according to its strength and structure. Depending on the magnetic field dissipation behaviour, the spin-down

will be slower or faster (Pons et al., 2007). Beyond this, the magnetic field changes the rotational properties of the star by inducing prolateness or oblateness according to the field geometry. Owed to the large number of free parameters, different models for the magnetic field decay fit the data. The curve interpretation becomes less significant.

The theory behind glitches is based on the pinning behaviour of superfluid core vortices onto the crust. However, this region inside the star is poorly understood and strongly influenced by the magnetic field (Graber et al., 2015). Analogously, the implementation of superconductivity in the neutron star model is complicated by the unknown magnetic field strength as well. For field strengths of 10^{15} G in the interior for example, proton superconductivity would be entirely suppressed. Therefore, the spatial extent of the superconducting region is unclear (Sedrakian et al., 1997).

After the first successful detection of gravitational waves, it is a highly topical task to prepare the theory for the new neutron star detection channel of gravitational waves. In order to find out which gravitational wave signals are to be expected from neutron stars, mechanisms creating a deviation from the stellar rotational symmetry need to be simulated. For isolated stars, r-modes and magnetic deformations need to be studied, which is obviously complicated by the unknown field structure. In low mass X-ray binaries, accretion caused deformations, unstable modes and magnetically confined mountains of accreted matter can generate gravitational waves (Melatos & Payne, 2005). The inspiral and merger phase of the companions is expected to be detectable best in the gravitational wave spectrum. However, the entire simulation of the binary system is subject to large uncertainties due to the unknown initial magnetic fields of the companions (Haskell et al., 2015).

Neutron star seismology, aiming on constraining the equation of state from QPOs, is hindered by the unknown magnetic field. In order to infer the interior composition from surface observations, the behaviour of oscillation modes at the crust-core boundary region needs to be well-known. The magnetic field penetrating both media is the crucial coupling mechanism, strongly affecting the oscillation spectrum (Colaiuda & Kokkotas, 2011; Gabler et al., 2012). Another important investigation channel for neutron star oscillation modes is the CFS instability. Its growth rate is influenced by the neutron star magnetic field as well (Kokkotas, 2011).

Besides the complications the unknown magnetic field structure enforces on general neutron star investigations, magnetic field related studies are clearly challenged as well. For example, the origin and evolution of the magnetic field, possibly involving dynamo processes, is unclear (Mastrano & Melatos, 2011). The time scale of ohmic field decay cannot be estimated due to the unknown length scale of the magnetic field structure (Pons et al., 2007). Outbursts such as giant flares allow for a variety of interior field structures fitting to the same set of observables (Perna et al., 2014).

Summarising, the stability problem of magnetised neutron stars hinders the highly desired determination of the equation of state and the understanding of the neutron star evolution itself.

Aside from the disadvantages, all correlations between observations and the magnetic field listed above also represent possibilities to constrain the magnetic field by measurements. The interpretation of this data, however, is very difficult due to the large number of free parameters, such as uncertainties concerning the neutron star mass, radius, equation

of state, effects of superfluidity and superconductivity etc.

After all, one might ask how reasonable it is to perform neutron star studies applying magnetic field configurations that are known to be unstable in simple systems. Universal results that are produced for different field assumptions might still be reliable, but it is highly desirable to rather solve the stability problem of magnetised neutron stars.

3.2. Main idea of the semi-analytic method

As demonstrated in the previous sections, it is more than worthwhile to address the stability problem of neutron stars. This is what is implemented in this work.

Sections 3.1.2 and 3.1.3 discussed the incapability of purely analytical and numerical approaches in finding concrete universal answers to the stability problem. Therefore, in this work we present and implement a semi-analytic method that has never been used before. It combines the advantages of both analytical and numerical approaches, avoiding their weak points.

> The innovative idea of the semi-analytic method for stability analysis presented here is to set up the energy variation density for the variational principle analytically, and to compute the integral required to calculate the energy variation numerically.
>
> That way, the system can be kept general by parametrisation and many previously required simplifications are not mandatory. The systematic investigation of system classes allows it to constrain realistic magnetic field and composition structures.
>
> **Main idea of the stability analysis method presented in this work**

Compared to a purely analytical approach, the semi-analytic method allows for a treatment of more realistic stars. Compared to a simulation study, the magnetic field and composition structure as well as the imposed perturbation can be parametrised. Varying these parameters, various model systems can be studied at once. The energy variation can be computed systematically for all sets of parameters and provides information about the corresponding model systems, according to the stability criterion (2.45).

The results for δW can be scanned for systematic trends. That way, we might find areas in the parameter space that produce stars that are stable with a high possibility.

Once we find evidence for possibly stable configurations, these candidates can be investigated applying time evolution codes, that potentially confirm their stability. This procedure is by far more promising and expedient than constructing test systems for numerical codes on the basis of intelligent guesses, which is the procedure simulations currently rely on.

The findings of potentially stable magnetised stars can then be applied to make models that are assumed for various studies more realistic, cf. section 3.1.4.

Beyond the stability analysis of magnetised neutron stars and the determination of realistic configurations, the method set up in this work is capable of investigating other systems as well. It is generally applicable to issues where the energy variation of a system is required and it is possibly difficult to access analytically at the same time.

In this work, the derivation and implementation of the method is explicitly referred to magnetised neutron stars.

4. Realisation of the semi-analytic method

For the purpose of implementing the idea of the semi-analytic method presented in the previous chapter, the analytic expression for the energy variation derived in equation (2.116) needs to be integrated numerically. This procedure requires the analytical preparation of the integral on one hand, as well as the numerical integration setup on the other hand.

The first goal of this work is to reproduce known results in order to ensure the functionality of the method. Secondly, we intend to make the investigated system more realistic by incorporating new effects into the framework, that have been difficult or impossible to address analytically so far.

Consequently, a numerical integration pattern is required. Beyond that, the additional features need to be depicted mathematically to test their influence on the energy variation.

In this chapter, we first derive the newly appearing terms in the energy variation caused by the additional neutron star features. Subsequently, the applied numerical setup and integration pattern will be explained.

The analytic extensions implemented here aim for a more realistic model system that might solve the stability problem of the possibly oversimplified current neutron star model.

For one thing, we will investigate stratified stars as opposed to the polytropic stars Tayler applied in his studies.

The barotropicity commonly assumed in former studies implies a homogeneous proton-neutron fraction throughout the star and represents a strong simplification towards real stars, cf. paragraph “Stratification” in section 2.2.3. The consideration of stratification is a promising attempt to make progress in solving the stability issue of neutron stars.

Although stratification has been suggested several times before, only very few attempts have been made to realise a stratified model system. The reason is that the implementation of stratification complicates an analytic study decisively. The polytropic equation of state chosen in numerous studies before, allows for an exact solution for the density distribution inside the star. A non-polytropic equation of state, however, requires a numerical solution for the pressure and density distribution that influences all investigation steps.

In this work, the numerical consideration of the density distribution can easily be realised due to the semi-analytic character of the investigation method. Beyond that, we will keep the polytropic description for the background system and consider the impact of stratification in a perturbative approach following Akgün et al. (2013).

Secondly, we will drop the Cowling approximation in this work.

Previous stability studies on magnetised neutron stars were based on the negligence of the gravitational Euler perturbation. Here, it will be observed how $\delta\Phi$ affects the system stability, indicated by the energy variation.

This step is essential in modern neutron star stability analysis for the following reason. Tayler (1973) showed that the Cowling approximation is a valid simplification when

performing an instability proof. A system that is found to be unstable in Cowling approximation is still unstable in full description. The additional term in the energy variation caused by the disturbed gravitational potential is negative. Nowadays, however, we are less concerned with finding instabilities rather than explaining the actual stability of real neutron stars. The final goal in this field is the ultimate proof of the stability of magnetised neutron stars. For this task, the validity of the Cowling approximation is no longer obvious. An estimate is needed on how strongly the stability of a system state is affected, whether it is detected in Cowling approximation or in an exact approach.

Akgün et al. (2013) discussed the stabilisation of a dominant toroidal field instability by a poloidal field component and stratification. This result indicates that mixed magnetic fields and stratification might be relevant for the global stability of arbitrary modes. Nevertheless, this study has been performed in Cowling approximation. We will investigate whether this assumption was justified and whether the result is reliable.

In this work, the impact on the energy variation for this peculiar case will be derived. This represents a first concrete application of removing the Cowling approximation, which has never been done before. However, the provided procedure is exemplaric and represents a generic scheme that can be applied on further issues in the future. Generally, the approach is analogous for other perturbation modes or system properties.

The consideration of stratified stars without Cowling approximation requires an extension of the energy variation for polytropes in Cowling approximation set up in section 2.3.2. Stratification and the perturbation induced change in the gravitational potential cause additional terms in δW as given by (2.116) with (2.117).

These expressions will be derived in sections 4.1 and 4.2. Starting point is the implicit form for the energy variation (2.78) with (2.79), as it is valid for arbitrary equations of state and it holds in full non-Cowling description.

4.1. Energy variation with stratification

In this section, the impact of stratification on the energy variation formula will be derived. Note that Akgün et al. (2013) derived an analogous expression for the stratified star. The agreement between both derivations is shown in the appendix C.3.3.

The impact of stratification on the mathematical framework set up in chapter 2, is given by the change in the equation of state when the system is deflected from its equilibrium state.

The polytropic equation of state (2.22) is replaced by its perturbed form (2.38). The equation of state enters the mathematical framework only in the course of deriving the Euler pressure perturbation δp, as can be seen in section 2.3.2. Accordingly, the only contribution to the energy variation (2.78) with (2.79), which is affected by stratification, is $\mathcal{E}_{\text{fluid}}$.

The Euler pressure perturbation δp and subsequently the fluid contribution δW_{fluid} to the energy variation will be derived here for $\Gamma_0 \neq \Gamma_1$, in analogy to section 2.3.2.

4.1.1. Calculation of the Eulerian pressure perturbation

The Euler and Lagrange perturbations δp and Δp of the fluid pressure follow from the density perturbations (2.101a) and (2.83) with the use of the equation of state (2.38). The assumption of a non-barotropic equation of state $p = p(\rho, x)$, with the definition of Γ_1 by (2.39), yields

$$\left(\frac{\partial p_0}{\partial \rho_0}\right)_{x^p} = \frac{p_0}{\rho_0}\left(\frac{\partial \ln p_0}{\partial \ln \rho_0}\right)_{x^p} = \frac{p_0}{\rho_0}\Gamma_1. \tag{4.1}$$

In this step, relation (A.21) has been used for the connection between derivatives of scalar functions and derivatives of their logarithms.

The further consideration will be based on the assumption that the fluid displacement happens on a short time-scale, prohibiting particle conversions during the perturbation. Therefore, the proton fraction stays constant inside a displaced fluid element: $\Delta x^p = 0$. With connection (2.48), $\delta x^p = -\boldsymbol{\xi} \cdot \nabla x_0^p$ follows. This assumption is equivalent to an adiabatic process, reminding that x^p plays the role of an effective entropy, as stated in section 2.2.3.

Therefore,

$$\Delta p = \left(\frac{\partial p_0}{\partial \rho_0}\right)_{x^p} \Delta\rho + \left(\frac{\partial p_0}{\partial x_0^p}\right)_{\rho} \underbrace{\Delta x^p}_{0} = \frac{\Gamma_1 p_0}{\rho_0}\Delta\rho. \tag{4.2}$$

Making use of the density perturbation (2.83), the Lagrange pressure perturbation reads

$$\Delta p = -\Gamma_1 p_0 \nabla \cdot \boldsymbol{\xi} + \mathcal{O}(\boldsymbol{\xi}^2). \tag{4.3}$$

The Euler pressure perturbation follows with connection (2.48):

$$\delta p = \Delta p - \boldsymbol{\xi} \cdot \nabla p_0 + \mathcal{O}(\boldsymbol{\xi}^2). \tag{4.4}$$

Thus,

$$\delta p = -\Gamma_1 p_0 \nabla \cdot \boldsymbol{\xi} - \boldsymbol{\xi} \cdot \nabla p_0 + \mathcal{O}(\boldsymbol{\xi}^2). \tag{4.5}$$

Explicit Euler pressure perturbation for stratified stars, in full description

The pressure perturbation in the case of considering stratification is equivalent to the pressure perturbation (2.86) and (2.101b) of a polytrope, where the equilibrium polytropic index Γ_0 is replaced by the polytropic index Γ_1 of the perturbed state. The pressure perturbation in the polytropic case δp^{poly} represents a special case of (4.5), for $\Gamma_1 = \Gamma_0$.

4.1.2. Fluid pressure contribution to the energy variation

According to the equivalence in δp concerning polytropes, as given by expression (2.101b), and stratified stars, as given by expression (4.5), the further derivation of $\delta W_{\mathrm{fluid}}$ in the stratified case is structurally identical to the polytropic case shown in section 2.3.2.

Neglecting surface integral terms, the fluid pressure gradient contribution to the energy variation is thus given by

$$\mathcal{E}_{\text{fluid}} = \frac{1}{4}\,\Re\left\{\Gamma_1\, p_0\,(\nabla\cdot\boldsymbol{\xi}^*)\;(\nabla\cdot\boldsymbol{\xi}) + \boldsymbol{\xi}\cdot\nabla p_0\,(\nabla\cdot\boldsymbol{\xi}^*)\right\}. \tag{4.6}$$

Explicit fluid pressure energy variation for stratified stars, in full description

This expression can be rearranged to give the form given by Akgün et al. (2013):

$$\mathcal{E}_{\text{fluid}} = \frac{1}{2}\,\Re\left\{(\Gamma_1-\Gamma_0)\;p_0\,(\nabla\cdot\boldsymbol{\xi}^*)\;(\nabla\cdot\boldsymbol{\xi}) + \frac{\Gamma_0\,p_0}{\rho_0^2}\;(\nabla\cdot(\rho_0\,\boldsymbol{\xi}^*))\;(\nabla\cdot(\rho_0\,\boldsymbol{\xi}))\right\}. \tag{4.7}$$

The derivation is shown in the appendix section C.3.3. Note that formulation (4.7) involves the difference $\Delta\Gamma$ between both polytropic indices and therefore directly shows the stabilising/destabilising impact of stable/unstable stratification mathematically. Stable/unstable stratification as explained in paragraph "Stratification" of section 2.2.3, contributes a positive/negative part to the energy variation density.

Further note that the fluid contribution to the energy variation in the polytropic case $\mathcal{E}^{\text{poly}}_{\text{fluid}}$, given by expression (2.114), represents a special case of (4.6), for $\Gamma_1 = \Gamma_0$.

4.2. Energy variation without Cowling approximation

In this section, the impact of dropping the Cowling approximation on the energy variation formula will be derived.

The Cowling approximation implies that the change in the gravitational potential due to the displacement is negligible, i.e. $\delta\Phi = 0$, as stated in section 2.3.2. If this approximation is removed, a $\delta\Phi$-dependent contribution $\delta W^{\text{nC}}_{\text{grav}}$ arises in the energy variation. The superscript 'nC' indicates that $\delta W^{\text{nC}}_{\text{grav}}$ is the additional term appearing in a full **n**on-**C**owling treatment as opposed to a Cowling treatment:

$$\delta W_{\text{grav}} = \delta W^{\text{Cowl}}_{\text{grav}} + \delta W^{\text{nC}}_{\text{grav}}. \tag{4.8}$$

The additional term has been neglected in the explicit form of the energy variation given in (2.116). According to the implicit form given by (2.78) and (2.79c), it reads

$$\mathcal{E}^{\text{nC}}_{\text{grav}} = \mp\frac{1}{4}\,\Re\left\{\rho_0\,(\boldsymbol{\xi}^*\cdot\nabla\delta\Phi)\right\}. \tag{4.9}$$

Remember the sign convention, determined by the choice of the gravitational field vector in (2.17).

For the purpose of determining the impact of dropping the Cowling approximation, $\mathcal{E}_{\mathrm{grav}}^{\mathrm{nC}}$ needs to be calculated. This requires the calculation of $\delta\Phi$, which is implicitly given by (2.101c):

$$\delta\Phi = \pm G \iiint \rho_0(\boldsymbol{r}')\,\boldsymbol{\xi}(\boldsymbol{r}')\cdot\nabla_{\boldsymbol{r}'}\frac{1}{|\boldsymbol{r}-\boldsymbol{r}'|}\,\mathrm{d}V' + \mathcal{O}(\boldsymbol{\xi}^2). \tag{4.10}$$

Since $\delta\Phi$ depends on the displacement field in a non-trivial way, the explicit calculation of $\delta\Phi$ requires a specific choice for the displacement field. In the subsequent paragraphs, we will thus derive an explicit expression for $\delta\Phi$ for two different choices of $\boldsymbol{\xi}$.

Afterwards, the expressions will be used to set up an explicit expression for $\mathcal{E}_{\mathrm{grav}}^{\mathrm{nC}}$.

4.2.1. $\delta\Phi$ explicitly for $\boldsymbol{\xi}$ expressed by spherical harmonics

The first choice we assume for the displacement field is its expression via spherical harmonics Y_l^m, according to assumption (2.136) with (2.137).

The explicit form for the Euler perturbation of the gravitational potential in this case can be found in Chandrasekhar (1965):

$$\delta\Phi(\boldsymbol{r}) = \delta\Phi(r)\,Y_l^m(\vartheta,\varphi) + \mathcal{O}(\boldsymbol{\xi}^2), \tag{4.11}$$

with

$$\delta\Phi(r) = \pm\frac{4\pi G}{2l+1}\left[\frac{J_l(r)}{r^{l+1}} - r^l K_l(r)\right] \tag{4.12}$$

and

$$J_l(r) = \int_0^r \rho_0(r')\,r'^l\left[l\,\frac{g(r')}{r'} + d_{r'}h(r')\right]\mathrm{d}r' \tag{4.13a}$$

$$K_l(r) = \int_r^R \frac{\rho_0(r')}{r'^{l+1}}\left[(l+1)\,\frac{g(r')}{r'} - d_{r'}h(r')\right]\mathrm{d}r'. \tag{4.13b}$$

Explicit Euler perturbation of the gravitational potential for $\boldsymbol{\xi}$ expressed by spherical harmonics according to (2.136)**, in full description**

Here, m and l denote the spherical harmonics' mode indices. The radial functions $J_l(r)$, respectively $K_l(r)$, at the position r are given by integrations from the stellar centre up to r, respectively from r up to the stellar surface. Singularities at $r' = 0$ in the first term of $J_l(r)$ are avoided for $l \geq 1$, while for $l = 0$ the term vanishes. The integral in $K_l(r')$ does not extend to $r' = 0$, and thus stays finite as well.

The derivation of expression (4.11) with (4.12) and (4.13) is outlined in the appendix section B.5.1.

4.2.2. δW^{nC} explicitly for $\boldsymbol{\xi}$ expressed by spherical harmonics

With the use of the Euler perturbation of the gravitational potential shown in the previous section, the gravitational energy variation can be derived in full description.

The derivation is shown in the appendix B.5.2. The result can be found in Chandrasekhar & Lebovitz (1964):

$$\delta W_{\text{grav}}^{\text{nC}} = -2\pi G \int_0^R \frac{\rho_0^2(r)\, g^2(r)}{r^2}\,\mathrm{d}r - \frac{2\pi G}{2l+1}\int_0^R \Big\{ J_l(r)\,\mathrm{d}_r K_l(r) - K_l(r)\,\mathrm{d}_r J_l(r)\Big\}\,\mathrm{d}r \tag{4.14a}$$

$$\delta W_{\text{grav}}^{\text{nC}} = -2\pi G \int_0^R \frac{\rho_0^2(r)\, g^2(r)}{r^2}\,\mathrm{d}r + \frac{4\pi G}{2l+1}\int_0^R \mathrm{d}_r J_l(r)\, K_l(r)\,\mathrm{d}r. \tag{4.14b}$$

Explicit non-Cowling contribution to the energy variation for $\boldsymbol{\xi}$ expressed by spherical harmonics according to (2.136)

4.2.3. $\delta\Phi$ explicitly for $\boldsymbol{\xi}$ according to the mixed field choice of Akgün et al.

In this work, we will in investigate the relevance of the Cowling approximation particularly by testing whether the stability analysis performed by Akgün et al. (2013) stays valid when the approximation is dropped.

For this purpose, the gravitational Euler perturbation will be derived for Akgün's choice (2.130) of the displacement field. Note that expression (4.11) is not applicable in this case because the ϑ-dependence of $\boldsymbol{\xi}$ cannot be expressed by the general form (2.136) of $\boldsymbol{\xi}$ that has been used in the previous section.

The procedure is analogous to the case where the displacement field was expressed by spherical harmonics, where the derivation is shown in the appendix section B.5.1.

Starting from equation (4.10), we use spherical coordinates (2.4) and assume axisymmetry:

$$\delta\Phi(\boldsymbol{r}) = \pm G \iiint \rho_0(\boldsymbol{r}')\,\boldsymbol{\xi}(\boldsymbol{r}')\cdot\nabla_{\boldsymbol{r}'}\left(\frac{1}{|\boldsymbol{r}-\boldsymbol{r}'|}\right) r'^2 \sin\vartheta'\,\mathrm{d}r'\,\mathrm{d}\vartheta'\,\mathrm{d}\varphi' + \mathcal{O}(\boldsymbol{\xi}^2). \tag{4.15}$$

The integral extends over the total stellar volume.

Following the procedure in the appendix, the absolute value can be expanded in terms of spherical harmonics $Y_\lambda^\mu(\vartheta',\varphi')$ as defined in (2.137). Then, according to relations (B.25) and (B.26):

$$\frac{1}{|\boldsymbol{r}-\boldsymbol{r}'|} = \sum_{\lambda=0}^{\infty} \frac{4\pi}{2\lambda+1}\, f_\lambda(r,r') \sum_{\mu=-\lambda}^{\lambda} Y_\lambda^\mu(\vartheta,\varphi)\, Y_\lambda^\mu(\vartheta',\varphi'), \tag{4.16}$$

with the radial function

$$f_\lambda(r,r') = \begin{cases} \frac{r'^\lambda}{r^{\lambda+1}} & \text{if } r' \le r \\ \frac{r^\lambda}{r'^{\lambda+1}} & \text{if } r' \ge r. \end{cases} \tag{4.17}$$

The expansion (4.16) is inserted into (4.15). Due to the linearity of the gradient and the distributive property, all quantities independent of $\boldsymbol{r}'$ and the summations can be pulled out of the integral. Keeping the integrand real according to section A.5.4 in the appendix,

the Euler perturbation then is

$$\delta\Phi(\boldsymbol{r}) = \pm \sum_{\lambda=0}^{\infty} \sum_{\mu=-\lambda}^{\lambda} \frac{4\pi G}{2\lambda+1} Y_\lambda^\mu(\vartheta,\varphi) \cdot \tag{4.18}$$
$$\iiint \rho_0(r') \left\{ \boldsymbol{\xi}^*(\boldsymbol{r}') \cdot \nabla_{\boldsymbol{r}'} \left[f_\lambda(r,r') \, Y_\lambda^\mu(\vartheta',\varphi') \right] \right\} r'^2 \sin\vartheta' \, \mathrm{d}r' \, \mathrm{d}\vartheta' \, \mathrm{d}\varphi' + \mathcal{O}(\boldsymbol{\xi}^2).$$

Note that $\boldsymbol{\xi}$ as well as $Y_\lambda^\mu(\vartheta',\varphi')$ denote generally complex functions. However, the azimuthal integral over the scalar product is always real as it has been shown in the appendix section A.5.4. Thus, we do not need to take the real part over the integrand or add the factor 1/2 as it is necessary for the energy variation. Further, the spherical symmetry of the unperturbed system was taken into account by applying $\rho_0(\boldsymbol{r}') = \rho_0(r')$.

Next, the mixed field choice (2.130) for the displacement field is utilised:

$$\xi_r^* = \tilde{R}(r,\vartheta) \, r \sin\vartheta \, \mathrm{e}^{-\mathrm{i}m'\varphi} \tag{4.19a}$$
$$\xi_\vartheta^* = \tilde{S}(r,\vartheta) \, r \sin\vartheta \, \mathrm{e}^{-\mathrm{i}m'\varphi} \tag{4.19b}$$
$$\xi_\varphi^* = -\mathrm{i}\tilde{T}(r,\vartheta) \, r \sin\vartheta \, \mathrm{e}^{-\mathrm{i}m'\varphi} \, . \tag{4.19c}$$

Note that the sign of ξ_φ^* is negative due to the complex conjugation. Beyond that, the mode index of $\boldsymbol{\xi}_{m'}$ is denoted as m' because it generally differs from the mode index m of the spherical harmonics describing $\delta\Phi$. Further, the gradient is evaluated in spherical coordinates. The exponential dependence on φ' can be factored out by defining

$$Y_\lambda^\mu(\vartheta',\varphi') \equiv \Theta_\lambda^\mu(\vartheta') \, \mathrm{e}^{\mathrm{i}\mu\varphi'}, \tag{4.20}$$

with $\Theta_\lambda^\mu(\vartheta') = N_{\lambda\mu} \, P_{\lambda\mu}(\cos\vartheta')$. Thus,

$$\delta\Phi(\boldsymbol{r}) = \pm \sum_{\lambda=0}^{\infty} \sum_{\mu=-\lambda}^{\lambda} \frac{4\pi G}{2\lambda+1} Y_\lambda^\mu(\vartheta,\varphi) \cdot \tag{4.21}$$
$$\iiint \rho_0(r') \Big\{ \big[\tilde{R}(r',\vartheta') \, r' \sin\vartheta' \, \partial_{r'} f_\lambda(r,r') \, \Theta_\lambda^\mu(\vartheta')$$
$$+ \tilde{S}(r',\vartheta') \, \sin\vartheta' \, f_\lambda(r,r') \, \partial_{\vartheta'} \Theta_\lambda^\mu(\vartheta')$$
$$-\mathrm{i}^2 \mu \tilde{T}(r',\vartheta') \, f_\lambda(r,r') \, \Theta_\lambda^\mu(\vartheta') \big] \mathrm{e}^{\mathrm{i}(\mu-m)\varphi'} \Big\} \cdot$$
$$r'^2 \sin\vartheta' \, \mathrm{d}r' \, \mathrm{d}\vartheta' \, \mathrm{d}\varphi' + \mathcal{O}(\boldsymbol{\xi}^2),$$

where we already evaluated the azimuthal derivative $\partial_{\varphi'} Y_\lambda^\mu(\vartheta',\varphi') = \mathrm{i}\mu \, \Theta_\lambda^\mu(\vartheta') \, \mathrm{e}^{\mathrm{i}\mu\varphi'}$.

In equation (4.21), the only actually complex contribution to the integrand is the expo-

nential function. Thus, with relation (A.10):

$$\delta\Phi(\boldsymbol{r}) = \pm \sum_{\lambda=0}^{\infty} \sum_{\mu=-\lambda}^{\lambda} \frac{4\,\pi\,G}{2\,\lambda+1}\, Y_\lambda^\mu(\vartheta,\varphi) \cdot \tag{4.22}$$
$$\int_0^\pi \int_0^R \rho_0(r') \Big[\tilde{R}(r',\vartheta')\, r' \sin\vartheta'\, \partial_{r'} f_\lambda(r,r')\, \Theta_\lambda^\mu(\vartheta')$$
$$+ \tilde{S}(r',\vartheta')\, \sin\vartheta'\, f_\lambda(r,r')\, \partial_{\vartheta'} \Theta_\lambda^\mu(\vartheta')$$
$$+ \mu\, \tilde{T}(r',\vartheta')\; f_\lambda(r,r')\, \Theta_\lambda^\mu(\vartheta') \Big] \cdot$$
$$\underbrace{\int_0^{2\pi} \mathrm{e}^{\mathrm{i}(\mu-m)\varphi'}\, \mathrm{d}\varphi'}_{2\pi\delta_{\mu m}}\; r'^2 \sin\vartheta'\, \mathrm{d}r'\, \mathrm{d}\vartheta' + \mathcal{O}(\boldsymbol{\xi}^2).$$

The φ'-integral in (4.22) vanishes if both mode indices differ, as shown by equation (A.10). This implies that for all non-vanishing terms in $\delta\Phi$, the mode index μ of the $\frac{1}{|\boldsymbol{r}-\boldsymbol{r}'|}$-expansion is equivalent to the mode index m of the displacement field. The μ-summation in (4.22) can be dropped, keeping only the non-vanishing term with $\mu = m$.

Subsequently, the λ-summation cannot include terms with $\lambda < m$ and its summation index is adjusted:

$$\delta\Phi(\boldsymbol{r}) = \pm \sum_{\lambda=m}^{\infty} \frac{8\,\pi^2\,G}{2\,\lambda+1}\, Y_\lambda^m(\vartheta,\varphi) \int_0^\pi \int_0^R \rho_0(r') \Big[\tilde{R}(r',\vartheta')\, r'\, \partial_{r'} f_\lambda(r,r')\, \Theta_\lambda^m(\vartheta') \tag{4.23}$$
$$+ \tilde{S}(r',\vartheta')\, f_\lambda(r,r')\, \partial_{\vartheta'} \Theta_\lambda^m(\vartheta') + \frac{m\,\tilde{T}(r',\vartheta')}{\sin\vartheta'}\, f_\lambda(r,r')\, \Theta_\lambda^m(\vartheta') \Big] \cdot$$
$$r'^2 \sin^2\vartheta'\, \mathrm{d}r'\, \mathrm{d}\vartheta' + \mathcal{O}(\boldsymbol{\xi}^2).$$

The f_λ-derivative is evaluated based on (4.17), yielding

$$f_\lambda(r,r') = \begin{cases} \frac{r'^\lambda}{r^{\lambda+1}} & \text{if } r' \le r \\ \frac{r^\lambda}{r'^{\lambda+1}} & \text{if } r' \ge r \end{cases} \qquad d_{r'} f_\lambda(r,r') = \begin{cases} \lambda\, \frac{r'^{\lambda-1}}{r^{\lambda+1}} & \text{if } r' \le r \\ -(\lambda+1)\, \frac{r^\lambda}{r'^{\lambda+2}} & \text{if } r' \ge r. \end{cases} \tag{4.24}$$

For the purpose of inserting (4.24) into (4.23), the integral is split into two integration

areas with $r' \leq r$ and $r' \geq r$:

$$\begin{aligned}\delta\Phi(\boldsymbol{r}) = \pm \sum_{\lambda=m}^{\infty} \frac{8\pi^2 G}{2\lambda+1} Y_\lambda^m(\vartheta,\varphi) \cdot \\ \left\{ \int_0^\pi \int_0^r \rho_0(r') \left[\lambda \tilde{R}(r',\vartheta') \frac{r'^\lambda}{r^{\lambda+1}} \Theta_\lambda^m(\vartheta') + \tilde{S}(r',\vartheta') \frac{r'^\lambda}{r^{\lambda+1}} \partial_{\vartheta'} \Theta_\lambda^m(\vartheta') \right.\right. \\ \left. + \frac{m\tilde{T}(r',\vartheta')}{\sin\vartheta'} \frac{r'^\lambda}{r^{\lambda+1}} \Theta_\lambda^m(\vartheta') \right] r'^2 \sin^2\vartheta' \,\mathrm{d}r' \,\mathrm{d}\vartheta' \\ + \int_0^\pi \int_r^R \rho_0(r') \left[-(\lambda+1) \tilde{R}(r',\vartheta') \frac{r^\lambda}{r'^{\lambda+1}} \Theta_\lambda^m(\vartheta') + \tilde{S}(r',\vartheta') \frac{r^\lambda}{r'^{\lambda+1}} \partial_{\vartheta'} \Theta_\lambda^m(\vartheta') \right. \\ \left.\left. + \frac{m\tilde{T}(r',\vartheta')}{\sin\vartheta'} \frac{r^\lambda}{r'^{\lambda+1}} \Theta_\lambda^m(\vartheta') \right] r'^2 \sin^2\vartheta' \,\mathrm{d}r' \,\mathrm{d}\vartheta' \right\} + \mathcal{O}(\boldsymbol{\xi}^2).\end{aligned} \tag{4.25}$$

In analogy to (4.13), radial functions $J_\lambda^m(r)$ and $K_\lambda^m(r)$ are defined as

$$\begin{aligned} J_\lambda^m(r) = \int_0^\pi \int_0^r \rho_0(r')\, r'^\lambda \left[\lambda \tilde{R}(r',\vartheta') \Theta_\lambda^m(\vartheta') + \tilde{S}(r',\vartheta') \partial_{\vartheta'} \Theta_\lambda^m(\vartheta') \right. \\ \left. + \frac{m\tilde{T}(r',\vartheta')}{\sin\vartheta'} \Theta_\lambda^m(\vartheta') \right] r'^2 \sin^2\vartheta' \,\mathrm{d}r' \,\mathrm{d}\vartheta' \end{aligned} \tag{4.26a}$$

$$\begin{aligned} K_\lambda^m(r) = \int_0^\pi \int_r^R \frac{\rho_0(r')}{r'^{\lambda+1}} \left[(\lambda+1) \tilde{R}(r',\vartheta') \Theta_\lambda^m(\vartheta') - \tilde{S}(r',\vartheta') \partial_{\vartheta'} \Theta_\lambda^m(\vartheta') \right. \\ \left. - \frac{m\tilde{T}(r',\vartheta')}{\sin\vartheta'} \Theta_\lambda^m(\vartheta') \right] r'^2 \sin^2\vartheta' \,\mathrm{d}r' \,\mathrm{d}\vartheta'. \end{aligned} \tag{4.26b}$$

Note that as opposed to r, ϑ does not appear in the integration boundaries. It is therefore irrelevant whether the polar integration variable is named ϑ' or ϑ.

Finally, the Euler perturbation of the gravitational potential can be written in analogy to (4.11) with (4.12) and (4.13) as

$$\delta\Phi(\boldsymbol{r}) = \sum_{\lambda=m}^{\infty} \delta\Phi_\lambda^m(r)\, Y_\lambda^m(\vartheta,\varphi) + \mathcal{O}(\boldsymbol{\xi}^2) \tag{4.27}$$

with

$$\delta\Phi_\lambda^m(r) = \pm\frac{8\,\pi^2\,G}{2\,\lambda+1}\left[\frac{J_\lambda^m(r)}{r^{\lambda+1}} - r^\lambda\, K_\lambda^m(r)\right] \tag{4.28}$$

and

$$J_\lambda^m(r) = \int_0^\pi\!\!\int_0^r \rho_0(r')\, r'^{\lambda+2}\left[\left(\lambda\,\tilde{R}(r',\vartheta') + \frac{m\,\tilde{T}(r',\vartheta')}{\sin\vartheta'}\right)\Theta_\lambda^m(\vartheta') + \tilde{S}(r',\vartheta')\,\partial_{\vartheta'}\Theta_\lambda^m(\vartheta')\right]\sin^2\vartheta'\,\mathrm{d}r'\,\mathrm{d}\vartheta' \tag{4.29a}$$

$$K_\lambda^m(r) = \int_0^\pi\!\!\int_r^R \frac{\rho_0(r')}{r'^{\lambda-1}}\left[\left((\lambda+1)\,\tilde{R}(r',\vartheta') - \frac{m\,\tilde{T}(r',\vartheta')}{\sin\vartheta'}\right)\Theta_\lambda^m(\vartheta') - \tilde{S}(r',\vartheta')\,\partial_{\vartheta'}\Theta_\lambda^m(\vartheta')\right]\sin^2\vartheta'\,\mathrm{d}r'\,\mathrm{d}\vartheta'. \tag{4.29b}$$

Explicit Euler perturbation of the gravitational potential for the mixed field choice (2.130) **of $\boldsymbol{\xi}$, in full description**

Note that unlike λ, m is not a summation index but the mode index stemming from the displacement field $\boldsymbol{\xi}(\boldsymbol{r}) \sim \mathrm{e}^{\mathrm{i}m\varphi}$. The r'-integrations in $J_\lambda^m(r)$ and $K_\lambda^m(r)$ run in the intervals $[0,r]$ and $[r,R]$. The ϑ'-integration covers the full angular range $[0,\pi]$.

In comparison with expressions (4.13), equations (4.29) comprise an additional angular integration. The reason is that the displacement field here does not show symmetry properties which could be utilised in the case where $\boldsymbol{\xi}$ was expressed by spherical harmonics.

Due to the missing symmetry properties, the λ-summation in (4.27) could not be evaluated as easily as it was the case for the μ-summation.

A detailed search for symmetries in the appendix B.5.7 shows: The λ-summation cannot be removed in the mixed field case if we take into account the explicit choice we make for $\tilde{R}$, $\tilde{S}$ and $\tilde{T}$ in the application section 5.3 in accordance with Akgün et al. (2013). Instead, when applying $\delta\Phi(\boldsymbol{r})$ on the mixed field system with stratification, we will approximate the sum by focussing on the most dominant terms with $\lambda \le 2$ for $m = 1$:

$$\delta\Phi(\boldsymbol{r}) = \delta\Phi_1^1(r)\, Y_1^1(\vartheta,\varphi) + \delta\Phi_2^1(r)\, Y_2^1(\vartheta,\varphi) + \mathcal{O}(\boldsymbol{\xi}^2) + \mathcal{O}\left(\int_0^r \frac{r'^5}{r^4}\, f(r')\,\mathrm{d}r'\right) + \mathcal{O}\left(\int_r^R \frac{r^3}{r'^2}\, f(r')\,\mathrm{d}r'\right). \tag{4.30}$$

Keeping in mind that the λ-sum stems from the expansion of $\frac{1}{|\boldsymbol{r}-\boldsymbol{r}'|}$ in spherical harmonics, the most dominant terms belong to the lowest values of λ.

With our choice, we neglect terms of the order $\frac{r'^5}{r^4}$ and higher in the J_λ^m-contribution and terms of the order $\frac{r^3}{r'^2}$ and higher in the K_λ^m-contribution. In both cases, the fraction is small, because $r' \leq r$ holds for the J_λ^m-integral and $r' \geq r$ holds for the K_λ^m-integral. The approximation is valid.

4.2.4. δW^{nC} explicitly for $\boldsymbol{\xi}$ according to the mixed field choice of Akgün et al.

Starting from the expression for the gravitational potential derived in the previous section, the non-Cowling contribution $\delta W_{\text{grav}}^{\text{nC}}$ to the energy variation needs to be set up.

We derive $\delta W_{\text{grav}}^{\text{nC}}$ for the mixed field choice of $\boldsymbol{\xi}$, in analogy to the derivation shown in the appendix B.5.2, where the displacement field was expressed by spherical harmonics.

According to (4.9) and (2.78), the non-Cowling contribution to the energy variation is

$$\delta W_{\text{grav}}^{\text{nC}} = \mp\frac{1}{4} \iiint \rho_0(r)\, \Re\left\{\boldsymbol{\xi}^* \cdot \nabla \delta\Phi(\boldsymbol{r})\right\} \mathrm{d}V. \tag{4.31}$$

The integral extends over the total stellar volume. We insert the expression for $\delta\Phi(\boldsymbol{r})$ given by equations (4.27) and (4.28), keeping first order $\boldsymbol{\xi}$-terms in $\delta\Phi(\boldsymbol{r})$. Thus, $\delta W_{\text{grav}}^{\text{nC}}$ is on the order of $\boldsymbol{\xi}^2$ as demanded:

$$\delta W_{\text{grav}}^{\text{nC}} = -\sum_{\lambda=m}^{\infty} \frac{2\,\pi^2\,G}{2\,\lambda+1} \iiint \rho_0(r)\, \Re\left\{\boldsymbol{\xi}^* \cdot \nabla\left[\left(\frac{J_\lambda^m(r)}{r^{\lambda+1}} - r^\lambda K_\lambda^m(r)\right) Y_\lambda^m(\vartheta,\varphi)\right]\right\} \mathrm{d}V. \tag{4.32}$$

As shown in the appendix A.5.4, the real part ensures the integral to be physically reasonable even though $\boldsymbol{\xi}$ and $Y_\lambda^m(r)$ are both generally complex functions.

In analogy to the previous paragraph, the lack of symmetry in $\boldsymbol{\xi}$ prohibits the application of an orthogonality relation similar to (B.29) at this point. Instead, the scalar product of $\boldsymbol{\xi}^*$ with the gradient will be evaluated step by step. First, we express the gradient in spherical coordinates and define the abbreviation $F_\lambda^m(r) \equiv \left(\frac{J_\lambda^m(r)}{r^{\lambda+1}} - r^\lambda K_\lambda^m(r)\right)$ to obtain

$$\begin{aligned}\delta W_{\text{grav}}^{\text{nC}} = -\sum_{\lambda=m}^{\infty} \frac{2\,\pi^2\,G}{2\,\lambda+1} \iiint \rho_0(r)\, \Re\Bigg\{&\xi_r^*\, \mathrm{d}_r F_\lambda^m(r)\, Y_\lambda^m(\vartheta,\varphi) + \xi_\vartheta^*\, F_\lambda^m(r)\, \frac{\partial_\vartheta Y_\lambda^m(\vartheta,\varphi)}{r} \\ &+\xi_\varphi^*\, F_\lambda^m(r)\, \frac{\partial_\varphi Y_\lambda^m(\vartheta,\varphi)}{r\sin\vartheta}\Bigg\} r^2 \sin\vartheta\, \mathrm{d}r\, \mathrm{d}\vartheta\, \mathrm{d}\varphi.\end{aligned} \tag{4.33}$$

Next, the mixed field choice (2.130) for the displacement field is utilised. The complex conjugation was shown in equation (4.19). Note that the sign of ξ_φ^* is negative due to the complex conjugation and that the mode index m' of $\boldsymbol{\xi}_{m'}$ generally differs from the mode index m of the spherical harmonics describing $\delta\Phi$.

We insert (4.19) into (4.33) and split the spherical harmonics into polar and azimuthal parts according to definition (4.20). Further, the derivation with respect to φ is evaluated

as $\partial_\varphi \mathrm{e}^{\mathrm{i}m\varphi} = \mathrm{i}\,m\,\mathrm{e}^{\mathrm{i}m\varphi}$. Thus,

$$\delta W_{\mathrm{grav}}^{\mathrm{nC}} = -\sum_{\lambda=m}^{\infty} \frac{2\,\pi^2\,G}{2\,\lambda+1} \iiint \rho_0(r)\,\Re\Big\{\Big[\tilde{R}(r,\vartheta)\,r\sin\vartheta\,\mathrm{d}_r F_\lambda^m(r)\,\Theta_\lambda^m(\vartheta) + \tilde{S}(r,\vartheta)\,\sin\vartheta\,\cdot \\ F_\lambda^m(r)\,\partial_\vartheta\Theta_\lambda^m(\vartheta) - \mathrm{i}^2\,m\,\tilde{T}(r,\vartheta)\,F_\lambda^m(r)\,\Theta_\lambda^m(\vartheta)\Big]\mathrm{e}^{\mathrm{i}(m-m')\varphi}\Big\}\,r^2\sin\vartheta\,\mathrm{d}r\,\mathrm{d}\vartheta\,\mathrm{d}\varphi, \tag{4.34}$$

where the exponential terms have been factorised.

The exponential terms are the only complex contribution to the integrand. The real part can be evaluated utilising expression (A.32) while the azimuthal integration is carried out according to relation (A.10):

$$\delta W_{\mathrm{grav}}^{\mathrm{nC}} = -\sum_{\lambda=m}^{\infty} \frac{2\,\pi^2\,G}{2\,\lambda+1} \int_0^\pi\int_0^R \rho_0(r)\,\Big[\tilde{R}(r,\vartheta)\,r\,\mathrm{d}_r F_\lambda^m(r)\,\Theta_\lambda^m(\vartheta) \\ + \tilde{S}(r,\vartheta)\,F_\lambda^m(r)\,\partial_\vartheta\Theta_\lambda^m(\vartheta) + \frac{m\,\tilde{T}(r,\vartheta)}{\sin\vartheta}\,F_\lambda^m(r)\,\Theta_\lambda^m(\vartheta)\Big]\cdot \\ \underbrace{\frac{1}{2}\int_0^{2\pi}\left(\mathrm{e}^{\mathrm{i}(m-m')\varphi} + \mathrm{e}^{\mathrm{i}(m'-m)\varphi}\right)\mathrm{d}\varphi}_{2\pi(\delta_{mm'}+\delta_{m'm})}\,r^2\sin^2\vartheta\,\mathrm{d}r\,\mathrm{d}\vartheta. \tag{4.35}$$

Renaming m' as m, this is

$$\delta W_{\mathrm{grav}}^{\mathrm{nC}} = -\sum_{\lambda=m}^{\infty} \frac{4\pi^3 G}{2\,\lambda+1} \int_0^\pi\int_0^R \rho_0(r)\,\Big[\tilde{R}(r,\vartheta)\,r\,\mathrm{d}_r F_\lambda^m(r)\,\Theta_\lambda^m(\vartheta) + \tilde{S}(r,\vartheta)\,F_\lambda^m(r)\,\partial_\vartheta\Theta_\lambda^m(\vartheta) \\ + \frac{m\,\tilde{T}(r,\vartheta)}{\sin\vartheta}\,F_\lambda^m(r)\,\Theta_\lambda^m(\vartheta)\Big]\,r^2\sin^2\vartheta\,\mathrm{d}r\,\mathrm{d}\vartheta. \tag{4.36}$$

The radial derivative of $F_\lambda^m(r)$ is given by

$$\mathrm{d}_r\left[\frac{J_\lambda^m(r)}{r^{\lambda+1}} - r^\lambda K_\lambda^m(r)\right] = -\frac{\lambda+1}{r^{\lambda+2}}\,J_\lambda^m(r) - \lambda\,r^{\lambda-1}\,K_\lambda^m(r) \\ + (2\,\lambda+1)\,r\,\rho_0(r)\int_0^\pi \tilde{R}(r,\vartheta')\,\Theta_\lambda^m(\vartheta')\,\sin^2\vartheta'\,\mathrm{d}\vartheta', \tag{4.37}$$

as proven in the appendix section B.5.4.

We insert (4.37) as well as $F_\lambda^m(r)$ into (4.36) and sort the terms by the appearance of

$J_\lambda^m(r)$ and $K_\lambda^m(r)$ to obtain

$$\delta W_{\text{grav}}^{\text{nC}} = -\sum_{\lambda=m}^{\infty} 4\pi^3 G \int_0^\pi\!\!\int_0^R \rho_0^2(r)\, r^4\, \tilde{R}(r,\vartheta)\, \Theta_\lambda^m(\vartheta)\, \sin^2\vartheta\, I_\lambda^m(r)\, \mathrm{d}r\, \mathrm{d}\vartheta - \sum_{\lambda=m}^{\infty} \frac{4\pi^3 G}{2\lambda+1} \cdot \tag{4.38}$$
$$\int_0^\pi\!\!\int_0^R \left\{ -\frac{\rho_0(r)}{r^{\lambda-1}} \left((\lambda+1)\, \tilde{R}(r,\vartheta)\, \Theta_\lambda^m(\vartheta) - \tilde{S}(r,\vartheta)\, \partial_\vartheta \Theta_\lambda^m(\vartheta) - \frac{m\tilde{T}(r,\vartheta)}{\sin\vartheta}\, \Theta_\lambda^m(\vartheta) \right) J_\lambda^m(r) \right.$$
$$\left. - r^{\lambda+2}\, \rho_0(r) \left(\lambda\, \tilde{R}(r,\vartheta)\, \Theta_\lambda^m(\vartheta) + \tilde{S}(r,\vartheta)\, \partial_\vartheta \Theta_\lambda^m(\vartheta) + \frac{m\tilde{T}(r,\vartheta)}{\sin\vartheta}\, \Theta_\lambda^m(\vartheta) \right) K_\lambda^m(r) \right\} \cdot$$
$$\sin^2\vartheta\, \mathrm{d}r\, \mathrm{d}\vartheta,$$

with

$$I_\lambda^m(r) \equiv \int_0^\pi \tilde{R}(r,\vartheta')\, \Theta_\lambda^m(\vartheta')\, \sin^2\vartheta'\, \mathrm{d}\vartheta'. \tag{4.39}$$

Based on their definition in (4.29), the radial derivatives of $J_\lambda^m(r)$ and $K_\lambda^m(r)$ are

$$\mathrm{d}_r J_\lambda^m(r) = +\int_0^\pi \rho_0(r)\, r^{\lambda+2} \left[\left(\lambda\, \tilde{R}(r,\vartheta) + \frac{m\tilde{T}(r,\vartheta)}{\sin\vartheta} \right) \Theta_\lambda^m(\vartheta) \right. \tag{4.40a}$$
$$\left. + \tilde{S}(r,\vartheta)\, \partial_\vartheta \Theta_\lambda^m(\vartheta) \right] \sin^2\vartheta\, \mathrm{d}\vartheta$$
$$\mathrm{d}_r K_\lambda^m(r) = -\int_0^\pi \frac{\rho_0(r)}{r'^{\lambda-1}} \left[\left((\lambda+1)\, \tilde{R}(r,\vartheta) - \frac{m\tilde{T}(r,\vartheta)}{\sin\vartheta} \right) \Theta_\lambda^m(\vartheta) \right. \tag{4.40b}$$
$$\left. - \tilde{S}(r,\vartheta)\, \partial_\vartheta \Theta_\lambda^m(\vartheta) \right] \sin^2\vartheta\, \mathrm{d}\vartheta.$$

This result is derived in the appendix section B.5.5. Note that the polar angle represents an integration variable that can be named ϑ' as well as ϑ. Further note that $\mathrm{d}_r K_\lambda^m(r)$ is equivalent to the negative radial integrand in $K_\lambda^m(r)$ which follows from the definition of the integration boundaries in $K_\lambda^m(r)$.

The derivatives (4.40) can be identified in (4.38) and thus, the non-Cowling energy variation term is expressible as

$$\delta W_{\text{grav}}^{\text{nC}} = -\sum_{\lambda=m}^{\infty} 4\pi^3 G \int_0^\pi\!\!\int_0^R \rho_0^2(r)\, r^4\, \tilde{R}(r,\vartheta)\, \Theta_\lambda^m(\vartheta)\, \sin^2\vartheta\, I_\lambda^m(r)\, \mathrm{d}r\, \mathrm{d}\vartheta \tag{4.41}$$
$$- \sum_{\lambda=m}^{\infty} \frac{4\pi^3 G}{2\lambda+1} \int_0^R \left\{ \mathrm{d}_r K_\lambda^m(r)\, J_\lambda^m(r) - \mathrm{d}_r J_\lambda^m(r)\, K_\lambda^m(r) \right\} \mathrm{d}r.$$

This result can be further simplified by applying relation (B.71) derived in the appendix

section B.5.6:

$$\int_0^R \left\{ J_\lambda^m(r)\, \mathrm{d}_r K_\lambda^m(r) - K_\lambda^m(r)\, \mathrm{d}_r J_\lambda^m(r) \right\} \mathrm{d}r = -2 \int_0^R \mathrm{d}_r J_\lambda^m(r)\, K_\lambda^m(r)\, \mathrm{d}r. \tag{4.42}$$

Using expression (4.42) in (4.41), the alternate formulation of the additional energy variation term is

$$\begin{aligned} \delta W_{\mathrm{grav}}^{\mathrm{nC}} = &- \sum_{\lambda=m}^{\infty} 4\pi^3 G \int_0^\pi \int_0^R \rho_0^2(r)\, r^4\, \tilde{R}(r,\vartheta)\, \Theta_\lambda^m(\vartheta)\, \sin^2\vartheta\, I_\lambda^m(r)\, \mathrm{d}r\, \mathrm{d}\vartheta \\ &+ \sum_{\lambda=m}^{\infty} \frac{8\pi^3 G}{2\lambda+1} \int_0^R \mathrm{d}_r J_\lambda^m(r)\, K_\lambda^m(r)\, \mathrm{d}r. \end{aligned} \tag{4.43}$$

Finally, based on the results in equations (4.41) and (4.43) the non-Cowling contribution to the energy variation in the mixed field case is

$$\begin{aligned} \delta W_{\mathrm{grav}}^{\mathrm{nC}} = &- \sum_{\lambda=m}^{\infty} 4\pi^3 G \int_0^\pi \int_0^R \rho_0^2(r)\, r^4\, \tilde{R}(r,\vartheta)\, \Theta_\lambda^m(\vartheta)\, \sin^2\vartheta\, I_\lambda^m(r)\, \mathrm{d}r\, \mathrm{d}\vartheta \\ &- \sum_{\lambda=m}^{\infty} \frac{4\pi^3 G}{2\lambda+1} \int_0^R \left\{ \mathrm{d}_r K_\lambda^m(r)\, J_\lambda^m(r) - \mathrm{d}_r J_\lambda^m(r)\, K_\lambda^m(r) \right\} \mathrm{d}r \end{aligned} \tag{4.44a}$$

$$\begin{aligned} \delta W_{\mathrm{grav}}^{\mathrm{nC}} = &- \sum_{\lambda=m}^{\infty} 4\pi^3 G \int_0^\pi \int_0^R \rho_0^2(r)\, r^4\, \tilde{R}(r,\vartheta)\, \Theta_\lambda^m(\vartheta)\, \sin^2\vartheta\, I_\lambda^m(r)\, \mathrm{d}r\, \mathrm{d}\vartheta \\ &+ \sum_{\lambda=m}^{\infty} \frac{8\pi^3 G}{2\lambda+1} \int_0^R \mathrm{d}_r J_\lambda^m(r)\, K_\lambda^m(r)\, \mathrm{d}r, \end{aligned} \tag{4.44b}$$

with

$$I_\lambda^m(r) \equiv \int_0^\pi \tilde{R}(r,\vartheta')\, \Theta_\lambda^m(\vartheta')\, \sin^2\vartheta'\, \mathrm{d}\vartheta'. \tag{4.45}$$

Explicit non-Cowling contribution to the energy variation for the mixed field choice (2.130) **of ξ**

4.3. Numerical implementation

In this section, the numerical framework applied in this work will be presented.

Statement of the problem After the energy variation has been analytically prepared and extended in the previous sections, the total integral that needs to be solved is

$$\delta W = \delta W_{\mathrm{magn}} + \delta W_{\mathrm{fluid}} + \delta W_{\mathrm{grav}} \tag{4.46}$$

$$= \iiint \left\{ \mathcal{E}_{\mathrm{magn}} + \mathcal{E}_{\mathrm{fluid}} + \mathcal{E}_{\mathrm{grav}}^{\mathrm{Cowl}} \right\} \mathrm{d}V + \delta W_{\mathrm{grav}}^{\mathrm{nC}} \tag{4.47}$$

with

$$\mathcal{E}_{\mathrm{magn}} = \frac{1}{4} \Re \left\{ \frac{\delta \boldsymbol{B}^* \cdot \delta \boldsymbol{B}}{4\pi} - \boldsymbol{j}_0 \cdot \frac{\delta \boldsymbol{B} \times \boldsymbol{\xi}^*}{c} \right\}, \qquad \delta \boldsymbol{B} = \nabla \times (\boldsymbol{\xi} \times \boldsymbol{B}_0) \tag{4.48a}$$

$$\mathcal{E}_{\mathrm{fluid}} = \frac{1}{4} \Re \left\{ \Gamma_1 p_0 (\nabla \cdot \boldsymbol{\xi}^*) \, (\nabla \cdot \boldsymbol{\xi}) + \boldsymbol{\xi} \cdot \nabla p_0 (\nabla \cdot \boldsymbol{\xi}^*) \right\} \tag{4.48b}$$

$$\mathcal{E}_{\mathrm{grav}}^{\mathrm{Cowl}} = \pm \frac{1}{4} \Re \left\{ \boldsymbol{\xi} \cdot \nabla \Phi_0 (\nabla \cdot (\rho_0 \boldsymbol{\xi}^*)) \right\}. \tag{4.48c}$$

This form is composed of the original expressions for the energy variation (2.78) with (2.117) and the new fluid pressure contribution considering stratification in equation (4.6), as well as the additional non-Cowling term in the gravitational contribution (4.8).

In the mixed field case, $\delta W_{\mathrm{grav}}^{\mathrm{nC}}$ is given by equations (4.44b), (4.45) and (4.29):

$$\delta W_{\mathrm{grav}}^{\mathrm{nC}} = -\sum_{\lambda=m}^{\infty} 4\pi^3 G \int_0^{\pi} \int_0^{R} \rho_0^2(r) \, r^4 \, \tilde{R}(r,\vartheta) \, \Theta_\lambda^m(\vartheta) \, \sin^2\vartheta \, I_\lambda^m(r) \, \mathrm{d}r \, \mathrm{d}\vartheta \tag{4.49}$$

$$+ \sum_{\lambda=m}^{\infty} \frac{4\pi^3 G}{2\lambda+1} \int_0^{R} \mathrm{d}_r J_\lambda^m(r) \, K_\lambda^m(r) \, \mathrm{d}r$$

with

$$I_\lambda^m(r) = \int_0^{\pi} \tilde{R}(r,\vartheta') \, \Theta_\lambda^m(\vartheta') \, \sin^2\vartheta' \, \mathrm{d}\vartheta' \tag{4.50}$$

and

$$J_\lambda^m(r) = \int_0^{\pi} \int_0^{r} \rho_0(r') \, r'^{\lambda+2} \left[\left(\lambda \, \tilde{R}(r',\vartheta') + \frac{m \, \tilde{T}(r',\vartheta')}{\sin\vartheta'} \right) \Theta_\lambda^m(\vartheta') \right. \tag{4.51a}$$

$$\left. + \tilde{S}(r',\vartheta') \, \partial_{\vartheta'} \Theta_\lambda^m(\vartheta') \right] \sin^2\vartheta' \, \mathrm{d}r' \, \mathrm{d}\vartheta'$$

$$K_\lambda^m(r) = \int_0^{\pi} \int_r^{R} \frac{\rho_0(r')}{r'^{\lambda-1}} \left[\left((\lambda+1) \, \tilde{R}(r',\vartheta') - \frac{m \, \tilde{T}(r',\vartheta')}{\sin\vartheta'} \right) \Theta_\lambda^m(\vartheta') \right. \tag{4.51b}$$

$$\left. - \tilde{S}(r',\vartheta') \, \partial_{\vartheta'} \Theta_\lambda^m(\vartheta') \right] \sin^2\vartheta' \, \mathrm{d}r' \, \mathrm{d}\vartheta'.$$

As stated in section 2.2.3, we assume the model system to be axisymmetric. The symmetry reduces the number of integrations that need to be performed numerically in order to calculate δW by one. The integral over the azimuthal angle φ will be evaluated analytically, the same way it has been done in the J_λ^m- and K_λ^m-integrals in equation (4.35). The remaining numerical integration will be carried out in the (ϖ, z)-plane in cylindrical coordinates.

Explicit expression of the integrand In the course of the numerical integration, the continuous stellar volume is replaced by a discrete grid. At the grid points, the integrand value must be known numerically. That means, numerical values are required at these positions for all quantities appearing in the integrand.

According to the respective choice illustrated in section 2.3.3, the displacement field can be expressed as a function of constants, coordinates and $\boldsymbol{\xi}$-defining functions X and Z or $\tilde{R}$ and $\tilde{S}$. The $\boldsymbol{\xi}$-defining functions will be chosen as functions of constants, coordinates and also equilibrium system quantities Q_0, as shown by equations (2.122), (2.126), (2.132) and (2.133). The same applies for the magnetic field structure chosen in section 2.2.3.

At every integration grid point, we can allocate numerical values to these quantities depending on constants and coordinates, as long as the system quantities Q_0 are known. Considering this, the only remaining unknowns are the background system quantities pressure, density and gravitational potential.

Problem solving plan According to the statement of the problem in the previous paragraphs, we can give a problem solving plan and list the numerical methods that will be required.

First, we need to calculate the equilibrium quantities $Q_0(r)$ in the code before solving the integral. For this task, the system equations are numerically solved using the classical Runge-Kutta method, as it will be described in section 4.3.1.

The geometry of the grid points where the integrand is numerically known as provided by the system equations differs from the grid required for the two-dimensional integration. We thus need to calculate the numerical values of the system quantities at the required positions before the integration can be performed. This can be achieved by spatial interpolation, most conveniently employing cubic splines, as it will be explained in section 4.3.2.

Finally, a numerical integration algorithm based on Simpson's rule will be utilised. The algorithm is illustrated in section 4.3.3.

In the case of a full non-Cowling treatment, the $\delta\Phi$-describing radial functions J and K require additional integrations. Their computation is described in section 4.3.4.

The integration code for the calculation of δW has been set up successively and extended gradually to keep track of its functionality while the treatment of more complex systems was enabled. The code development process is depicted in section 4.3.5. The final code structure will be presented in section 4.3.6.

Remember that the dimensionless unit system introduced in section 2.2.2 is utilised in order to keep the astrophysical values, that are represented by large numbers, numerically treatable.

4.3.1. Solving the background system equations with Runge-Kutta

General problem The system equations given by expressions (2.26) form a first-order set of nonlinear ordinary explicit differential equations for the equilibrium quantities $Q_0(r) \in \{m_0(r), p_0(r), \Phi_0(r)\}$:

$$\mathrm{d}_r Q(r) = f(r, Q(r)) \qquad Q(r_0) = Q_0. \tag{4.52}$$

System of nonlinear ordinary differential equations

In this section, we will skip the lower index 0 denoting an equilibrium quantity, in order to avoid confusion. Instead, the index s labels the numerical grid points from $s = 0$ to $s = s(\max)$.

The exact boundary conditions are given at the stellar centre $r_0 = 0$. For the application, however, an approximation or exclusion of the central point will become necessary to avoid singularities if the numerical procedure requires terms involving $1/r_0$.

Further note that the structure of this problem would still be maintained in a relativistic or post-Newtonian approach based on TOV equations in future applications.

Runge-Kutta method A system of differential equations as shown in equation (4.52) can be solved applying the Runge-Kutta method which we prefer over a multistep method for convenience.

That means, starting from the boundary condition at the stellar centre, the solution Q_{s+1} at each numerical grid point $s+1$ is calculated based on the previously calculated solution Q_s of the neighbouring grid point s:

$$Q_{s+1} = Q_s + h_r \sum_{j=1}^{J} b_j \, k_j + \mathcal{O}\left(h_r^{J+1}\right) \qquad r_{s+1} = r_s + h_r \qquad s = 0, ..., s(\max). \tag{4.53}$$

***J*-th order Runge-Kutta method, solving the system of differential equations** (4.52)

The step width h_r is the distance between neighbouring grid points, b_j and k_j are prefactors and intermediate values of f, and J corresponds to the order of the Runge-Kutta method applied.

The classical forth order Runge-Kutta method ($J = 4$) provides an optimised ratio between effort and accuracy. Although the local truncation error of every iteration is of fifth order in h_r, the total error is of the order $\mathcal{O}(h_r^4)$. With this method, the solution of the differential equation is calculated on the basis of four intermediate stages k_j:

$$Q_{s+1} = Q_s + \frac{h_r}{6}\left(k_1 + 2k_2 + 2k_3 + k_4\right) + \mathcal{O}\left(h_r^4\right) \quad r_{s+1} = r_s + h_r \quad s = 0, ..., s(\max) \tag{4.54}$$

with

$$k_1 = f\left(r_s,\, Q_s\right) \tag{4.55a}$$

$$k_2 = f\left(r_s + \frac{h_r}{2},\, Q_s + \frac{h_r}{2}\, k_1\right) \tag{4.55b}$$

$$k_3 = f\left(r_s + \frac{h_r}{2},\, Q_s + \frac{h_r}{2}\, k_2\right) \tag{4.55c}$$

$$k_4 = f\left(r_s + h_r,\, Q_s + h_r\, k_3\right). \tag{4.55d}$$

Classical Runge-Kutta method, solving the system of differential equations (4.52)

In our case, the method is explicit and does not require the solution of further systems of equations.

Boundary conditions The application of the classical Runge-Kutta method for solving the background system equations (2.26) requires a detailed consideration of the problem and the establishment of numerically formulated boundary conditions.

The system equations (2.26) comprise three differential equations for equilibrium mass m_0, pressure p_0 and gravitational potential Φ_0. The mass density ρ is related to the pressure by the equation of state (2.22) and can easily be calculated once a solution for $p_0(r)$ has been found:

$$\rho(r) = \left(\frac{p(r)}{\kappa}\right)^{1/\Gamma_0}. \tag{4.56}$$

The neutron star is subject to the boundary conditions

$$m(r_0) = 0 \qquad p(R) = 0 \qquad \Phi(R) = \Phi_{\text{ext}}, \tag{4.57}$$

which can be explained as follows. The mass $m(r)$ included inside a sphere with radius r is zero for $r_0 = 0$. The fluid pressure drops to zero at the stellar surface $r_{s(\max)} = R$ matching the surrounding vacuum. The gravitational potential at the stellar surface $r_{s(\max)} = R$ equals the total gravitational potential Φ_{ext} a test particle experiences at the neutron star surface.

As explained above, the classical Runge-Kutta method operates by calculating the system quantities stepwise starting from a set of initial values.

We thus need to create a set of boundary conditions either located at the stellar centre or at the stellar surface. We choose to solve the equations from the inside outwards and set the solving pattern as follows.

First, the central density $\rho_c \equiv \rho_0 = \rho(r_0)$ is chosen appropriately to fit a typical neutron star density profile. From that, the polytropic equation of state (2.22) provides the central

pressure

$$p_c \equiv p_0 = p(r_0) = \kappa \rho_c^{\Gamma_0}. \tag{4.58}$$

The boundary condition for the gravitational potential at the stellar centre can be arbitrarily chosen as the third system equation is linear in Φ. The addition of a constant value to the solution $\Phi(r)$ can thus fulfil the surface boundary condition $\Phi(R) = \Phi_{\text{ext}}$.

Note that we skipped the equilibrium index again. The index $s = 0$ denotes the system quantity at the innermost grid point.

In order to avoid singularities in the numerical procedure, the initial radial grid point is located slightly off-centred by choosing $r_0 = r_c$ with $r_c \gtrsim 0$, for example $r_c = 10^{-5}$. That way, the possible singularity at $r = 0$ is excluded from the numerical grid. The initial mass follows from r_c and ρ_c by integration of system equation (2.26a):

$$\mathrm{d}_r m_0 = 4\pi r^2 \rho_c \qquad\qquad m_0 = \frac{4\pi}{3} {r_c}^3 \rho_c. \tag{4.59}$$

Altogether, the boundary conditions for the numerical procedure are

$$m_0 = \frac{4\pi}{3} {r_c}^3 \rho_c \qquad p_0 = \kappa \rho_c^{\Gamma_0} \qquad \Phi_0 = \Phi_c \qquad \text{with} \qquad r_0 = r_c \qquad \rho_0 = \rho_c. \tag{4.60}$$

Boundary conditions for the Runge-Kutta solving of the background system equations

Remember that the index 0 denotes the innermost grid point $s = 0$.

Numerical solving pattern Starting from suitable initial values established in the previous paragraph, the numerical solving scheme for the problem needs to be set up next.

The routine given by (4.54) and (4.55) solves the equations stepwise for increasing values of r_s. We store the solutions $m(r_s)$, $p(r_s)$ and r_s in order to receive a full radial profile of these quantities at discrete positions.

Note that currently we have no use for the gravitational potential inside the star. The gravitational potential enters the integrand (4.48) in the differentiated form via $(\boldsymbol{\xi} \cdot \nabla)\, \Phi_0$ only. According to the spherical symmetry of the equilibrium star, the only non-vanishing component of this expression is the radial one, $\xi_r\, \mathrm{d}_r \Phi_0$. The derivative $\mathrm{d}_r \Phi_0$ in this expression is given by the right hand side of the third system equation (2.26c). The Φ_0-dependent terms appearing in the integrand $\mathcal{E}$ can thus be fully expressed by p_0 and m_0. This is why we abstain from solving the third system equation. However, the code is capable of storing $\Phi(r_s)$ as well if needed and if it is supposed to fit an external value of the gravitational potential Φ_{ext}.

The solving iteration must stop when the stellar surface is reached at $r_s = R$ or $s = s(\max)$. This requirement can be translated into a numerical exit condition: The solving algorithm runs until the fluid pressure drops below a critical value $p_\varepsilon \gtrsim 0$, small enough to be a valid approximation of the vacuum pressure level. The computed pressure is checked in each iteration step. As long as it exceeds p_ε, that means $p(r_{s+1}) > p_\varepsilon$, the solving

algorithm continues. Once the fluid pressure equals the critical value or falls below it, i.e. $p(r_{s+1}) \leq p_\varepsilon$, the iteration stops. The value last computed for r is allocated to the stellar radius $R = r_s$. The mass included inside this radius is identified as the total stellar mass $M = m(r_s)$.

Applying the numerical scheme set up above, the variation of central density ρ_c, polytropic index Γ_0 and equation of state prefactor κ enables the construction of different compact objects, varying in mass M, radius R and compactness M/R.

In this work, we prefer specific models characterised by $(M, R, M/R)$ as code input over parameter sets of $(\rho_c, \Gamma_0, \kappa)$. The determination of stellar mass, radius and compactness is intuitively far more meaningful than choosing the internal density or the polytropic index. That way, the model star under investigation can directly be compared to compact objects from observations or other studies, naturally characterised by M, R and M/R.

The usage of $(M, R, M/R)$ as predefined values can be realised as follows. In preparatory code runs, various sets of input parameters have been tested to construct realistic neutron star models that are appropriate for the usage in this work. Using these results, the parameter values for ρ_c, Γ_0 and κ required for the construction of a desired model $(M, R, M/R)$, can be assigned. One further advantage of this procedure is that the numerical grid can be chosen in such a way that the outermost grid point $r_{s(\max)}$ coincides exactly with the given stellar radius R. The utilised step width h_r follows from R and the demanded number of grid points $s(\max)$. The exit condition is pre-fulfilled and the only remaining task during the code run is to compute and store the radial values $m(r_s)$ and $p(r_s)$.

4.3.2. Grid adjustment with cubic spline interpolation

Problem According to the spherical symmetry of the equilibrium system, the discrete solutions calculated with the Runge-Kutta method for the system quantities $Q(r_s)$ are located on concentric spheres with radii r_s. For constant φ, the positions of numerically known values form a poloidal grid. It is represented by a series of concentric semi-circles in the (ϖ, z)-plane and by a family of straight lines in the (r, ϑ)-plane, cf. figures 4.1a and 4.1b.

The numerical integration on the other hand will be performed on a non-equidistant cartesian grid in the (ϖ, z)-plane as shown in figure 4.1c. Currently, a universal number of z-grid points is utilised at every ϖ-grid point for convenience, resulting in an inhomogeneous spacing. In the long term, however, an equidistant cartesian grid can be utilised instead, resulting in a spatially homogeneous accuracy of the numerical integration.

Either way, the grid transformation from the Runge-Kutta-known points to the points demanded for the Simpson integration requires an interpolation of generally all system quantities.

Grid definition For the purpose of interpolating the Runge-Kutta calculated values to the integration grid, both grids need to be mathematically well defined.

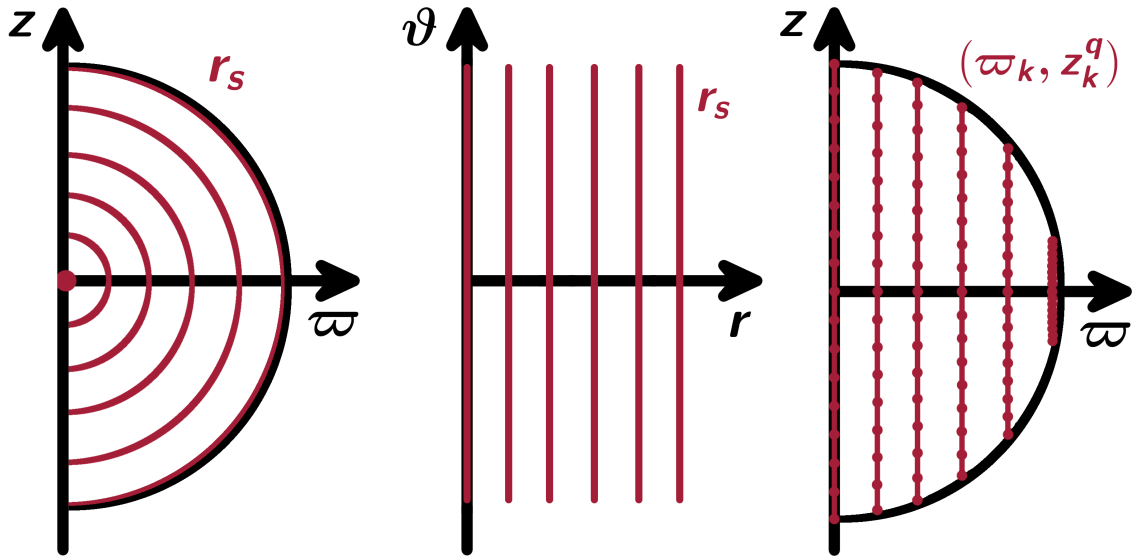

(a) Runge-Kutta grid in cylindrical coordinates.

(b) Runge-Kutta grid in spherical coordinates.

(c) Simpson integration grid in cylindrical coordinates.

Figure 4.1.: Grid of Runge-Kutta calculated values displayed in the (ϖ, z)-plane of cylindrical coordinates (a) and the (r, ϑ)-plane of spherical coordinates (b). Simpson integration grid in the (ϖ, z)-plane of cylindrical coordinates (c).

The original grid shown in figures 4.1a and 4.1b is defined by the Runge-Kutta solving scheme:

The number of intervals in r-direction is $s(\max)$ with an interval width h_r.
The grid is spherically symmetric. The grid points are located at

$$r_s = r_0 + s\,h_r \qquad \vartheta \text{ arbitrary}, \tag{4.61}$$

where $s(\max)$ is reasonably chosen and $s = 0, ..., s(\max)$.

Original Runge-Kutta grid in the (r, ϑ)-plane

The basic structure of the integration grid we choose for the (ϖ, z)-plane is shown in figure 4.1c. Along ϖ, the grid points (ϖ_k, z_k^q) are equidistant and labelled by the index $k = 0, ..., n_\varpi$. For each k, $n_z + 1$ grid points are spread along z, labelled by the index $q = 0, ..., n_z$. In this work, we use a universal number of intervals along z for all ϖ_k-knots, i.e. $n_z(k) = n_z \,\forall\, k$. Therefore, the grid points for different k are not equally spaced along z. As explained above, a cartesian grid could easily be constructed instead for future applications.

According to the requirement of the Simpson integration, the number of intervals in both directions must be even, i.e. $n_\varpi \mod 2 = 0$ and $n_z \mod 2 = 0$.

Beyond that, the numbers of intervals n_ϖ and n_z need to be chosen large enough to provide a sufficient level of accuracy in the numerical integration while keeping the effort and calculation time still reasonable.

Finally, the integration grid should be in reasonable proportion to the Runge-Kutta grid with $s(\max)$ grid points. The accuracy cannot be increased arbitrarily by refining the integration grid, it is ultimately determined by the Runge-Kutta background computation. In the extreme case of very small localisation areas, we allow for the situation that all grid points utilised in the (ϖ, z)-integration stem from interpolations of one single Runge-Kutta grid point r_s. In other cases with spatially extended integration areas, this scenario should be avoided in order to guarantee a sufficient level of accuracy.

According to this considerations, the integration grid we choose for the (ϖ, z)-plane can be constructed as follows.

The numbers of intervals along ϖ and z are

$$n_\varpi = \frac{s(\max)}{u_\varpi} \begin{cases} +0 & \text{if } \frac{s(\max)}{u_\varpi} \text{ even} \\ +1 & \text{if } \frac{s(\max)}{u_\varpi} \text{ odd} \end{cases} \qquad n_z = \frac{s(\max)}{u_z} \begin{cases} +0 & \text{if } \frac{s(\max)}{u_z} \text{ even} \\ +1 & \text{if } \frac{s(\max)}{u_z} \text{ odd} \end{cases} \tag{4.62}$$

with the according interval widths

$$h_\varpi = \frac{\varpi(\max) - \varpi(\min)}{n_\varpi} \qquad h_z(k) = \frac{z_k(\max) - z_k(\min)}{n_z}, \tag{4.63}$$

where $\varpi(\max)$, $\varpi(\min)$, $z_k(\max)$ and $z_k(\min)$ denote the upper and lower boundaries of the grid along ϖ and z. The grid points are located at

$$\varpi_k = \varpi_0 + k\, h_\varpi \qquad z_k^q = z_k^0 + q\, h_z(k), \tag{4.64}$$

where $k = 0, ..., n_\varpi$ and $q = 0, ..., n_z$.

Numerical integration grid for the δW-calculation in the (ϖ, z)-plane, general form

Note that the interval size $h_z(k)$ along z depends on the ϖ-index k. The numerical factors u_ϖ and u_z determine the choice of n_ϖ and n_z on the basis of $s(\max)$.

Simpson integration grids applied in this work Based on the general form for the Simpson grid in cylindrical coordinates, the concrete two-dimensional integration areas applied in this work can be defined.

Depending on the individual system the semi-analytic method is applied to, cf. chapter 5, we will use different choices for the numerical integration area.

For the application on purely toroidally magnetised neutron stars in section 5.1, the three-dimensional integration area we chose extends over the full stellar volume. The reason is that the localisation of the displacement field described in equation (2.124) keeps the computation time manageable. There is no need for an integration area reduction. Beyond that, we do not expect singularities inside the integration area that might perturb the integration result.

The subsequent two-dimensional area for the numerical integration in the (ϖ, z)-plane corresponds to one half of the stellar cross section.

The integration boundaries are given by

$$\varpi^i = 0 \qquad z_k^i = -\sqrt{R^2 - \varpi_k^2} \tag{4.65}$$
$$\varpi^f = R \qquad z_k^f = +\sqrt{R^2 - \varpi_k^2}.$$

Numerical integration boundaries for the δW-calculation in the toroidal field case

The indices i and f denote initial and final integration bounds.

The explicit integration grid follows from the general form shown by (4.62), (4.63) and (4.64):

The explicit interval widths are

$$h_\varpi = \frac{R}{n_\varpi} \qquad h_z(k) = \frac{2\sqrt{R^2 - \varpi_k^2}}{n_z}. \tag{4.66}$$

The grid points are located at

$$\varpi_k = \varpi_{\text{init}} + k\, h_\varpi \qquad z_k^q = z_{\text{mid}} + \left(q - \frac{n_z}{2}\right) h_z(k), \tag{4.67}$$

where $k = 0, ..., n_\varpi$ and $q = 0, ..., n_z$, $\varpi_{\text{init}} = 0$ and $z_{\text{mid}} = 0$.

Numerical integration grid for the δW-calculation in the toroidal field case

The chosen integration area is symmetric to the equator. The grid point $(\varpi_0, z_0^{n_z/2}) = (0, 0)$ is located at the stellar centre and for constant k, the z_k^q-grid points are arranged axisymmetrically with respect to the ϖ-axis: $z_k^0 = -z_k^{n_z}$ etc.

For the poloidal field application shown in section 5.2, we assume the integration area to be identical to the localisation area of the displacement field. In three dimensions, its shape is the torus around the symmetry axis including the neutral line. It is given by equation (2.129). In two dimensions, it is illustrated in figure 2.16. With this choice, possible singularities at the stellar symmetry axis are excluded from the integration area.

The integration boundaries are given by

$$\varpi^i = R_{\text{tor}} - \bar{r}_{\text{tor}} \qquad z_k^i = -\sqrt{\bar{r}^2 - (R_{\text{tor}} - \varpi)^2} \tag{4.68}$$
$$\varpi^f = R_{\text{tor}} + \bar{r}_{\text{tor}} \qquad z_k^f = +\sqrt{\bar{r}^2 - (R_{\text{tor}} - \varpi)^2}.$$

Numerical integration boundaries for the δW-calculation in the poloidal field case

For the application on stars with mixed magnetic fields and stratification, described in section 5.3, the integration area chosen for the δW-computation extends over the entire stellar volume.

The two-dimensional area for the numerical integration is equivalent to the toroidal field case (4.65).

The integration boundaries are given by

$$\begin{aligned} \varpi^i &= 0 & z_k^i &= -\sqrt{R^2 - \varpi_k^2} \\ \varpi^f &= R & z_k^f &= +\sqrt{R^2 - \varpi_k^2}. \end{aligned} \tag{4.69}$$

Numerical integration boundaries for the δW-calculation in the mixed field case

However, in the case of the full non-Cowling treatment, a smaller integration area will be applied in the mixed field case for the computation of J and K. That way, the computation time is reduced. This procedure will be described in section 4.3.4.

Spline interpolation For the purpose of performing the transformation from the Runge-Kutta grid to the integration grid, we will make use of a spline interpolation.

It is based on the approximation of an exact function $Q(r)$ by polynomials. The full domain is divided into intervals where the function is represented by different polynomials $P_s(r)$ inside each interval $[s, s+1]$. The interpolation accuracy increases with the degree of the employed polynomials.

The cubic spline interpolation that is used here is a specifically favourable method, since it provides a comparably small error for low efforts.

It is based on polynomials of third degree. Polynomials of neighbouring intervals are matched at the grid points as well as their first and second derivatives:

$$P_s(r) = P_{s+1}(r) \qquad \mathrm{d}_r P_s(r) = \mathrm{d}_r P_{s+1}(r) \qquad d_r^2 P_s(r) = d_r^2 P_{s+1}(r). \tag{4.70}$$

The additional condition of fitting derivatives increases the interpolation accuracy over the expected value for third degree polynomials. Under certain circumstances, the interpolation can even be exact. The method is illustrated in the appendix section D.1.

Implementation In order to apply the cubic spline interpolation to our specific problem, an implementation plan must be determined.

First, we need to specify the coordinate system we want to perform the interpolation in. According to the geometry of the neutron star and its magnetic field, reasonable options are cylindrical coordinates or spherical coordinates. It is more convenient to use spherical coordinates for the following reasons.

For one thing, spherical coordinates provide the advantage that the known points form a cartesian grid in the (r, ϑ)-plane, as can be seen in figure 4.1b. This allows for a straightforward choice of interpolation intervals. The cartesian structure of the original grid strongly

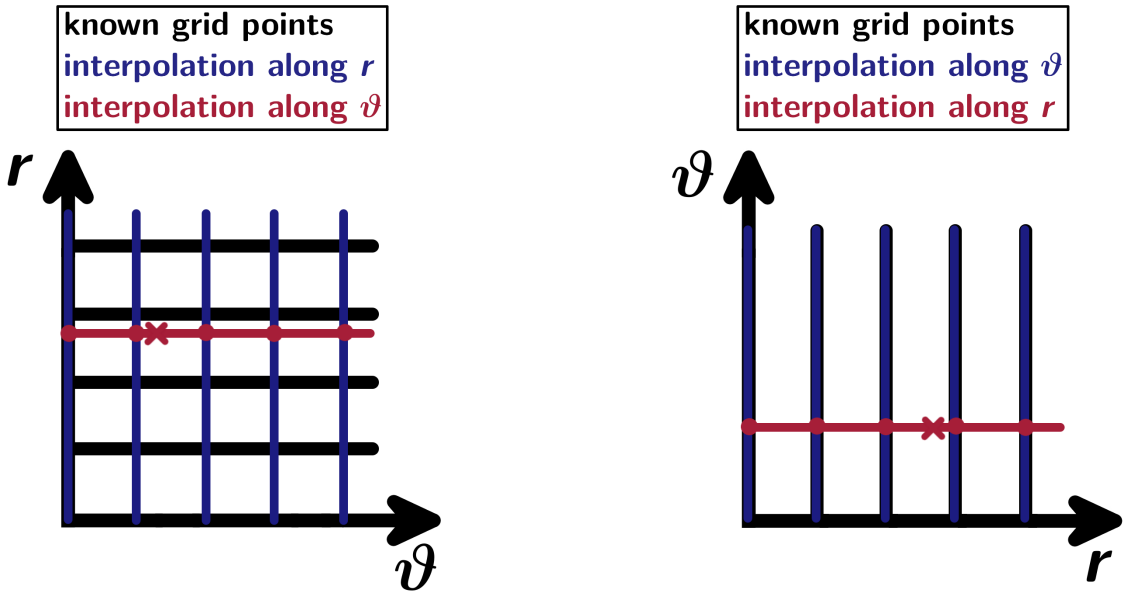

(a) Interpolation first along r.

(b) Interpolation first along ϑ.

Figure 4.2.: Two-dimensional spline interpolation in the the (r, ϑ)-plane of spherical coordinates. If the interpolation is first executed along r, cubic splines need to be utilised twice (a). If the continuously known values along ϑ are utilised instead of the first interpolation, cubic splines are only required along r (b).

simplifies the procedure, because the interpolation method relies on reasonably structured intervals.

The final grid, on the other hand, does not need to show any kind of structure, because the final grid points can be calculated at arbitrary positions.

Furthermore, the spherical symmetry of the system background quantities $m_0(r)$, $p_0(r)$, $\rho_0(r)$ and $\Phi_0(r)$ can be exploited in spherical coordinates by reducing the number of required interpolation processes by one. This becomes obvious with the following explanation.

The required grid transformation takes place on a two-dimensional plane. Therefore, generally two spline interpolations are necessary. In spherical coordinates, the interpolation can either be first performed along r or be first performed along ϑ, cf. figure 4.2.

If the interpolation is first performed along the r-coordinate, the determined intermediate grid points can be used to perform a second spline interpolation along ϑ afterwards. According to the spherical symmetry, all splines along r are identical, which provides a calculation advantage.

However, if we decide to first interpolate along ϑ and then along r, we find that the first interpolation is not necessary at all. The Runge-Kutta calculated values form a discrete grid in the r-direction, but they provide continuous values along ϑ.

One single cubic spline interpolation along r is therefore sufficient to find the required values at every (r, ϑ)- or (ϖ, z)-position inside the star.

It is thus sufficient to perform a one-dimensional cubic spline interpolation along r.

The interval boundaries coincide with the grid points of the numerically computed system quantities. The interval width is given by the Runge-Kutta step width h_r with equidistant grid points, $h_s = h_r \; \forall \; s$.

Based on the general formulas (D.1), (D.5) and (D.10) given in the appendix, the specific procedure we apply in this work is as follows.

System quantities $Q(r)$ are interpolated by

$$Q(r) = a_s\,(r - r_s)^3 + b_s\,(r - r_s)^2 + c_s\,(r - r_s) + d_s \qquad h_s = r_{s+1} - r_s, \tag{4.71}$$

with the interpolation coefficients

$$a_s = \frac{S_{s+1} - S_s}{6\,h_r} \qquad b_s = \frac{S_s}{2} \qquad c_s = \frac{Q_{s+1} - Q_s}{h_r} - \frac{2\,h_r\,S_s + h_r\,S_{s+1}}{6} \qquad d_s = Q_s \tag{4.72}$$

$\forall\; s = 0, ..., n-1$ and the linear system of equations for $S_0, ..., S_n$:

$$\left(\begin{array}{ccccccccc|c}
6 & 0 & 0 & 0 & ... & 0 & 0 & 0 & 0 & 6/h\,(Q_2 - 2\,Q_1 + Q_0) \\
h_r & 4\,h_r & h_r & 0 & ... & 0 & 0 & 0 & 0 & 6/h\,(Q_3 - 2\,Q_2 + Q_1) \\
0 & h_r & 4\,h_r & h_r & ... & 0 & 0 & 0 & 0 & 6/h\,(Q_4 - 2\,Q_3 + Q_2) \\
... & ... & ... & ... & ... & ... & ... & ... & ... & ... \\
0 & 0 & 0 & 0 & ... & h_r & 4\,h_r & h_r & 0 & 6/h\,(Q_{n-2} - 2\,Q_{n-3} + Q_{n-4}) \\
0 & 0 & 0 & 0 & ... & 0 & h_r & 4\,h_r & h_r & 6/h\,(Q_{n-1} - 2\,Q_{n-2} + Q_{n-3}) \\
0 & 0 & 0 & 0 & ... & 0 & 0 & 0 & 6 & 6/h\,(Q_n - 2\,Q_{n-1} + Q_{n-2})
\end{array}\right) \tag{4.73}$$

Cubic spline interpolation with linear extrapolation at the boundaries.

The linear system of equations (4.73) is tridiagonal and diagonally dominant. It can be solved applying the Gauß-Seidel method explained below.

Gauß-Seidel method

The Gauß-Seidel method is an iterative routine for the solution of linear systems of equations.

It is based on the procedure of solving the i-th system equation for the unknown S_i in each iteration step, taking into account the variables S_j with $j < i$ that have previously been calculated during this step.

The linear system of equations

$$\begin{array}{ccccccc}
a_{00}\,S_0 & + & ... & + & a_{0n}\,S_n & = & b_0 \\
a_{10}\,S_0 & + & ... & + & a_{1n}\,S_n & = & b_1 \\
... & + & ... & + & ... & = & ... \\
a_{n0}\,S_0 & + & ... & + & a_{nn}\,S_n & = & b_n
\end{array} \tag{4.74}$$

is approximately solved by the solution vector $\boldsymbol{S}^{(m)}$ in the m-th iteration. In the $(m+1)$-th

iteration, the components of the solution vector are

$$S_i^{(m+1)} = \frac{1}{a_{ii}} \left(b_i - \sum_{j=0}^{i-1} a_{ij} S_j^{(m+1)} - \sum_{j=i+1}^{n} a_{ij} S_j^{(m)} \right), \qquad i = 0, ..., n. \tag{4.75}$$

With an increasing number of iterations, the solution vector approaches the exact solution. The method converges definitely if the linear system of equations is diagonally dominant. This is especially the case for the system given in expression (4.73).

4.3.3. Computing the energy variation with Simpson's integration method

Simpson method For the actual integration part of the code we draw on Simpson's $h/3$-rule in two dimensions.

According to this method, the integrand is approximated by different polynomials in different intervals of the integration area. The integral value follows as the sum of their contributions.

The approximation error of the method is of forth order, although the applied polynomials are only of second degree. The reason is that the third order error term vanishes. The method thus features an optimised ratio between effort and accuracy.

Symmetry The neutron stars investigated in this work are represented by a three-dimensional model system in axisymmetry. Thanks to the symmetry, one of the integrals required to calculate the energy variation (4.47) can be solved analytically.

After the φ-integration has been carried out, the ϖ- and z-integral in cylindrical coordinates, or the r- and ϑ-integral in spherical coordinates, respectively, remain to be evaluated numerically. In order to perform the two-dimensional integration, Simpson's method is applied twice here.

Implementation The integration grid we use in cylindrical coordinates has been defined in section 4.3.2. Based on that, the numerical integration can be mathematically formulated.

Expressed in cylindrical coordinates, the integral we need to solve is

$$I = \iint f(\varpi, z)\, \mathrm{d}z\, \mathrm{d}\varpi. \tag{4.76}$$

First, we apply Simpson's method on the inner z-integral for all ϖ-grid points k. Afterwards, the results for $k = 0, ..., n_\varpi$ are entered as integrand values into the Simpson formula of the outer ϖ-integral.

According to that, the approximated integral is

$$I = \frac{h_\varpi}{3}\left(G_0 + 4\sum_{j=0}^{\frac{n_\varpi}{2}-1} G_{2j+1} + 2\sum_{j=1}^{\frac{n_\varpi}{2}-1} G_{2j} + G_{n_\varpi} \right) + \mathcal{O}(h_\varpi^4), \quad G_k \equiv G(\varpi_k) \tag{4.77a}$$

$$G_k = \frac{h_z}{3}\left(f_k^0 + 4\sum_{j=0}^{\frac{n_z}{2}-1} f_k^{2j+1} + 2\sum_{j=1}^{\frac{n_z}{2}-1} f_k^{2j} + f_k^{n_z} \right) + \mathcal{O}(h_z^4), \qquad f_k^q \equiv f(z_k^q). \tag{4.77b}$$

Two-dimensional Simpson integration in the (ϖ, z)-plane in cylindrical coordinates

Remember that lower indices denote ϖ-grid points labelled by k, and upper indices denote z-grid points labelled by q.

In this work, we are going to compute the energy variation integral (4.47) in cylindrical coordinates based on the framework set up in this section.

However, the integration can equally be performed in spherical coordinates. In this case, the corresponding integration grid and Simpson procedure are equivalent to the ones we use for the calculation of the radial functions J and K. Their computation will be performed in spherical coordinates as shown in the subsequent section.

Computational effort The two-dimensional numerical integration requires a noticeable amount of computation time compared to a one-dimensional integration. However, for the problems considered in this work and the achieved accuracies, the computational effort is still limited and manageable.

For future treatments of actual three-dimensional systems, the numerical integration will still be feasible in finite computation time. In this case, however, one might consider the precalculation and storing of certain terms, to directly use their values when needed. That way, it will not be necessary to re-solve all system equations for each new parameter combination we choose. This idea requires a detailed investigation on which terms stay unchanged during the variation of certain parameters.

4.3.4. Calculation of the radial functions J_λ^m and K_λ^m in $\delta W_{\mathsf{grav}}^{\mathsf{nC}}$

Problem The numerical scheme set up in the previous section is suitable to calculate the energy variation in Cowling approximation. For a full non-Cowling description of the system, however, the radial functions J and K need to be known at all grid points r_s in order to compute δW.

The calculation of J and K strongly depends on the choice we make for the displacement field. In the case of the mixed field choice for $\boldsymbol{\xi}$, the additional integral I_λ^m, given by expression (4.45), needs to be computed as well.

Note that in this section, J and K will be named in the general form without indices as long as we do not specify a particular choice for the displacement field.

If $\boldsymbol{\xi}$ is expressed by spherical harmonics according to choice (2.136), there are two options

to calculate the radial functions given by equation (4.13):

$$J_l(r) = \int_0^r \rho_0(r')\, r'^l \left[l\, \frac{g(r')}{r'} + d_{r'} h(r') \right] \mathrm{d}r' \tag{4.78a}$$

$$K_l(r) = \int_r^R \frac{\rho_0(r')}{r'^{l+1}} \left[(l+1)\, \frac{g(r')}{r'} - d_{r'} h(r') \right] \mathrm{d}r'. \tag{4.78b}$$

The first and obvious possibility is to compute these integrals numerically, for example applying the Simpson method in one dimension.

On the other hand, the derivatives $\mathrm{d}_r J_l$ and $\mathrm{d}_r K_l$ are related to the integrands in the following way:

$$\mathrm{d}_r J_l(r) = +j_l(r) = \rho_0(r)\, r^l \left[\frac{l\, g(r)}{r} + d_r h(r) \right] \tag{4.79a}$$

$$\mathrm{d}_r K_l(r) = -k_l(r) = -\frac{\rho_0(r)}{r^{l+1}} \left[(l+1)\, \frac{g(r)}{r} - d_r h(r) \right], \tag{4.79b}$$

as shown in the appendix equation (B.42). With this formulation, the second option becomes evident: J_l and K_l can be calculated as solutions of one-dimensional ordinary differential equations (4.79), for example applying the classical Runge-Kutta method.

Both numerical procedures have already been implemented in the code as explained in sections 4.3.1 and 4.3.3. Therefore, the basis to apply the methods in a straightforward way is prepared.

Tests showed that both procedures provide comparable results regarding accuracy and computing time. The second option of the Runge-Kutta treatment is thus preferable to the Simpson integration due to its reduced programming effort.

In this work, however, we are going to remove the Cowling approximation for the neutron star model with mixed magnetic fields, where the displacement field obeys the specific choice (2.130). J_λ^m and K_λ^m are given by equations (4.51).

According to equations (4.40), their radial derivatives are

$$\mathrm{d}_r J_\lambda^m(r) = + \int_0^\pi \rho_0(r)\, r^{\lambda+2} \left[\left(\lambda\, \tilde{R}(r,\vartheta) + \frac{m\, \tilde{T}(r,\vartheta)}{\sin\vartheta} \right) \Theta_\lambda^m(\vartheta) \right. \tag{4.80a}$$
$$\left. + \tilde{S}(r,\vartheta)\, \partial_\vartheta \Theta_\lambda^m(\vartheta) \right] \sin^2\vartheta\, \mathrm{d}\vartheta$$

$$\mathrm{d}_r K_\lambda^m(r) = - \int_0^\pi \frac{\rho_0(r)}{r'^{\lambda-1}} \left[\left((\lambda+1)\, \tilde{R}(r,\vartheta) - \frac{m\, \tilde{T}(r,\vartheta)}{\sin\vartheta} \right) \Theta_\lambda^m(\vartheta) \right. \tag{4.80b}$$
$$\left. - \tilde{S}(r,\vartheta)\, \partial_\vartheta \Theta_\lambda^m(\vartheta) \right] \sin^2\vartheta\, \mathrm{d}\vartheta.$$

In contrast to the previous case where $\boldsymbol{\xi}$ was expressed by spherical harmonics, these equations are no ordinary differential equations. The application of a Runge-Kutta method would still require the integration over the polar angle ϑ.

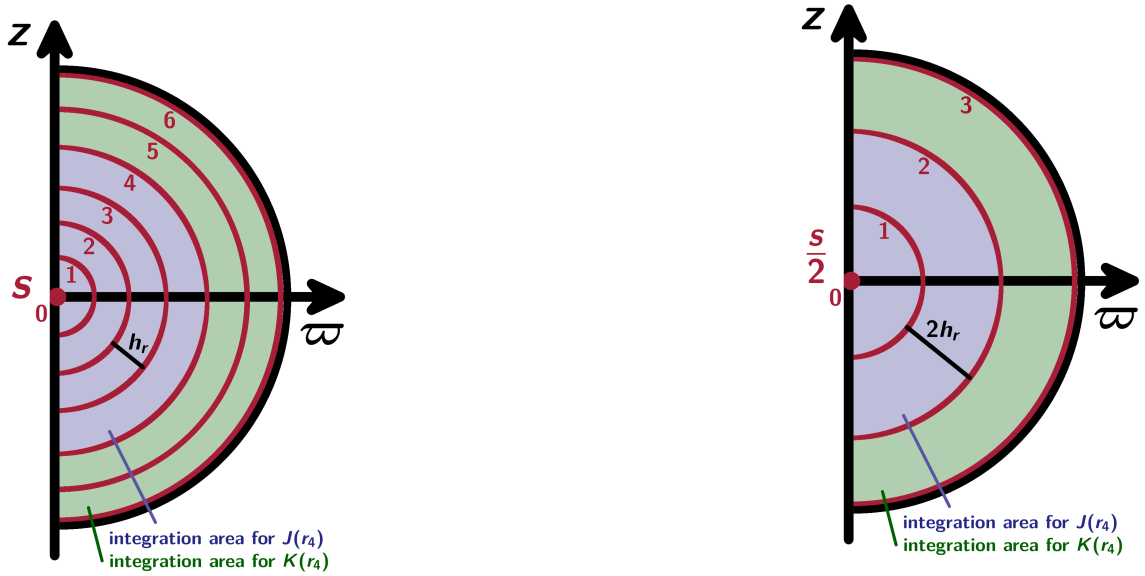

(a) Runge-Kutta grid.

(b) Integration grid for the (J, K)-calculation.

Figure 4.3.: The step width of the (J, K)-calculation grid (b) is twice as large as in the Runge-Kutta grid of the background quantities (a) in order to guarantee an even number of intervals for the radial Simpson integration. In this highly simplified sketch, it is $s(\max) = 6$.

Therefore in this work, J_λ^m and K_λ^m will be entirely calculated by Simpson integrations in two dimensions.

Integration grid In analogy to the integration grid set up in cylindrical coordinates for the computation of δW in section 4.3.3, we now define an integration grid in spherical coordinates for the J, K-calculation.

We first need to choose an adequate set of known points we can base the integration on. Remember the original Runge-Kutta grid (4.61) of known background quantities. It consists of $s(\max)$ intervals of width h_r and grid points r_s, as shown in figure 4.1b. The background quantities are known at the concentric spheres forming the Runge-Kutta grid. We are going to place the (J, K)-integration grid points inside this set. That way, all required quantities for the J- and K-calculation are directly known at the (J, K)-Simpson grid points without further interpolation, cf. figure 4.3.

Secondly, we need to consider the points where the computed values of J and K are required. Equation (4.47) shows that the δW-calculation requires computed values of J and K at all δW-Simpson integration grid points (ϖ_k, z_k^q). We will therefore compute J and K for all Runge-Kutta grid points r_s where the equilibrium quantities are known as well. Afterwards, the computed values for $J(r_s)$ and $K(r_s)$ will be interpolated to the cylindrical integration grid points (ϖ_k, z_k^q), applying the same procedure we established for the background quantities in section 4.3.2.

In order to construct the radial structure of the (J, K)-integration grid, the geometry

of J and K needs to be considered. In comparison to the energy variation integral, the calculation of J and K shows one decisive difference: Integrals (4.51a) and (4.51b) are not onetime integrations extending from the stellar centre $r = 0$ to the surface $r = R$, but they need to be computed for different integration areas $[0, r_s]$ in the case of J and $[r_s, R]$ in the case of K, with $s = 0, ..., s(\max)$.

For the calculation of $J(r_s)$ and $K(r_s)$, we are going to utilise a two-dimensional Simpson method. It is based on the even grid points of the Runge-Kutta grid. For each value of r_s, the upper integral boundary for the $J(r_s)$-calculation and the lower integral boundary for the $K(r_s)$-calculation are determined by the respective grid point r_s itself.

With this approach, the necessary condition of an even number of intervals for the radial Simpson integration can only be fulfilled for even grid points $s = 2$, $s = 4$, ..., $s = s(\max)$ in the J-calculation and $s = 0$, $s = 2$, ..., $s = s(\max) - 2$ in the K-calculation. This is why the utilised (J, K)-integration grid has a doubled step width $2\,h_r$ compared to the Runge-Kutta grid. Apart from that, both grids are congruent as can be seen in figure 4.3. Once J and K have been computed for the even Runge-Kutta grid points, they are interpolated to the uneven grid points $s = 1$, $s = 3$, ..., $s = s(\max) - 1$.

Besides its radial structure, the (J, K)-integration grid must provide a discrete angular structure as well, in order to enable the angular integration. Due to the spherical symmetry of the background, the equilibrium quantities are independent of ϑ. That means, the angular position of the (J, K)-integration grid points can be chosen arbitrarily inside the Runge-Kutta set of concentric spheres. We choose an even number n_ϑ of intervals in the ϑ-direction and set the interval width h_ϑ and grid point location ϑ_s subsequently.

Overall, the integration grid we use for J and K in the (r, ϑ)-plane is described as follows.

The integration boundaries are given by

$$\begin{aligned} r^i &= (x_0 - \delta_r)\, R & \qquad \vartheta^i &= \vartheta_0 - \delta_\vartheta \\ r^f &= (x_0 + \delta_r)\, R & \qquad \vartheta^f &= \vartheta_0 + \delta_\vartheta . \end{aligned} \tag{4.81}$$

Numerical integration boundaries for the J^m_λ-, K^m_λ-calculation in the (r, ϑ)-plane

We choose an integration area that is slightly bigger than the localisation region given by equation (2.135), cf. figure 2.17. For convenience, the integration area has a rectangular shape in the (r, ϑ)-plane. The extent of the integration area is kept small because in the mixed field case, the calculation of J and K requires additional integrations for each grid point.

Additionally, the explicit integration grid for the J_λ^m- and K_λ^m-computation is defined.

For the Simpson integration, the number of intervals along r is $\bar{n}_r = \frac{s(\max)}{2}$.

The number n_ϑ of intervals along ϑ is arbitrarily chosen by

$$n_\vartheta = \frac{s(\max)}{u_\vartheta} \begin{cases} +0 & \text{if } \frac{s(\max)}{u_\vartheta} \text{ even} \\ +1 & \text{if } \frac{s(\max)}{u_\vartheta} \text{ odd.} \end{cases} \tag{4.82}$$

The according interval widths and grid point locations are given by

$$2\,h_r = \frac{R}{\bar{n}_r} \qquad h_\vartheta = \frac{\pi}{n_\vartheta} \qquad r_{\bar{s}} = r_{\min} + 2\,\bar{s}\,h_r \qquad \vartheta^t = \vartheta_{\min} + t\,h_\vartheta, \tag{4.83}$$

where $\bar{s} = 0, ..., \bar{n}_r$ and $t = 0, ..., n_\vartheta$.

The computed values of J and K are next interpolated to a finer grid described by

$$h_r = \frac{R}{n_r} \qquad h_\vartheta = \frac{\pi}{n_\vartheta} \qquad r_s = r_{\min} + s\,h_r \qquad \vartheta^t = \vartheta_{\min} + t\,h_\vartheta, \tag{4.84}$$

where $s = 0, ..., n_r = s(\max)$ and $t = 0, ..., n_\vartheta$.

Numerical integration grid for the J_λ^m-, K_λ^m-calculation in the (r, ϑ)-plane

The numerical factor u_ϑ determines the choice of n_ϑ on the basis of $s(\max)$.

Simpson integration In analogy to the approximated integral (4.77) in cylindrical coordinates, the two-dimensional integral (4.51) will be calculated by a twice-done application of the Simpson method.

The J- and K-integrals in spherical coordinates can be expressed by

$$I = \iint f(r, \vartheta)\,\mathrm{d}\vartheta\,\mathrm{d}r. \tag{4.85}$$

They are approximately solved by

$$I = \frac{2\,h_r}{3}\left(G_0 + 4 \sum_{j=0}^{\frac{\bar{n}_r}{2}-1} G_{2j+1} + 2 \sum_{j=1}^{\frac{\bar{n}_r}{2}-1} G_{2j} + G_{\bar{n}_r} \right) + \mathcal{O}((2\,h_r)^4), \quad G_{\bar{s}} \equiv G(r_{\bar{s}}) \tag{4.86a}$$

$$G_k = \frac{h_\vartheta}{3}\left(f_{\bar{s}}^0 + 4 \sum_{j=0}^{\frac{n_\vartheta}{2}-1} f_{\bar{s}}^{2j+1} + 2 \sum_{j=1}^{\frac{n_\vartheta}{2}-1} f_{\bar{s}}^{2j} + f_{\bar{s}}^{n_\vartheta} \right) + \mathcal{O}(h_\vartheta^4), \qquad f_{\bar{s}}^t \equiv f(\vartheta_{\bar{s}}^t). \tag{4.86b}$$

Two-dimensional Simpson integration in the (r, ϑ)-plane in spherical coordinates

In the mixed field case, the calculation of $\delta W_{\mathrm{grav}}^{\mathrm{nC}}$ shown in equation (4.49) requires not only the computation of J_λ^m and K_λ^m, but the computation of the additional integral I_λ^m shown in expression (4.50) as well.

It will be calculated in a one-dimensional Simpson integration along ϑ for all radial grid points r_s. The integration grid we use is equivalent to the angular part of the integration grid (4.83) utilised for the $(J_\lambda^m, K_\lambda^m)$-computation.

If the additional integral (4.50) is expressed by

$$I_s = \int f(r, \vartheta)\, \mathrm{d}\vartheta, \tag{4.87}$$

it can be approximately solved by

$$I_s = \frac{h_\vartheta}{3}\left(f_s^0 + 4 \sum_{j=0}^{\frac{n_\vartheta}{2}-1} f_s^{2j+1} + 2 \sum_{j=1}^{\frac{n_\vartheta}{2}-1} f_s^{2j} + f_s^{n_\vartheta} \right) + \mathcal{O}(h_\vartheta^4), \qquad f_s^t \equiv f(r_s, \vartheta_s^t). \tag{4.88}$$

One-dimensional Simpson integration along ϑ in spherical coordinates

Reduction of the computational effort The calculation pattern described here for the mixed field case includes $s(\max)/2$ two-dimensional numerical integrations for J_λ^m and the same number of two-dimensional integrations for K_λ^m that need to be executed before the actual δW-computation can be performed.

The computation time required for two-dimensional integrations is significant, as discussed in the previous section 4.3.3. Therefore, the non-Cowling part will become the decisive term determining the computation time. It is thus desired to find mechanisms simplifying the calculation of J and K concerning the processing power.

First of all, we can save time by efficiently arranging the programming structure.

The radial functions J and K will be precalculated and stored before the actual code run. In cases where J and K do not depend on certain parameters that are being varied, this procedure is an efficient time-saving method. One precode run allows for a whole series of δW-calculations with different parameters as long as they do not impact J and K in (4.51).

For the application on mixed fields presented in this work, the explicit dependencies are

$$J_\lambda^m = J_\lambda^m(Q_0, \tilde{R}, \tilde{S}, \tilde{T}, \Theta_\lambda^m) \tag{4.89a}$$
$$K_\lambda^m = K_\lambda^m(Q_0, \tilde{R}, \tilde{S}, \tilde{T}, \Theta_\lambda^m) \tag{4.89b}$$

with

$$\tilde{R} = \tilde{R}(\xi_0, x_0, \vartheta_0, \delta_r, \delta_\vartheta) \tag{4.90}$$
$$\tilde{S} = \tilde{S}(\xi_0, x_0, \vartheta_0, \delta_r, \delta_\vartheta) \tag{4.91}$$
$$\tilde{T} = \tilde{T}(Q_0, \tilde{R}, \tilde{S}, \Gamma_1, B_0, \eta_{\mathrm{tor}}). \tag{4.92}$$

That means, the radial functions do depend on the magnetic field and composition parameters. However, they are independent of the poloidal field parameter η_{pol}. Therefore, it is possible to generate lookup tables of J- and K-values for each polytropic index Γ_1 that will be utilised.

Besides the programming manner, there is also an opportunity to simplify the underlying calculation structure directly.

As explained above, the computation of J at each grid point r_{2s} requires an integration from 0 to r_{2s}. This procedure can be simplified thanks to the additivity of integration on intervals, for an illustration cf. figure 4.3. For $s > 1$, the computation of $J_\lambda^m(r_{2s})$ can be performed by making use of the previously calculated value for $J_\lambda^m(r_{2s-2})$. In analogy, the computation of $K(r_{2s})$ requires an integration from r_{2s} to R. The additivity of integration can be exploited here as well if the integration is carried out from the stellar surface inwards:

$$J(r_{2s}) = \int_0^{r_{2s}} j \,\mathrm{d}r' = \int_0^{r_{2s-2}} j \,\mathrm{d}r' + \int_{r_{2s-2}}^{r_{2s}} j \,\mathrm{d}r' \tag{4.93a}$$

$$K(r_{2s}) = \int_{r_{2s}}^{R} k \,\mathrm{d}r' = -\int_R^{r_{2s}} k \,\mathrm{d}r' = -\int_R^{r_{2s+2}} k \,\mathrm{d}r' - \int_{r_{2s+2}}^{r_{2s}} k \,\mathrm{d}r'. \tag{4.93b}$$

In the mixed field case, the angular integration over ϑ included in j_λ^m and k_λ^m must be performed in any case. Therefore, we do not exploit the opportunity described above in the first code applications shown in this work. Instead, we apply the two-dimensional Simpson integration framework for the J- and K-computation we prepared in the previous section.

In future applications, however, when more systems should be analysed without Cowling approximation, the simplification based on (4.93) might be a convenient tool for the reduction of computation time. We need to keep in mind that depending on the magnetic field and composition structure, future applications will require displacement fields different from the choices shown in this work, which causes different forms of J and K accordingly. For realistic model systems, their structure is expected to be rather complex, similar to the mixed field case, than simple, as for spherically symmetric systems. This method will thus become helpful, especially when complex structures occur inside the integration area, that slow down the integration process.

Finally, it is always advisable to exploit existing symmetries of the system.

For example, the ϑ-integral values in J_λ^m and K_λ^m are preserved for given r as long as we only change parameters of the spherically symmetric background. Features like this should be considered to save computation time in future applications.

4.3.5. Code development

The integration code built in this work is written in the programming language C. It has been set up in a very reduced form at first and has been extended ever since to gradually include more and more features of realistic neutron stars. That way, the code development

process could be controlled in every step, guaranteeing that the produced results are in accordance with previously known facts.

In this section, the code construction progress will be presented chronologically.

Stability of unmagnetised spherically symmetric equilibrium polytropes The first test application for a simplified version of the code was the stability analysis of equilibrium compact objects constructed with different polytropic indices.

This setup required the following steps. Since the calculation of the energy variation is grounded on the background stellar model, the very first required code fragment was the solution of the equilibrium system equations. The classical Runge-Kutta solver was implemented as explained in section 4.3.1, providing the radial distributions of mass $m_0(r)$, pressure $p_0(r)$ and gravitational potential $\Phi_0(r)$.

Next, the expression for the energy variation density was expressed by numerically known values. In this first application, fluid pressure terms and gravitational contributions were relevant.

Afterwards, the code fragment performing the actual integration was established. According to the spherical symmetry of the equilibrium system, a one-dimensional Simpson integration over r was sufficient. It was implemented in spherical coordinates. The applied integration grid was chosen equivalently to the well-established Runge-Kutta grid.

Finally, the opportunity of automatic parameter variation during the code run was implemented. The energy variation can be calculated for different sets of parameters. The result δW is output tabularly depending on the parameters and can be plotted on the parameter space. In the simplified code, the polytropic index Γ_0 and the central density ρ_c were varied in order to investigate different background models.

Stability of toroidally magnetised polytropes The second step in the code development process enabled the treatment of magnetised systems.

This involves the extension of the energy variation density by the Lorentz term as well as choices for the magnetic field parametrisation. Accordingly, the displacement field has been chosen as explained in section 2.3.3. Due to the Newtonian description of the magnetic field, the relativistic corrections in the system equations needed to be dropped in order to maintain consistency.

With this new situation, the following arrangements in the code became necessary. Since the newly added magnetic field structure breaks the spherical symmetry of the background system, the one-dimensional Simpson integration was replaced by the two-dimensional one shown in section 4.3.3. It was implemented in cylindrical coordinates.

The two-dimensional integration requires an integration grid in the (ϖ, z)-plane, which was set up next. The according system quantities $Q_0(\varpi, z)$ were interpolated from the spherically symmetric solutions $Q_0(r)$ of the system equations. At first, a simple approximation method had been implemented. Subsequently, it has been replaced by the more accurate cubic spline interpolation explained in section 4.3.2.

The first code test for magnetised systems was the investigation of toroidally magnetised neutron stars subject to 'sausage' (m=0) and 'kink' (m=1) mode displacement fields defined by Tayler (1973). The code presented here was the first one to reproduce the Tayler instabilities of neutron stars with toroidal magnetic fields using a semi-analytic method. This result will be shown in section 5.1.

Stability of poloidally magnetised polytropes In order to enable the code for the treatment of arbitrary magnetic field structures, the investigation of poloidal magnetic fields needed to be implemented next.

The required model adjustments regarding the magnetic field parametrisation and the displacement field structure have been shown in sections 2.2.3 and 2.3.3. All quantities have been transformed from toroidal coordinates used by Markey & Tayler (1973) to cylindrical coordinates, according to (2.8). That way, the code structure performing the Simpson integration in cylindrical coordinates could be maintained.

The required code enhancement in this step was the adaption of the integration area. The integral extending over the stellar volume has been replaced by an integral over the localisation area of $\boldsymbol{\xi}$, in accordance with the explanation given in section 2.3.3.

Applying the adapted code, the poloidal field instability was verified by a negative energy variation for arbitrary magnetic field strengths, as will be shown in section 5.2.

Stability of unmagnetised stratified stars The implementation of stratification in the model was first introduced by investigating the stability of stratified unmagnetised stars against g-mode type displacement fields.

According to section 4.1, the energy variation was adjusted to stratified stars. The displacement field was expressed by stellar eigenmodes, approximated by a homogeneous background star, as shown in expression (2.140).

The implementation of stratification in the model did not require a restructuring of the code per se. An extension was nevertheless added to enable a validation mechanism for the produced results. For displacement fields of the form of stellar eigenfunctions, the code can calculate the corresponding eigenfrequencies from the computed energy variation, see equation (5.73).

Beyond that, a perturbative method was implemented to derive the eigenfunctions of the stratified star. Starting functions equivalent to the eigenfunctions of the homogeneous star are gradually corrected to converge to the actual eigenfunctions of the considered system. The method will be shown in section 5.4.2.

The code confirmed the expected qualitative stability behaviour of stratified stars subject to g-mode type displacements for $\Gamma_1 \gtrless \Gamma_0$. Literature values of eigenfrequencies of polytropic neutron stars were reproduced to affirm the quantitative functionality of the code, cf. section 5.4.1.

Stability of stratified stars with mixed magnetic fields The investigation of mixed magnetic fields considering stratification required the combination of all fragments set up in the code development process so far.

Energy variation, magnetic field and displacement field were chosen in accordance with Akgün et al. (2013) in order to facilitate the validation of results, cf. sections 2.2.3 and 2.3.3.

This step did not require further structural code modifications thanks to the programming groundwork depicted above. Still, the integration code has been restructured again to adjust the integration area to the displacement field localisation.

Beyond that, the automatic variation of the level of stratification has been implemented. Note that in the first application we performed, the stability of hydrostatic equilibria constructed with different values of Γ_0 was tested. In contrast, for the application described here, the background system was kept constant and we tested the impact of stratification and the magnetic field structure on the stability of these equilibria. Therefore, we kept Γ_0 constant here, while Γ_1 has been varied.

The calculated energy variation depending on the poloidal field strength and the level of stratification reproduced the stability criterion derived by Akgün et al. (2013) for stratified neutron stars with mixed magnetic fields. The results will be shown in section 5.3.

Stability of polytropic stars without Cowling approximation The final step to receive the code in its current form was the removal of the Cowling approximation.

This was first realised in a spherically symmetric toy system with one-dimensional integration and displacement fields expressed by spherical harmonics, in accordance with Chandrasekhar (1965). The analytical extension of the energy variation is depicted in sections 4.2.1 and 4.2.2.

The computational requirements for the J- and K-calculation are the additional Simpson integrations, that have been implemented according to section 4.3.4.

Furthermore, the storing of computed values for $J(r)$ and $K(r)$ in arrays and their reuse in subsequent code runs has been realised in order to save calculation time.

Stability of stratified stars with mixed magnetic fields without Cowling approximation After the consideration of the toy model, the non-Cowling contribution was set up for the actual mixed field system with stratification and the according mixed field choice for the displacement field.

The analytical groundwork is shown in sections 4.2.3 and 4.2.4.

The numerical implementation required modifications in the computation of the radial functions J and K. According to the axisymmetry of the star and the mixed field choice for $\boldsymbol{\xi}$, the one-dimensional integration has been replaced by the two-dimensional Simpson method explained in section 4.3.4.

The full non-Cowling treatment was applied on the mixed field system with stratification we investigated before in Cowling approximation. That way, the assumption of the Cowling approximation from Akgün et al. (2013) could be validated. The results will be shown in section 5.3.

4.3.6. Code structure

This section illustrates the structure of the final code at the end of the development process described above. The current code is capable of treating mixed magnetic fields, stratification and non-Cowling problems.

The code run consists of two precodes that will be described first in this section and the main code described afterwards.

Precodes

Before we run the actual integration code, two precodes computing input values for the main code are called in order to save calculation time. As explained above, the precodes provide lookup tables of system quantity values the actual main code has recourse to. This is especially expedient for quantities that are not influenced by the parameter variation performed in the main code.

Specifically, the first precode constructs typical background neutron star models. The second precode computes the radial functions $J^m_\lambda(r^s)$ and $K^m_\lambda(r^s)$ describing $\delta\Phi$.

Construction of neutron star models This precode generates typical neutron star models characterised by mass, radius and compactness on the basis of different input parameter sets $(\rho_c, \Gamma_0, \kappa)$. It is based on the Runge-Kutta solver described in section 4.3.1. With the precode results, the input parameters and grid assumptions required to yield a desired model neutron star can be read from a lookup table.

Calculation of radial functions J^m_λ and K^m_λ As discussed in section 4.3.4, this precode creates lookup tables for values of J, K, $\mathrm{d}_r J$ and $\mathrm{d}_r K$ at all Runge-Kutta grid points inside the localisation area. The main code can call these results in every run during the parameter variation, for which the parameter change does not impact the radial functions.

The precode structure concerning the calculation of the background quantities is equivalent to the main code structure. The integration part differs from the main code by computing J^m_λ and K^m_λ instead of δW, cf. section 4.3.4.

For the sake of accuracy, the numerical values for the derivatives $\mathrm{d}_r J^m_\lambda$ and $\mathrm{d}_r K^m_\lambda$ are not numerically derived from J and K but directly calculated from the integrands in (4.29) based on known quantities at the grid points.

Main code

Prespecified constants and input parameters The main code first requires physical and technical input parameters that can be arbitrarily chosen within a reasonable range.

The computational input parameters determine the Runge-Kutta solver as well as the Simpson-grid definition. The remaining parameters describe the model system under consideration, the magnetic field and the displacement field vector. They represent potential members of the parameter space on which the energy variation is investigated. In this case, a new value is assigned to them in each code run during a loop.

Finally, the required physical constants c, $M_\odot$ and G are defined.

Setup numerical grids The first computational step in the main code is the determination of the Runge-Kutta step width h_r based on the given neutron star model with radius R and the desired accuracy, determined by $s(\max)$. Next, the numbers of intervals for the Simpson integration in the (ϖ, z)-plane in both directions are set via relations (4.62), according to $s(\max)$ and the factors u_ϖ and u_z chosen before. Tests ensure that the numbers of integration grid intervals for both integrals are even, sufficiently large, and in a reasonable relation to one another.

Once the numerical grids are defined, the remaining variables required for the Simpson integration, $(J^m_\lambda, K^m_\lambda)$-calculation and the localisation are declared and initialised.

Solution of the system equations After the numerical setup is complete, the system equations (2.26) are solved with the Runge-Kutta routine described in section 4.3.1. In contrast to the precode, this time the solver is not mainly focussed on identifying total mass and radius, but on computing the background quantities mass, pressure and gravitational potential for all Runge-Kutta grid points. The results $m_0(r_s)$, $p_0(r_s)$ and $\Phi_0(r_s)$ are stored in one common array together with the radial distance from the stellar centre r_s.

Validation tests are performed in order to ensure that the routine produces the correct values for the prespecified values of M and R and that the fluid pressure decreases below the required critical value p_ε at the surface.

Setup numerical integration grid Once the radial profiles of the equilibrium quantities are available, the numerical grid points defining the localisation area can be identified. First, the radial grid points $r_{\min}$ and $r_{\max}$ comprising the localisation region are determined. The precalculated values for J and K are allocated to the arrays that describe their radial distribution.

Afterwards, the radially known background quantities m_0 and p_0 as well as J and K are interpolated to the Simpson grid points utilised in the two-dimensional numerical integration. Further, the position variables defining the integration grid in the (ϖ, z)-plane are stored in arrays.

Computation of the energy variation After all required system quantities are numerically set, the Simpson integration in two dimensions is performed, first along z and afterwards along ϖ, cf. section 4.3.3. The integration code is executed in a series of loops where the input parameters are varied. That way, the energy variation is computed for different sets of parameters at once.

Variable parameters are the neutron star model $(M, R, M/R)$, the background composition parameters ρ_c and κ, the polytropic indices Γ_0 and Γ_1, the magnetic field parameters such as B_0, η_{tor} and η_{pol}, the displacement field amplitude as well as the localisation choices described by x_0, ϑ_0, δ_r and δ_ϑ for example.

Finally, the code produces an output, listing the computed energy variation values for the corresponding parameter sets being used. In addition, the constants and model parameters that were not being varied are output.

5. Applications of the semi-analytic method

After the idea of the semi-analytic method has been realised in the previous chapter, it will be applied to actual problems, testing its functionality and producing new insights about the stability of neutron stars.

On one hand, the method will be employed on magnetised neutron stars in order to address the stability issue. By testing gradually more complex systems and incorporating more and more features of realistic neutron stars, systems shall be found that might be potentially stable. Translated into a mathematical approach, this means, the particular parameter combinations generating the most positive energy variations shall be found.

On the other hand, further application possibilities of the semi-analytic method will be shown in section 5.4. For one thing, these general applications are helpful steps during the development of the method. Beyond that, they show the broad range of applications and the universality of the method.

Concerning the application of the method to magnetised neutron stars, we will begin with the attempt of verifying Tayler's known analytical results on unstable neutron stars with purely toroidal and purely poloidal magnetic fields in sections 5.1 and 5.2. That way, the functionality of the method and the applied code is guaranteed, as explained in section 4.3.5.

Afterwards, the extensions analytically derived in chapter 4 are incorporated in the method. Subsequently, more complex neutron star models will be investigated, as presented in section 5.3. This study can be compared to the work by Akgün et al. (2013), where the semi-analytic approach allows for a more realistic modelling in comparison to the analytic study presented by Akgün et al. We will be able to remove simplifications and constraints that were necessary in the analytical approach. Especially, the Cowling approximation will be removed.

This chapter is structured in the following way. For each application of the semi-analytic method to magnetised neutron stars, we describe the specific model setup first, including the parametrisation we use for the magnetic field, the displacement field and the localisation area. Next, we present the subsequent explicit expression for the energy variation. After the case-dependent numerical specialities have been discussed, the results are finally presented and interpreted.

Supporting calculations and derivations are shown in the appendix C for reasons of clarity.

As explained in section 2.3.3 and proven in the appendix B.4, the displacement fields we constructed are chosen in such a way that the surface integral contributions do not need to be considered in any of the applications shown in this chapter.

Moreover, all applications shown here address neutron stars in a vacuum environment. The stars do not have an atmosphere which could provide any magnetic field or energy contributions.

5.1. Stars with purely toroidal magnetic fields

For the toroidally magnetised neutron star, we will mainly discuss non-axisymmetric displacement fields with mode indices $m \neq 0$. They cause instabilities in the cylindrical fluid discharge which are expected to persist in the presence of gravity as well, cf. Tayler (1973).

The "kink" mode with $m = 1$ discussed here causes the strongest instability. This becomes apparent in a straightforward instability proof that will be outlined below.

For the geometry of the displacement field see figure 2.12b.

5.1.1. System setup

In this section, the semi-analytic method will be applied to the model used by Tayler (1973). That is, an axisymmetric polytropic star with a purely toroidal magnetic field in Cowling approximation.

Rotation is neglected, as well as the crust and the potential inner core. The star solely consists of normal fluid neutrons and normally conductive protons and electrons. The magnetic field lines form concentric circles around the symmetry axis of the system, cf. figure 2.8. According to the axisymmetric geometry of the system, cylindrical coordinates will be utilised in this application.

In order to describe the unmagnetised background system, we will apply the hydrostatic equilibrium equation (2.29) as defined in section 2.2.3. Note that Tayler, on the contrary, considers the magnetic field contribution in the hydrostatic equilibrium equation in order to simplify the expressions in δW. According to this circumstance, our terms will slightly differ from the form given by Tayler (1973). These deviations will be discussed in detail below.

In this section, rationalised geometrised Gaussian cgs units will be applied in order to be consistent with Tayler's work.

Magnetic field

At first, Tayler chooses a magnetic field of purely toroidal geometry and an otherwise arbitrary structure. The azimuthal component B_φ is finite, while the other components vanish.

In addition and as explained above, in this work the magnetic field is claimed to vanish at the stellar axis as well as at the stellar surface. The assumptions $B_\varphi \sim \varpi$ and $B_\varphi \sim \rho$ prevent inconsistencies at the stellar axis on one hand and the extension of the field into the vacuum exterior on the other hand. The magnetic field choice (2.31) was presented in the fundamental setup section 2.2.3. It is depicted in figure 2.8.

In cylindrical coordinates, with the constant amplitude B_{tor}, it is

$$B_\varpi = 0 \qquad B_\varphi = \varpi\, \rho_0\, B_{\mathrm{tor}} \qquad B_z = 0. \tag{5.1}$$

Stellar composition

In the simple system Tayler chose, stratification is not taken into account, the star is polytropic. Therefore, the equilibrium system and the perturbed state are described by the very same equilibrium polytropic index, $\Gamma_1 = \Gamma_0$.

The fluid contribution to the energy variation density is thus given by (2.117b).

Description of the gravitational energy contribution

This first application of the semi-analytic method on magnetised neutron stars will be performed in Cowling approximation, i.e. $\mathcal{E}^{\mathrm{nC}}_{\mathrm{grav}} = 0$.

The gravitational contribution to the energy variation is thus given by (2.117c).

Beyond that, we keep both sign conventions for the gravitational field vector with $\boldsymbol{g} = \pm\nabla\Phi_0$, where the upper sign corresponds to the notation used by Tayler (1973).

Displacement field

For the construction of a non-axisymmetric displacement field revealing the instability of toroidally magnetised stars, we follow Tayler's approach.

After ansatz (2.121) has been chosen for the displacement field, the $\boldsymbol{\xi}$-defining functions need to be defined in such a way that the Tayler instability is detectable.

The derivation of this explicit form for $\boldsymbol{\xi}$ is based on the explicit expression for the energy variation in the toroidal field case, which will be given below in equations (5.11) and (C.52). The derivation of this explicit form will be outlined in the subsequent section. The detailed derivation is presented in the appendix section C.1.5. However, equation (5.11) has been derived applying the general ansatz (2.121) for the displacement field and the minimisation of $\mathcal{E}(Y)$ only, without further assumptions on the $\boldsymbol{\xi}$-defining functions.

In comparison to Tayler's approach, the form of equation (5.11) derived here, includes additional terms following from the fact that we do not include the magnetic field contribution in the equilibrium equation (2.29). More details on that will be given in the subsequent section and in the appendix section C.1.5. For the construction of the explicit displacement field form presented here, we just need to keep track of these additional terms.

In Tayler (1973), three stability criteria for the neutron star are set up. Their equivalents derived from equation (5.11) are

$$\bar{A} \overset{!}{>} 0 \qquad\qquad \bar{C} \overset{!}{>} 0 \qquad\qquad \bar{B}^2 \overset{!}{<} 4\,\bar{A}\,\bar{C}, \tag{5.2}$$

with

$$\begin{aligned}
\bar{A} = {} & B_\varphi^2\,\frac{m^2-2}{\varpi^2} - \frac{2\,B_\varphi\,\partial_\varpi B_\varphi}{\varpi} \pm \partial_\varpi\Phi_0\,\partial_\varpi\rho_0 - \frac{\rho_0^2\,\partial_\varpi\Phi_0^2}{\Gamma_0\,p_0} - \frac{B_\varphi^2}{2\,\Gamma_0\,p_0}\left(\frac{\partial_\varpi\left(\varpi B_\varphi\right)}{\varpi}\right)^2 \\
& \mp \frac{\rho_0\,B_\varphi}{\Gamma_0\,p_0\,\varpi}\,\partial_\varpi\Phi_0\,\partial_\varpi\left(\varpi B_\varphi\right)
\end{aligned} \tag{5.3a}$$

$$\begin{aligned}
\bar{B} = {} & -\frac{2\,B_\varphi\,\partial_z B_\varphi}{\varpi} \pm \partial_\varpi\Phi_0\,\partial_z\rho_0 \pm \partial_z\Phi_0\,\partial_\varpi\rho_0 - \frac{2\rho_0^2}{\Gamma_0\,p_0}\,\partial_\varpi\Phi_0\,\partial_z\Phi_0 - \frac{B_\varphi^2}{\Gamma_0\,p_0\,\varpi}\,\partial_\varpi\left(\varpi B_\varphi\right)\,\partial_z B_\varphi \\
& \mp \frac{\rho_0\,B_\varphi}{\Gamma_0\,p_0}\left(\frac{\partial_\varpi\left(\varpi B_\varphi\right)}{\varpi}\,\partial_z\Phi_0 + \partial_z B_\varphi\,\partial_\varpi\Phi_0\right)
\end{aligned} \tag{5.3b}$$

$$\bar{C} = B_\varphi^2\,\frac{m^2}{\varpi^2} \pm \partial_z\Phi_0\,\partial_z\rho_0 - \frac{\rho_0^2\,\partial_\varpi\Phi_0^2}{\Gamma_0\,p_0} - \frac{B_\varphi^2}{2\,\Gamma_0\,p_0}\left(\partial_z B_\varphi\right)^2 \mp \frac{\rho_0\,B_\varphi}{\Gamma_0\,p_0}\,\partial_z\Phi_0\,\partial_z B_z. \tag{5.3c}$$

The derivation of these criteria is shown in the appendix section C.1.1.

Tayler finds that if one of the stability criteria (5.2) is violated, a displacement field causing a negative energy variation can always be found.

Close to the stellar symmetry axis, the first stability criterion is violated for $B_\varphi \neq 0$, as validated in the appendix section C.1.2:

$$\bar{A} < 0 \qquad \text{for} \qquad B_\varphi \neq 0. \tag{5.4}$$

This violation is obvious only for $m = 1$, which will be assumed from now on.

Based on (5.4), the displacement field can be constructed in such a way that the energy variation becomes negative for an integration around the localisation (ϖ_0, z_0) of the instability. Particularly, this implies to choose suitable values for the $\boldsymbol{\xi}$-defining functions X and Z in the ansatz (2.121) for the displacement field.

Despite the fact that the stability criteria (5.2) with (5.3) differ from Tayler's approach due to the differences in equation (5.11), the argumentation for the displacement field construction stays unchangedly applicable. The justification of this statement as well as the detailed description of all construction steps outlined here are given in the appendix section C.1.4.

Considering the detectability of the Tayler instability and a vanishing surface integral contribution, the assumptions made in section 2.3.3 for the displacement field ansatz

$$\xi_\varpi = X(\varpi, z)\, \mathrm{e}^{\mathrm{i}m\varphi} \qquad \xi_\varphi = \frac{\mathrm{i}Y(\varpi, z)}{m}\, \mathrm{e}^{\mathrm{i}m\varphi} \qquad \xi_z = Z(\varpi, z)\, \mathrm{e}^{\mathrm{i}m\varphi} \tag{5.5}$$

follow:

$$\left.\begin{aligned} X(\varpi, z) &= X_0\, \varpi\, \sin(k_A\,(\varpi - \epsilon_A))\, \cos(l_A\, z) \\ Z(\varpi, z) &= Z_0\, \varpi\, \cos(k_A\,(\varpi - \epsilon_A))\, \sin(l_A\, z) \end{aligned}\right\} \quad \text{in } A, \qquad \left.\begin{aligned} X(\varpi, z) &= 0 \\ Z(\varpi, z) &= 0 \end{aligned}\right\} \quad \text{else,} \tag{5.6}$$

and the value for Y that minimises the energy variation with respect to Y:

$$\begin{aligned} Y(\varpi, z) = Y_{\min} \equiv \partial_\varpi(\varpi X) + \varpi\, \partial_z Z \pm \frac{\varpi\, \rho_0}{\Gamma_0\, p_0} \left(g_\varpi X + g_z Z \right) \\ + \frac{\varpi B_\varphi}{2\,\Gamma_0\, p_0} \left(\frac{\partial_\varpi\,(\varpi B_\varphi)}{\varpi} X + \partial_z B_\varphi Z \right). \end{aligned}$$

The localisation area is

$$A = \left\{ \varpi \in \mathbb{R} \,\middle|\, \epsilon_A - \frac{\pi}{k_A} < \varpi < \epsilon_A + \frac{\pi}{k_A}\ ,\ z \in \mathbb{R} \,\middle|\, -\frac{\pi}{l_A} < z < \frac{\pi}{l_A} \right\}. \tag{5.7}$$

The geometry of the toroidally magnetised model system is illustrated in figure 2.8a. The parameters must fulfil

$$\epsilon_A > \frac{\pi}{k} \qquad k_A\, X_0 + l_A\, Z_0 = 0 \qquad |X_0| \gg |Z_0| \qquad |l_A| \gg |k_A| \gg \frac{1}{h}, \tag{5.8}$$

with the typical scale height h of the system quantities.

The precise motivation for this displacement field choice is given in the appendix section C.1.4.

The geometry of the utilised displacement field and its localisation are visualised in figures 2.12b and 2.15.

The "kink" mode with $m = 1$ and choice (5.5) in general describes a non-axisymmetric deflection that is periodic with φ, according to the proportionality $\boldsymbol{\xi} \sim \mathrm{e}^{im\varphi}$. The displacement field components in ϖ- and z-direction are each periodic with both ϖ and z, according to the proportionalities $\xi_\varpi \sim \sin(k_A\,(\varpi - \epsilon_A))$, $\xi_\varpi \sim \cos(l_A\,z)$ and $\xi_z \sim \cos(k_A\,(\varpi - \epsilon_A))$, $\xi_z \sim \sin(l_A\,z)$. The dependency of ξ_φ on ϖ and z is not trivial, due to the dependency $\xi_\varphi \sim Y(X, Z, \partial_\varpi(\varpi X), \partial_z Z)$.

Finally, we are going to define the constants k_A and l_A in terms of the dimensionless stellar radius $\tilde{R}$ via

$$k_A = \frac{\pi}{\tilde{R}}\,u_k \qquad\qquad l_A = \frac{\pi}{\tilde{R}}\,u_l, \tag{5.9}$$

where u_k and u_l are numerical parameters that need to be chosen.

5.1.2. Energy variation explicitly

Applying the assumptions (5.1) and (5.5) made above for $\boldsymbol{B}$ and $\boldsymbol{\xi}$ in its general form (2.116) with (2.117), the energy variation becomes

$$\begin{aligned}
\delta W = \; & \frac{1}{4} \iiint \Re\Bigg\{ \frac{B_\varphi^2\, m^2}{\varpi^2} \Big(X^* X + Z^* Z \Big) + \Big(\partial_\varpi \left(X\, B_\varphi \right) + \partial_z \left(Z\, B_\varphi \right) \Big) \\
& \cdot \Big(\partial_\varpi \left(X^*\, B_\varphi \right) + \partial_z \left(Z^*\, B_\varphi \right) - \frac{\partial_\varpi \left(\varpi B_\varphi \right)}{\varpi}\, X^* - \partial_z B_\varphi\, Z^* \Big) \\
& - \frac{B_\varphi}{\varpi^2}\, \partial_\varpi \left(\varpi B_\varphi \right) Y^* X - \frac{B_\varphi}{\varpi}\, \partial_z B_\varphi\, Y^* Z \\
& + \Gamma_0\, p_0 \left(\frac{\partial_\varpi \left(\varpi X^* \right)}{\varpi} - \frac{Y^*}{\varpi} + \partial_z Z^* \right) \cdot \left(\frac{\partial_\varpi \left(\varpi X \right)}{\varpi} - \frac{Y}{\varpi} + \partial_z Z + X\, \partial_\varpi p_0 + Z\, \partial_z p_0 \right) \\
& \pm \Big(X\, \partial_\varpi \Phi_0 + Z\, \partial_z \Phi_0 \Big) \left[\rho_0 \left(\frac{\partial_\varpi \left(\varpi X^* \right)}{\varpi} - \frac{Y^*}{\varpi} + \partial_z Z^* \right) + X^*\, \partial_\varpi \rho_0 + Z^*\, \partial_z \rho_0 \right] \Bigg\}\, \mathrm{d}V.
\end{aligned} \tag{5.10}$$

Note the additional factor 1/2 that appears here compared to Tayler's form as long as the real part has not been evaluated yet. It is caused by our differing definition of the displacement field, cf. appendix section A.5.4. In comparison to the general expression (2.117), the magnetic contribution terms in (5.10) are missing the factor $1/(4\pi)$ that stemmed from the non-rationalised Maxwell equations (2.14). It is neglected here since we switched to geometrised rationalised Gaussian cgs units in this chapter.

Expression (5.10) can be further transformed by splitting the $\boldsymbol{\xi}$-defining functions into real and imaginary parts. Since they provide equivalent contributions to δW, they can be chosen real without restriction: $X = X_R$, $Y = Y_R$ and $Z = Z_R$. The real part in the integrand can be evaluated and the φ-integral can be performed. Beyond that, the

integrand can be minimised with respect to Y. This derivation is shown the appendix section C.1.5.

Finally, the explicit energy variation is

$$\begin{aligned}\delta W = \frac{\pi}{2} \iint \Bigg\{ & B_\varphi^2 \left(\varpi\, \partial_\varpi \left(\frac{X}{\varpi} \right) + \partial_z Z \right)^2 + B_\varphi^2 \, \frac{(m^2-2)\, X^2 + m^2\, Z^2}{\varpi^2} \\ & - \frac{2\, B_\varphi\, X}{\varpi} \left(\partial_\varpi B_\varphi\, X + \partial_z B_\varphi\, Z \right) \pm \left(X\, \partial_\varpi \Phi_0 + Z\, \partial_z \Phi_0 \right) \left(X\, \partial_\varpi \rho_0 + Z\, \partial_z \rho_0 \right) \\ & - \frac{\rho_0^2}{\Gamma_0\, p_0} \left(X\, \partial_\varpi \Phi_0 + Z\, \partial_z \Phi_0 \right)^2 - \frac{B_\varphi^2}{4\, \Gamma_0\, p_0} \left(\frac{\partial_\varpi \left(\varpi B_\varphi \right)}{\varpi}\, X + \partial_z B_\varphi Z \right)^2 \\ & \mp \frac{\rho_0 B_\varphi}{\Gamma_0\, p_0} \left(X\, \partial_\varpi \Phi_0 + Z\, \partial_z \Phi_0 \right) \left(\frac{\partial_\varpi \left(\varpi B_\varphi \right)}{\varpi}\, X + \partial_z B_\varphi\, Z \right) \Bigg\} \varpi \, \mathrm{d}\varpi \, \mathrm{d}z. \end{aligned} \tag{5.11}$$

Note that the last two terms in (5.11) are additionally appearing compared to Tayler's form. This circumstance is caused by the different use of the equilibrium equation mentioned above.

Furthermore, we kept the mode index $m \neq 0$ arbitrary, whereas Tayler assumed $m = 1$.

The difference in taking the real part between our approach and Tayler's approach, however, is only reflected during the derivation but not in the end result. We applied the real part to the complete integrand, whereas Tayler takes the real part of the displacement field only, compare appendix section A.5.4.

Energy variation contributions explicitly

During the derivation of the energy variation formula in the appendix, we kept track of the separate contributions stemming from different stellar forces: the Lorentz force, the fluid pressure gradient and the gravitational force.

This procedure will allow for a detailed interpretation of the results.

With the minimising value

$$Y_{\min} = \partial_\varpi \left(\varpi X \right) + \varpi\, \partial_z Z \pm \frac{\rho_0 \varpi}{\Gamma_0\, p_0} \left(X\, \partial_\varpi \Phi_0 + Z\, \partial_z \Phi_0 \right) + \frac{\varpi B_\varphi}{2\, \Gamma_0\, p_0} \left(\frac{\partial_\varpi \left(\varpi B_\varphi \right)}{\varpi} X + \partial_z B_\varphi Z \right) \tag{5.12}$$

from equation (C.43), the contributions to the energy variation density are

$$\begin{aligned}\mathcal{E}_{\text{magn}}(X, Y_{\min}, Z) = \; & \frac{1}{4}\left\{\frac{B_\varphi^2 m^2}{\varpi^2}\left(X^2+Z^2\right)+\left(\partial_\varpi\left(XB_\varphi\right)+\partial_z\left(ZB_\varphi\right)\right)^2\right. \\ & -\left(\partial_\varpi\left(XB_\varphi\right)+\partial_z\left(ZB_\varphi\right)\right)\left(\frac{\partial_\varpi\left(\varpi B_\varphi\right)}{\varpi}X+\partial_z B_\varphi Z\right) \\ & \left.-\frac{B_\varphi}{\varpi^2}\partial_\varpi\left(\varpi B_\varphi\right)Y_{\min}X-\frac{B_\varphi}{\varpi}\partial_z B_\varphi Y_{\min}Z\right\}\end{aligned} \tag{5.13a}$$

$$\begin{aligned}\mathcal{E}_{\text{fluid}}^{\text{poly}}(X, Y_{\min}, Z) = \; & \frac{1}{4}\left\{\Gamma_0 p_0\left(\frac{\partial_\varpi\left(\varpi X\right)}{\varpi}-\frac{Y_{\min}}{\varpi}+\partial_z Z\right)^2\right. \\ & \left.+\left(\frac{\partial_\varpi\left(\varpi X\right)}{\varpi}-\frac{Y_{\min}}{\varpi}+\partial_z Z\right)\left(X\,\partial_\varpi p_0+Z\,\partial_z p_0\right)\right\}\end{aligned} \tag{5.13b}$$

$$\begin{aligned}\mathcal{E}_{\text{grav}}^{\text{Cowl}}(X, Y_{\min}, Z) = \pm\frac{1}{4}\left\{\left(X\,\partial_\varpi\Phi_0+Z\,\partial_z\Phi_0\right)\right.\Bigg[\rho_0\left(\frac{\partial_\varpi\left(\varpi X\right)}{\varpi}-\frac{Y_{\min}}{\varpi}+\partial_z Z\right) \\ \left.+X\,\partial_\varpi\rho_0+Z\,\partial_z\rho_0\Bigg]\right\}.\end{aligned} \tag{5.13c}$$

The explicit form, after $Y_{\min}$ has been inserted, follows from equations (C.45), (C.49) and (C.50):

$$\begin{aligned}\mathcal{E}_{\text{magn}}(X, Y_{\min}, Z) = \frac{1}{4}\Bigg\{ \; & B_\varphi^2\left(\varpi\,\partial_\varpi\left(\frac{X}{\varpi}\right)+\partial_z Z\right)^2+B_\varphi^2 m^2\,\frac{X^2+Z^2}{\varpi^2}-\frac{2\,B_\varphi^2\,X^2}{\varpi^2} \\ & -\frac{2\,B_\varphi\,X}{\varpi}\left(\partial_\varpi B_\varphi\,X+\partial_z B_\varphi\,Z\right)\mp\frac{\rho_0\,B_\varphi}{\Gamma_0\,p_0}\left(\frac{\partial_\varpi\left(\varpi B_\varphi\right)}{\varpi}X+\partial_z B_\varphi Z\right) \\ & \cdot\left(X\,\partial_\varpi\Phi_0+Z\,\partial_z\Phi_0\right)-\frac{B_\varphi^2}{2\,\Gamma_0\,p_0}\left(\frac{\partial_\varpi\left(\varpi B_\varphi\right)}{\varpi}X+\partial_z B_\varphi Z\right)^2\Bigg\}\end{aligned} \tag{5.14a}$$

$$\begin{aligned}\mathcal{E}_{\text{fluid}}^{\text{poly}}(X, Y_{\min}, Z) = \frac{1}{4}\Bigg\{ & \pm\frac{\rho_0\,B_\varphi}{2\,\Gamma_0\,p_0}\left(\frac{\partial_\varpi\left(\varpi B_\varphi\right)}{\varpi}X+\partial_z B_\varphi\,Z\right)\left(X\,\partial_\varpi\Phi_0+Z\,\partial_z\Phi_0\right) \\ & +\frac{B_\varphi^2}{4\,\Gamma_0\,p_0}\left(\frac{\partial_\varpi\left(\varpi B_\varphi\right)}{\varpi}X+\partial_z B_\varphi\,Z\right)^2\Bigg\}\end{aligned} \tag{5.14b}$$

$$\begin{aligned}\mathcal{E}_{\text{grav}}^{\text{Cowl}}(X, Y_{\min}, Z) = \frac{1}{4}\Bigg\{ & \pm\left(X\,\partial_\varpi\Phi_0+Z\,\partial_z\Phi_0\right)\left(X\,\partial_\varpi\rho_0+Z\,\partial_z\rho_0\right) \\ & -\frac{\rho_0^2}{\Gamma_0\,p_0}\left(\partial_\varpi\Phi_0+Z\,\partial_z\Phi_0\right)^2 \\ & \mp\frac{\rho_0\,B_\varphi}{2\,\Gamma_0\,p_0}\left(X\,\partial_\varpi\Phi_0+Z\,\partial_z\Phi_0\right)\left(\frac{\partial_\varpi\left(\varpi B_\varphi\right)}{\varpi}X+\partial_z B_\varphi\,Z\right)\Bigg\}.\end{aligned} \tag{5.14c}$$

For a better understanding, the terms appearing in this notation can be traced back to their origin in equation (2.116) with (2.117), where

$$\delta W = \delta W_1 + \delta W_2 + \delta W_3 + \delta W_4 + \delta W_5 \tag{5.15}$$

with

$$\delta W_1 = \frac{1}{4}\Re\left\{\delta \boldsymbol{B}^* \cdot \delta \boldsymbol{B}\right\} \tag{5.16a}$$

$$\delta W_2 = -\frac{1}{4}\Re\left\{\boldsymbol{j}_0 \cdot (\delta \boldsymbol{B} \times \boldsymbol{\xi}^*)\right\} \tag{5.16b}$$

$$\delta W_3 = \frac{1}{4}\Re\left\{\Gamma_0 p_0 (\nabla \cdot \boldsymbol{\xi}^*)(\nabla \cdot \boldsymbol{\xi})\right\} \tag{5.16c}$$

$$\delta W_4 = \frac{1}{4}\Re\left\{\boldsymbol{\xi} \cdot \nabla p_0 (\nabla \cdot \boldsymbol{\xi}^*)\right\} \tag{5.16d}$$

$$\delta W_5 = \pm\frac{1}{4}\Re\left\{\boldsymbol{\xi} \cdot \nabla \Phi_0 (\nabla \cdot (\rho_0 \boldsymbol{\xi}^*))\right\}. \tag{5.16e}$$

The positive magnetic contribution terms in expression (5.14a) stem from δW_1, the negative and mixed sign terms from δW_2. The last term in the magnetic contribution represents the additional term compared to Tayler's form.

The first fluid contribution in equation (5.14b) added up from terms of both δW_3 and δW_4, while the second fluid contribution follows from δW_3 alone and appears additionally compared to Tayler (1973).

The gravitational contribution (5.14c) corresponds to δW_5. The last gravitational contribution is an additional term.

5.1.3. Computation

Parameter set choice

Once the system setup has been prepared, the numerical integration requires an appropriate choice for the parameters of the background model, the magnetic field and the displacement field, as well as suitable computation parameters.

In order to create a typical neutron star with Newtonian system equations (2.26), the background polytropic index of $\Gamma_0 = 2$ will be used. The central density ρ_c and the proportionality constant $\tilde{\kappa}^*$ will be varied within a reasonable range to cover a variety of neutron star models differing in mass, radius and compactness.

Cf. the current list of observed neutron stars in Lattimer & Prakash (2005); Lattimer (2016).

The models applied here are shown in table 5.1.

The magnetic field strength will be varied within the range that is relevant for toroidal magnetic fields in neutron stars. According to previous studies indicating a much stronger interior field than the observable exterior field, we also cover high magnetic field strengths.

The calculations will be performed for varying B_{tor} from 10^{10} to 10^{15} G and for $B_{\mathrm{tor}} = 0$.

Table 5.1.: Background model parameter set used for the Tayler instability proof on toroidally magnetised neutron stars. The remaining parameters for magnetic field, displacement field and computation are given in the text.

ρ_c in $10^{15}\,\mathrm{g/cm^3}$	$\tilde{\kappa}^*$ in $10^{11}\,\mathrm{cm^2}$	M in $\mathrm{M}_\odot$	R in km	M/R
1.24	8	1.12	11.2	0.15
1.1	10	1.39	12.5	0.16
1.15	10	1.45	12.5	0.17
1.2	10	1.51	12.5	0.18

The displacement field parameters must be chosen in accordance with the requirements shown in equation (5.8). The discussion regarding the optimal choice is shown in the appendix section C.1.4.

We use the mode index $m = 1$, the amplitudes $X_0 = 1$, $Z_0 = -0.1$, the constants $u_k = 10$, $u_l = 10^2$ and the dimensionless localisation parameter $\tilde{\epsilon}_A = 0.001\,\tilde{R}/u_k = 0.0001\,\tilde{R}$.

For the computational parameters, one universal parameter set will be utilised for all models under investigation.

The radial coordinate is approximated at the stellar centre by $r_c = 1\,\mathrm{cm}$. The vacuum pressure level introduced in section 4.3.1 is set to $\tilde{p}_\varepsilon = 10^{-10}$. Remember that $\tilde{p}$ denotes the dimensionless pressure value, i.e. $p_\varepsilon = 5.55 \times 10^{38}\,\mathrm{g\ cm^{-1}\ s^{-2}}$. Note that this value is smaller than the central pressure by approximately four orders of magnitude. For example, $p_c = 5.34 \times 10^{42}\,\mathrm{g\ cm^{-1}\ s^{-2}}$ for $\Gamma_0 = 2$, $\rho_c = 10^{15}\,\mathrm{g\ cm^{-3}}$ and $\tilde{\kappa}^* = 8 \times 10^{11}\,\mathrm{cm^2}$. The Simpson integration grid is defined by $u_\varpi = 10$ and $u_z = 10$.

Numerical features

The two-dimensional integration area used for the toroidal field was constructed in section 4.3.2 and presented in equation (4.65).

According to the manageable computation time, the numerical integration area is chosen as one half of the stellar cross section. That way, we do not need to construct an integration region with a cartesian geometry, adjusted to the shape of the localisation region.

5.1.4. Results

The total energy variation (5.11) and its individual contributions (5.13) have been calculated for exemplaric model systems. In this section, we present the results.

The qualitative behaviour of $\delta\widetilde{W}(B_{\mathrm{tor}})$ and especially its sign are presented in figure 5.1. The quantitative behaviour can be visualised by plotting the absolute value $\left|\delta\widetilde{W}\right|(B_{\mathrm{tor}})$. The absolute values of the energy variation and the separate contributions are plotted in figure 5.2 for different model neutron stars.

We show both graphs as we are primarily interested in the stability behaviour of the system which is described by the sign of the energy variation. On the other hand, figure 5.1 cannot provide information about the quantitative behaviour of $\delta\widetilde{W}(B_{\mathrm{tor}})$. The result must be plotted in a log-log plot in order to read out the quantitative relation between energy variation and magnetic field strength. However, the logarithmic scaling requires

positive values. We can create graph 5.2 which contains the desired information about the quantitative behaviour at the price of loosing the qualitative sign information. The picture becomes complete by combining both graphs.

Also note that we focus on models that provide a positive gravitational energy variation δW_{grav} in order to avoid possible g-mode type instabilities affecting the consideration.

Finally, figure 5.3 presents a measurement for the numerical error caused by the integration. It shows the absolute difference between the total energy variation and the sum of its contributions,

$$\left| \delta\widetilde{W} - \sum_{i=1}^{3} \delta\widetilde{W}_i \right|, \tag{5.17}$$

with $\delta\widetilde{W}_i = \delta\widetilde{W}_{\text{magn}}, \delta\widetilde{W}_{\text{fluid}}, \delta\widetilde{W}_{\text{grav}}$.

The total energy variation has been computed based on the explicit form (5.11), whereas the separate contributions have been calculated according to equations (5.13), where the minimising value (5.12) has been specified separately.

Note that this consideration represents a restricted estimate for the numerical error range. It only reflects the obvious deviation between different numerical approaches, providing the minimum numerical error range. The actual error generated by the integration might be even larger.

The results presented here contain the following information.

Before we focus on the impact of the magnetic field, we check the conditions of the unmagnetised system.

The total energy variation of the unmagnetised star is positive for all models, i.e. $\delta\widetilde{W}(B_{\text{tor}} = 0) > 0$. That means, without the toroidal magnetic field, the system is stable against the kink mode type displacement field (5.5) which is imposed on the star. This fact eliminates the possibility of mistaking a potential negative energy variation caused by the fluid or gravitational contribution for the Tayler instability. This result creates the foundation for a verification of the Tayler instability.

The qualitative behaviour of the energy variation follows from figure 5.1.

The magnetic contribution is negative for all finite field strengths, $\delta\widetilde{W}_{\text{magn}} < 0 \,\forall\, B_{\text{tor}} \neq 0$. Its absolute value $|\delta\widetilde{W}_{\text{magn}}|$ increases with the field strength.

The fluid and gravitational contributions are independent of the magnetic field strength as expected. The fluid part is slightly negative, $\delta\widetilde{W}_{\text{fluid}} < 0$, and the gravitational part is slightly positive, $\delta\widetilde{W}_{\text{grav}} > 0$. Compared to the magnetic part, both are increasingly negligible for growing B_{tor}.

The dominating magnetic contribution causes the total energy variation to be negative for magnetic field strengths exceeding a critical value: $\delta\widetilde{W} < 0 \,\forall\, B_{\text{tor}} > B_{\text{tor}}^{\text{crit}}$. In terms of the stability criterion (2.45), this implies that the system is unstable against the kink mode perturbation if the system's toroidal magnetic field is sufficiently strong. The significance of this finite critical value will be discussed below.

The quantitative result is expressed in figure 5.2.

The magnetic contribution to the energy variation, and thereby the total energy variation as well, shows a linear behaviour in the log-log plot. This relation translates into a

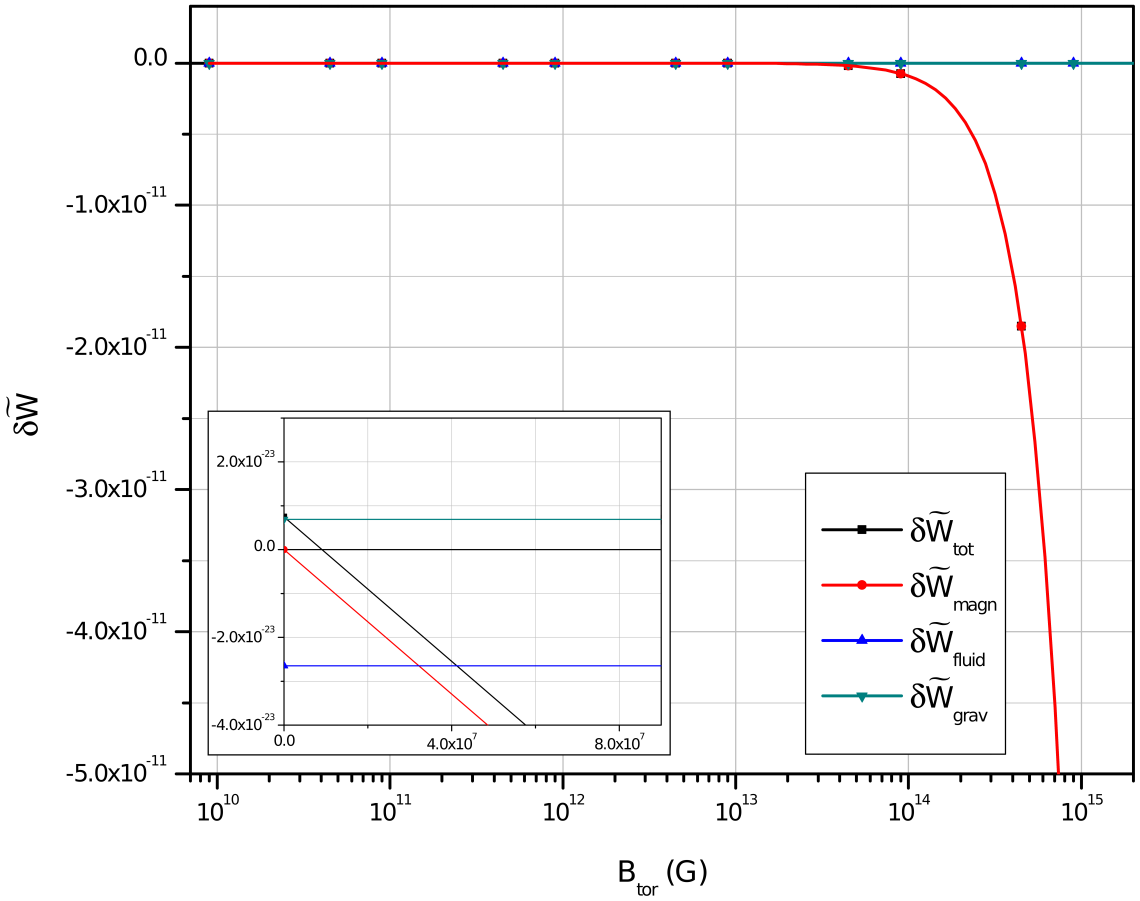

Figure 5.1.: Dimensionless energy variation of the toroidally magnetised neutron star for the $m = 1$ mode displacement, calculated with the semi-analytic method. The graph shows the total energy variation as well as the separate contributions from magnetic field, fluid pressure and gravity. The energy variation is negative for magnetic field strengths of $B_{\mathrm{tor}} > B_{\mathrm{tor}}^{\mathrm{crit}} = 2.86 \times 10^8\,\mathrm{G}$. Note that $\delta W_{\mathrm{magn}} < 0$, $\delta W_{\mathrm{fluid}} < 0$ and $\delta W_{\mathrm{grav}} > 0 \,\forall\, B_{\mathrm{tor}} \neq 0$. Separate contributions do not add up to the total energy variation due to numerical inaccuracies, as it will be discussed in section 5.1.5. The model system is described by $M = 1.12\,\mathrm{M}_\odot$ and $R = 11.2\,\mathrm{km}$. The parameters are defined in the text.

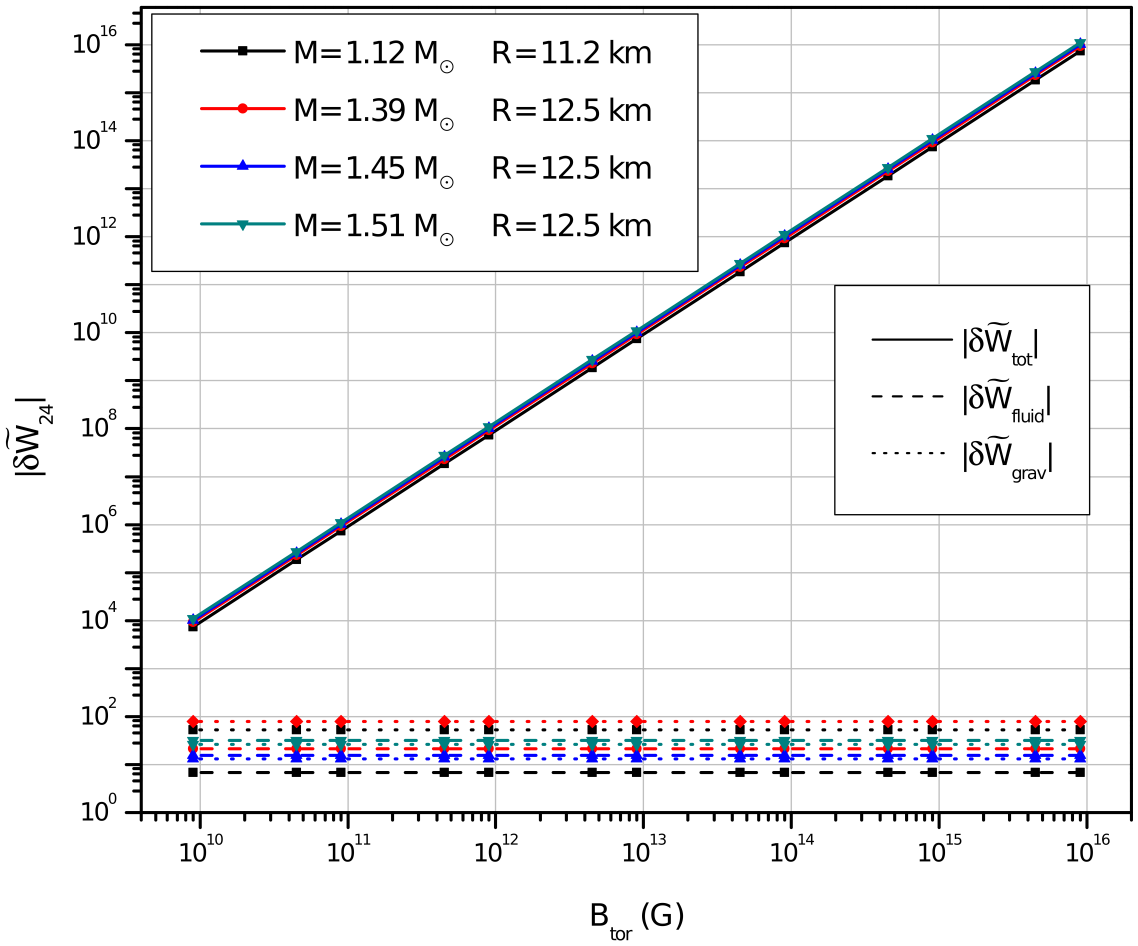

Figure 5.2.: Dimensionless energy variation of the toroidally magnetised neutron star for the $m = 1$ mode displacement, calculated with the semi-analytic method. The graph shows the absolute value $\left|\delta\widetilde{W}_{24}\right| \equiv 10^{24}\left|\delta\widetilde{W}\right|$ of the total energy variation $\delta\widetilde{W}$ (solid line), the fluid contribution $\delta\widetilde{W}_{\mathrm{fluid}}$ (dashed line) and the gravitational contribution $\delta\widetilde{W}_{\mathrm{grav}}$ (dotted line). Note that $\delta W_{\mathrm{magn}} < 0$, $\delta W_{\mathrm{fluid}} < 0$ and $\delta W_{\mathrm{grav}} > 0 \,\forall\, B_{\mathrm{tor}} \neq 0$. The magnetic contribution dominates the behaviour of the total energy variation. The parameters are defined in the text.

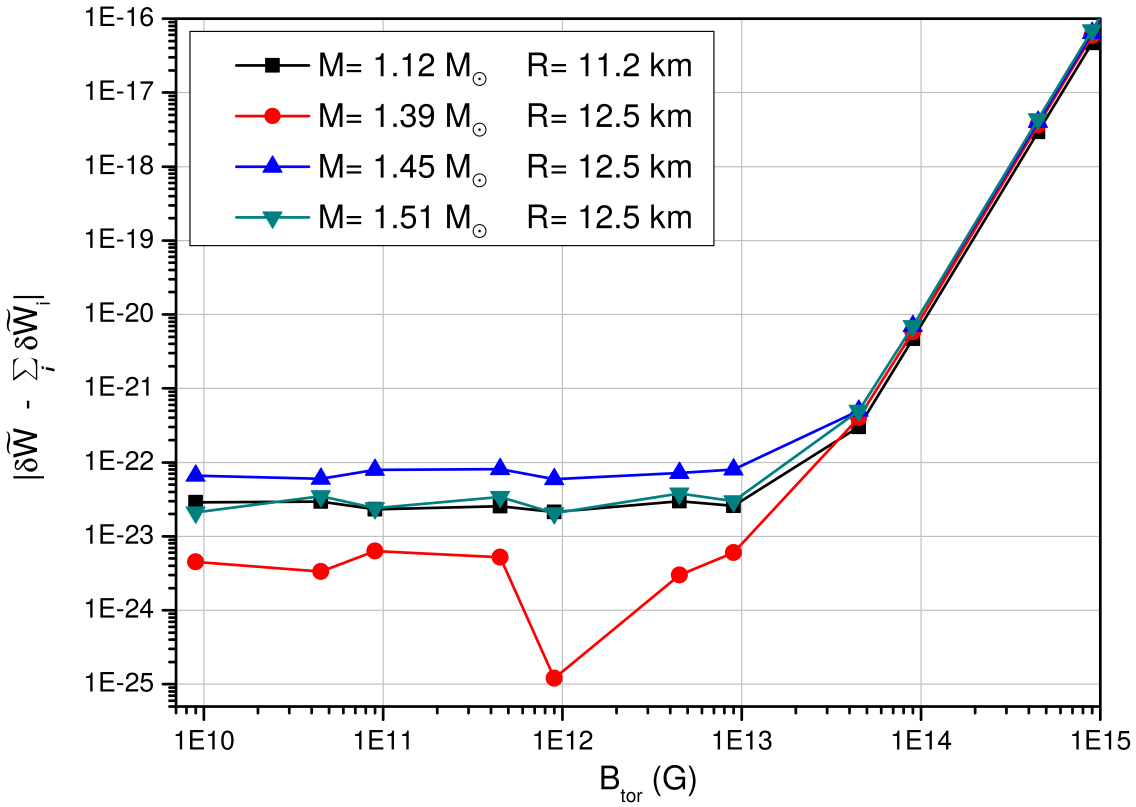

Figure 5.3.: Error estimation for the numerical integration of the semi-analytic method, regarding the application of the method on the toroidally magnetised neutron star.

quadratic dependency $\delta W_{\text{magn}} \sim B_{\text{tor}}^2$. The magnetic contribution increases quadratically with the magnetic field strength, while fluid and gravitational contribution stay constant independent of B_{tor}.

This can be seen from the separate contributions (5.13) to the energy variation as well. From assumption (5.1) it is

$$B_\varphi = \varpi\, \rho_0\, B_{\text{tor}} \qquad \frac{\partial_\varpi (\varpi B_\varphi)}{\varpi} = (2\,\rho_0 + \varpi\, \partial_\varpi \rho_0)\, B_{\text{tor}} \qquad \partial_z B_\varphi = \varpi\, \partial_z \rho_0\, B_{\text{tor}}. \tag{5.18}$$

Therefore, the magnetic contribution (5.13a) obeys $\mathcal{E}_{\text{magn}} \sim B_{\text{tor}}^2$, while the fluid contribution (5.13b) as well as the gravitational contribution (5.13c) do not depend on B_{tor}.

The root of $\delta W(B_{\text{tor}})$ in graph 5.1 determines the critical field strength for instability.

We give a rough estimate by fitting the energy variation for $B_{\text{tor}} \leq 9 \times 10^9\,\text{G}$ with a quadratic function and calculating the root.

For an estimate of the $B_{\text{tor}}^{\text{crit}}$-accuracy, we calculate the minimal and maximal values the energy variation can take, according to the numerical error range. These minima and maxima are denoted by $\delta\widetilde{W}^{\min}$ and $\delta\widetilde{W}^{\max}$.

We approximate the energy variation error within the range 0 G to 9×10^9 G restrictively. That means, we assume the smaller value at $B_{\text{tor}} = 0$ rather than the larger value at $B_{\text{tor}} = 9 \times 10^9\,\text{G}$. That way, we ensure not to overestimate the error and mistake an actual physical feature for a numerical inaccuracy.

According to the computed values

$$\delta\widetilde{W}(B_{\text{tor}} = 0) = \quad 7.470\,92 \times 10^{-24} \tag{5.19}$$

$$\delta\widetilde{W}(B_{\text{tor}} = 9 \times 10^9\,\text{G}) = -7.402\,34 \times 10^{-21} \tag{5.20}$$

$$\left|\delta\widetilde{W}(B_{\text{tor}}) - \sum_i \delta\widetilde{W}_i(B_{\text{tor}})\right| = \quad 2.704\,92 \times 10^{-23}, \tag{5.21}$$

the energy variation and the minimal and maximal values of the error range can be described by the quadratic equation

$$\delta\widetilde{W} \approx \delta\widetilde{W}(B_{\text{tor}} = 0) + c_q\, \left(B_{\text{tor}}[G]\right)^2 \tag{5.22}$$

with

$$c_q = 9.147\,91 \times 10^{-41}\,\text{G}^{-2} \qquad \delta\widetilde{W}_{\min} = -1.957\,828 \qquad \delta\widetilde{W}_{\max} = 3.452\,012. \tag{5.23}$$

The roots follow as

$$B_{\text{tor}}^{\text{crit}} = 2.857\,76 \times 10^8\,\text{G} \qquad B_{\text{tor}}^{\text{crit, min}} = 0 \qquad B_{\text{tor}}^{\text{crit, max}} = 6.142\,92 \times 10^8\,\text{G}. \tag{5.24}$$

Note that the minimal possible value of the energy variation is already negative for $B_{\text{tor}} = 0$ and does not have a change in sign within the range 0 G to 9×10^9 G.

Thus, the minimal critical value is $B_{\text{tor}}^{\text{crit, min}} = 0$.

5.1.5. Interpretation

After the results have been presented in the previous section, the next step is to evaluate whether the analytically known Tayler instability could be verified applying the semi-analytic method.

Summarising from the previous section, the total energy variation is negative for all magnetic field strengths exceeding a critical value. Therefore, the system is in fact unstable against the imposed perturbation as expected.

In the unmagnetised state, δW is positive which implies a stable system in the presence of the same perturbation mode. That means, the instability is caused by the magnetic field indeed.

It must be noted that the results in figure 5.1 imply $\delta W(B_{\mathrm{tor}} = 0) > 0$, while figure 5.2 provides $\delta W_{\mathrm{fluid}}(B_{\mathrm{tor}} = 0) + \delta W_{\mathrm{grav}}(B_{\mathrm{tor}} = 0) < 0$ for the presented model system. However, the small values $\delta W_{\mathrm{fluid}}(B_{\mathrm{tor}} = 0)$ and $\delta W_{\mathrm{grav}}(B_{\mathrm{tor}} = 0)$ lie within the error range of the numerical integration, estimated in figure 5.3. The negative energy variation resulting for $B_{\mathrm{tor}} = 0$ by adding fluid and gravitational contribution is rather a consequence of the numerical inaccuracy then an actual physical feature. This interpretation is supported by the fact that δW has been computed directly from the explicit minimised form (5.11) of the energy variation. The calculation of $\delta W_{\mathrm{fluid}}$ and δW_{grav}, in contrast, involved the additional step of precomputing Y_{min} and inserting it into the integral. It is therefore a justified assumption that the accuracy of δW is higher than the accuracy of the sum of the separate contributions.

Furthermore, the possibility that the detected negative energy variation could be caused by another instability, not the Tayler-instability, has been broadly eliminated by focussing on a model where the gravitational contribution is stable against the applied perturbation. In fact, the fluid and gravitational contributions to the energy variation are almost vanishingly small for all values of B_{tor}, and might even vanish strictly according to the numerical error range.

Therefore, it is very likely that the detected instability is of magnetic nature.

However, the instability analytically found by Tayler (1973) represents a structural instability which is present for all magnetic field strengths $B_{\mathrm{tor}} > 0$. In contrast, the semi-analytical results produced here suggest a finite critical field strength $B_{\mathrm{tor}}^{\mathrm{crit}} > 0$. This fact needs to be discussed in order to decide whether the instability detected here functions as a verification of the Tayler instability.

First, we must mention that a structural character of the instability found here is not excluded by the results. As explained above, the fluid and gravitational contribution to the energy variation are so small that $\delta W_{\mathrm{fluid}}(B_{\mathrm{tor}} = 0) = 0$ and $\delta W_{\mathrm{grav}}(B_{\mathrm{tor}} = 0) = 0$ are compatible with the restrictive numerical error range. This scenario would imply a critical magnetic field strength of $B_{\mathrm{tor}}^{\mathrm{crit}} = 0$.

Secondly, we need to take into account that Tayler's stability consideration was based on the assumption that the $\boldsymbol{\xi}$-defining functions X and Z vary quickly spatially compared to the system quantities. This assumption was based on the requirement $|l_A| \gg |k_A| \gg 1/h_A$, as explained in the appendix section C.1.4. However, this condition might be violated in the limit of small magnetic field strengths. That means, for very small field strengths, $|\boldsymbol{B}|$ might increase steeply with r. If this is the case and the second requirement in

equation (5.8) is violated, the argumentation concerning the stability consideration is not longer valid. Specifically, the estimates made for $\bar{A}'$ and $\bar{B}'$, both depending on B_{tor}, are untenable: $\bar{A}'$ might not be negative everywhere inside the localisation region and $\bar{B}'$ might not be negligible. For the definition of $\bar{A}'$ and $\bar{B}'$, see appendix section C.1.4. This possible violation might explain why the structural character of the Tayler instability cannot be verified with the approach presented here. Due to the fact that the analytical investigation in Tayler (1973) was based on approximations, the character of the instability might in fact not even be structural.

Summarising, the existence of the Tayler instability has been verified. The character of the detected instability is not in agreement with the analytical result yet, but neither do the two methods contradict each other within their range of accuracy.

Overall, the detected instability is clearly driven by the magnetic field. The semi-analytic method has proven its functionality for the first application on simple magnetised neutron stars.

5.2. Stars with purely poloidal magnetic fields

After the semi-analytic method has been successfully applied to the toroidally magnetised star, the next step is to also investigate the poloidally magnetised neutron star with the slightly more complex magnetic field structure.

This application will be based on the analytical study by Markey & Tayler (1973). Altering the geometry, the model system under consideration is basically equivalent to the toroidal field model described in the previous section. We will make use of this situation by utilising toroidal coordinates. Consequently, the applied displacement field will be the analogue to the perturbation applied in the toroidal field case, although this time various modes m will be considered.

5.2.1. System setup

In accordance to the model definition of the toroidal field case, the system will be kept as simple as possible. The semi-analytic method will be applied to an axisymmetric polytropic background star with a purely poloidal magnetic field, described in Cowling approximation.

Uniform and differential rotation as well as the neutron star crust are neglected in the model. The neutron star consists of a fluid with normal neutrons and normally conductive protons and electrons.

The magnetic field lines form concentric circles around the magnetic field symmetry axis, which is the neutral line shown in figure 2.9. The neutral line represents a circular toroidal line around the stellar symmetry axis. Therefore, with the usage of toroidal coordinates (2.8), the system appears as a cylindrical fluid discharge that is toroidally wrapped up around the symmetry axis, cf. figure 2.13b.

The hydrostatic equilibrium equation (2.29) describes the unperturbed system. In contrast, Markey & Tayler (1973) comment that the equilibrium equation includes the magnetic field. However, the analytic consideration does not require the determination of the background system quantities p_0, ρ_0 and Φ_0. Therefore, the equations shown by Markey

and Tayler have been derived independently of the equilibrium equation and are directly comparable to the expressions shown here.

For the poloidal field application, geometrised rationalised Gaussian cgs units will be applied in order to keep the consistency with Markey & Tayler (1973).

Magnetic field

The magnetic field has been defined in section 2.2.3 in such a way that it shows a purely poloidal structure with a vanishing azimuthal component $B_\varphi = 0$, while the other components can be expressed by the stream function ψ in cylindrical coordinates:

$$B_\varpi = -\frac{1}{\varpi}\,\partial_z\psi \qquad\qquad B_z = \frac{1}{\varpi}\,\partial_\varpi\psi, \tag{5.25}$$

cf. appendix section B.2. Next, the toroidal coordinate system (2.8) has been chosen in such a way that the amount of magnetic flux streaming through the torus along the stellar symmetry axis is prespecified to a certain value of $2\,\pi\,\psi$. This procedure is shown in the appendix section C.2.1. With this, choice (2.32) follows:

$$B_\psi = 0 \qquad\qquad B_\varphi = 0 \qquad\qquad B_\chi = B_{\mathrm{pol}}\,\frac{\bar{r}}{\varpi}. \tag{5.26}$$

The distance $\bar{r}$ to the neutral line has been defined in equation (2.9). The field amplitude is described by the constant prefactor B_{pol} of the dimension cm^{-2}.

Note that the magnetic field smoothly approaches zero at the neutral line. Beyond that, the prefactor B_{pol} is constant, which means the dependency of the magnetic field on the stream function $\boldsymbol{B} = \boldsymbol{B}(\psi)$ is hidden in the proportionality $B_\chi \sim \bar{r}/\varpi$ in equation (5.26).

Stellar composition

In analogy to the previous application on toroidally magnetised stars, stratification is not considered in the simple neutron star model applied here. The polytropic indices of background system and perturbed state are identical, $\Gamma_1 = \Gamma_0$.

The fluid part of the energy density variation is given by form (2.117b).

Description of the gravitational energy contribution

Just like in the toroidal field case, the stability analysis of the poloidally magnetised star will be performed in Cowling approximation, $\mathcal{E}^{\mathrm{nC}}_{\mathrm{grav}} = 0$.

Therefore, the gravitational part of the energy variation density is given by expression (2.117c).

Both sign conventions $\boldsymbol{g} = \pm\nabla\Phi_0$ will be kept, in order to facilitate the comparison to the toroidal field case.

For comparison, in Markey & Tayler (1973), the sign convention is not defined. As shown in the subsequent section, the gravitational contribution vanishes there, according to the particular displacement field choice applied, and does not need to be discussed.

Displacement field

For the stability investigation of the poloidally magnetised neutron star, Markey & Tayler (1973) first argue that the system is equivalent to the toroidal field case with respect to the magnetic field symmetry axis. Therefore, the displacement field has a similar structure to the perturbation applied in the toroidally magnetised neutron star, if the poloidally magnetised star is described in toroidal coordinates.

The analogue (2.125) to Markey and Tayler's ansatz utilised in this work is

$$\xi_\psi = \frac{X(\psi,\chi)}{\varpi B_\chi}\, \mathrm{e}^{\mathrm{i}m\varphi} \tag{5.27a}$$

$$\xi_\varphi = \frac{\mathrm{i}\,\varpi\, Y(\psi,\chi)}{m}\, \mathrm{e}^{\mathrm{i}m\varphi} \tag{5.27b}$$

$$\xi_\chi = B_\chi\, Z(\psi,\chi)\, \mathrm{e}^{\mathrm{i}m\varphi}\,. \tag{5.27c}$$

There are two differences compared to Markey and Tayler's approach.

First, as in the toroidal field case, we use the actually complex displacement field vector in the integrand and ensure the physical meaningfulness of δW by taking the real part over the total integrand. Markey & Tayler (1973), in contrast, apply the real part of $\boldsymbol{\xi}$ only.

Secondly, according to our definition (5.27), Y is a real function, whereas Markey and Tayler include the imaginary unit in $Y^{\mathrm{MT}} = i\, Y_I^{\mathrm{MT}}$.

Beyond the displacement field ansatz, Markey & Tayler (1973) formulate two additional constraints for $\boldsymbol{\xi}$ which will be assumed in this work as well.

These conditions simplify the energy variation and facilitate the actual instability proof:

$$\boldsymbol{\xi}\cdot\boldsymbol{g} \overset{!}{=} 0 \qquad\qquad \nabla\cdot\boldsymbol{\xi} \overset{!}{=} 0. \tag{5.28}$$

These requirements state that the applied displacement field is perpendicular to the gravitational field vector and divergence free.

Conditions (5.28) imply that the neutron star fluid is incompressible towards the type of perturbation being imposed on the system, which means $\delta\rho = 0$. The local density ρ at a fixed position is not influenced by $\boldsymbol{\xi}$. This consequence is mathematically derived in the appendix section C.2.2.

Note that this limitation to a subclass of perturbations is possible, since this study aims on the verification of an instability. According to the stability criterion (2.45), the detection of one unstable perturbation mode is sufficient to prove instability.

With conditions (5.28), the $\boldsymbol{\xi}$-defining functions Y and Z can be expressed as functions of X. The derivation is shown in the appendix section C.2.2.

Furthermore, X is chosen in such a way that the displacement field can be localised inside a torus extending around the symmetry axis and including the neutral line, cf. figure 2.16. The torus surface is given by $\psi = \psi_{\mathrm{tor}}$. The detailed discussion concerning the localisation is presented in the appendix as well.

We assume

$$X = f(\psi,\chi)\,(\psi-\psi_{\mathrm{tor}})^2\,. \tag{5.29}$$

The explicit form of Y and Z resulting from this choice is shown in equation (2.126).

The remaining structure of X besides the localisation is described by the function $f(\chi,\psi)$. It is chosen in such a way that the Tayler instability is detectable, while $f(\chi,\psi)$ is still in accordance with the localisation of $\boldsymbol{\xi}$.

As shown in the appendix section C.2.2, the structural character of the Tayler instability becomes evident in cases where the energy variation is negative independently of the magnetic field strength. This is the case particularly if the magnetic field amplitude B_{pol} can be factorised out of the δW-integrand.

The appropriate choice (C.92) fulfils this requirement. It reads

$$f(\psi,\chi) = \frac{X_0 \sin\chi}{B_{\mathrm{pol}}^2}, \tag{5.30}$$

so that finally

$$\left.\begin{array}{ll} X(\psi,\chi) = \frac{X_0 \sin\chi}{4}\left(\bar{r}^2 - \bar{r}_{\mathrm{tor}}^2\right)^2 & \\ Y(\psi,\chi) = X\frac{\cos\chi}{\varpi\,\bar{r}\,B_{\mathrm{pol}}} + B_{\mathrm{pol}}\frac{\partial_\chi Z}{\varpi} + \partial_\psi X & \text{in } A, \\ Z(\psi,\chi) = -X_0\left(\bar{r}^2 - \bar{r}_{\mathrm{tor}}^2\right)^2 \frac{\varpi\,(R_{\mathrm{tor}}\cos\chi - \bar{r})}{4\,\bar{r}^2\,B_{\mathrm{pol}}^2\,R_{\mathrm{tor}}} & \end{array}\right\} \quad \left.\begin{array}{l} X(\psi,\chi) = 0 \\ Y(\psi,\chi) = 0 \\ Z(\psi,\chi) = 0 \end{array}\right\} \quad \text{else,} \tag{5.31}$$

with

$$\partial_\psi X = -\frac{X_0 \sin\chi}{B_{\mathrm{pol}}}\left(\bar{r}^2 - \bar{r}_{\mathrm{tor}}^2\right) \tag{5.32}$$

and

$$\partial_\chi Z = \frac{X_0}{B_{\mathrm{pol}}^2}\frac{\left(\bar{r}^2 - \bar{r}_{\mathrm{tor}}^2\right)^2}{4\,\bar{r}^2\,R_{\mathrm{tor}}}\left[\frac{R_{\mathrm{tor}}^2 + \bar{r}^2 - \bar{r}\,R_{\mathrm{tor}}\cos\chi\left(\sin^2\chi + 2\right)}{\sin\chi} - \frac{\varpi\,(R_{\mathrm{tor}}\cos\chi - \bar{r})}{\tan\chi}\right]. \tag{5.33}$$

Note that the dependency $X \sim X_0 \sin\chi$ in ansatz (5.31) is borrowed from Markey and Tayler's approach, where $X^{\mathrm{MT}} = X_0 \sin\chi$ is used. Apart from this resemblance, our assumption is more specified. We ensure the localisation of $\boldsymbol{\xi}$ and exclude the magnetic field strength from the integral.

Close to the neutral line, this approach is equivalent to the $m = 1$ mode applied in the toroidal field case, where the reference axis of the displacement field was straight. This equivalence holds for Markey and Tayler's choice of X as well as for our assumption (5.31). The additional term $\left(\bar{r}^2 - \bar{r}_{\mathrm{tor}}^2\right)^2/4$ reduces to a constant amplitude in the case of $\bar{r} = 0$.

For the purpose of revealing the magnetic field independency of δW, the $\boldsymbol{\xi}$-defining functions are finally redefined, as shown in equation (C.94):

$$\begin{array}{ll} f_{\mathrm{B}} \equiv B_{\mathrm{pol}}^2\, f & \left(\partial_\psi X\right)_{\mathrm{B}} \equiv B_{\mathrm{pol}}\,\partial_\psi X \\ X_{\mathrm{B}} \equiv X & \left(\partial_\chi X\right)_{\mathrm{B}} \equiv \partial_\chi X \\ Y_{\mathrm{B}} \equiv B_{\mathrm{pol}}\, Y & \left(\partial_\chi Y\right)_{\mathrm{B}} \equiv B_{\mathrm{pol}}\,\partial_\chi Y \\ Z_{\mathrm{B}} \equiv B_{\mathrm{pol}}^2\, Z & \left(\partial_\chi\partial_\psi X\right)_{\mathrm{B}} \equiv B_{\mathrm{pol}}\,\partial_\chi\partial_\psi X. \end{array} \tag{5.34}$$

5.2.2. Energy variation explicitly

Remember the assumptions (5.28) made for the displacement field. Displacement fields of this type do not contribute to the fluid or gravitational part of the energy variation, as can be seen from equation (2.117).

The remaining energy variation density is the magnetic part,

$$\delta W = \delta W_{\mathrm{magn}}. \tag{5.35}$$

Applying choices (5.26) and (5.27) for $\boldsymbol{B}$ and $\boldsymbol{\xi}$ to the general form (2.116) with (2.117) of the energy variation, δW reads

$$\begin{aligned}\delta W = \frac{1}{4} \iiint \Re \Bigg\{ & \frac{\partial_\chi X^* \, \partial_\chi X}{\varpi^2 \, B_\chi^2 \, J} + \frac{\varpi^2 \, \partial_\chi Y^* \, \partial_\chi X}{m^2 \, J} + B_\chi^2 \, J \left(\partial_\psi X - Y\right) \left(\partial_\psi X^* - Y^*\right) \\ & - \partial_\psi \left(B_\chi^2 \, J\right) \left(X \, \partial_\psi X^* - X \, Y^* + \frac{Z}{J} \, \partial_\chi X^*\right) \Bigg\} \, \mathrm{d}\psi \, \mathrm{d}\varphi \, \mathrm{d}\chi.\end{aligned} \tag{5.36}$$

In this step, the transformation equations (2.8) for the toroidal coordinate system as well as the corresponding volume element (2.10) have been applied. The Jacobi determinant is given by $J = \varpi / B_{\mathrm{pol}}$, cf. equation (C.67).

Expression (5.36) contains the additional factor 1/2 compared to Markey and Tayler's form that arises from the fact that we apply actually complex displacement fields in this work, cf. appendix section A.5.4.

Beyond that, we neglected the factor $1/(4\,\pi)$ in (5.36) compared to the original expression (2.117a), since we switched to rationalised units in this chapter. This prefactor stemmed from the non-rationalised Maxwell equations (2.14) and it is suppressed in Markey and Tayler's formulation. However, in this application the factor would only represent a constant amplitude of the total energy variation, because only magnetic contributions are considered in δW.

Analogously to the previous application, the $\boldsymbol{\xi}$-defining functions are next split into real and imaginary parts that contribute equivalent terms to δW. According to that, X, Y and Z are chosen real without restriction.

Note that with our choice (5.27) for the displacement field, this also applies for the azimuthal displacement field component. This is not the case for Markey and Tayler's formulation. We use

$$\xi_\varphi = i \, \frac{\varpi \, Y}{m} \, \mathrm{e}^{\mathrm{i}m\varphi} \qquad \text{with} \qquad Y = Y_R. \tag{5.37}$$

In contrast, Markey & Tayler (1973) define

$$\xi_\varphi^{\mathrm{MT}} = \frac{\varpi \, Y^{\mathrm{MT}}}{m} \, \mathrm{e}^{\mathrm{i}m\varphi} \qquad \text{with} \qquad Y^{\mathrm{MT}} = i \, Y_I^{\mathrm{MT}}. \tag{5.38}$$

The φ-integral can next be performed analytically while the real part is evaluated. The

particular steps are shown in the appendix section C.2.3.

The result is the explicit energy variation for the poloidal field case (C.103):

$$\delta W = \frac{\pi}{2} \iint \left\{ \frac{(\partial_\chi X)^2}{\varpi\, \bar{r}^2} + \frac{\varpi\, B_{\mathrm{pol}}^2}{m^2} (\partial_\chi Y)^2 + \frac{\bar{r}^2\, B_{\mathrm{pol}}^2}{\varpi} \left(\partial_\psi X - Y\right)^2 \right. \tag{5.39}$$
$$\left. + B_{\mathrm{pol}} \frac{2\, R_{\mathrm{tor}} - \bar{r}\, \cos\chi}{\varpi^2} \left(X\, \partial_\psi X - X\, Y + \frac{B_{\mathrm{pol}}}{\varpi}\, Z\, \partial_\chi X \right) \right\} \mathrm{d}\varpi\, \mathrm{d}z.$$

We transformed the integral to cylindrical coordinates because the numerical integration will be performed in ϖ and z. The $\boldsymbol{\xi}$-defining functions are chosen according to equations (5.31). The subsequent transformation steps of δW are given in the appendix.

Finally, the magnetic field dependency can be factored out applying choice (5.34), and the simplified energy variation becomes

$$\delta W = \frac{\pi}{2} \iint \left\{ \frac{(\partial_\chi X)_{\mathrm{B}}^2}{\varpi\, \bar{r}^2} + \frac{\varpi}{m^2} (\partial_\chi Y)_{\mathrm{B}}^2 + \frac{\bar{r}^2}{\varpi} \left(\left(\partial_\psi X\right)_{\mathrm{B}} - Y_{\mathrm{B}} \right)^2 \right. \tag{5.40}$$
$$\left. + \frac{2\, R_{\mathrm{tor}} - \bar{r}\, \cos\chi}{\varpi^2} \left(X_{\mathrm{B}} \left(\partial_\psi X\right)_{\mathrm{B}} - X_{\mathrm{B}}\, Y_{\mathrm{B}} + \frac{Z_{\mathrm{B}}\, (\partial_\chi X)_{\mathrm{B}}}{\varpi} \right) \right\} \mathrm{d}\varpi\, \mathrm{d}z,$$

as shown in equation (C.104). Note that quantities with the index B are truly independent of B_{pol}, without implicit dependencies.

Therefore, according to form (5.40) of the energy variation, a possibly detectable instability must indeed be independent of the magnetic field strength.

Beyond that, the analytic elimination of B_{pol} from the integrand reduces the numerical integration error.

5.2.3. Computation

Parameter set choice

Similar to the previous application on toroidally magnetised neutron stars, the parameter values for the equilibrium system, magnetic field and displacement field need to be specified.

Additionally, the magnetic field geometry and displacement field localisation are determined by the parameters R_{tor} and $\bar{r}_{\mathrm{tor}}$ of the toroidal coordinate system.

The background model will be constructed by solving the Newtonian system equations (2.26) for a $\Gamma_0 = 2$ polytrope. The model parameters we choose generate typical neutron stars. They are listed in table 5.2.

The mode index m will be varied within the range 1.6 to 6.0, depending on the model under consideration. The covered range is chosen large enough for a potential change in sign to be detected.

Note that by its definition in equation (2.119), the mode index is defined as an integer. Here, however, rational numbers are applied in order to better resolve the area around a potential root, i.e. a potential change in the stability behaviour.

Table 5.2.: Background model parameter set used for the Tayler instability proof on poloidally magnetised neutron stars. The remaining parameters for magnetic field, displacement field, computation and the geometrical parameters are given in the text.

ρ_c in $10^{15}\,\mathrm{g/cm^3}$	$\tilde{\kappa}^*$ in $10^{11}\,\mathrm{cm}^2$	M in $\mathrm{M}_\odot$	R in km	M/R
1.1	8	0.99	11.2	0.13
1.05	9	1.13	11.9	0.14
1.0	10	1.26	12.5	0.15
1.3	8.5	1.28	11.5	0.16

For the sake of numerical accuracy, form (5.40) of the energy variation density will be entered in the integration code rather than form (5.39). That means, the magnetic field strength cancels out exactly from the integrand and B_{pol} does not need to be defined.

The only remaining $\boldsymbol{\xi}$-defining parameter that has not been set yet is X_0. It acts as the displacement field vector amplitude and is arbitrarily chosen as $X_0 = 1 \times 10^{-3}$. From equation (5.40) with (5.31) and (5.34), it can be inferred that it solely determines the absolute value of the energy variation $|\delta W|$.

The position of the neutral line and the extent of the localisation area are set to

$$R_{\mathrm{tor}} = \frac{R}{2} \qquad \frac{\bar{r}_{\mathrm{tor}}}{R_{\mathrm{tor}}} = 0.8. \tag{5.41}$$

The torus centre is located at the half stellar radius, which allows for a variation of $\bar{r}_{\mathrm{tor}}$ up to high values. The actual extent of the localisation area we assume here ensures that the localisation torus completely lies within the star.

The numerical parameters are chosen as follows.

The vacuum pressure level for the Runge-Kutta solver of the background equations is set to $\tilde{p}_\varepsilon = 10^{-10}$. The corresponding step width is $h_r = 4 \times 10^{-4}$, while the Simpson integration grids are determined by $u_\varpi = 10$ and $u_z = 100$.

Note that these parameters create relatively coarse grids. This choice was motivated by the following fact. For the specific case investigated here, the numerical result diverges with an increasing grid resolution, as it will be discussed in the subsequent section. Therefore, we do not want to choose an overly fine grid here, for the sake of computation time.

Numerical features

The two-dimensional integration area used for the poloidal field application was constructed in section 4.3.2 and presented in equation (4.68). It is identical to the localisation area cross section.

Note that the integrand $\mathcal{E}$ in equations (5.36) or (5.40) shows a pole at the neutral line.

The pole is not caused by numerical inaccuracies, but it is of physical nature. That means, its occurrence can be expected from the formula. All terms besides V diverge

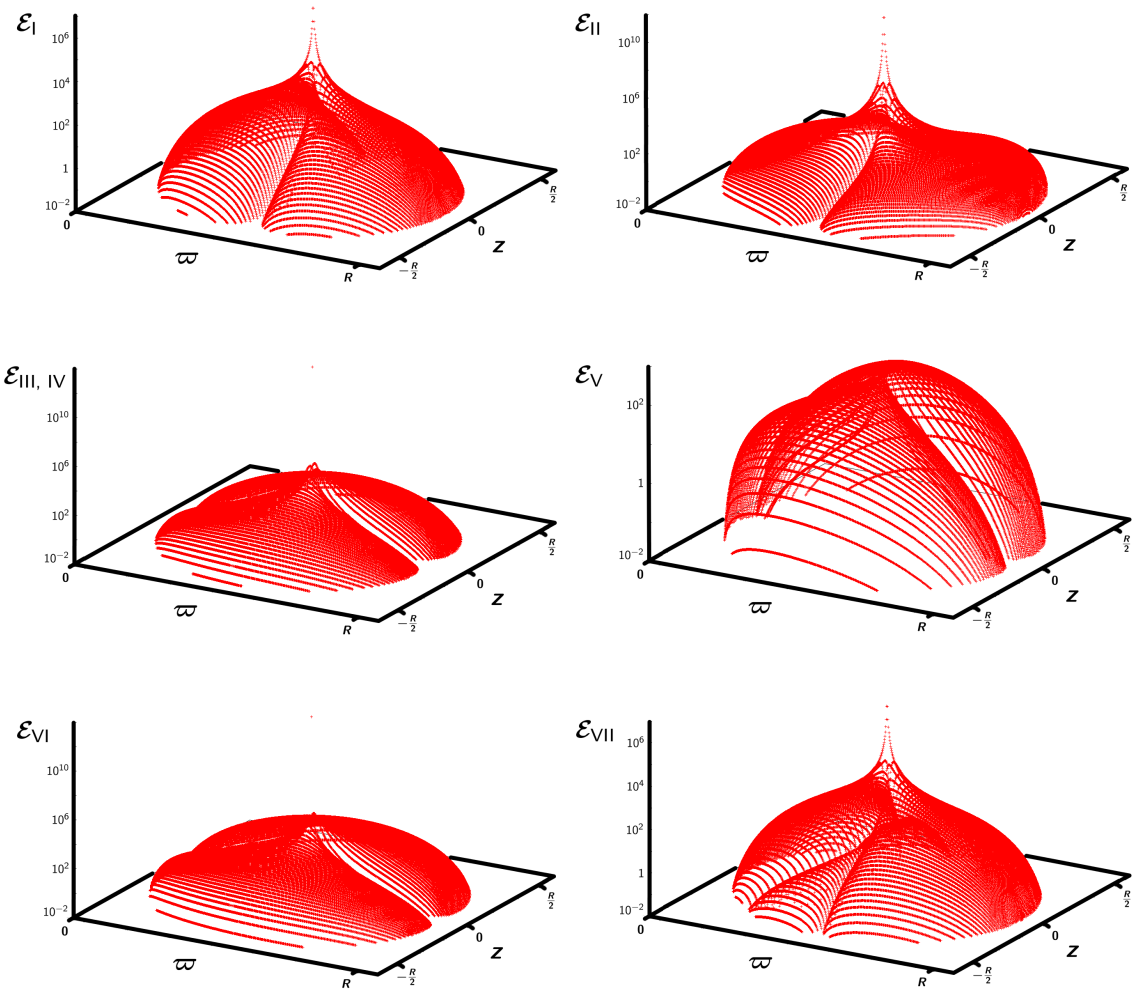

Figure 5.4.: Integrand terms for the poloidally magnetised neutron star, defined by equations (C.86) and (5.42). All terms besides $\mathcal{E}_{\mathrm{V}}$ show a pole at the neutral line. The system quantities are defined in the text. The numerical resolution is given by the Runge-Kutta stepwidth $h_r = 1 \times 10^{-3}$.

for $(\varpi = R_{\mathrm{tor}}, z = 0)$, where the separate integrand terms have been defined in equation (C.86).

For an illustration, the integrand terms $\mathcal{E}_{\mathrm{I}}$ -$\mathcal{E}_{\mathrm{VII}}$ are plotted in figure 5.4, where

$$\mathcal{E}_{\mathrm{III,\,IV}} \equiv \frac{\bar{r}^2\, B_{\mathrm{pol}}^2}{\varpi} \left(\partial_\psi X - Y\right)^2 . \tag{5.42}$$

Due to the physical pole, the Simpson method is not a suitable integration method for this specific application. The computed integrand value δW does not converge with increasing integration accuracy, as it is strongly affected by the extremely high values of $\mathcal{E}$ close to the pole.

One possibility to avoid this problem would be the construction of an alternative dis-

placement field which removes the divergent terms from the integrand.

However, this task might be extremely difficult if not impossible, as $\boldsymbol{\xi}$ still needs to simultaneously fulfil the conditions that have been imposed earlier: Markey and Tayler's assumptions (5.28), the ability of being localised in order to neglect the surface integral terms, and the potential of revealing the Tayler instability, which translates into conditions for the choice of $f(\psi, \chi)$.

Alternatively, we could replace the Simpson integration we use for the semi-analytic routine by an adaptive integration method which is suitable for divergent integrands.

However, at this stage, the purpose of this application is only to test the functionality of the semi-analytic method and the corresponding code at large. Precise values for the energy variation are not required. The instability verification is based on the qualitative consideration of $\delta W \gtrless 0$. Future projects might be adequately describable by the Simpson method. The appropriate integration routine will need to be chosen for each newly investigated system anyway. Concerning the effort, the replacement of the integration routine is not a reasonable choice for the test system considered here.

Therefore, we are going to apply the displacement field defined above as well as the Simpson integration routine, and exclude the pole from the integration area by cutting the integrand values at a certain maximum. That way, only grid points that are located far enough from the pole at the neutral line ($\varpi = R_{\mathrm{tor}}, z = 0$) are considered during the numerical integration. The grid points closest to the singularity, providing integrand contributions that exceed the average by orders of magnitude, are excluded.

Note that the procedure of cutting the pole removes the quantitative significance of the results. They need to be considered as qualitative results instead.

In order to assure their meaningfulness, it has been ascertained that the qualitative result is not influenced by the computation parameter choice. The extent of the localisation region as well as the numerical grid resolution do not have an impact on the sign of δW or its separate contributions.

5.2.4. Results

The energy variation (5.40) has been calculated for different model systems and varying mode indices. The results are presented in this section.

The result $\delta\widetilde{W}(m)$ is presented in figure 5.5. Remember that the mode index m is varied continuously for a higher resolution of a possible change in the stability behaviour, although m has actually been defined as an integer, according to assumption (5.27).

The interpretation of figure 5.5 shows, all model systems feature an equivalent $\delta W(m)$-dependency.

The energy variation is positive for small mode indices and becomes negative for increasing m, exceeding a critical value, $m > m^{\mathrm{crit}}$. The change in sign implies a change in the system's stability behaviour.

That means, for all neutron star models considered here, a displacement field $\boldsymbol{\xi} \sim \mathrm{e}^{\mathrm{i}m\varphi}$ can be found that decreases the total system energy. There is an infinite number of perturbations with $m > m^{\mathrm{crit}}$ against which the investigated systems are unstable.

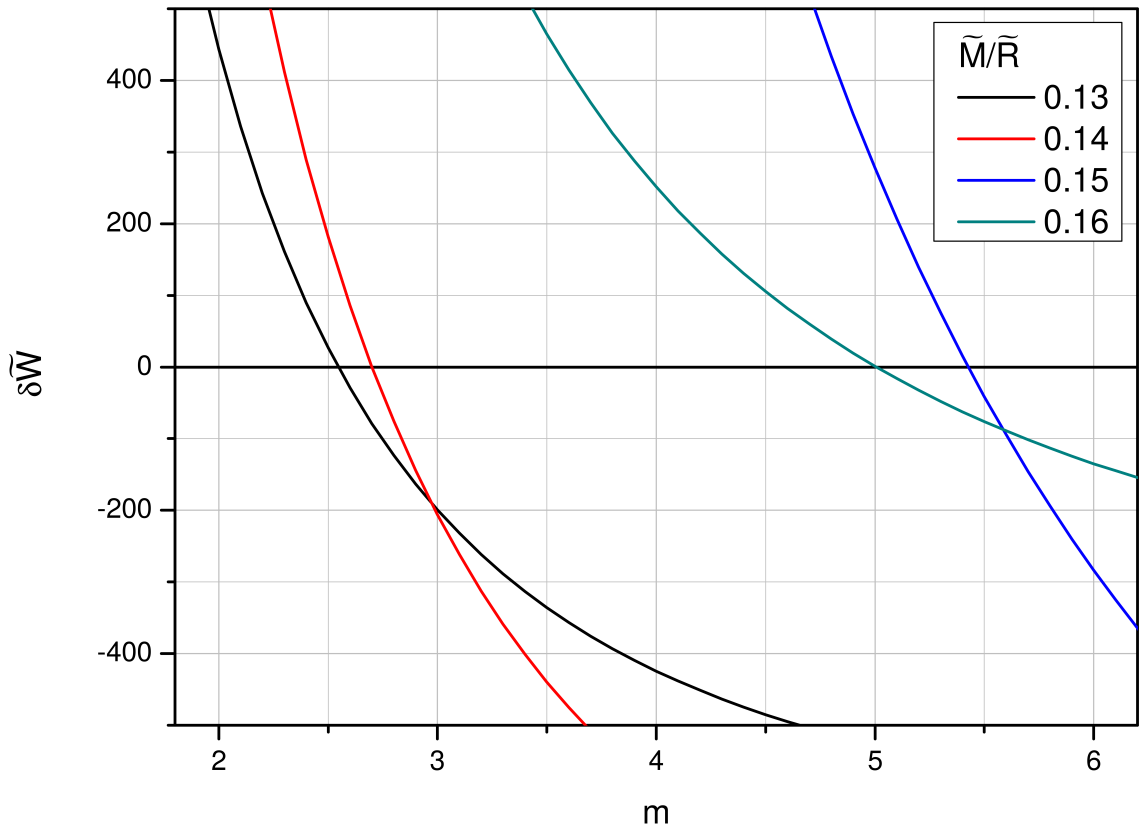

Figure 5.5.: Dimensionless energy variation $\delta\widetilde{W}$ of the poloidally magnetised neutron star, calculated with the semi-analytic method. The energy variation is plotted against the displacement field mode index m for neutron star models with different compactness. The parameters are defined in table 5.2 and in the text.

According to stability criterion (2.45), one unstable mode is sufficient to prove the instability of the equilibrium state. From graph 5.5 we can therefore deduce that the purely poloidally magnetised models we tested are unstable.

Furthermore, the detected instability is evidently driven by the magnetic field. The Lorentz term is the only contribution to the energy variation we considered when we imposed conditions (5.28) on the displacement field, cf. equation (5.35).

Once the detected instability has been identified as a magnetic field instability, we can also deduce its structural character.

The magnetic field strength has no impact on the $\delta W(m)$-behaviour. The onset of the instability is therefore independent of the field strength.

This observation is confirmed by the analytical consideration formulated above: The energy variation (5.40) is independent of the magnetic field strength B_{pol}. That means, the instability is always present as long as a poloidal magnetic field exists which is of the structure defined in equation (5.26). The field strength can become arbitrarily small, as long as the corresponding energy variation is significant compared to other contributions in the star.

As soon as the magnetic field is removed from the model system, the magnetic field contribution δW_{magn} vanishes. For the displacement field structure applied here, the energy variation vanishes as well, $\delta W = 0$, i.e. the system is metastable.

5.2.5. Interpretation

Based on the results presented in the previous section, we need to evaluate whether the Tayler instability of the poloidal field could be verified applying the semi-analytic method.

The results suggest: The instability found in the previous section is indeed the Tayler instability of neutron stars with purely poloidal magnetic fields detected by Markey & Tayler (1973).

This conclusion is supported by the fact that the instability both is magnetically caused and shows a structural character.

The verification of the Tayler instability was accomplished for the models shown in table 5.2 and for the displacement field choices (5.27), (5.31). However, the uniform behaviour of $\delta W(m)$ found for all investigated systems suggests that the validity of this result might hold as well in generalised cases.

On the contrary, graph 5.5 suggests a connection between the critical mode index and the mass, radius or compactness of the neutron star model. This potential dependency could be investigated if the numerical Simpson integration would be replaced by an adaptive integration method that is able to provide quantitative results, in spite of the diverging integrand in (5.40). The qualitative results we produced cannot serve for this kind of analysis.

Note that the stability analysis provided here is based on a stationary picture. Although higher mode indices produce stronger negative energy variations, these perturbations do not necessarily represent the “strongest instability”. As explained in section 2.3.3, this term typically describes the fastest growing mode.

The detected tendency of the instability onset with an increasing mode index $m > m^{\text{crit}}$ is in accordance with the analytic stability evaluation given by Markey & Tayler (1973). The instability proof provided there is based on the assumption $m \to \infty$. For the detailed analytic stability consideration given by Markey & Tayler (1973), see appendix section C.2.4.

Finally, it can be remarked that the qualitative nature of the results produced here does not keep us from drawing valid conclusions.

This emphasises the great advantage of the semi-analytic method of delivering statements about the stability requiring little effort. The semi-analytic method can produce results without providing additional quantitative information that would complicate the study considerably. It is therefore perfectly suitable for a first evaluation of a system's stability behaviour, before simulations or normal mode analysis are applied to the system.

For future applications, however, the semi-analytic method can be adapted optimally to the system under consideration by choosing the ideal integration method, in order to receive reliable quantitative results directly from the method as well.

Summarising, the application of the semi-analytic method on poloidally magnetised stars proved the functionality of the method as well as the code that has been set up so far. After the verification of the toroidal field Tayler instability, this validation demonstrates that the method works on structurally distinct problems of different geometry.

5.3. Stars with mixed magnetic fields and stratification

Once the semi-analytic method proved itself as a functional tool to investigate purely toroidal as well as purely poloidal magnetic field structures in the previous sections, the next step is to apply it to a system with a mixed magnetic field consisting of both components. Furthermore, the simple polytropic composition structure will be altered into a stratified density profile. And the Cowling approximation will be lifted. This approach represents an ideal test of the method, since it involves the combination of all energy variation terms and all code fragments derived and set up so far, cf. chapter 4.

The application presented in this section aims on the verification of the analytic study performed by Akgün et al. (2013). The semi-analytic method is challenged to reproduce the stability criterion analytically derived in this study.

This test first indicates whether the semi-analytic method is capable of reproducing quantitatively known results, after the qualitative verifications of the Tayler instabilities.

For the sake of comparability of the results, the model system used here will be chosen in accordance to the model defined by Akgün et al.

However, several simplifying assumptions that were necessary in the analytical study will be lifted. The most prominent one is the removal of the Cowling approximation.

Magnetic and displacement field structure are chosen in such a way that the star would be unstable with the toroidal magnetic field component alone. The magnetic field component which is tested for its stability behaviour is the toroidal one.

Therefore, the displacement field applied here is equivalent to the one used in the toroidal field case model described in section 5.1. The poloidal field component is superimposed to this system, possibly stabilising the Tayler instability in the presence of stratification.

5.3.1. System setup

In this application, we consider stratified stars with mixed magnetic fields in Cowling approximation as well as in a full non-Cowling treatment.

Rotation, neutron star crust and inner stellar core are not taken into account. The star is assumed to be a fluid consisting of neutrons, protons and electrons, without superfluidity or superconductivity. The poloidal part of the magnetic field pervades the stellar interior and exterior, taking on a dipole structure outside the star. The toroidal component is confined into the torus-shaped region inside the star that is enclosed by the outermost poloidal field line which still closes inside the star. According to the presence of both field components and for the sake of comparison with Akgün et al. (2013), spherical coordinates will be used for this application.

Note that in contrast to the previously shown applications, non-rationalised Gaussian cgs units will be applied in the mixed field case. That way, in accordance to Akgün et al., the magnetic contributions to the energy variation consistently contain the factor $1/(4\pi)$ stemming from the Maxwell equations (2.14).

Magnetic field

The toroidal and poloidal magnetic field components in the mixed field case can be described separately. For a visualisation see Akgün et al. (2013).

The poloidal field extending everywhere is assumed to have a simple but realistic field structure. It simulates the magnetic field of a point dipole outside the star. It corresponds to the lowest non-vanishing order in a multipole expansion, considering that magnetic monopoles do not exist. This assumption is quite a good approximation for exterior neutron star magnetic fields, according to observational data. The neutral line defined by $\boldsymbol{B}_{\mathrm{pol}} = 0$ represents the symmetry axis of the poloidal field in the mixed field picture. Note that the poloidal field lines are not necessarily circles around the neutral line as in the previous application. Their shape is more realistic with straighter lines towards the stellar symmetry axis and more curved lines towards the equator region.

The toroidal field component is spatially confined into a torus-like region including the neutral line. Since the model star is situated in vacuum, the toroidal field cannot be sustained outside the star, cf. section 2.2.3. Therefore, the region with $\boldsymbol{B}_{\mathrm{tor}} \neq 0$ is bounded by the outermost poloidal field line that still closes inside the star. The symmetry axis of the toroidal field component is equivalent to the stellar symmetry axis, due to the lack of rotation.

An arbitrary magnetic field is divergence free. Additionally, the field we assume here is axisymmetric and can thus be expressed in terms of a stream function, as shown in equation (B.11). Akgün et al. (2013) utilise this approach to construct ansatz (2.33) for

the mixed magnetic field:

$$\begin{aligned} \boldsymbol{B}_{\mathrm{tor}} &= B_0\, \eta_{\mathrm{tor}}\, R\, \hat{\beta}(r,\vartheta)\, \nabla_r \varphi \\ \boldsymbol{B}_{\mathrm{pol}} &= B_0\, \eta_{\mathrm{pol}}\, R^2\, \nabla_r \hat{\alpha}(r,\vartheta) \times \nabla_r \varphi. \end{aligned} \tag{5.43}$$

The remaining structure is determined by choices (2.34) and (2.35):

$$\hat{\alpha}(r,\vartheta) = f(x)\, \sin^2 \vartheta \qquad \hat{\beta}(r,\vartheta) = \begin{cases} (\hat{\alpha}-1)^2 & \text{for } \hat{\alpha} \geq 1 \\ 0 & \text{for } \hat{\alpha} < 1, \end{cases} \tag{5.44}$$

and

$$f(x) = f_2\, x^2 - f_4\, x^4 + f_6\, x^6. \tag{5.45}$$

These assumptions ensure that the poloidal field is continuous at the stellar surface, matching the exterior field, and finite at the stellar centre. The toroidal field component is continuous at the boundary of the toroidal field confinement region.

The maximum field strengths of the poloidal and toroidal field are determined by the amplitude parameters η_{pol} and η_{tor}, as explained in section 2.2.3.

Stellar composition

In the mixed field case, we assume a polytropic background star, described by the polytropic index Γ_0. The equilibrium quantities pressure, mass, density and gravitational potential will be computed by solving the system equations (2.26) with the polytropic equation of state (2.22).

Note that Akgün et al. use an explicit density distribution approximating the polytrope instead in order to make it analytically treatable. Thanks to the semi-analytic method, this simplification is not necessary here.

The perturbations are described by the polytropic index $\Gamma_1 \neq \Gamma_0$, which generally differs from the background polytropic index which implies stratification, as explained in section 2.2.3. This procedure is in accordance with the description in Akgün et al. (2013).

However, Akgün et al. distinguish between two background polytropic indices, one for the unmagnetised equilibrium system and one for the magnetised one. Thus, they work with three polytropic indices in total. For a straightforward comparison with their work, see table E.3 providing an overview on the notations of polytropic indices applied by different authors.

According to the consideration of stratification, the fluid contribution to the energy variation density is given by equation (4.6).

Description of the gravitational energy contribution

Since the study performed by Akgün et al. was purely analytical, it relied on the assumption of the Cowling approximation. For the purpose of a direct comparison of the results and an evaluation of the semi-analytic method's functionality, we first apply the Cowling approximation as well.

The gravitational contribution to the energy variation is given by equation (2.117c).

Afterwards, the system under investigation is gradually made more complex by removing the Cowling approximation and applying the full non-Cowling treatment instead.

The additional contribution to the energy variation is given by expressions (4.44a) or (4.44b). The total gravitational contribution is given by equation (4.8), with an unchanged Cowling part.

Both sign conventions $\boldsymbol{g} = \pm\nabla\Phi_0$ for the gravitational field vector are kept. The lower sign corresponds to the notation applied by Akgün et al. (2013).

Displacement field

In the mixed field case investigated here, the toroidal field component is tested regarding its stability behaviour. Ansatz (2.130) chosen by Akgün et al. for the displacement field is thus equivalent to the choice (5.5) that has been used in the toroidal field case in section 5.1. Both approaches are identical if the $\boldsymbol{\xi}$-defining functions fulfil relation (2.131), as shown in the appendix section C.3.1.

The $\boldsymbol{\xi}$-defining functions are set up similarly to the toroidal field case in section 5.1.

They are chosen in such a way that the Tayler instability of the toroidal field component is detectable in the absence of the poloidal field component. That means, with assumptions (2.132) and (2.133) for $\tilde{R}$, $\tilde{S}$ and $\tilde{T}$, the energy variation density is negative at the position (x_0, ϑ_0) of the localisation area if only fluid and gravitational contributions and the toroidal field part $\mathcal{E}_{\mathrm{tor}}$ of the magnetic contribution are taken into account.

In order to achieve this, the energy variation density $\mathcal{E}_{\mathrm{tor}} + \mathcal{E}_{\mathrm{fluid}} + \mathcal{E}_{\mathrm{grav}}$ of the toroidally magnetised star is minimised with respect to the $\boldsymbol{\xi}$-defining function $\tilde{T}$ of the azimuthal component.

Beyond that, the displacement field is localised to an axisymmetric region with an ellipse-like cross section in the (r, ϑ)-plane, as explained in section 2.3.3 and illustrated in figure 2.17.

Constraints on the $\boldsymbol{\xi}$-defining functions follow from the requirement of a vanishing surface integral contribution and the avoidance of singularities when the poloidal field is added to the system. The exact procedure is shown in the appendix section C.3.1.

The final choice is, cf. equations (2.132), (2.133) and (2.134):

$$\left.\begin{aligned} \tilde{R}(r,\vartheta) &= -\frac{\xi_0}{r}\,\sigma\left(1-\bar{\chi}^2\right)^{\sigma-1}\,\partial_\vartheta\bar{\chi}^2 \\ \tilde{S}(r,\vartheta) &= \frac{\xi_0}{R}\,\sigma\left(1-\bar{\chi}^2\right)^{\sigma-1}\,\partial_x\bar{\chi}^2 \end{aligned}\right\} \quad \text{in } A, \qquad \left.\begin{aligned} \tilde{R}(r,\vartheta) &= 0 \\ \tilde{S}(r,\vartheta) &= 0 \end{aligned}\right\} \quad \text{else,} \tag{5.46}$$

with

$$\tilde{T}(r,\vartheta) = \tilde{T}_{\min} \equiv -\frac{E_1(r,\vartheta)}{2\,m\,E_2(r,\vartheta)} \tag{5.47}$$

and

$$\bar{\chi}^2(r,\vartheta) = \left(\frac{x-x_0}{\delta_r}\right)^2 + \left(\frac{\vartheta-\vartheta_0}{\delta_\vartheta}\right)^2 \qquad \partial_\vartheta\bar{\chi}^2 = 2\,\frac{\vartheta-\vartheta_0}{\delta_\vartheta^2} \qquad \partial_x\bar{\chi}^2 = 2\,\frac{x-x_0}{\delta_r^2}. \tag{5.48}$$

Expressions E_1 and E_2 are contributions to the energy variation integrand, and will be defined in the subsequent section.

This assumption for the displacement field was derived for mode indices $m \neq 0$.

In accordance with the toroidal field application 5.1 and Akgün et al. (2013), we will use $m = 1$ for the calculations. It represents the particular Tayler unstable mode that is expected to be the strongest one in a toroidally magnetised system. That way, the possible finding of a stabilisation of the considered mode would be more significant.

5.3.2. Energy variation explicitly

The energy variation of a stratified star is given by the general form (4.47) with (4.48). In Cowling approximation, we assume $\delta W_{\text{grav}}^{\text{nC}} = 0$. In the case of the full non-Cowling treatment, the non-Cowling gravitational contribution must be additionally considered. For displacement field choice (2.130), $\delta W_{\text{grav}}^{\text{nC}}$ is given by equation (4.49) with relations (4.50) and (4.51).

In order to achieve the explicit form for the energy variation in the mixed field case, the magnetic field and displacement field choices (5.43) and (2.130) with (5.44), (5.45), (5.46) and (5.47) are inserted into the expression. After some rearrangements, definitions and algebra, Akgün et al. express the energy variation in a compact form.

Since the derivation is shown in Akgün et al. (2013), we will only outline the essential transformation steps and present the end result for the total energy variation in this section.

In extension to the formulas presented by Akgün et al., we keep track of the origin of each term in the energy variation. That way, we are able to calculate the impact of every contribution to the energy variation separately.

In analogy to Akgün et al., we split the magnetic contribution into a toroidal, poloidal and mixed part,

$$\mathcal{E}_{\text{magn}} = \mathcal{E}_{\text{tor}} + \mathcal{E}_{\text{pol}} + \mathcal{E}_{\text{cross}}, \tag{5.49}$$

and combine the fluid and gravitational contributions to the energy variation into one hydrostatic term

$$\mathcal{E}_{\text{hyd}} \equiv \mathcal{E}_{\text{fluid}} + \mathcal{E}_{\text{grav}}. \tag{5.50}$$

With assumption (5.43), the magnetic contribution consists of terms purely involving $\boldsymbol{B}_{\text{tor}}$, described by $\mathcal{E}_{\text{tor}}$, terms purely involving $\boldsymbol{B}_{\text{pol}}$, described by $\mathcal{E}_{\text{pol}}$, and terms involving both field components, described by $\mathcal{E}_{\text{cross}}$. The mathematical illustration is shown in the appendix section C.3.2.

Next, Akgün et al. define the notations

$$\Lambda(u) = \tilde{R}\,\partial_r u + \frac{\tilde{S}\,\partial_\vartheta u}{r} \tag{5.51}$$

and

$$D_m = \frac{3\tilde{R}}{r} + \partial_r \tilde{R} + \frac{2\tilde{S}}{r}\cot\vartheta + \frac{\partial_\vartheta \tilde{S}}{r} - \frac{m\tilde{T}}{r\sin\vartheta}, \tag{5.52}$$

where $u = \{m_0, \rho_0, p_0, \Phi_0, \alpha, \beta\}$ can be an arbitrary axisymmetric system quantity and D_m denotes the prefactor of the displacement field divergence

$$\nabla \cdot \boldsymbol{\xi} = D_m \, r \, \sin\vartheta \, \mathrm{e}^{\mathrm{i}m\varphi} \,. \tag{5.53}$$

With these definitions and choice (5.43) for the magnetic field, Akgün et al. receive expressions for $\mathcal{E}_{\mathrm{tor}}$, $\mathcal{E}_{\mathrm{pol}}$ and $\mathcal{E}_{\mathrm{hyd}}$, which are shown in equation (C.120).

The $\boldsymbol{\xi}$-defining functions can be chosen real without restriction as their real and imaginary parts contribute equivalent terms to the energy variation density, analogously to the previous applications.

The mixed term $\mathcal{E}_{\mathrm{cross}}$ is purely imaginary and will eventually not contribute to the energy variation as demonstrated in the appendix.

The expression (C.120c) Akgün et al. give for the hydrostatic part is indeed identical to the sum of fluid and gravitational contributions (4.6) and (2.115) set up in this work for the stratified star, as proven in the appendix section C.3.3.

The final form of the energy variation that will be used for the computation is

$$\delta W = \frac{\pi}{2} \iint \left\{ E_0 - \frac{E_1^2}{4\,E_2} + 2\,E_{\mathrm{pol}} \right\} \varpi \, \mathrm{d}\varpi \, \mathrm{d}z \tag{5.54}$$

with

$$E_0 = E_0^{\mathrm{tor}} + E_0^{\mathrm{hyd}} \qquad E_1 = E_1^{\mathrm{tor}} + E_1^{\mathrm{hyd}} \qquad E_2 = E_2^{\mathrm{hyd}}. \tag{5.55}$$

The contributions caused by the toroidal magnetic field component are

$$E_0^{\mathrm{tor}} = \frac{\beta^2}{4\,\pi} D_0^2 + \left(\frac{\beta\,\Lambda(\beta)}{4\,\pi} - \frac{\beta^2\,\Lambda(\varpi)}{\pi\,\varpi} \right) D_0 - \frac{\beta\,\Lambda(\beta)\,\Lambda(\varpi)}{2\,\pi\,\varpi} + \frac{\beta^2\,\Lambda^2(\varpi)}{\pi\,\varpi^2} \tag{5.56a}$$

$$E_1^{\mathrm{tor}} = -\frac{\beta\,\Lambda(\beta)}{4\,\pi\,\varpi}. \tag{5.56b}$$

Note that $E_2^{\mathrm{tor}} = 0$.

The fluid and gravitational parts, combined in the hydrostatic contribution provide

$$E_0^{\mathrm{hyd}} = \varpi^2\,\Gamma_1\,p_0\,D_0^2 + \left(\varpi^2\,\Lambda(p_0) \pm \varpi^2\,\rho_0\,\Lambda(\Phi_0)\right) D_0 \pm \varpi^2\,\Lambda(\rho_0)\,\Lambda(\Phi_0) + \frac{m^2\,\beta^2\left(\tilde{R}^2 + \tilde{S}^2\right)}{4\,\pi\,\varpi^2} \tag{5.57a}$$

$$E_1^{\mathrm{hyd}} = -2\,\varpi\,\Gamma_1\,p_0\,D_0 - \varpi\,\Lambda(p_0) \mp \varpi\,\rho_0\,\Lambda(\Phi_0) \tag{5.57b}$$

$$E_2^{\mathrm{hyd}} = \Gamma_1\,p_0. \tag{5.57c}$$

The poloidal field contributes

$$E^{\mathrm{pol}} = \frac{1}{8\,\pi\,\varpi^2\,r^2}\Bigg[r^2\left(m\,\tilde{T}\,\partial_r\alpha - \frac{\varpi\,\Lambda(\alpha)}{r} - \varpi\,\partial_r\Lambda(\alpha)\right)^2 + \left(m\,\partial_\vartheta\alpha\,\tilde{T} - z\,\Lambda(\alpha) - \varpi\,\partial_\vartheta\Lambda(\alpha)\right)^2$$
$$+\varpi\,r\,\Delta^*\alpha\,\tilde{S}\left(m\,\partial_\vartheta\alpha\,\tilde{T} - z\,\Lambda(\alpha) - \varpi\,\partial_\vartheta\Lambda(\alpha)\right) + \varpi^2\left(\partial_\vartheta\alpha\,\partial_r\tilde{T} - \partial_r\alpha\,\partial_\vartheta\tilde{T}\right)^2$$
$$+\varpi\,r^2\,\Delta^*\alpha\,\tilde{R}\left(m\,\partial_r\alpha\,\tilde{T} - \frac{\varpi\,\Lambda(\alpha)}{r} - \varpi\,\partial_r\Lambda(\alpha)\right)\Bigg], \tag{5.58}$$

where

$$\Delta^* \equiv \partial_r^2 + \frac{\sin\vartheta}{r^2}\,\partial_\vartheta\left(\frac{\partial_\vartheta}{\sin\vartheta}\right) \tag{5.59}$$

denotes the Grad-Shafranov operator.

The total toroidal, hydrostatic and combined contributions to the energy variation density are

$$\mathcal{E}_{\mathrm{tor}} = E_1^{\mathrm{tor}}\,m\,\tilde{T} + E_0^{\mathrm{tor}} \tag{5.60a}$$
$$\mathcal{E}_{\mathrm{hyd}} = E_2^{\mathrm{hyd}}\left(m\,\tilde{T}\right)^2 + E_1^{\mathrm{hyd}}\,m\,\tilde{T} + E_0^{\mathrm{hyd}} \tag{5.60b}$$
$$\mathcal{E}_{\mathrm{tor}} + \mathcal{E}_{\mathrm{hyd}} = E_2\left(m\,\tilde{T}\right)^2 + E_1\,m\,\tilde{T} + E_0. \tag{5.60c}$$

Note that the integrand in equation (5.54) has been minimised with respect to $\tilde{T}$, whereas expression (5.60c) has not been minimised yet.

Remember that the minimising value $\tilde{T}_{\mathrm{min}}$ has been defined in equation (5.47), depending on E_1 and E_2. These functions are the sums of the magnetic and hydrostatic parts (5.56) and (5.57).

Finally, Akgün et al. approximate the poloidal contribution to

$$E^{\mathrm{pol}} \approx \frac{\left(\partial_\vartheta\alpha\,\partial_r\tilde{S}\right)^2}{8\,\pi\,r^2}\left(1 + \frac{4\,z^2}{m^2\,r^2}\right), \tag{5.61}$$

which facilitates the analytic consideration.

In contrast to the analytic study, this approximated form is not necessary for an investigation with the semi-analytic method. However, the semi-analytic method can be used to test the validity of this approximation by comparing the stability criteria derived from the exact and the approximated energy variation densities (5.58) and (5.61).

In the unmagnetised system, the energy variation is

$$\delta W_{\mathrm{hyd}} = \frac{\pi}{2}\iint\left(\frac{1}{\Gamma_0} - \frac{1}{\Gamma_1}\right)\frac{\left(\boldsymbol{\xi}\cdot(\nabla p_0)\right)^2}{p_0}\,\varpi\,\mathrm{d}\varpi\,\mathrm{d}z \qquad \text{for} \qquad \boldsymbol{B} = 0. \tag{5.62}$$

In contrast to the previous applications, Akgün et al. apply the same procedure that we use to ensure that the energy variation is real and physically meaningful. They take

the real part over the total integrand. Therefore, the expressions (5.56), (5.57) and (5.58) shown here are identical to the expressions given by Akgün et al. (2013) without additional prefactors, as long as the real parts have been evaluated in both formulas, respectively have not been evaluated in both formulas yet.

The prefactor $1/(4\pi)$ arising from the non-rationalised Maxwell equations (2.14) and appearing in the magnetic field terms, is present in both studies.

Note that in this work, the energy variation density is defined via $\delta W = \iint \mathcal{E}\,\mathrm{d}V$, while Akgün et al. define $\delta W^{\mathrm{A}} = 1/2 \iint \mathcal{E}^{\mathrm{A}}\,\mathrm{d}V$. Therefore, $\mathcal{E}^{\mathrm{A}} = 2\,\mathcal{E}$.

The analytical consideration presented by Akgün et al. (2013) is further based on an approximation of the derived energy variation terms, as shown in the appendix section C.3.4.

Beyond that, the extent of the localisation region is assumed to be infinitesimal by setting $\delta_r \to 0$ and $\delta_\vartheta \to 0$ simultaneously.

Finally, a stability criterion (C.139) is analytically derived which describes the minimal poloidal field strength necessary for the stabilisation of the toroidal field Tayler instability.

The verification of this criterion represents a quantitative test for the semi-analytic method. Due to the advantages of the semi-analytic method, the energy variation does not require approximations applied in the approach of Akgün et al. We use the exact expressions (5.56), (5.57) and (5.58) derived for $\mathcal{E}$ instead.

5.3.3. Computation

Parameter set choice

In the mixed field application, the parameter values for the equilibrium system, stratified composition, magnetic field and displacement field, including the localisation region, must be specified.

For the background system, a polytrope will be utilised that is similar to the analytic density profile Akgün et al. (2013) assume.

In particular, the equilibrium polytropic index will be chosen as $\Gamma_0 = 2.287\,757\,4$ and the proportionality constant as $\kappa = 65\,\mathrm{cm}^{2\Gamma_0 - 2}$. The central density is choosen as $\rho_c = 2.087 \times 10^{15}\,\mathrm{g\ cm^{-3}}$. The resulting stellar mass and stellar radius are $M = 0.0764\,\mathrm{M}_\odot$ and $R = 3.53\,\mathrm{km}$.

The considered model thus does not represent a neutron star. However, as it will be seen below, the specific model system does not impact the resulting general stability criterion.

According to the analytic density profile applied by Akgün et al., the central pressure can be calculated via

$$p_c = \frac{15\,G\,M^2}{16\,\pi\,R^4}. \tag{5.63}$$

This value is required for the analytic stability criterion (C.137) and the ratio (C.136) of the localisation area parameters.

In this work, the central pressure value for the Runge-Kutta solution of the background system equations follows from Γ_0, κ and ρ_c. For the evaluation of the stability criterion, we still apply formula (5.63), in order to be as consistent with the analytic study as possible. Note that both approaches to calculate p_c are nevertheless aligned, since the background

system parameters have been chosen in such a way that they reproduce the model (M, R) applied by Akgün et al.

For the computation, we apply geometrised rationalised Gaussian cgs units, where the geometrised gravitational constant is $\tilde{G}^* = 1$.

The stellar composition will be varied by altering the polytropic index for the perturbations in such a way that

$$\frac{\Delta\Gamma}{\Gamma_0} \in [0, 0.25], \tag{5.64}$$

where $\Delta\Gamma = \Gamma_1 - \Gamma_0$ has been defined in equation (2.41). Remember that Δ denotes a simple difference here, not a Lagrangian perturbation.

The stable stratification implied by $\Delta\Gamma > 0$ ensures that the neutron star under investigation is not subject to unstable g-modes which might cause a negative energy variation even in the unmagnetised case. That way, the Tayler instability of the magnetised star that is investigated is prevented from being covered by other unstable effects inducing $\delta W < 0$.

The exact values applied for Γ_1 are shown in table 5.3.

In contrast to the investigation here, Akgün et al. assume a constant ratio of $\Gamma_1/\Gamma_0 = 5/4$ for the polytropic indices, corresponding to a typical main sequence star. However, this ratio does not enter the derivation of the analytic stability criterion (C.139). Therefore, the criterion is applicable to typical stratification levels of neutron stars assumed in (5.64) as well.

The toroidal magnetic field strength is set by assuming $\eta_{\mathrm{tor}} = 1/0.0254$, in accordance to Akgün et al.

This value is an arbitrary choice since the analytically derived stability criterion (C.139) provides the critical poloidal field strength that is necessary for stability in terms of the toroidal field strength.

The general field amplitude is set to $\tilde{B}_0 = 3.663\,623\,96 \times 10^{-5}$.

The poloidal magnetic field strength η_{pol} is varied within a range that covers the change in sign in the energy variation. This range differs for the distinct choices of Γ_1. The specific intervals are given in table 5.3.

According to the assumption made in the analytic study, the poloidal field shall be sufficiently weaker than the toroidal component for all η_{pol} applied, where we keep in mind that η_{tor} and η_{pol} determine the maximum field strengths of both components.

The displacement field parameters are chosen as $\xi_0 = 1$, $\sigma = 2.366\,025$ from equation (C.135) and $m = 1$, in accordance to the analytic study. That way, we consider the mode causing the so called "strongest" instability.

The localisation region is positioned at $x_0 = 0.772$, $\vartheta_0 = 1.37$. The angular extent of the localisation region in the semi-analytic study is set by $\delta_\vartheta = 0.05$, while the radial extent follows from relation (C.136) with the parameters chosen above as

$$\delta_r = 2.617 \times 10^{-4}\, \delta_\vartheta \sqrt{\frac{\Gamma_0\,\Gamma_1}{\Gamma_1 - \Gamma_0}}. \tag{5.65}$$

The list of applied parameter combinations is given in table 5.3.

Table 5.3.: Parameter combinations applied for the Tayler instability proof on neutron stars with mixed magnetic fields and stratification. The combinations of the polytropic indices for the perturbations and the radial extent of the localisation area are shown, together with the corresponding parameter range where the poloidal field strength is varied. This table is valid for $\Gamma_0 = 2.287\,757\,4$, $\eta_{\mathrm{tor}} = 1/0.0254$ and $B_0 = 3.663\,623\,96 \times 10^{-5}$. The remaining parameters are given in the text.

Γ_1	$\frac{\Gamma_1-\Gamma_0}{\Gamma_0}$	δ_r	η_{pol} range
2.859 696 8	0.25	$4.426\,29 \times 10^{-5}$	$[1.0 \times 10^{-5}, 1.2 \times 10^{-5}]$
2.700 000 0	0.18	$5.065\,946\,172\,5 \times 10^{-5}$	$[1.3 \times 10^{-5}, 1.4 \times 10^{-5}]$
2.600 000 0	0.14	$5.712\,098\,92 \times 10^{-5}$	$[1.4 \times 10^{-5}, 1.5 \times 10^{-5}]$
2.500 000 0	9.3×10^{-2}	$6.793\,738\,852\,5 \times 10^{-5}$	$[1.7 \times 10^{-5}, 1.9 \times 10^{-5}]$
2.400 000 0	4.9×10^{-2}	$9.153\,388\,272\,5 \times 10^{-5}$	$[1.9 \times 10^{-5}, 2.8 \times 10^{-5}]$
2.300 000 0	5.35×10^{-3}	$2.713\,202\,515 \times 10^{-4}$	$[3.0 \times 10^{-5}, 8.0 \times 10^{-5}]$
2.290 000 0	9.8×10^{-4}	$6.325\,530\,517\,5 \times 10^{-4}$	$[1.0 \times 10^{-4}, 4.0 \times 10^{-4}]$

The considerations underlying this choice are as follows. In the analytical study, the localisation region is assumed to be infinitesimally small with $\delta_r \to 0$ and $\delta_\vartheta \to 0$. For the purpose of keeping the validity of the analytically derived stability criterion acceptable, we assume a rather small value for the angular extent of the localisation area here. Beyond that, Akgün et al. assume relation (C.136) for the ratio $\delta_r/\delta_\vartheta$ in deriving the stability criterion (C.139). Inserting the parameters chosen above and using relations (C.140), the ratio becomes

$$\left(\frac{\delta_r}{\delta_\vartheta}\right)^2 = \frac{k_{\mathrm{tor}}}{2\,k_{\mathrm{hyd}}(\Gamma_1)}\,\frac{b_{\mathrm{tor}}^2\,B_0^2}{8\,\pi\,p_c}\,\frac{\Gamma_0}{\Gamma_1-\Gamma_0} = 6.851\,09 \times 10^{-8}\,\frac{\Gamma_0\,\Gamma_1}{\Gamma_1-\Gamma_0}. \tag{5.66}$$

For a definition of the parameters, see appendix section C.3.4.

As explained in the appendix, the comparison between the results from the semi-analytic method and the analytic study requires the same assumptions in both studies. Especially, the $\delta_r/\delta_\vartheta$-ratio (5.66) of Akgün et al. must be obeyed in the semi-analytic study in order to keep the validity of the analytic stability criterion (C.139) for our application. This ratio is a function of Γ_1, which is varied in the semi-analytic study. Therefore, in contrast to Akgün et al., one of the localisation area parameters defining its extent must be adjusted in our study for each choice of Γ_1 in such a way that (5.66) stays valid. We choose to keep δ_ϑ constant and to adapt δ_r accordingly. For all choices of Γ_1, it has been ensured that the resulting radial extent δ_r is small enough to keep the error for the comparison between the analytic stability criterion and the semi-analytic method sufficiently low.

The computational parameters are chosen similarly to the previous applications.

At the stellar centre, the radial coordinate is approximated by $r_c = 10\,\mathrm{cm}$. The vacuum pressure level is set to $\tilde{p}_\varepsilon = 10 \times 10^{-10}$, i.e. $p_\varepsilon = 5.55 \times 10^{38}\,\mathrm{g\,cm^{-1}\,s^{-2}}$. The Simpson grid is constructed with $u_\varpi = 10$ and $u_z = 100$. The grid for the J_λ^μ, K_λ^μ-calculation in the full non-Cowling treatment is defined by $u_\vartheta = 10$. The mode indices for the spherical harmonics describing the Euler perturbation of the gravitational potential are chosen as $m = 1$ and $l = 2$.

For the parameter values defined here, the analytic stability criterion derived by Akgün et al. (C.139) explicitly reads

$$\eta_{\mathrm{pol}} > \eta_{\mathrm{pol}}^{\mathrm{crit}} = 6.759 \times 10^{-5}\, \delta_{\vartheta} \sqrt{\frac{\Gamma_0 \Gamma_1}{\Gamma_1 - \Gamma_0}}. \tag{5.67}$$

Numerical features

The two-dimensional integration area applied to compute δW in the mixed field case was constructed in section 4.3.2 and presented in equation (4.69). The integration is performed in cylindrical coordinates to avoid changes in the integration code structure.

The two-dimensional integration area for the computation of J_λ^m and K_λ^m in the non-Cowling treatment was constructed in section 4.3.4 and presented in equation (4.81). The integration is performed in spherical coordinates. This choice facilitates the integrations that need to be performed during the $(J_\lambda^m, K_\lambda^m)$-calculation for all radial grid points r_s.

The localisation of the displacement field in the integration code is realised in the following way. For all integration grid points fulfilling the localisation condition $\bar{\chi}^2 < 1$ from equation (2.135), the $\boldsymbol{\xi}$-defining functions are set according to the choices discussed above. For grid points outside the localisation area, the $\boldsymbol{\xi}$-defining functions are set to zero.

5.3.4. Results

The total energy variation and its individual contributions have been calculated for different poloidal magnetic field strengths and stratification levels. In this section, the results are presented.

The energy variation (5.54) has been calculated for a varying poloidal field strength, applying different levels of stratification. The result $\delta\widetilde{W}(\eta_{\mathrm{pol}})$ is shown in figure 5.6. For this calculation, the full non-Cowling treatment has been applied. The corresponding energy variation in the case of $\eta_{\mathrm{pol}} = 0$ is listed in table 5.4 for all investigated levels of stratification.

In this section, the energy variation is presented in the dimensionless form $\delta\widetilde{W}_8 \equiv 10^8\, \delta\widetilde{W}$.

The separate contributions to the energy variation caused by both magnetic field components, the hydrostatic part and the removal of the Cowling approximation are plotted in figure 5.7 for one particular level of stratification $\Delta\Gamma/\Gamma_0$. The corresponding expressions for these contributions are given by equations (5.56), (5.57), (5.58) and (4.49). Graph 5.7 also compares the energy variation in Cowling approximation with the energy variation resulting in full treatment.

The computed energy variation presented in figure 5.6 shows the expected change in stability with an increasing poloidal field strength that was found in the analytic study by Akgün et al. (2013). In order to verify this result quantitatively, the roots from graph 5.6, representing the critical poloidal field strength $\eta_{\mathrm{pol}}^{\mathrm{crit}}$ necessary for stability, are plotted against the level of stratification in figure 5.8.

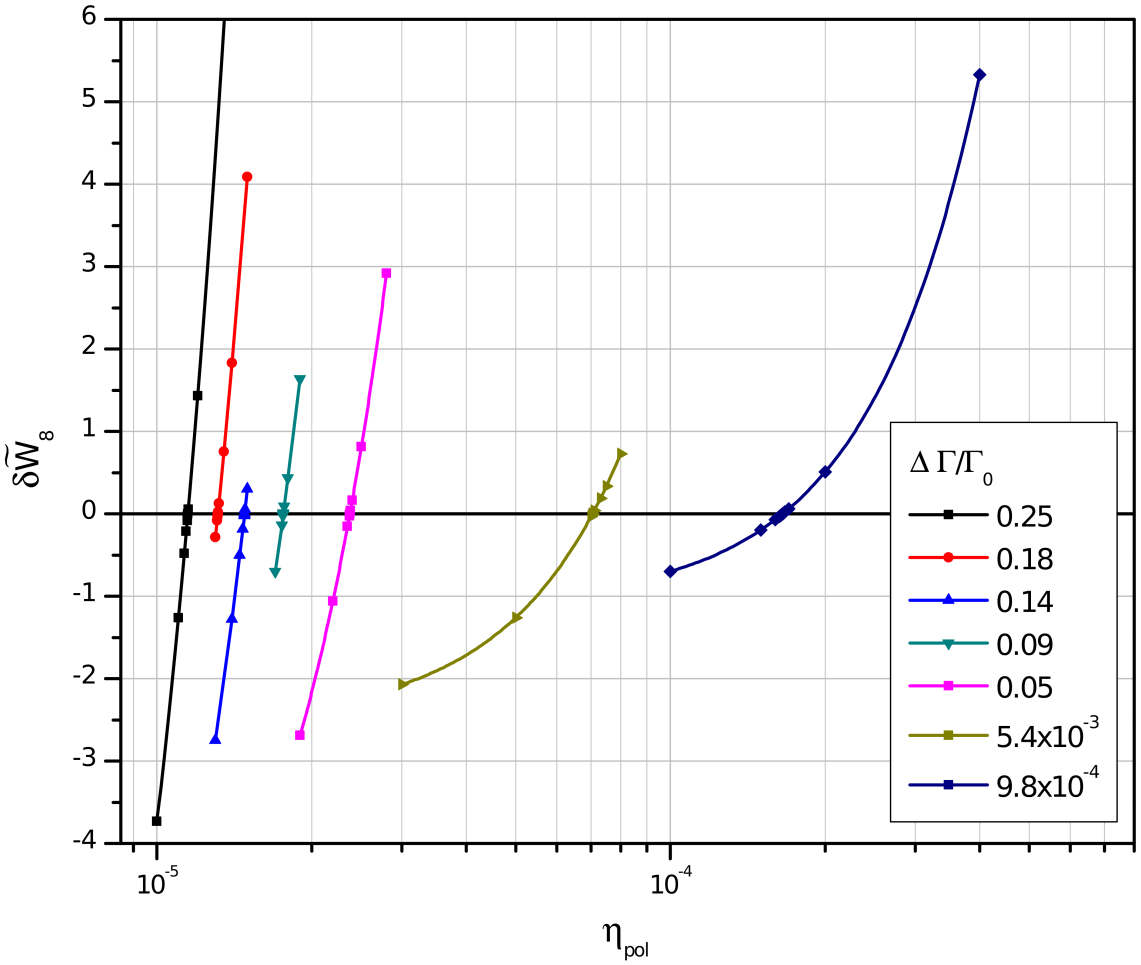

Figure 5.6.: Dimensionless energy variation $\delta\widetilde{W}_8 \equiv 10^8\,\delta\widetilde{W}$ of the neutron star with mixed magnetic fields, calculated with the semi-analytic method. The energy variation is plotted against the field strength of the poloidal field component $\eta_{\rm pol}$ for neutron star models with different levels of stratification $\Delta\Gamma/\Gamma_0$. The curves have been interpolated according to the discrete computed values. The parameters are defined in table 5.3 and in the text.

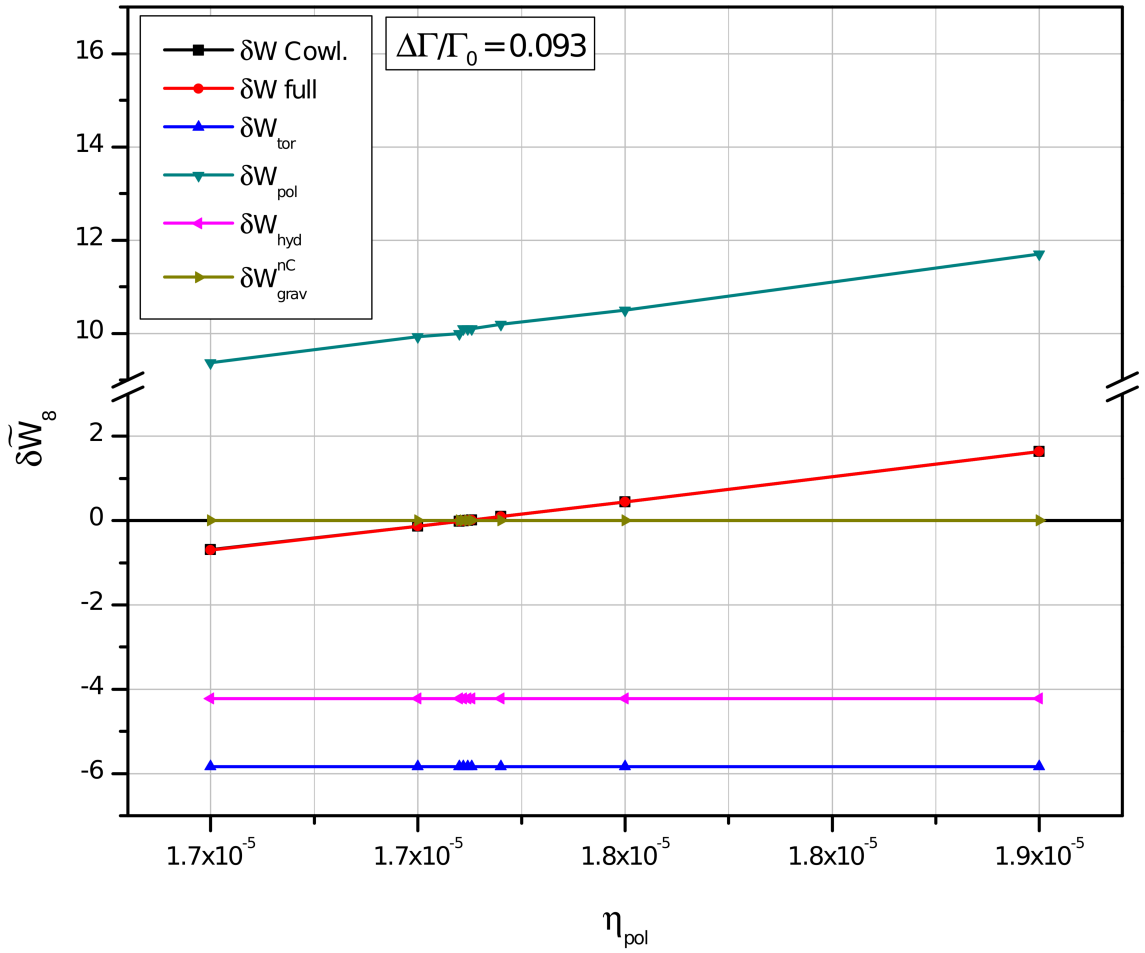

Figure 5.7.: Dimensionless contributions to the energy variation $\delta\widetilde{W}_i$ of the neutron star with mixed magnetic fields, calculated with the semi-analytic method. The graph shows $\delta\widetilde{W}_8 \equiv 10^8\,\delta\widetilde{W}$. The total energy variation with and without the assumption of the Cowling approximation is presented. The total energy variation and its contributions are plotted against the field strength of the poloidal field component $\eta_{\rm pol}$ for $\Delta\Gamma/\Gamma_0 = 0.093$. The parameters are defined in table 5.3 and in the text.

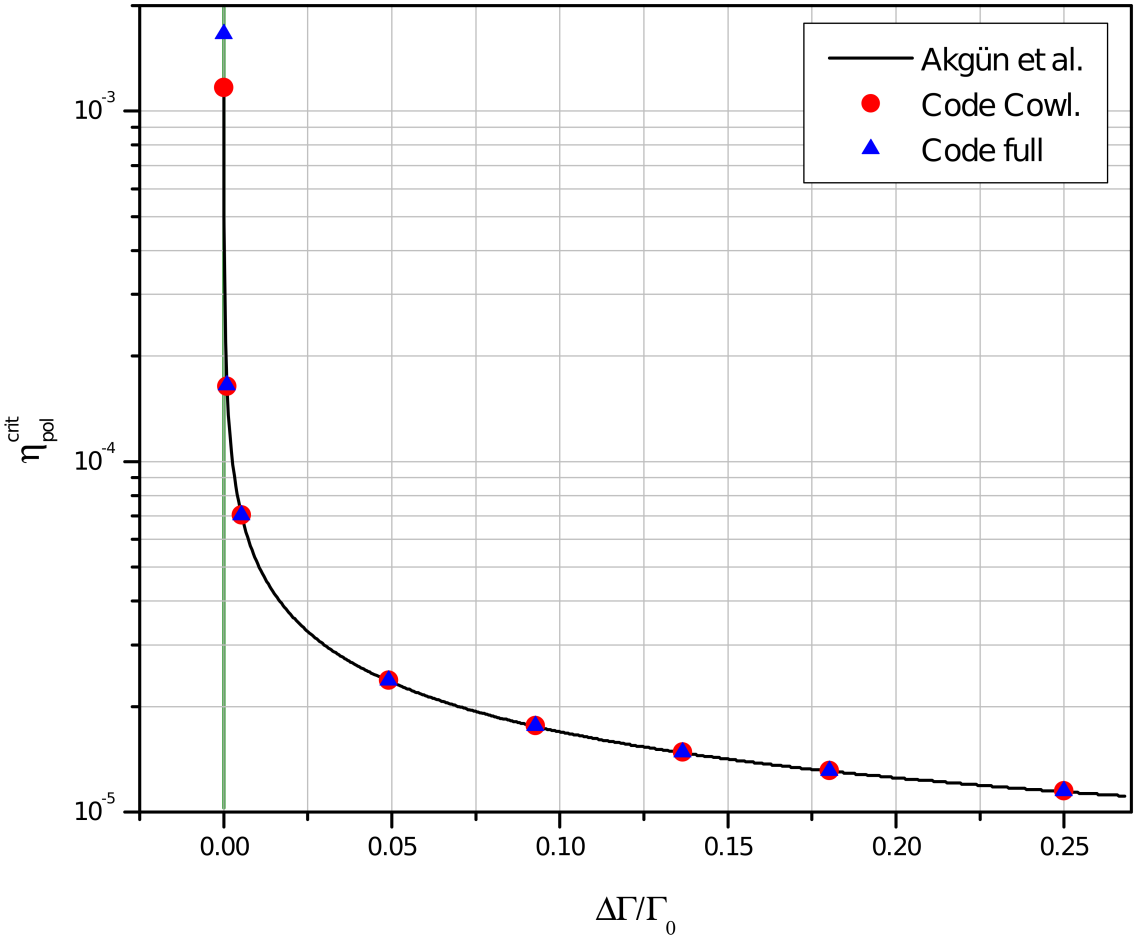

Figure 5.8.: Critical minimum poloidal field strength necessary to stabilise the toroidal field Tayler instability, plotted against the level of stratification. The discrete values follow from graph 5.6 which has been produced applying the semi-analytic method. The result is shown for both cases, with and without Cowling approximation. The parameter values are defined in the text. The continuous curve has been computed for the same system applying the analytical stability criterion derived by Akgün et al. (2013).

Table 5.4.: Dimensionless energy variation $\delta\widetilde{W}_8 \equiv 10^8\,\delta\widetilde{W}$ of the mixed field case model system for $\eta_{\mathrm{pol}} = 0$, calculated with the semi-analytic method. The results are presented for the different levels of stratification, cf. figure 5.6, in Cowling approximation as well as in the full non-Cowling treatment. The underlying formula for the energy variation is given by (5.54) with (5.55), (5.56), (5.57) and $E_{\mathrm{pol}} = 0$. The parameters are defined in table 5.3 and in the text. The energy variation is negative in all cases.

Γ_1	$\Delta\Gamma/\Gamma_0$	$\delta\widetilde{W}_8$ in Cowling appr.	$\delta\widetilde{W}_8$ in full treatment
2.859 696 8	0.25	−15.444 533 52	−15.445 924 04
2.70	0.18	−13.494 405 84	−13.495 998 95
2.60	0.14	−11.967 915 72	−11.969 712 16
2.50	0.093	−10.062 476 96	−10.064 613 39
2.40	0.049	−7.468 438 961	−7.471 318 096
2.30	5.35×10^{-3}	−2.519 344 759	−2.527 887 708
2.29	9.8×10^{-4}	−1.080 092 219	−1.100 074 9

From the data, the following results can be deduced.

The energy variation of the purely toroidally magnetised star is negative, according to table 5.4:

$$\delta W(\eta_{\mathrm{pol}} = 0) < 0 \qquad \forall \qquad \frac{\Delta\Gamma}{\Gamma_0}. \tag{5.68}$$

That means, the model system investigated in graph 5.6 and in table 5.4 is unstable for all applied levels of stratification if $\eta_{\mathrm{pol}} = 0$. Remember that the displacement field constructed in the appendix section C.3.1 was designed precisely to provide this result.

For $\eta_{\mathrm{pol}} \neq 0$, the energy variation increases with the growing field strength and experiences a change in sign, cf. figure 5.6. This behaviour is qualitatively independent of the degree of stratification, for all polytropic indices Γ_1 applied here.

The positive energy variation for large poloidal field strengths implies the stabilisation of the instability that has been active for small poloidal field strengths. This consideration is referred to the specific displacement field mode applied here.

Figure 5.7 shows that the toroidal field contribution to the energy variation is negative, $\delta W_{\mathrm{tor}} < 0$. That means, the toroidal field component has a destabilising impact on the system.

The poloidal field contribution, in contrast, is positive for all considered field strengths, $\delta W_{\mathrm{pol}} > 0\ \forall\ \eta_{\mathrm{pol}}$, and increases with η_{pol}. That means, the stabilising impact of the poloidal field component becomes stronger the stronger the poloidal field is.

The hydrostatic contribution $\delta W_{\mathrm{hyd}} = \delta W_{\mathrm{fluid}} + \delta W_{\mathrm{grav}}^{\mathrm{Cowl}}$ and the additional non-Cowling part $\delta W_{\mathrm{grav}}^{\mathrm{nC}}$ are negative.

The non-Cowling part is negligibly small, $\left|\delta W_{\mathrm{grav}}^{\mathrm{nC}}\right| \ll |\delta W|$. Therefore, the total energy variation in Cowling approximation is approximately equivalent to the total energy variation in the full non-Cowling approach, $\delta W^{\mathrm{Cowl}} \approx \delta W^{\mathrm{full}}$.

The critical poloidal field strength $\eta_{\mathrm{pol}}^{\mathrm{crit}}$ necessary for stability from figure 5.8 increases with a decreasing value of $\Delta\Gamma/\Gamma_0$.

In the limiting case $\Delta\Gamma = 0$ of an unstratified star, the solid curve following from the analytical stability criterion (5.67) diverges. That means, the toroidal field instability of the applied displacement field cannot be stabilised by an arbitrarily strong poloidal magnetic field if the star is unstratified.

The discrete data points in graph 5.8 following from the semi-analytically produced results in figure 5.6 cannot reproduce the actual divergence for $\Gamma_1 = \Gamma_0$. Due to the usage of numerical methods, a possible divergence cannot manifest as an actual infinite value, but as a very large finite numerical value. That means, the semi-analytic result is in accordance with the analytical result.

Beyond this, the semi-analytic results are in great accordance with the analytically calculated curve.

The semi-analytic results are almost identical for both approaches with and without the assumption of the Cowling approximation, as already seen from graph 5.7. The largest deviation between the semi-analytic study and the analytical criterion, as well as between the Cowling approach and the full treatment in graph 5.8 occurs for $\Delta\Gamma = 0$. However, the critical poloidal field strength found for $\Delta\Gamma \to 0$ is very large and does not fulfil the requirement of $\left|\boldsymbol{B}_{\mathrm{pol}}\right| \ll |\boldsymbol{B}_{\mathrm{tor}}|$ anymore. Therefore, in the limiting case of $\Gamma_1 \to \Gamma_0$, the assumptions for the stability consideration are violated and the significance of the result as well as the comparability of both studies are restricted.

5.3.5. Interpretation

According to the results from the investigation of the mixed field system with stratification presented in the previous section, we can now estimate the quantitative validity of the semi-analytic method.

Besides this, the impact of the removal of the Cowling approximation will be discussed.

Summarising the outcome from the previous section, the analytically found stabilising impact of the poloidal field component on the toroidal field instability in the presence of stratification has been verified with the semi-analytic method.

This fact represents one further qualitative confirmation of the semi-analytic method's functionality. Beyond that, figure 5.8 convincingly confirms the quantitative prediction capacity of the code and the method as well.

The great accordance between the analytic study by Akgün et al. (2013) and the semi-analytic one further provides the justification for the simplifications Akgün et al. made for the analytic approach. Since we did not rely on these simplifications, the semi-analytic approach was based on their exact equivalents instead.

In particular, the analytic density profile Akgün et al. assumed was an adequate approximation of the $\left(\Gamma_0 = 2.287\,757\,4, \kappa = 65\,\mathrm{cm}^{2\Gamma_0 - 2}\right)$-polytrope we applied in the semi-analytic study.

Akgün et al. based the analytical stability criterion on approximated expressions for the energy variation contributions. This simplification seems to be perfectly valid for the purpose of stability analysis. For the largest range of tested $\Delta\Gamma$-values, the analytic criterion coincides with the semi-analytic result, which has been derived from the exact expressions for δW_i instead.

Finally, the assumption of the infinitesimally small localisation area of the displacement field made by Akgün et al. was sufficiently approximated by the choices made in this work

for δ_ϑ and δ_r. Although we kept the localisation area finite, apparently the chosen extent of A was small enough to keep the validity of the analytic stability criterion (5.67) for our model as well.

Nevertheless, the semi-analytic method offers a larger flexibility than the analytic approach concerning the investigation of versatile model systems.

The comparison of the studies in Cowling approximation and in the full non-Cowling treatment shows no significant differences in the results for the particular application here. The impact of the additional non-Cowling term $\delta W_{\mathrm{grav}}^{\mathrm{nC}}$ is negligible in the investigated system.

This agreement holds for all tested finite levels of stratification, even for the star with the strongest level of stratification $\Delta\Gamma/\Gamma_0 = 0.25$. In fact, the maximum difference in the critical poloidal field strength calculated with both approaches is present for the lowest tested level of stratification $\Delta\Gamma/\Gamma_0 = 1.86 \times 10^{-5}$, cf. figure 5.8. However, this deviation does not seem to be a physical feature. It seems to be caused by a numerically induced inaccuracy. The limiting case $\Delta\Gamma \to 0$ corresponds to the transition between existent g-modes for $\Gamma_1 \neq \Gamma_0$ and non-existent g-modes for $\Gamma_1 = \Gamma_0$, cf. section 2.3.1. Therefore, the numerical error is expected to increase for $\Delta\Gamma \to 0$. The deviation between both approaches is thus most probably covered by the numerical error range.

The overall insignificant difference between the Cowling and the non-Cowling approach for the particular application shown here is a consequence of the infinitesimally small localisation area Akgün et al. assume for the displacement field.

The additional non-Cowling contribution $\delta W_{\mathrm{grav}}^{\mathrm{nC}}$ to the energy variation is a function of J_λ^m, K_λ^m and the integral I_λ^m, as can be seen from equation (4.49). Functions I_λ^m, J_λ^m and K_λ^m are given by equations (4.50) and (4.51).

For each radial grid point r, I_λ^m, J_λ^m and K_λ^m are calculated by angular and, in the case of J_λ^m and K_λ^m, radial integrations from 0 to r or r to R, respectively. None of their integrands includes terms that do not linearly depend on one of the $\boldsymbol{\xi}$-defining functions $\tilde{R}$, $\tilde{S}$ or $\tilde{T}$. Since these functions are non-vanishing only inside the strongly restricted localisation area, only very few grid points contribute finite integrand values to I_λ^m, J_λ^m and K_λ^m.

In particular, the effective angular integration area is constrained by $\delta_\vartheta = 0.05$ and the effective radial integration area by $\delta_r \in [4.4 \times 10^{-5}, 9.5 \times 10^{-2}]$, depending on the polytropic index Γ_1.

The absolute values of the functions I_λ^m, J_λ^m and K_λ^m following as the sums of these contributions are thus very small, considering that the integrands are finite and not extraordinarily big.

In the limiting case of an infinitesimally small localisation area extent, as assumed for the analytic consideration by Akgün et al., these functions even vanish identically:

$$I_\lambda^m(\delta_r \to 0, \delta_\vartheta \to 0) \to 0 \tag{5.69}$$

$$J_\lambda^m(\delta_r \to 0, \delta_\vartheta \to 0) \to 0 \tag{5.70}$$

$$K_\lambda^m(\delta_r \to 0, \delta_\vartheta \to 0) \to 0. \tag{5.71}$$

Concerning the above discussion, one should remark that the behaviour found here holds for the particular assumptions made by Akgün et al. indeed, but it is not to be expected in general by any means.

Especially, the displacement field applied in this section is not expected to be present in realistic stars. The displacement field assumed by Akgün et al. is truly artificial due to its infinite localisation. Spatially extended displacement fields might lead to a significant difference between δW^{Cowl} and δW^{full} and require the full non-Cowling treatment.

Displacement fields involving a strong radial motion or the consideration of rotating stars might necessitate the non-Cowling treatment as well.

The same holds for the consideration of relativistic corrections. Compared to the Newtonian approach portrayed here, they might cause the Eulerian gravitational perturbation $\delta\Phi$ to have a larger impact on the system, due to the altered effect of gravity in the relativistic treatment.

The construction and development of the semi-analytic method thus has its justification.

It has been shown that the semi-analytic method is capable of removing the Cowling approximation in a straightforward way, also for finite localisation regions, which would be infeasible in an analytic treatment.

The computation time of the results presented above and other trial code runs was manageable, even for larger localisation regions, i.e. larger effective integration areas. That means, there are still computational capacities for possible future investigations on 3D-systems that will require significantly more computation time.

The physical outcome of the neutron star investigation with mixed fields and stratification applying the semi-analytic method is equivalent to the result found by Akgün et al.

The stabilisation of the particular Tayler unstable displacement field mode applied here is possible for a sufficiently strong poloidal magnetic field component if the star is stably stratified.

Although this result provides a possible indication on which effects might be relevant to explain the observed stability of magnetised neutron stars, it does not imply the solution of the neutron star stability problem by any means.

First, the detected stabilising impact has been found for one single perturbation mode only. According to the general stability criterion (2.45), a complete stability proof would require the investigation of all possible displacement fields.

Secondly, the above consideration is based on the unrealistic assumption of an infinitesimally small localisation area. In real systems, we expect mode coupling, which prevents the occurrence of isolated mode excitations. According to energy transfers, an active mode will excite other modes on one hand and propagate through the whole stellar system on the other hand, especially if the mode is unstable and the star is broadly homogeneous. Even if one mode might dominate in an actual star and if spatial anomalies facilitate the confinement of this mode, it will neither be fully constrained nor partially constrained to an infinitesimal region.

To summarise, the results presented in this section represent one further proof of the functionality of the semi-analytic method. Beyond that, for the first time, new physical insights were gained applying the method.

5.4. Application to further issues

Beyond the stability analysis investigations on magnetised neutron stars shown above, the semi-analytic method can be applied to further problems.

In section 5.4.1, the method will be applied for the computation of eigenvalues and eigenfunctions of the system under investigation. That way, we can test the potential of the semi-analytic method to make quantitative predictions.

Beyond that, the semi-analytic method provides the potential of creating a perturbative method for the computation of eigenfrequencies and eigenfunctions of the investigated system. This approach is shown in section 5.4.2.

5.4.1. Computation of neutron star eigenfrequencies

Idea

As explained in the appendix section B.6.1, the perturbation of the Euler equation can be understood as an eigenvalue problem.

The eigenfrequencies ω_n of the perturbed system can be calculated from the eigenfunctions $\boldsymbol{u}_n^{(0)}$ of the equilibrium system and the eigenvalue operator $\mathbf{L}$, given by the Euler equation. The corresponding formula is shown in equation (B.110),

$$\omega_n^2 = \frac{\iiint {\boldsymbol{u}_n^{(0)}}^* \cdot \mathbf{L}\, \boldsymbol{u}_n^{(0)}\, \rho \,\mathrm{d}V}{\iiint {\boldsymbol{u}_n^{(0)}}^* \cdot \boldsymbol{u}_n^{(0)}\, \rho \,\mathrm{d}V} + \mathcal{O}(\delta L^2), \tag{5.72}$$

where the equilibrium system is denoted by the superscript (0). Appendix section B.6.3 further shows that due to the connection with the Euler equation, the numerator of expression (5.72) is related to the expression for the energy variation (B.115) in the following way:

$$\omega^2 = \frac{4\,\delta W\left(\boldsymbol{\xi} = \boldsymbol{u}_n^{(0)}\right)}{\Re\left\{{\boldsymbol{u}_n^{(0)}}^* \cdot \boldsymbol{u}_n^{(0)}\, \rho \,\mathrm{d}V\right\}}. \tag{5.73}$$

Therefore, the expression analytically derived for δW in this work can be applied for a quantitative calculation of the eigenfrequencies of the considered system.

The numerical setup implemented here provides the required computational framework.

Implementation and outlook

First test applications of the idea described above have been implemented.

For the continuing development of the method, the eigenfrequencies of a homogeneous star shall be calculated. According to the underlying formula (5.72), this procedure requires the input of the eigenfunctions $\boldsymbol{u}_n^{(0)}$ of the homogeneous star. We use the formulation shown in section 2.3.3. The eigenfunctions are given in the appendix section A.7.

For first test runs on polytropic stars, the numerically calculated eigenfunctions provided by other studies can be utilised.

Note that in this procedure, f-mode type displacement fields cannot be investigated in the case of a homogeneous star, since they obey $\nabla \cdot \boldsymbol{\xi} = 0$.

According to equation (2.101a),

$$\delta\rho = -\rho_0 \nabla\cdot\boldsymbol{\xi} - \boldsymbol{\xi}\cdot\nabla\rho_0 = -\rho_0\nabla\cdot\boldsymbol{\xi}, \tag{5.74}$$

where we took into account that $\nabla\rho_0 = 0$ in the homogeneous star. Further, the f-mode type displacements are always incompressible, i.e. $\delta\rho = 0$, as explained in section 2.3.1. Therefore, $\nabla\cdot\boldsymbol{\xi} = 0$.

5.4.2. Eigenmode determination in non-homogeneous stars

In this section, the idea of the previous section is extended for the purpose of creating a method to calculate eigenfunctions and eigenfrequencies of non-homogeneous stars.

Motivation

While the eigenmodes and eigenfrequencies of polytropic stars are well known, the investigations presented in section 5.3 for instance involve stratified stars whose eigenmodes and eigenfrequencies have not been determined yet. Generally spoken, in the course of applying the semi-analytic method, we will regularly deal with specific systems and parameter choices for which the eigenfunctions are not necessarily known.

However, the determination of the system's eigenfrequencies and eigenmodes might be helpful to gain information about its oscillation properties. It would be desirable to calculate these quantities with the aid of the semi-analytic method as opposed to a full complex time-dependent normal mode analysis. Beyond that, the global stability analysis test, based on the semi-analytic method and suggested above, requires the given eigenfunctions of the system as well.

Idea

The idea of determining eigenfunctions and eigenfrequencies with the semi-analytic method is based on the fact that the energy variation is related to the eigenfrequency as explained in section 2.3.1.

The basic assumption is that the eigenfrequency of a system changes slightly when the star is polytropic or stratified as compared to purely homogeneous. In this case, the star can be described by a perturbative approach, where the deviation from homogeneity creates a small deviation in the stellar eigenfrequency.

Starting from analytically known eigenfrequencies of the homogeneous star, the corrections caused by the radius dependent density profile are calculated with the semi-analytic method. Afterwards, these frequencies can be inserted to calculate the new corrected eigenfunctions. This procedure can be repeated in an iterative method.

According to equation (5.72), the eigenfrequencies of the system can be calculated from the eigenfunctions of the equilibrium system and the eigenvalue operator describing the system. In the first step, we approximately apply the eigenfunctions $\boldsymbol{u}_{\mathrm{hom}}$ of the homogeneous star in the formula. The eigenvalue operator $\mathbf{L}_{\mathrm{poly}}$ is chosen according to the actual polytropic system:

$$\omega^2_{(1)} = \omega^2_{\mathrm{hom}} + \frac{\iiint \boldsymbol{u}^*_{\mathrm{hom}}\cdot\mathbf{L}_{\mathrm{poly}}\,\boldsymbol{u}_{\mathrm{hom}}\,\rho\,\mathrm{d}V}{\iiint \boldsymbol{u}^*_{\mathrm{hom}}\cdot\boldsymbol{u}_{\mathrm{hom}}\,\rho\,\mathrm{d}V} + \mathcal{O}(\delta L^2), \tag{5.75}$$

where we consider an arbitrary non-degenerate mode n. The subscript (1) denotes the order of the correction method.

The result of (5.75) is the square of an eigenfrequency $\omega_{(1)}$ which is expected to differ from the original eigenfrequency $\omega_{(0)} = \omega_{\mathrm{hom}}$ of the homogeneous star, corresponding to $\boldsymbol{u}_{(0)} = \boldsymbol{u}_{\mathrm{hom}}$. The computed eigenfrequency is expected to fit the polytropic star better than ω_{hom}, since it has been corrected by applying the actual operator $\mathbf{L}_{\mathrm{poly}}$ of the polytrope.

Subsequently, the newly calculated eigenfrequency $\omega_{(1)}$ can be applied in equation (B.99), in order to calculate the corresponding first-order corrected eigenfunction $\boldsymbol{u}_{(1)}$:

$$\boldsymbol{u}_{(1)} = \boldsymbol{u}_{\mathrm{hom}} + \frac{1}{N} \sum_p \frac{\boldsymbol{u}_{\mathrm{hom}}(p)}{\omega^2_{(1)}(n) - \omega^2_{(1)}(p)} \iiint \boldsymbol{u}^*_{\mathrm{hom}}(p) \cdot \mathbf{L}_{\mathrm{poly}}\, \boldsymbol{u}_{\mathrm{hom}}(n)\, \rho \, \mathrm{d}V, \tag{5.76}$$

where N has been defined in equation (B.102). In this step, the system is again described as a polytrope via $\mathbf{L}_{\mathrm{poly}}$.

These steps can now be repeated in an iteration procedure. For each iteration step j, the calculated eigenfrequency $\omega_{(j)}$ and eigenfunction $\boldsymbol{u}_{(j)}$ are expected to more accurately approach the actual eigenfrequency ω_{poly} and eigenfunction $\boldsymbol{u}_{\mathrm{poly}}$ of the polytropic star. Finally, the method shall converge to the exact values.

Test runs and outlook

The perturbative correction method for the calculation of eigenmodes in arbitrary systems has been examined in several test runs. Apparently, the mutual computation of ω^2 and $\boldsymbol{u}$ is essential for the method to work.

A more extended study of the functionality of this method and quantitative tests of the results shall be performed in future studies.

Once the method works for the computation of eigenmodes on polytropic stars, it shall be extended to stratified systems.

This step would provide a valuable tool, since modern and future neutron star stability studies must investigate complex systems, as proven in this work. The more realistic the considered system will be, the reduced the possibilities are to describe it analytically, and the more beneficial the semi-analytic determination of its eigenmodes will be.

6. Conclusions

Based on the results from the application chapter 5, we can now make concluding remarks on the technical and physical outcome of this work. First, we estimate whether the construction and implementation of the semi-analytic method worked as desired. Second, the newly gained physical insights on neutron stars will be summed up.

6.1. Functionality of the semi-analytic method

The functionality of the semi-analytic method will be evaluated considering the expectations described in chapter 3. We will estimate whether the requirements for the semi-analytic method could be implemented and whether the fundamental idea of the semi-analytic procedure could prove itself.

System complexity The first requirement for the semi-analytic method was to provide an opportunity to keep the investigated system more complex and realistic than possible in an analytic study. This demand has been clearly fulfilled.

The semi-analytic approach allowed us to successively include a variety of additional neutron star characteristics relevant for its stability behaviour compared to the simple analytic investigations by Tayler (1973); Markey & Tayler (1973).

In particular, we could add the possibility of stratified model neutron stars in section 4.1, investigate mixed magnetic fields in a straightforward way and combine these effects in section 5.3.

Even compared to the analytic study of more complex magnetised neutron stars provided by Akgün et al. (2013), the strong and previously essential Cowling approximation could be removed in section 4.2. This achievement represents the main confirmation of the fact that the complexity of the considered system has been increased.

The analytic derivation of the non-Cowling term has been kept general, so that it can easily be adapted to future applications on different systems. Additionally, the required code structure for this extension has been prepared, cf. section 4.3.4. The first test application on mixed magnetic fields with stratification in section 5.3 finally proved that the semi-analytic method is indeed capable of investigating systems without Cowling approximation.

This step represents a major improvement in the field of stability analysis of magnetised neutron stars. So far, basically all studies relied on the assumption of the Cowling approximation, which is an unsatisfying circumstance given that gravity plays an important role for the physical characteristics of compact objects. Especially for future investigations focussing on the search for stability rather than on the detection of instabilities, where the Cowling approximation might not be valid, this achievement is essential.

Removal of simplifications Furthermore, several approximations that were necessary for the previous analytical stability investigations could be avoided in this work.

In particular, the stability considerations in Tayler (1973) and Markey & Tayler (1973) relied on estimations and argumentations. The semi-analytic method in sections 5.1 and 5.2, in contrast, provided a statement about the stability of the system directly produced from the theoretical model assumptions.

It was possible to consistently neglect the magnetic field in the unmagnetised neutron star equilibrium in contrast to Tayler (1973). Tayler assumed the magnetised neutron star background in order to avoid additional terms in the energy variation density in the analytic consideration. Applying the semi-analytic method, these additional terms in the energy variation (5.11) and in the minimising $\boldsymbol{\xi}$-defining function $Y_{\min}$ in (5.12) could easily be carried along. This example demonstrates the flexibility of the semi-analytic method to treat systems with altered fundamental equations or composition profiles.

Compared to Akgün et al. (2013), the analytic density profile approximating a polytrope could be replaced by an actual polytropic composition structure, cf. section 5.3. This achievement indicates that the constructed code is capable of processing arbitrary and for example precalculated density profiles for the background system in a straightforward way.

Similar to the simple neutron star models, Akgün et al. derived the analytic stability criterion based on approximated expressions for the energy variation. Even in the highly complex system with mixed magnetic fields, stratification and full consideration of the gravitational Euler perturbation, these approximations were not necessary in the semi-analytic approach. The full and – within the frame of the applied model system – exact expressions for the energy variation density could be processed easily and in manageable computation time by the integration code, cf. section 5.3.

Finally, the analytically required assumption of an artificial infinitely strongly confined displacement field was not necessary in the semi-analytic treatment in section 5.3. Even though the extent of the localisation area was kept relatively small for the application shown here in order to produce results comparable to the analytic study, larger localisation areas can equally be chosen. The application presented in this work was a first test verifying the functionality of the code. Further test runs indicate that realistic extended localisation areas are assumable in future applications.

As explained in section 2.3.3, larger localisation areas involve the complication of an aggravated distinction between the spatial regions contributing positive or negative terms to the total energy variation and to localise a possible instability. The straightforward possibility to adjust the localisation region when working with the semi-analytic method, will allow for a systematic scanning of the questionable region. Beyond this, the code set up in this work even holds the opportunity to directly plot the energy variation integrand depending on the spatial parameters, as shown in figure 5.4. This allows a fast visualisation of the problem at hand, which is not accessible with purely analytic or numerical approaches, and provides an extremely valuable overview.

Generality Finally, the semi-analytic approach was expected to offer the opportunity of an easy and systematic parameter variation, especially for the magnetic field and displacement field. That way, the considered system shall be kept general and different classes

of systems shall be examinable at once. The semi-analytic method provides this feature which has already been utilised in all applications shown above.

The method proved that it is possible to vary different system parameters and to scan the parameter space for values and combinations producing systems that are more likely to be stable. The functionality of the parameter variation has been confirmed for parameters describing different aspects of the neutron star, such as the magnetic field, displacement field, background system and the stellar composition.

For the toroidal field application in section 5.1, the toroidal magnetic field strength B_{tor} has been varied and the increasingly destabilising impact of the field with higher field strengths has been detected. Beyond that, the background model parameters Γ_0 and κ have been varied in order to ensure that the findings are universal.

In section 5.2, the displacement field has been parametrised and the mode index m has been varied. It has been proven that for mode indices exceeding a critical value, the system is unstable. Again, the background parameters have been varied for the sake of generality. The parameters being varied were the central density ρ_c and the proportionality constant κ of the polytropic equation of state.

Finally, in the mixed field case in section 5.3, the poloidal magnetic field strength η_{pol} and the polytropic index for the perturbations Γ_1 have been varied. The stabilising tendency has been detected for poloidal field strengths exceeding a critical value, where a stronger degree of stratification lowers the minimum field strength.

In test runs, different sizes of the displacement field localisation area have been applied in all applications. This type of parameter variation proved to be easily feasible as well.

Overall, one can say that the possibilities of parameter variation are by far more diverse than demonstrated in the test applications implemented so far. The semi-analytic method thus offers a very broad range of investigation options for future projects.

Concluding, the semi-analytic method is capable of treating complex systems while keeping the generality of the study at the same time.

Therefore, the semi-analytic method indeed proved itself as a valuable tool for preinvestigations prior to simulation studies.

6.2. Theoretical insights about magnetised neutron stars

In this section, the physical aspects of the insights newly gained by applying the semi-analytic method will be summarised.

In accordance to the simple analytic study by Tayler (1973), the semi-analytic method detected an instability in the toroidally magnetised neutron star for non-axisymmetric displacement fields of an exponential angular dependence, cf. section 5.1.

This result holds for polytropic stars consisting of a neutron proton electron fluid without rotation. The occurrence of this instability, identified as the Tayler instability, was found for magnetic field strengths exceeding a vanishingly low minimum magnetic field strength for interior field standards. However, the instability might occur for lower field strengths as well which cannot be ruled out from the semi-analytic investigation. According to the localisation of the displacement field, it can be deduced that the origin of the instability

is located close to the symmetry axis of the star which coincides with the magnetic field symmetry axis.

The same simple neutron star model with a purely poloidal magnetic field shows an analogous instability that has been detected with the semi-analytic method in section 5.2.

The unstable perturbation mode has the same structure as in the toroidal field case, with respect to the symmetry axis of the geometrically altered magnetic field. This Tayler instability of the poloidal magnetic field is detectable for arbitrary non-vanishing field strengths. This result verifies the work by Markey & Tayler (1973). The localisation of the displacement field confirmed that the origin of the instability is located close to the magnetic field symmetry axis again, which for the poloidally magnetised star is equivalent to the neutral line.

Beyond these instability proofs, the semi-analytic method detected stabilising impacts of more complex physical features that are present in real stars, in comparison to the variety of simple analytic studies such as Tayler (1973); Markey & Tayler (1973); Wright (1973). Section 5.3 showed that the poloidal magnetic field component in a mixed field star can have a stabilising impact on the toroidal field Tayler instability. The fundamental condition for this effect is a deviation from the polytropic composition of the star. These results confirm the outcome of Akgün et al. (2013).

This result implies that the non-barotropic stratified density distribution might have a tendency to stabilise the neutron star system against magnetic field instabilities in general. Equally, the interaction of toroidal and poloidal field components might in general be a relevant factor to solve the stability problem of magnetised neutron stars. However, the investigation presented here does not consider the global stability of the system or the properties of an actual mixed magnetic field with interacting components.

In comparison with the advanced analytical study by Akgün et al. (2013), the semi-analytic method confirmed the validity of the Cowling approximation for the specific conditions assumed there, cf. section 5.3.

In the application shown here, the displacement field was infinitely strongly localised. This fact prohibited a meaningful investigation on whether the Cowling approximation shows tendencies to become invalid in the case of stability proofs, as compared to its validity for the detection of instabilities. However, the possibility of becoming invalid cannot be ruled out according to the study performed here. The hypothesis should therefore be investigated again for a different system in order to test to what extent the Cowling approximation affects the result and whether it must be removed for future stability verifications similar to the one shown here.

Overall, the semi-analytic method was able to provide numerous new insights compared to the simple analytic studies.

The more advanced analytical study by Akgün et al. could be confirmed. The general framework to apply the semi-analytic method to more complex systems in the future is prepared. According to the results found so far, one can feel confident that the method will make its contribution to gain a more detailed knowledge about magnetised neutron stars.

7. Outlook

After summarising the achievements of the semi-analytic method presented in this work in the previous chapter, the future perspectives of the method, concrete applications and possible followup projects will be discussed here.

7.1. Applications on magnetised neutron stars

The first thing to mention is that the stability investigation of magnetised neutron stars started in section 5 can be continued.

On the one hand, the system under consideration shall successively be made more realistic, including additional physical features that might be relevant for the stellar stability behaviour. In doing so, the semi-analytic approach shall be applied in order to test the stability properties of the system, based on the energy variation method.

On the other hand, the method can be adapted to other neutron star related application fields, such as the calculation of eigenfrequencies of the system.

Twisted torus field configurations

The most natural extension to the method in its current form and according to the present state of research is the investigation of actual mixed magnetic fields.

The application shown in section 5.3 investigated the impact of a weak poloidal field component on the toroidal field Tayler instability. An actual star, however, is expected to posses an interior field consisting of both field components, forming a twisted-torus structure as illustrated in figure 3.1. The result from the work by Akgün et al. (2013) is not directly applicable to this situation as it is not clear how both field components interact, regarding the field instabilities of the other component. New instabilities might arise in the actual mixed field compared to the superposition of both independent components.

The twisted-torus field showed indications of stability in numerical studies before, for example in Braithwaite & Spruit (2006).

The semi-analytic method shall be applied to investigate if this configuration shows in fact stronger stability tendencies then others. The investigation of the twisted-torus field first requires the construction of an appropriate displacement field that is optimally adjusted to the mixed field geometry in order to impose effective perturbations on the field lines. Next, the system should be perturbed while its energy variation is computed applying the semi-analytic method.

As demonstrated in the applications presented in this work, the construction of an adequate displacement field is not a direct process with one single solution. It might be a difficult task to find the perturbation mode that causes a fast growing instability.

The recognition of such modes, however, is highly desired. They allow for deductions concerning the global stability behaviour of the system, which is predominantly driven by these fast growing unstable modes.

The semi-analytic method offers a helpful possibility to address this issue.

First, a general form for the displacement field shall be constructed for the twisted-torus field. It will be based on the geometrical considerations that underlie the displacement field choices applied above to perturb the separate magnetic field components. The twisted-torus field follows by vectorial addition of the toroidal and poloidal magnetic field components. Therefore, the appropriate mixed case displacement field is expected to be a vectorial combination of choices (2.121), respectively (2.130), for the toroidal field case and (2.125) for the poloidal field case.

This displacement field ansatz shall next be expressed in a parametrised form where the parameters can be constrained applying the semi-analytic method. As proven in this work, the semi-analytic approach is capable of varying certain mode parameters easily. The parameter space can be scanned for displacement fields that might cause strong instabilities.

Indications for unstable modes as well as possible stabilising effects can be verified afterwards by an investigation with time resolved simulation codes.

One possible intermediate step towards the mixed field investigation is to study the impact of an isolated toroidal field component on the poloidal field instability discussed in section 5.2.

This investigation can be performed in analogy to the procedure shown in section 5.3 with interchanged magnetic field components. Fast growing unstable modes have been discussed before by Markey & Tayler (1973) and can be tested on the simple purely poloidally magnetised star. The required analytical and numerical framework has already been prepared.

Therefore, this study is expected to be implemented in a more straightforward way than the actual mixed case and it might complete the picture about the stability related interaction of both field components towards each other. This information might then facilitate the construction of an actual mixed field perturbation in the next step.

Extensions of the model system

Besides the consideration of mixed magnetic fields, further neutron star characteristics have been neglected in the investigations so far that might have an impact on stability.

All investigations shown here and all studies cited in this work are based on the description of the neutron star as a fluid. Actual stars, however, possess a solid crust of nuclei, as explained in section 2.1.2.

This solid crust might have a stabilising impact on the perturbation modes of the interior magnetised fluid. The crust is assumed to be elastic and deformable, but it cannot be displaced as easily as the fluid elements that move with very little resistance. Since the poloidal magnetic field lines penetrate the surface of the neutron star, as visualised in figure 2.9a, they pass through the solid crust as well. It is expected that the fixation of the field lines by the relatively rigid crust might have a stabilising impact on the system. Compared to an entirely fluid star, the field lines fixated by the crust cannot move arbitrarily with the fluid elements.

The implementation of the solid crust in the energy variation principle would imply an additional term in the energy variation caused by the elastic energy of the crust. The derivation of this term can be done by assuming a full elastic sphere at first and passing on to the spherical shell in a second step. For the transition region between the solid crust and the fluid core, appropriate boundary conditions must be found. The simplest possibility would be to describe the fluid interior and the solid crust with the same model, but different parameters for their distinct elasticity behaviour.

However, even the neutron star crust is not able to stabilise all expected instabilities, especially not in the case of the very strong magnetic field strengths appearing in magnetars. Therefore, the consideration of stability in fluid stars, as presented in this work, is still relevant as well.

Furthermore, the fluids assumed in this work, and other studies concerning neutron star stability, are based on the assumption of normal neutrons and protons. This implies another simplification, since the temperature and density conditions in the neutron star interior suggest that the neutrons form a superfluid and the protons form a superconductor, cf. section 2.1.2.

Since superfluidity and superconductivity were able to explain other neutron star characteristics such as glitches, it stands to reason that these effects might be essential for the neutron star properties in general (Ruderman et al., 1998; Scholz et al., 2017).

The description of superfluid neutrons or superconducting protons would require a new consideration of the established energy terms in the energy variation. The altered properties of neutrons and protons impact the fluid pressure contribution as well as the treatment of the magnetic field.

Validity tests of the Cowling approximation

As explained in the previous chapter, a reasonable follow-up step to the studies performed in this work is to test the validity of the Cowling approximation for stability verifications on further systems.

This information is important due to the increasing interest to search for stability rather than to detect instabilities in upcoming studies. For investigations of this kind, it is not clear whether the Cowling approximation is still applicable. For example in the case of the toroidal field instability, the investigated system appears more stable than it actually is due to the Cowling approximation. If this effect is noticeably strong, the assumption of the Cowling approximation would implicate that unstable systems mistakenly appear stable and the results were not reliable.

Since the analytical and numerical environment for these validity studies has been set up in sections 4.2 and 4.3 already, this step involves little effort and provides interesting insights for future applications.

Relativistic neutron star models

Another natural improvement of the semi-analytic method is the replacement of the Newtonian description by a relativistic approach.

The Newtonian approach applied in this work was justified since we performed tests and produced first results, and because the investigated systems do not involve major mass movements or the like. For a long-range application of the method, however, the

relativistic framework is essential to gain an optimally suitable description of neutron stars, being highly compact objects.

The simplest way to incorporate relativistic corrections in the method is to replace the Newtonian system equations (2.26) by TOV equations. However, this procedure creates inconsistencies if the Newtonian description of the magnetic field used so far is being kept.

Therefore, a relativistic framework can only be achieved by a complete replacement of the Newtonian description by the relativistic one. The entire energy consideration must be set up again in analogy to the existing Newtonian case.

Alternatively, the magnetic field description can be adjusted to a relativistic approach by computing an actual relativistic magnetic equilibrium by solving the Grad-Shafranov equation.

Minor improvements

Besides the additional effects that are worthwhile to be studied and some major structural extensions, there is a number of small improvements that can be implemented in the model and in the code.

Concerning the model, the solving of the system equations (2.26) can be replaced by the use of a prespecified composition profile. That way, the large effort of a complete relativistic description of the background system can be avoided, while we can still estimate to what extent various more realistic composition structures would affect stability. The numerically specified density profiles can for instance be taken from computational studies that showed indications of stability for these models.

Analogously, the approximated magnetic equilibrium applied in this work can be replaced by an actual magnetic equilibrium. So far, the equilibrium state is constructed under the assumption of superimposing the magnetic field to an unmagnetised equilibrium, cf. section 2.2.1. The semi-analytic method, however, is also compatible with a prespecified numerically constructed magnetic equilibrium, which follows from the solution of the Grad-Shafranov equation.

One useful possible code improvement is for example the application of an equidistant cartesian integration grid in the (ϖ, z)-plane. That way, the numerical accuracy stays spatially homogeneous.

Regarding the removal of the Cowling approximation and due to the additionally required integrations, it is important to exhaust the full potential of possible reductions of the computation time. In particular, the J- and K-calculation should be improved by drawing on the previously calculated values of J and K at the neighbouring grid points.

Input parameter construction for simulations

According to all previously discussed phenomena and ideas for future projects, the semi-analytic method can be applied to construct more realistic model systems for magnetised neutron stars. Since they represent a still unresolved question of neutron star physics, this goal is highly desirable.

In particular, the semi-analytic method can be applied in order to systematically construct initial conditions for numerical simulation studies. These studies commonly rely on intelligent guesses for the initial parameter choices. The parameter combinations utilised

in modern studies are partially quite questionable regarding the system's stability behaviour. The usage of profound initial conditions would improve the significance of the simulation study. At the same time, the numerical study would provide a feedback on whether the determined parameters are actually realistic, concerning the outcome of the study or the possibly stable time evolution of the system.

Vice versa, the semi-analytic method can also be applied in order to test whether established initial parameters of numerical studies could tend to result in stable systems, and accordingly decide whether the applied parameters are suitable for these studies.

Global stability tests

The final goal in the field of stability analysis of magnetised neutron stars is to find stable model systems that satisfactorily explain the long and stable life of the observed pulsars.

This goal implies a global stability proof of the constructed model system. As explained in section 2.3.1, a global stability proof of an equilibrium state requires the stability proof of the system against all possible displacement fields. This task is a highly complex if not impossible challenge.

For example, the stabilising impact of the poloidal field component on the toroidal one in the study discussed in section 5.3 only took into account the system's stability behaviour against one specific perturbation mode.

Gaining a statement about the global stability of the system analytically is simply impossible. The semi-analytic method, however, offers a possibility to approach this goal at least.

As shown in chapter 5, the energy variation can be calculated for different choices of displacement field parameters at once. This property provides the opportunity to systematically investigate the impact of entire perturbation mode classes and possibly detect trends regarding which displacement field structures systematically induce instabilities.

The displacement field vectors can be expressed in terms of eigenfunctions of the system, which form a complete basis. That way, all possible displacement field modes can in principle be studied at once.

Even if the practical realisation is not at all a straightforward process, the sheer possibility is a chance the analytical approach cannot offer.

In a second step, these highly destabilising displacement fields can be applied to systems that are expected to be comparably stable. This might be systems involving certain features such as the twisted-torus magnetic field structure, stratification or a neutron star crust. That way, it can be tested whether the destabilising impact of the unstable perturbations is reduced or suppressed by the additional physical features.

7.2. Applications on further systems

Besides the stability analysis of magnetised neutron stars, there are several ideas to apply the semi-analytic method for stability tests on other neutron star related issues.

Eigenmode correction method

First of all, the perturbative correction method for the eigenmode calculation of polytropes or stratified neutron stars suggested in section 5.4.2 can be extended.

As explained above, the semi-analytic method in principle offers the possibility to calculate eigenfrequencies and eigenfunctions of polytropic and stratified stars from the eigenfrequencies and eigenfunctions of the homogeneous star. The advantage is the low time effort, that is expected compared to a time-resolved normal mode analysis approach.

Oscillation studies on neutron stars described in section 2.1.3 rely on the identification of stellar eigenmodes in computed or observed oscillation spectra. It is highly advantageous to have a method at hand that can provide the eigenmodes of arbitrary systems.

For stability analysis, the eigenfunctions are interesting as well. Especially the systematic approach of global stability analysis suggested in the previous paragraph requires the full set of stellar eigenfunctions. Arbitrary displacement fields can be expressed in the basis of eigenfunctions. Systems that are realistic enough in order to be of interest for future stability studies are not analytically treatable. The semi-analytic construction of their eigenmodes would be extremely helpful.

Stability of compact objects against radial displacements

Compact objects, constructed with a polytropic equation of state (2.22) and TOV equations (2.27), show a different stability behaviour depending on the input parameters applied in the construction (Shapiro & Teukolsky, 1983).

The semi-analytic method can be applied in order to investigate this behaviour.

Plotting the total mass of a series of compact objects depending on their central density, one can identify stable and unstable regions in the graph. The stability criterion is given by

$$\left\{ \begin{array}{c} \mathrm{d}_{\rho_c} M > 0 \\ \mathrm{d}_{\rho_c} M < 0 \end{array} \right\} \Leftrightarrow \left\{ \begin{array}{c} \text{stability} \\ \text{instability.} \end{array} \right\} \tag{7.1}$$

For comparably low central densities, the slope is positive. The corresponding objects are stable white dwarfs. With increasing central density, the stability behaviour changes. There is a density range where no stable objects exist. For even higher central densities, stable neutron stars occur. This region ends with a turning point $\mathrm{d}_{\rho_c} M = 0$ as well.

As shown by Shapiro & Teukolsky (1983), the proportionality

$$\mathrm{d}_{\rho_c} M \sim \Gamma_0 - \frac{4}{3} \tag{7.2}$$

can be derived. This translates into the stability criterion

$$\left\{ \begin{array}{c} \Gamma_0 > \frac{4}{3} \\ \Gamma_0 < \frac{4}{3} \end{array} \right\} \Leftrightarrow \left\{ \begin{array}{c} \text{stability} \\ \text{instability.} \end{array} \right\} \tag{7.3}$$

According to the achievements of the semi-analytic method presented in this work, we expect that the method is capable of confirming this stability criterion.

Different model systems can be constructed applying the TOV equations and versatile input parameters. The energy variation consists of fluid pressure and gravity terms. For the displacement field, a radial perturbation must be applied. The variation of the polytropic background parameter Γ_0 should then reveal the stability behaviour of compact objects.

Once this step has been achieved, the system equation for the model construction can be replaced by other choices. The impact of the relativistic description or a realistic equation of state can be investigated. For simplicity, one can even apply a numerically precalculated density profile. That way, it could be tested how realistic models are that are applied in other studies on compact objects.

g-mode stability of neutron stars

Removing the magnetic contribution from the energy variation, the semi-analytic method is able to investigate the stability of stratified neutron stars.

As explained in section 2.2.3, the level of stratification impacts the stability behaviour of the star towards g-mode type displacement fields.

In order to test this, one can apply the g-mode eigenfunctions of a homogeneous star, given in the appendix section A.7, as a displacement field first. Since the star is assumed to be stratified, this procedure is an approximation.

In the next step, the eigenmode of the actual stratified star shall be applied. It might be calculated applying the perturbative correction method suggested above.

The stability behaviour can then be tested, considering fluid and gravitational contributions in the energy variation.

CFS-instability of neutron stars

Another example for a possible application concerning stability analysis is the investigation of the CFS-instability.

Fast rotating neutron stars are subject to the CFS-instability, as mentioned in section 2.3.1. This stability is not dynamical, as opposed to the instabilities discussed in this work. An investigation of this type of instability would therefore be interesting.

For the application of the semi-analytic method to the possibly CFS-unstable system, we would need to consider rotation in the model. The corresponding rotational energy must be included in the expression for the energy variation density.

Beyond that, fluid pressure and gravitational contributions are still relevant. The non-Cowling treatment of the system derived in this work might become necessary as well when rotation is taken into account.

Choosing an adequate displacement field which induces the possible instability, would allow for an investigation of the CFS-instability.

There is a variety of opportunities to vary the system parameters, for example regarding the composition or the rotation of the star. One could even add the magnetic field and investigate its impact on the CFS instability.

Finally, beyond all opportunities described here, the semi-analytic method is not constrained to an investigation of neutron stars.

In principle, it is adaptable to all sorts of geometrically similar systems where a direct quick stability analysis is desired and less effort is preferred over time resolved results.

8. Summary

In this work, a new method for semi-analytic stability analysis based on the variational principle has been developed and implemented. Its functionality has been verified and its crucial advantages towards purely analytical and purely numerical studies have been shown. The method provides an excellent tool to address the so far unresolved stability problem of magnetised neutron stars, which represents one of the essential key questions of neutron star physics.

In particular, the general idea of the method has been presented and an implementation plan was built to set up the method.

The model used in previous stability analysis studies has been extended by adding more realistic and relevant neutron star features. The required analytical derivations have been presented. These were specifically the derivation of the Eulerian pressure perturbation and the fluid contribution to the energy variation density in a stratified star, as well as the Eulerian perturbation of the gravitational potential and the gravitational contribution to the energy variation density in a full non-Cowling treatment.

The numerical code involving the solution of the background system equations, two-dimensional Simpson integrations, grid interpolations and automatic parameter variation has been set up. Successively, the code has been adapted and refined to address more and more complex and realistic systems. Starting from spherical unmagnetised stars, axisymmetry and single magnetic field components have been added first. Afterwards, stratification and mixed magnetic fields have been taken into account. Finally, the Cowling approximation has been removed.

The implemented method has been applied to different problems in order to test the idea of the semi-analytic approach as well as the constructed numerical code. The Tayler instabilities of neutron stars with purely toroidal and purely poloidal magnetic fields have been verified. The stabilising impact of stratification and the poloidal field component on the toroidal Tayler instability has been confirmed. In order to gain first new physical insights from the method, the influence of the Cowling approximation has been investigated. While it does not affect the stability investigation in the specific application tested in this work, it still might not be valid for other applications.

Based on the achievements in this work, the semi-analytic method provides decisive improvements towards a more realistic description of magnetised neutron stars. There is room for further extensions such as the consideration of the neutron star crust, an actual mixed twisted-torus magnetic field structure or many others.

The essential goal of this work has been achieved. The result of this work is a functional method that enables promising potential applications. The semi-analytic method represents one further step towards a more detailed understanding of the interior neutron star structure, which impacts on our general knowledge of fundamental physics.

A. Mathematical identities

This chapter shows mathematical identities frequently used in this work (Bronstein et al., 2008).

A.1. Vector identities

Vectors $\boldsymbol{a}$, $\boldsymbol{b}$, $\boldsymbol{c}$ and generally complex scalars a, b fulfil:

$$\nabla \cdot (a\,\boldsymbol{b}) = a\,\nabla \cdot \boldsymbol{b} + \boldsymbol{b} \cdot \nabla a \tag{A.1}$$

$$\nabla \times (\boldsymbol{a} \times \boldsymbol{b}) = \boldsymbol{a}\,(\nabla \cdot \boldsymbol{b}) - \boldsymbol{b}\,(\nabla \cdot \boldsymbol{a}) + (\boldsymbol{b} \cdot \nabla)\,\boldsymbol{a} - (\boldsymbol{a} \cdot \nabla)\,\boldsymbol{b} \tag{A.2}$$

$$\boldsymbol{a} \times \boldsymbol{b} = -\boldsymbol{b} \times \boldsymbol{a} \tag{A.3}$$

$$\boldsymbol{a} \cdot (\boldsymbol{b} \times \boldsymbol{c}) = \boldsymbol{b} \cdot (\boldsymbol{c} \times \boldsymbol{a}) = \boldsymbol{c} \cdot (\boldsymbol{a} \times \boldsymbol{b}) \tag{A.4}$$

$$(\boldsymbol{a} \times \boldsymbol{b}) \times \boldsymbol{c} = (\boldsymbol{a} \cdot \boldsymbol{c})\,\boldsymbol{b} - (\boldsymbol{b} \cdot \boldsymbol{c})\,\boldsymbol{a} \tag{A.5}$$

$$\nabla \cdot (\boldsymbol{a} \times \boldsymbol{b}) = \boldsymbol{b} \cdot (\nabla \times \boldsymbol{a}) - \boldsymbol{a} \cdot (\nabla \times \boldsymbol{b}) \tag{A.6}$$

$$\nabla \cdot (\nabla \times \boldsymbol{b}) = 0. \tag{A.7}$$

A.2. Integral theorems

Integral theorems for the scalar a, vector $\boldsymbol{b}$ and normal vector $\boldsymbol{n}$ to the surface ∂V of the integration volume V are:

Gauß's theorem

$$\iiint_V \nabla \cdot \boldsymbol{b}\,\mathrm{d}V = \oiint_{\partial V} \boldsymbol{b} \cdot \boldsymbol{n}\,\mathrm{d}\boldsymbol{S}. \tag{A.8}$$

Partial integration in three dimensions

$$\iiint_V a\,\nabla \boldsymbol{b}\,\mathrm{d}V = \oiint_{\partial V} a\,\boldsymbol{b}\,\mathrm{d}\boldsymbol{S} - \iiint_V \boldsymbol{b} \cdot \nabla a\,\mathrm{d}V. \tag{A.9}$$

Integration of an exponential function over a full period

$$\int_0^{2\pi} \mathrm{e}^{\mathrm{i}(m_1 - m_2)\varphi}\,\mathrm{d}\varphi = 2\,\pi\,\delta_{m_1 m_2}. \tag{A.10}$$

A.3. Derivative identities

Gradient, divergence and curl

Spherical coordinates For spherical coordinates (2.4), the gradient of a scalar quantity a is

$$\nabla a = \partial_r a \, \boldsymbol{e}_r + \frac{\partial_\vartheta a}{r} \, \boldsymbol{e}_\vartheta + \frac{\partial_\varphi a}{r \sin\vartheta} \, \boldsymbol{e}_\varphi, \tag{A.11}$$

where $\boldsymbol{e}_i$ denote the unit vectors.

Cylindrical coordinates For cylindrical coordinates (2.6), the gradient of a scalar quantity a is

$$\nabla a = \partial_\varpi a \, \boldsymbol{e}_\varpi + \frac{\partial_\varphi a}{\varpi} \, \boldsymbol{e}_\varphi + \partial_z a \, \boldsymbol{e}_z, \tag{A.12}$$

where $\boldsymbol{e}_i$ denote the unit vectors.

The divergence of a vector quantity $\boldsymbol{b}$ is

$$\nabla \cdot \boldsymbol{b} = \frac{\partial_\varpi \left(\varpi \, b_\varpi \right)}{\varpi} + \frac{\partial_\varphi b_\varphi}{\varpi} + \partial_z b_z. \tag{A.13}$$

The curl of $\boldsymbol{b}$ is given by

$$\nabla \times \boldsymbol{b} = \left(\frac{\partial_\varphi b_z}{\varpi} - \partial_z b_\varphi \right) \boldsymbol{e}_\varpi + \left(\partial_z b_\varpi - \partial_\varpi b_z \right) \boldsymbol{e}_\varphi + \frac{1}{\varpi} \left(\partial_\varpi \left(\varpi \, b_\varphi \right) - \partial_\varphi b_\varpi \right) \boldsymbol{e}_z. \tag{A.14}$$

Orthogonal curvilinear coordinates Be $u_i = \{u_1, u_2, u_3\}$ orthogonal curvilinear coordinates. The curve element $\mathrm{d}\boldsymbol{r}$ and volume element $\mathrm{d}V$ are

$$\mathrm{d}\boldsymbol{r} = \sum_{i=1}^{3} h_\mathrm{i} \, \mathrm{d}\boldsymbol{u}_i \qquad\qquad \mathrm{d}V = J \prod_{i=1}^{3} \mathrm{d}u_i, \tag{A.15}$$

with $\mathrm{d}\boldsymbol{u}_i = \boldsymbol{e}_i \, \mathrm{d}u_i$. The normalised unit vectors $\boldsymbol{e}_i$, scale factors h_i and Jacobi determinant J are

$$\boldsymbol{e}_\mathrm{i} = \frac{\partial_{u_i} \boldsymbol{r}}{h_i} \qquad h_i = \left| \partial_{u_i} \boldsymbol{r} \right| \qquad J = \det \begin{pmatrix} \partial_{u_1} x & \partial_{u_2} x & \partial_{u_3} x \\ \partial_{u_1} y & \partial_{u_2} y & \partial_{u_3} y \\ \partial_{u_1} z & \partial_{u_2} z & \partial_{u_3} z \end{pmatrix}, \tag{A.16}$$

where $\{x, y, z\}$ are cartesian coordinates.

The gradient, divergence and curl of the scalar a and vector $\boldsymbol{b}$ in orthogonal curvilinear coordinates are

$$\nabla a = \frac{\partial_{u_1} a}{h_1} \, \boldsymbol{e}_1 + \frac{\partial_{u_2} a}{h_2} \, \boldsymbol{e}_2 + \frac{\partial_{u_3} a}{h_3} \, \boldsymbol{e}_3 \tag{A.17}$$

$$\nabla \cdot \boldsymbol{b} = \frac{1}{D} \left[\partial_{u_1} \left(h_2 \, h_3 \, b_1 \right) + \partial_{u_2} \left(h_1 \, h_3 \, b_2 \right) + \partial_{u_3} \left(h_1 \, h_2 \, b_3 \right) \right] \tag{A.18}$$

$$\nabla \times \boldsymbol{b} = \sum_{i,j,k=1}^{3} \varepsilon_{ijk} \frac{h_i}{D} \, \partial_{u_j} \left(h_k \, b_k \right) \boldsymbol{e}_i, \tag{A.19}$$

with $D = h_1\, h_2\, h_3$ and the Levi-Civita symbol ε_{ijk}.

Derivatives of logarithms

For scalar functions $x = x(\ln x(\ln y))$ and $\ln x = \ln x(\ln y(y))$, a relation between their derivatives and derivatives of their logarithms can be derived. These functions obey

$$x = \mathrm{e}^{\ln x} \qquad \frac{\mathrm{d}x}{\mathrm{d}\ln x} = \mathrm{e}^{\ln x} = x \qquad \frac{\mathrm{d}\ln y}{\mathrm{d}y} = \frac{1}{y}. \tag{A.20}$$

Thus,

$$\frac{\mathrm{d}x}{\mathrm{d}y} = \frac{\mathrm{d}x}{\mathrm{d}\ln x}\,\frac{\mathrm{d}\ln x}{\mathrm{d}y} = x\,\frac{\mathrm{d}\ln x}{\mathrm{d}\ln y}\,\frac{\mathrm{d}\ln y}{\mathrm{d}y} = \frac{x}{y}\,\frac{\mathrm{d}\ln x}{\mathrm{d}\ln y}. \tag{A.21}$$

Fluid pressure gradient

The gradient of the fluid pressure can be rewritten applying the chain rule on the dependence $p = p(\rho, x^p(\rho))$ from the equation of state (2.38) for the perturbed system:

$$\nabla p_0 = \left(\frac{\partial p_0}{\partial \rho_0}\right)_{x^p} \nabla\rho_0 + \left(\frac{\partial p_0}{\partial x_0^p}\right)_{\rho} \frac{\mathrm{d}x_0^p}{\mathrm{d}\rho_0}\,\nabla\rho_0 = \frac{p_0}{\rho_0}\left[\left(\frac{\partial \ln p_0}{\partial \ln \rho_0}\right)_{x^p} + \left(\frac{\partial \ln p_0}{\partial \ln x_0^p}\right)_{\rho} \frac{\mathrm{d}\ln x_0^p}{\mathrm{d}\ln \rho_0}\right]\nabla\rho_0. \tag{A.22}$$

In the second step, we made use of equation (A.21), relating derivatives and derivatives of their logarithms:

$$\left(\frac{\partial p_0}{\partial \rho_0}\right)_{x^p} = \frac{p_0}{\rho_0}\left(\frac{\partial \ln p_0}{\partial \ln \rho_0}\right)_{x^p} \qquad \left(\frac{\partial p_0}{\partial x_0^p}\right)_{\rho} = \frac{p_0}{x_0^p}\left(\frac{\partial \ln p_0}{\partial \ln x_0^p}\right)_{\rho} \qquad \frac{\mathrm{d}x_0^p}{\mathrm{d}\rho_0} = \frac{x_0^p}{\rho_0}\,\frac{\mathrm{d}\ln x_0^p}{\mathrm{d}\ln \rho_0}. \tag{A.23}$$

The polytropic index Γ_0 of the background system can be identified in (A.22) according to equation (2.40), yielding

$$\nabla p_0 = \frac{\Gamma_0\, p_0}{\rho_0}\,\nabla\rho_0. \tag{A.24}$$

A.4. Other relations

Trigonometric relation

The Pythagorean trigonometric identity reads

$$\sin^2\varphi + \cos^2\varphi = 1. \tag{A.25}$$

Transformation relations for vector components

For transformations from spherical coordinates (2.4) to cylindrical coordinates (2.6), the vector components of $\boldsymbol{b}$ obey

$$b_\varpi = b_r\,\sin\vartheta + b_\vartheta\,\cos\vartheta \tag{A.26a}$$

$$b_\varphi = b_\varphi \tag{A.26b}$$

$$b_z = b_r\,\cos\vartheta - b_\vartheta\,\sin\vartheta. \tag{A.26c}$$

A.5. Identities for complex functions

A.5.1. Notations and identities for complex numbers

Let a and b be complex functions, $\{a, b\} \in \mathbb{C}$. The complex number a and its complex conjugate a^* can be expressed as

$$a = a_r \, \mathrm{e}^{\,\mathrm{i}\varphi} = a_r \, (\cos\varphi + \mathrm{i}\sin\varphi) \qquad a = a_R + \mathrm{i}a_I \tag{A.27a}$$

$$a^* = a_r \, \mathrm{e}^{-\mathrm{i}\varphi} = a_r \, (\cos\varphi - \mathrm{i}\sin\varphi) \qquad a^* = a_R - \mathrm{i}a_I, \tag{A.27b}$$

where a_r is a real amplitude, while a_R and a_I denote real and imaginary parts of a.

The complex conjugation of sums and products obeys

$$(a+b)^* = a^* + b^* \qquad (a\,b)^* = a^*\,b^*. \tag{A.28}$$

A.5.2. Properties of real parts

The real parts of products of complex functions $\{a, b\} \in \mathbb{C}$ obey

$$\Re\left\{a^* b\right\} = \Re\left\{a \;\; b^*\right\} = \frac{1}{2}\left\{a^* b \;\; + a \;\; b^*\right\} = a_R\, b_R - a_I\, b_I \tag{A.29}$$

$$\Re\left\{a \;\; b\right\} = \Re\left\{a^* b^*\right\} = \frac{1}{2}\left\{a \;\; b \;\; + a^* b^*\right\} = a_R\, b_R + a_I\, b_I \tag{A.30}$$

$$\Re\left\{a^* + a\right\} = \Re\left\{2\, a_R\right\} = 2\, a_R, \tag{A.31}$$

which follows from the definition of complex numbers in equation (A.27).

Especially, the real part of an exponential function obeys

$$\Re\left\{\mathrm{e}^{\mathrm{i}(m_1 - m_2)\varphi}\right\} = \frac{1}{2}\left\{\mathrm{e}^{\mathrm{i}(m_1 - m_2)\varphi} + \mathrm{e}^{\mathrm{i}(m_2 - m_1)\varphi}\right\}. \tag{A.32}$$

A.5.3. Integrals of complex exponential functions

The integral of an exponential function $\mathrm{e}^{\mathrm{i}k\varphi}$ over a full period of φ vanishes for integers $k \in \mathbb{Z}$:

$$\int_0^{2\pi} \mathrm{e}^{\mathrm{i}k\varphi} \, \mathrm{d}\varphi = \int_0^{2\pi} \Big\{\cos(k\,\varphi) + \mathrm{i}\sin(k\,\varphi)\Big\} \, \mathrm{d}\varphi = \frac{1}{k}\Big[\sin(k\,\varphi)\Big]_0^{2\pi} - \frac{\mathrm{i}}{k}\Big[\cos(k\,\varphi)\Big]_0^{2\pi} = 0, \tag{A.33}$$

which follows from the definition of complex functions in exponential depiction in (A.27) and the periodicity of sine and cosine.

This property facilitates a consequent simplification in the integrand of the energy variation density. The energy variation density $\mathcal{E}$ depends on products of complex functions, such as $\boldsymbol{\xi}$ or δQ, that involve exponential parts like $\mathrm{e}^{\pm\mathrm{i}m\varphi}$. In these products, only terms where the exponential functions cancel out will provide a non-vanishing contribution during the φ-integration.

This circumstance can be expressed as a consequence of relation (A.33):

$$\int_0^{2\pi} \left(a\,\mathrm{e}^{\mathrm{i}m\varphi} + b\,\mathrm{e}^{-\mathrm{i}m\varphi}\right)\left(c\,\mathrm{e}^{\mathrm{i}m\varphi} + d\,\mathrm{e}^{-\mathrm{i}m\varphi}\right)\mathrm{d}\varphi = \int_0^{2\pi} (a\,d + b\,c)\,\mathrm{d}\varphi + \underbrace{\int_0^{2\pi} \left(a\,c\,\mathrm{e}^{2\mathrm{i}m\varphi} + b\,d\,\mathrm{e}^{-2\mathrm{i}m\varphi}\right)\mathrm{d}\varphi}_{0}, \tag{A.34}$$

where a, b, c and d are generally real functions.

This relation is applicable to all cases of this type considered in this work, since the mode index m always fulfils the condition $m \in \mathbb{Z}$.

Finally, in the case where a, b, c and d are independent of φ, (A.34) can be integrated to give

$$\int_0^{2\pi} \left(a\,\mathrm{e}^{\mathrm{i}m\varphi} + b\,\mathrm{e}^{-\mathrm{i}m\varphi}\right)\left(c\,\mathrm{e}^{\mathrm{i}m\varphi} + d\,\mathrm{e}^{-\mathrm{i}m\varphi}\right)\mathrm{d}\varphi = 2\,\pi\,(a\,d + b\,c)\,. \tag{A.35}$$

A.5.4. Ensuring the physical meaningfulness of the energy variation

As explained in section 2.3.2, there are two possible ways to guarantee a physically meaningful energy variation. Tayler (1973) and Markey & Tayler (1973) take the real part of $\boldsymbol{\xi}$ before inserting it into $\mathcal{E}$. In this work, the real part is taken over the total integrand $\mathcal{E}$ instead.

In this section, we derive the impact of both approaches on the form of δW. The result will enable the transformation between the equations given in this work and by Tayler et al., for direct comparison of the applications described in sections 5.1 and 5.2 with the original work.

We define complex functions

$$\bar{F} = F_0\,\mathrm{e}^{\mathrm{i}m\varphi} \qquad F = \Re\left(\bar{F}\right) = \Re\left(F_0\,e^{\mathrm{i}m\varphi}\right) \tag{A.36}$$

$$\bar{G} = G_0\,\mathrm{e}^{\mathrm{i}m\varphi} \qquad G = \Re\left(\bar{G}\right) = \Re\left(G_0\,e^{\mathrm{i}m\varphi}\right) \tag{A.37}$$

with generally complex amplitudes F_0, G_0 that do not depend on φ.

According to relation (A.30), the integral over the product of F and G can be calculated as

$$\int_0^{2\pi} F\,G\,\mathrm{d}\varphi = \int_0^{2\pi} \Re\left(F_0\,\mathrm{e}^{\mathrm{i}m\varphi}\right)\Re\left(G_0\,\mathrm{e}^{\mathrm{i}m\varphi}\right)\mathrm{d}\varphi \tag{A.38}$$

$$= \frac{1}{4}\int_0^{2\pi} \left(F_0\,\mathrm{e}^{\mathrm{i}m\varphi} + F_0^*\,\mathrm{e}^{-\mathrm{i}m\varphi}\right)\left(G_0\,\mathrm{e}^{\mathrm{i}m\varphi} + G_0^*\,\mathrm{e}^{-\mathrm{i}m\varphi}\right)\mathrm{d}\varphi \tag{A.39}$$

$$= \frac{\pi}{2}\left(F_0\,G_0^* + F_0^*\,G_0\right), \tag{A.40}$$

where the final step follows with relation (A.35).

Analogously, the integral over the real part of the product $\bar{F}\,\bar{G}$ can be calculated using equation (A.29):

$$\int_0^{2\pi} \Re\left(\bar{F}^*\bar{G}\right) \mathrm{d}\varphi = \int_0^{2\pi} \Re\left(F_0^*\ \mathrm{e}^{-im\varphi}\ G_0\ \mathrm{e}^{\mathrm{i}m\varphi}\right) \mathrm{d}\varphi \tag{A.41}$$

$$= \frac{1}{2}\int_0^{2\pi} \left(F_0^*\,G_0 + F_0\,G_0^*\right) \mathrm{d}\varphi \tag{A.42}$$

$$= \pi\left(F_0^*\,G_0 + F_0\,G_0^*\right). \tag{A.43}$$

Overall, the connection between both approaches can therefore be described by

$$\int_0^{2\pi} F\,G\,\mathrm{d}\varphi = \frac{1}{2}\int_0^{2\pi} \Re\left(\bar{F}^*\,\bar{G}\right) \mathrm{d}\varphi = \frac{1}{2}\int_0^{2\pi} \Re\left(\bar{F}\,\bar{G}^*\right) \mathrm{d}\varphi. \tag{A.44}$$

Note that relation (A.44) is valid, independently of whether the first or the second function is complex conjugated on the right hand side.

The components of the displacement field in this work are of the form of $\bar{F}$ and $\bar{G}$, while Tayler's $\boldsymbol{\xi}$-components are of the form of F and G.

Accordingly, all formulas shown in this work – where complex displacement fields are used and the real part is taken inside $\mathcal{E}$ – contain an extra factor of $1/2$ as long as the real part has not been evaluated yet, compared to Tayler's approach with real displacement fields.

Physical meaningful energy variation The additional factor of $1/2$ which ensures that the final explicit form of δW is identical with Tayler's form, particularly appears in the energy variation density in its implicit form in (2.79), as well as its explicit form in (2.117), and all transformation steps in between. The same applies for the fluid energy variation density contribution in the stratified star, shown in equation (4.6), and the non-Cowling gravitational contribution, given by equations (4.9) and (4.31) to (4.34). The summarised contributions in equation (4.48) still contain the unevaluated real part as well and therefore also the additional factor $1/2$ compared to Bernstein et al. (1958) or Tayler (1973). The same applies for the original δW-expressions in the application chapter, (5.10) and (5.36).

On the other hand, after the real part has been evaluated, the additional factor disappears. Expressions (4.14) of the non-Cowling gravitational contribution for displacement fields expressed by spherical harmonics are formally identical with their equivalents in Chandrasekhar & Lebovitz (1964). The same applies for the non-Cowling gravitational contributions in the mixed field case, shown by equations (4.35) to (4.44) and (4.49). In the application chapter, the final forms of the energy variation in equation (5.11), (5.39), (5.40) and (5.54), are identical with their equivalents in Tayler (1973), Markey & Tayler (1973) and Akgün et al. (2013).

Physical meaningful gravitational Euler perturbation For the derivation of the gravitational Euler perturbation $\delta\Phi$, the situation is different from the energy variation.

The calculation of $\delta\Phi$ involves the integration of a scalar product between the displacement field $\boldsymbol{\xi}$ and a gradient involving spherical harmonics Y_λ^μ, cf. equation (4.18). In contrast to δW, where Tayler inserted only the real part of the displacement field into the integrand, this time $\boldsymbol{\xi}$ and Y_λ^μ are actual complex functions. Nevertheless, the integral over the product is real which follows from the explicit form of their imaginary parts.

With

$$\boldsymbol{\xi}^* \sim \mathrm{e}^{-im\varphi} \qquad\qquad Y_\lambda^\mu \sim \mathrm{e}^{\mathrm{i}\mu\varphi}, \tag{A.45}$$

and according to relation (A.10), the azimuthal integral in $\delta\Phi$ becomes

$$\int_0^{2\pi} a\,\boldsymbol{\xi}^* \cdot \nabla\left[b\,Y_\lambda^\mu\right] \mathrm{d}\varphi = \int_0^{2\pi} c\,\mathrm{e}^{\mathrm{i}(\mu-m)\varphi}\,\mathrm{d}\varphi = 2\,\pi\,c\,\delta_{m\mu}, \tag{A.46}$$

where a, b and c denote real functions that are independent of φ. On the other hand, with relation (A.27),

$$\int_0^{2\pi} \Re\left\{a\,\boldsymbol{\xi}^* \cdot \nabla\left[b\,Y_\lambda^\mu\right]\right\} \mathrm{d}\varphi = \int_0^{2\pi} c\,\Re\left\{\mathrm{e}^{\mathrm{i}(\mu-m)\varphi}\right\} \mathrm{d}\varphi = \int_0^{2\pi} c\,\left\{\cos\left((\mu-m)\varphi\right)\right\} \mathrm{d}\varphi = 2\,\pi\,c\,\delta_{m\mu} \tag{A.47}$$

holds as well. Therefore,

$$\int_0^{2\pi} d\,\boldsymbol{\xi}^*\,Y_\lambda^\mu\,\mathrm{d}\varphi = \int_0^{2\pi} \Re\left\{d\,\boldsymbol{\xi}^*\,Y_\lambda^\mu\right\}\,\mathrm{d}\varphi, \tag{A.48}$$

with the real function d.

Note that this relation does not hold for arbitrary complex functions, cf. equation (A.29), it is rather caused by the particular form of $\boldsymbol{\xi}$ and Y_λ^μ.

According to (A.48) and the fact that Chandrasekhar & Lebovitz (1964) address actual complex functions in the $\delta\Phi$-integrand, there are no additional factors to be considered here compared to their form when we take the real part of the integrand.

Also note that the complex scalar product in the gravitational Euler perturbation integral (B.28), traces back – over the integral relation (B.29) – to the orthogonality relations (A.51) and (A.52) for spherical harmonics.

They involve actual complex functions whose scalar product integrals are real. The orthogonality relations stay unchanged when the real part is applied to the integrand:

$$\iint_S \Re\left\{Y_l^{m*}\,Y_{l'}^{m'}\right\} dS = \delta_{ll'}\,\delta_{mm'} \tag{A.49}$$

$$\iint_S \frac{1}{\sin^2\vartheta}\Re\left\{\sin^2\vartheta\,\partial_\vartheta Y_l^{m*}\,\partial_\vartheta Y_{l'}^{m'} + \partial_\varphi Y_l^{m*}\,\partial_\varphi Y_{l'}^{m'}\right\} dS = l(l+1)\,\delta_{ll'}\,\delta_{mm'}. \tag{A.50}$$

This feature eventually causes the $\delta\Phi$-integral to be intrinsically real as well.

A.6. Properties of spherical harmonics

Spherical harmonics, as defined in equation (2.137) with (2.138) and (2.139), and their derivatives fulfil the following orthogonality properties:

$$\iint Y_l^{m*}\, Y_{l'}^{m'}\, \mathrm{d}S = \delta_{ll'}\, \delta_{mm'} \tag{A.51}$$

$$\iint \frac{1}{\sin^2\vartheta} \left\{ \sin^2\vartheta\, \partial_\vartheta Y_l^{m*}\, \partial_\vartheta Y_{l'}^{m'} + \partial_\varphi Y_l^{m*}\, \partial_\varphi Y_{l'}^{m'} \right\} \mathrm{d}S = l(l+1)\, \delta_{ll'}\, \delta_{mm'}, \tag{A.52}$$

where $\mathrm{d}S$ denotes the angular surface element. For example, in spherical coordinates (2.4): $\mathrm{d}S = \sin\vartheta\, \mathrm{d}\vartheta\, \mathrm{d}\varphi$.

A.7. Eigenmodes of the homogeneous incompressible star

The stellar eigenmodes of homogeneous incompressible stars can be analytically described (Flügge, 1958; Smeyers & van Hoolst, 2010).

The explicit form of the radial functions defined in equation (2.144) is given in this section.

We define

$$y_1 = C_0\, \frac{\bar{E}\, \bar{U}}{r} \qquad\qquad y_2 = C_0\, \frac{\bar{V}}{r} \tag{A.53}$$

and

$$\begin{aligned} \bar{E} &= \frac{\Gamma_1\, \omega^2}{8\,\omega^2 + 2\,\omega^4 - 12} \\ \bar{F} &= \frac{14\,\Gamma_1\, \omega^2 - 8\,\omega^2 - 2\,\omega^4 + 12}{14\,\Gamma_1\, \omega^2} \\ \bar{G} &= \frac{1}{924} \left(\frac{-14\,\Gamma_1\, \omega^2 + 8\,\omega^2 + 2\,\omega^4 - 12}{\Gamma_1\, \omega^2} \right)^2 + \frac{52}{924}\, \frac{14\,\Gamma_1\, \omega^2 - 8\,\omega^2 - 2\,\omega^4 + 12}{\Gamma_1\, \omega^2}, \end{aligned} \tag{A.54}$$

with a constant amplitude C_0. For the homogeneous star, $c_1 = 1$.

The f-mode is described by

$$\bar{U}_f = \frac{2\, r}{\omega^2\, \bar{E}} \qquad\qquad \bar{V}_f = r \qquad\qquad \partial_r \bar{U}_f = \frac{2}{\omega^2\, \bar{E}}. \tag{A.55}$$

The g_1- and p_1-mode are described by

$$\begin{aligned} \bar{U}_{g_1,p_1} &= \left(4 + \frac{6}{\omega^2}\right) \frac{r^3}{R^2} - \left(2 + \frac{6}{\omega^2}\right) r \\ \bar{V}_{g_1,p_1} &= \left(\frac{6\,\bar{E}}{\omega^2} + \bar{E} + \frac{\Gamma_1}{2}\right) \frac{r^3}{R^2} - \left(\frac{6\,\bar{E}}{\omega^2} - \bar{E} + \frac{\Gamma_1}{2}\right) r \\ \partial_r \bar{U}_{g_1,p_1} &= 3\left(4 + \frac{6}{\omega^2}\right) \frac{r^2}{R^2} - \left(2 + \frac{6}{\omega^2}\right). \end{aligned} \tag{A.56}$$

The g_2- and p_2-mode are described by

$$\begin{aligned}
\bar{U}_{g_2,p_2} &= \left(6+\frac{6}{\omega^2}\right)\bar{F}\,\frac{r^5}{R^4}+\left(4+\frac{6}{\omega^2}\right)(1-\bar{F})\,\frac{r^3}{R^2}-\left(2+\frac{6}{\omega^2}\right)r \\
\bar{V}_{g_2,p_2} &= \left(\frac{6\,\bar{E}}{\omega^2}+3\,\bar{E}+\frac{\Gamma_1}{2}\right)\bar{F}\,\frac{r^5}{R^4}+\left(\frac{6\,\bar{E}}{\omega^2}+\bar{E}+\frac{\Gamma_1}{2}\right)(1-\bar{F})\,\frac{r^3}{R^2}-\left(\frac{6\,\bar{E}}{\omega^2}-\bar{E}+\frac{\Gamma_1}{2}\right)r \\
\partial_r\bar{U}_{g_2,p_2} &= 5\left(6+\frac{6}{\omega^2}\right)\bar{F}\,\frac{r^4}{R^4}+3\left(4+\frac{6}{\omega^2}\right)(1-\bar{F})\,\frac{r^2}{R^2}-\left(2+\frac{6}{\omega^2}\right).
\end{aligned} \tag{A.57}$$

The g_3- and p_3-mode are described by

$$\begin{aligned}
\bar{U}_{g_3,p_3} &= \left(8+\frac{6}{\omega^2}\right)\bar{G}\,\frac{r^7}{R^6}+\left(6+\frac{6}{\omega^2}\right)(\bar{F}-\bar{G})\,\frac{r^5}{R^4}+\left(4+\frac{6}{\omega^2}\right)(1-\bar{F})\,\frac{r^3}{R^2}-\left(2+\frac{6}{\omega^2}\right)r \\
\bar{V}_{g_3,p_3} &= \left(\frac{6\,\bar{E}}{\omega^2}+5\,\bar{E}+\frac{\Gamma_1}{2}\right)\bar{G}\,\frac{r^7}{R^6}+\left(\frac{6\,\bar{E}}{\omega^2}+3\,\bar{E}+\frac{\Gamma_1}{2}\right)(\bar{F}-\bar{G})\,\frac{r^5}{R^4} \\
&\quad+\left(\frac{6\,\bar{E}}{\omega^2}+\bar{E}+\frac{\Gamma_1}{2}\right)(1-\bar{F})\,\frac{r^3}{R^2}-\left(\frac{6\,\bar{E}}{\omega^2}-\bar{E}+\frac{\Gamma_1}{2}\right)r \\
\partial_r\bar{U}_{g_3,p_3} &= 7\left(8+\frac{6}{\omega^2}\right)\bar{G}\,\frac{r^6}{R^6}+5\left(6+\frac{6}{\omega^2}\right)(\bar{F}-\bar{G})\,\frac{r^4}{R^4}+3\left(4+\frac{6}{\omega^2}\right)(1-\bar{F})\,\frac{r^2}{R^2}-\left(2+\frac{6}{\omega^2}\right).
\end{aligned} \tag{A.58}$$

For homogeneous stars, the following analytical relations hold for the equilibrium quantities, inferred from the system equations (2.26):

$$\rho_0(r) = \rho_0 = \frac{M}{V} = \frac{3}{4\,\pi}\,\frac{M}{R^3} \tag{A.59}$$

$$p_0(r) = \frac{2\,\pi}{3}\,\rho_0^2\left(R^2-r^2\right) \tag{A.60}$$

$$g_r(r) = \mp\frac{4\,\pi}{3}\,\rho_0\,r \tag{A.61}$$

$$\Gamma_0 = \infty. \tag{A.62}$$

A.8. Unit systems

For an overview and the straightforward comparison with works by different authors, the most common choices for unit systems used in the field of magnetised neutron star stability analysis are presented in this section.

Generally, unit systems can be distinguished by the following characteristics.

SI and cgs unit systems In contrast to the SI unit system which is based on metre, kilogramme and second, the cgs system is based on the three fundamental units centimetre, gramme and second.

The expression of mechanical quantities in cgs units is unique. The transformation involves a simple unit change.

Electromagnetic quantities, in contrast, require an extension of the cgs unit system. A common choice is the so-called Gaussian cgs unit system. Electromagnetic quantities depicted in SI units and Gaussian cgs units are not transferable into each other by simple unit changes. The quantities and equations expressed in SI units and Gaussian cgs units differ in prefactors involving 4π, c, or vacuum permittivity and permeability ε_0 and μ_0.

Non-rationalised and rationalised unit systems The standard formulation of the fundamental electromagnetic equations in non-rationalised Gaussian cgs units involves the factor 4π in two of the Maxwell equations (2.14). On the contrary, rationalised unit systems are defined in such a way that these factors disappear.

The Maxwell equations expressed in rationalised units are symmetrical, while additional factors appear in Coulomb's law and the Biot-Savart law. The SI unit system is one example of a rationalised unit system, the rationalised Gaussian unit system discussed below is another one.

Non-geometrised and geometrised unit systems Fundamental equations describing phenomena of electromagnetism or gravity generally involve the appearance of the prefactors c and G. This can be seen for example in the Maxwell equations (2.14) or the Poisson equation (2.20). In a geometrised unit system, the physical units are defined in such a way that these factors equal unity, $c = 1$ and $G = 1$, and thus disappear from the fundamental equations.

Dimensionless set of quantities For calculations, and the numerical computation of physical quantities especially, it is convenient to work in a unit system where all physical quantities are dimensionless. All quantities are expressed in terms of non-dimensionless physical constants.

The dimensionless unit system can be based on an arbitrary set of constants that involves all three fundamental units in an independent way.

In the field of compact stellar objects, the usage of the solar mass $\mathrm{M}_\odot$, the speed of light c and the gravitational constant G is customary.

Gaussian cgs unit system

The typically so called "Gaussian unit system" labels a non-rationalised cgs system that represents an extension of the mechanical cgs unit system for electromagnetism.

It is for instance used by Akgün et al. (2013).

The basic equations that are relevant for this work, expressed in non-rationalised Gaus-

sian cgs units, are

$$\nabla \cdot \boldsymbol{E} = 4\,\pi\,\rho_e \tag{A.63a}$$

$$\nabla \times \boldsymbol{E} = -\frac{\partial_t \boldsymbol{B}}{c} \tag{A.63b}$$

$$\nabla \cdot \boldsymbol{B} = 0 \tag{A.63c}$$

$$\nabla \times \boldsymbol{B} = \frac{4\,\pi}{c}\,\boldsymbol{j} + \frac{\partial_t \boldsymbol{E}}{c} \tag{A.63d}$$

$$\boldsymbol{F}_e = q_e \left(\boldsymbol{E} + \frac{\boldsymbol{v} \times \boldsymbol{B}}{c} \right) \tag{A.63e}$$

$$\boldsymbol{F}_C = \frac{q_1\,q_2}{r^2}\,\frac{\boldsymbol{r}}{|\boldsymbol{r}|}, \tag{A.63f}$$

where equations (A.63a) to (A.63d) are the Maxwell equations, relation (A.63e) describes the electromagnetic force and equation (A.63f) represents Coulomb's law of two electric charges q_1 and q_2.

Geometrised rationalised Gaussian unit system

Compared to the Gaussian cgs unit system (A.63), the geometrised rationalised Gaussian cgs unit system does not involve the factor $4\,\pi$ in the Maxwell equations. The other equations, that might gain additional factors in the course of this, are not required in this work. Beyond that, the geometrisation involves $c = 1$ and $G = 1$.

This unit system is used by Bernstein et al. (1958); Tayler (1973); Markey & Tayler (1973) for instance.

The basic equations expressed in geometrised rationalised Gaussian cgs units are

$$\nabla \cdot \boldsymbol{E} = \rho_e \tag{A.64a}$$

$$\nabla \times \boldsymbol{E} = -\partial_t \boldsymbol{B} \tag{A.64b}$$

$$\nabla \cdot \boldsymbol{B} = 0 \tag{A.64c}$$

$$\nabla \times \boldsymbol{B} = \boldsymbol{j} + \partial_t \boldsymbol{E} \tag{A.64d}$$

$$\boldsymbol{F}_e = q_e\,(\boldsymbol{E} + \boldsymbol{v} \times \boldsymbol{B})\,. \tag{A.64e}$$

Dimensionless quantities in terms of $M_\odot, c$ and G

The set of dimensionless quantities $\{\tilde{Q}\}$ applied in this work is based on the solar mass, the speed of light and the gravitational constant. It is defined by the following relations.

$$\begin{aligned}
\tilde{r} &= \frac{c^2}{M_\odot G}\, r & \tilde{v} &= \frac{v}{c} & \tilde{F} &= \frac{G}{c^4}\, F & \tilde{W} &= \frac{W}{c^2\, M_\odot} \\
\tilde{t} &= \frac{c^3}{M_\odot G}\, t & \tilde{m} &= \frac{m}{M_\odot} & \tilde{p} &= \frac{M_\odot^2 G^3}{c^8}\, p & \tilde{\Phi} &= \frac{\Phi}{c^2} \\
\tilde{\rho} &= \frac{M_\odot^2 G^3}{c^6}\, \rho & \tilde{\boldsymbol{g}} &= \frac{M_\odot G}{c^4}\, \boldsymbol{g} & \tilde{\kappa} &= \frac{M_\odot^{2-2\Gamma_0} G^{3-3\Gamma_0}}{c^{8-6\Gamma_0}}\, \kappa & & \\
\tilde{\psi} &= \frac{c^6}{M_\odot^3 G^3}\, \psi & \tilde{\chi} &= \frac{c^6}{M_\odot^3 G^3}\, \chi & \tilde{J}_l &= \frac{c^{2l}}{M_\odot^{1+l} G^l}\, J_l & \tilde{K}_l &= \frac{M_\odot^l G^{1+l}}{c^{2+2l}}\, K_l \\
\tilde{q}_e &= \frac{q_e}{M_\odot G^{1/2}} & \tilde{\boldsymbol{j}} &= \frac{M_\odot^2 G^{5/2}}{c^7}\, \boldsymbol{j} & \tilde{\boldsymbol{B}} &= \frac{M_\odot G^{3/2}}{c^4}\, \boldsymbol{B} & &
\end{aligned} \tag{A.65}$$

Note that this definition holds for cgs as well as for SI units in the case of the mechanical or geometrical quantities $\{r, v, F, W, t, m, p, \Phi, \rho, \boldsymbol{g}, \kappa, \psi, \chi, J_l, K_l\}$. In the case of the electromagnetic quantities $\{q_e, \boldsymbol{j}, \boldsymbol{B}\}$, the relations are valid only in the cgs unit system.

The geometrised dimensionless quantities $\{\tilde{Q}^*\}$ are defined in analogy to relations (A.65) by choosing

$$\tilde{r}^*\,[\mathrm{cm}] = r \qquad \tilde{m}^*\,[\mathrm{cm}] = \frac{G}{c^2}\, m \qquad \tilde{t}^*\,[\mathrm{cm}] = c\, t. \tag{A.66}$$

B. Mathematical derivations

In this chapter, mathematical derivations that are relevant for this work are outlined.

B.1. Partial and material derivatives

The connection between material and partial time derivatives in floating fluids will be derived (Thompson, 2006).

The partial derivative $\partial_t Q$ describes the change of a quantity $Q(\boldsymbol{r}_0)$ at a fixed position:

$$\partial_t Q = \lim_{t \to t_0} \frac{Q(\boldsymbol{r}_0, t) - Q(\boldsymbol{r}_0, t_0)}{t - t_0}. \tag{B.1}$$

The material derivative $\mathrm{D}_t Q$ describes the change in Q within a fixed fluid element, that moves at a velocity $\boldsymbol{v}$ from $\boldsymbol{r}_0$ to $\boldsymbol{r}$ during the time interval $t - t_0$:

$$\mathrm{D}_t Q = \lim_{t \to t_0} \frac{Q(\boldsymbol{r}, t) - Q(\boldsymbol{r}_0, t_0)}{t - t_0} = \lim_{t \to t_0} \frac{Q(\boldsymbol{r}_0 + \boldsymbol{v}(t - t_0), t) - Q(\boldsymbol{r}_0, t_0)}{t - t_0}. \tag{B.2}$$

The connection between both derivatives can be derived as follows.

The total derivative $d_t Q$ of a quantity $Q(\boldsymbol{r}) = Q(r_1(t), r_2(t), r_3(t), t)$ is generally calculated by applying the chain rule:

$$d_t Q = \partial_1 Q \, d_t r_1 + \partial_2 Q \, d_t r_2 + \partial_3 Q \, d_t r_3 + \partial_t Q, \tag{B.3}$$

where $\partial_i \equiv \partial / \partial r_i$.

In fluid dynamics, any system quantity Q depends on position variables r_i that are also time-dependent, due to the fluid velocity $\boldsymbol{v} = \mathrm{d}_t \boldsymbol{r}$. The fluid velocity describes the change in the position vector for a fixed fluid element and is therefore denoted by the total derivative.

In this special case of fluid dynamics, the total derivative becomes

$$d_t Q = \partial_1 Q \, v_1 + \partial_2 Q \, v_2 + \partial_3 Q \, v_3 + \partial_t Q = \partial_t Q + \boldsymbol{v} \cdot \nabla Q \equiv \mathrm{D}_t Q. \tag{B.4}$$

It is called the material derivative.

If $\boldsymbol{Q} = (Q_1, Q_2, Q_3)$ is a vector quantity, the relation equally holds for its components:

$$\mathrm{D}_t \boldsymbol{Q} = \partial_t \boldsymbol{Q} + (\boldsymbol{v} \cdot \nabla) \, \boldsymbol{Q} = \begin{pmatrix} \partial_t \delta Q_1 \\ \partial_t \delta Q_2 \\ \partial_t \delta Q_3 \end{pmatrix} + \begin{pmatrix} (v_1 \partial_1 + v_2 \partial_2 + v_3 \partial_3) \, Q_1 \\ (v_1 \partial_1 + v_2 \partial_2 + v_3 \partial_3) \, Q_2 \\ (v_1 \partial_1 + v_2 \partial_2 + v_3 \partial_3) \, Q_3 \end{pmatrix}. \tag{B.5}$$

B.2. Magnetic field expressed by a stream function

Axisymmetric magnetic fields can be expressed by derivatives of a scalar stream function (Grad & Rubin, 1958; Lander & Jones, 2009). This feature is reasoned below.

According to Gauß's law for magnetism (2.14c), magnetic fields are divergence free. With relation (A.7), this Maxwell equation is fulfilled by default if the magnetic field is generated by a vector potential $\boldsymbol{A}$ via

$$\boldsymbol{B} = \nabla \times \boldsymbol{A}. \tag{B.6}$$

In cylindrical coordinates (2.6) with (A.14) and under the assumption of axisymmetry, this can be expressed as

$$\boldsymbol{B} = \left(\frac{\partial_\varphi A_z}{\varpi} - \partial_z A_\varphi\right) \boldsymbol{e}_\varpi + \left(\partial_z A_\varpi - \partial_\varpi A_z\right) \boldsymbol{e}_\varphi + \frac{1}{\varpi}\left(\partial_\varpi \left(\varpi\, A_z\right) - \partial_\varphi A_\varpi\right) \boldsymbol{e}_z \tag{B.7}$$

$$= -\frac{1}{\varpi}\,\partial_z u\, \boldsymbol{e}_\varpi + B_\varphi\, \boldsymbol{e}_\varphi + \frac{1}{\varpi}\,\partial_\varpi u\, \boldsymbol{e}_z, \tag{B.8}$$

with the cylindrical unit vectors $\boldsymbol{e}_i$ and a scalar stream function

$$u \equiv \varpi\, A_\varphi. \tag{B.9}$$

By the use of the gradient (A.12) in cylindrical coordinates and with the assumption of axisymmetry, $\partial_\varphi u = 0$, it is

$$\nabla u \times \boldsymbol{e}_\varphi = \left(\partial_\varpi u\, \boldsymbol{e}_\varpi + \partial_z u\, \boldsymbol{e}_z\right) \times \boldsymbol{e}_\varphi = -\partial_z u\, \boldsymbol{e}_\varpi + \partial_\varpi u\, \boldsymbol{e}_z. \tag{B.10}$$

Comparison of relations (B.8) and (B.10) finally shows that the axisymmetric magnetic field can be expressed by the stream function, the azimuthal magnetic field component and the azimuthal unit vector:

$$\boldsymbol{B} = \frac{1}{\varpi}\, \nabla u \times \boldsymbol{e}_\varphi + B_\varphi\, \boldsymbol{e}_\varphi. \tag{B.11}$$

B.3. Euler and Lagrange differentials

The connection between Lagrangian and Eulerian differentials in floating fluids will be derived in analogy to material and partial derivatives shown in section B.1 (Mestel, 1999).

The Euler differential δQ describes the change of a quantity $Q(\boldsymbol{r}_0)$ at a fixed position, see equation (2.46a):

$$\delta Q = Q^{\mathrm{E}}(\boldsymbol{r}_0, t) - Q_0(\boldsymbol{r}_0)\big|_t\,. \tag{B.12}$$

The Lagrange differential ΔQ describes the change in Q within a fixed fluid element, that is displaced from $\boldsymbol{r}_0$ to $\boldsymbol{r} = \boldsymbol{r}_0 + \boldsymbol{\xi}$, see equation (2.46b):

$$\Delta Q = Q^{\mathrm{L}}(\boldsymbol{r}, t) - Q_0(\boldsymbol{r}_0)\big|_t = Q^{\mathrm{L}}(\boldsymbol{r}_0 + \boldsymbol{\xi}, t) - Q_0(\boldsymbol{r}_0)\big|_t\,. \tag{B.13}$$

The connection between both definitions can be derived as follows.

The total differential dQ of a quantity $Q(\boldsymbol{r}) = Q(r_1(t), r_2(t), r_3(t), t)$ is generally calculated by applying the chain rule:

$$\mathrm{d}Q = \partial_1 Q\,\mathrm{d}r_1 + \partial_2 Q\,\mathrm{d}r_2 + \partial_3 Q\,\mathrm{d}r_3 + \delta Q. \tag{B.14}$$

In fluid dynamics, any system quantity Q depends on position variables r_i that are varied as well, by the displacement field $\boldsymbol{\xi} = \Delta\boldsymbol{r}$ acting on the fluid. The displacement field describes the change in the position vector for a fixed fluid element. It is therefore described by the Lagrange differential.

In this special case of fluid dynamics, the total differential becomes

$$\mathrm{d}Q = \partial_1 Q\,\xi_1 + \partial_2 Q\,\xi_2 + \partial_3 Q\,\xi_3 + \delta Q = \delta Q + (\boldsymbol{\xi}\cdot\nabla)\,Q \equiv \Delta Q. \tag{B.15}$$

It is called the Lagrange differential.

If $\boldsymbol{Q} = (Q_1, Q_2, Q_3)$ is a vector quantity, the relation equally holds for its components:

$$\Delta\boldsymbol{Q} = \delta\boldsymbol{Q} + (\boldsymbol{\xi}\cdot\nabla)\,\boldsymbol{Q} = \begin{pmatrix} \delta Q_1 \\ \delta Q_2 \\ \delta Q_3 \end{pmatrix} + \begin{pmatrix} (\xi_1\partial_1 + \xi_2\partial_2 + \xi_3\partial_3)\,Q_1 \\ (\xi_1\partial_1 + \xi_2\partial_2 + \xi_3\partial_3)\,Q_2 \\ (\xi_1\partial_1 + \xi_2\partial_2 + \xi_3\partial_3)\,Q_3 \end{pmatrix}. \tag{B.16}$$

Note that the displacement causing δQ and ΔQ is an instantaneous process as opposed to the actual fluid movement causing the partial and material time derivatives discussed in section B.1.

B.4. Surface integral contributions to the energy variation

Bernstein et al. (1958) showed how the energy variation for a magnetised neutron star can be split into surface integral terms δW_{surf} over the stellar surface, volume integral terms δW_{vac} over the exterior of the star and the actual volume integral δW_{star} over the stellar volume.

This finding is briefly outlined here for the purpose of proving that the only contribution that needs to be considered in this work is δW_{star}.

The total energy variation of a polytropic star in Cowling approximation, including volume integrations as well as surface integrals, is given by equations (2.78), (2.107), (2.113) and (2.115):

$$\begin{aligned} \delta W = \frac{1}{4}\iiint \Re\Bigg\{ & \frac{\delta\boldsymbol{B}^*\cdot\delta\boldsymbol{B}}{4\pi} - \boldsymbol{j}_0\cdot\frac{\delta\boldsymbol{B}\times\boldsymbol{\xi}^*}{c} + \Gamma_0 p_0\,(\nabla\cdot\boldsymbol{\xi}^*)\,(\nabla\cdot\boldsymbol{\xi}) \\ & + \boldsymbol{\xi}\cdot\nabla p_0\,(\nabla\cdot\boldsymbol{\xi}^*) \pm \boldsymbol{\xi}\cdot\nabla\Phi_0\,(\nabla\cdot(\rho_0\,\boldsymbol{\xi}^*))\Bigg\}\,\mathrm{d}V \\ - \frac{1}{4}\oiint \Re\Bigg\{ & \Gamma_0 p_0\,\boldsymbol{\xi}^*\,(\nabla\cdot\boldsymbol{\xi}) + \boldsymbol{\xi}^*\,(\boldsymbol{\xi}\cdot\nabla)\,p_0 + \frac{1}{4\pi}\underbrace{(\boldsymbol{\xi}^*\times\boldsymbol{B}_0)\times\delta\boldsymbol{B}}_{(\boldsymbol{\xi}^*\cdot\delta\boldsymbol{B})\boldsymbol{B}_0 - (\boldsymbol{B}_0\cdot\delta\boldsymbol{B})\boldsymbol{\xi}^*}\Bigg\}\,\boldsymbol{n}\,\mathrm{d}\boldsymbol{S}. \end{aligned} \tag{B.17}$$

The surface normal $\boldsymbol{n}$ points inwards. The cross product can be expressed by identity (A.5). Then,

$$\delta W = \delta W_{\mathrm{star}} - \frac{1}{4} \oiint \Re \left\{ \Gamma_0 \, p_0 \, (\nabla \cdot \boldsymbol{\xi}) + (\boldsymbol{\xi} \cdot \nabla) \, p_0 - \frac{\boldsymbol{B}_0 \cdot \delta \boldsymbol{B}}{4 \, \pi} \right\} \boldsymbol{\xi}^* \cdot \boldsymbol{n} \, \mathrm{d}\boldsymbol{S}, \tag{B.18}$$

if we take into account that the equilibrium magnetic field $\boldsymbol{B}_0$ penetrating the stellar surface is purely perpendicular to to the surface, i.e. $\boldsymbol{B}_0 \cdot \boldsymbol{n} = 0$. The magnetic field component parallel to the surface must vanish at the stellar surface, since the exterior neutron star magnetic field is purely poloidal in vacuum. This has been discussed in section 2.2.3.

The surface integral in (B.18) can be further transformed as shown by Bernstein et al. (1958), so that finally

$$\delta W = \delta W_{\mathrm{star}} + \delta W_{\mathrm{surf}} + \delta W_{\mathrm{vac}}, \tag{B.19}$$

with

$$\delta W_{\mathrm{surf}} = -\frac{1}{4} \oiint \Re \left\{ (\boldsymbol{n} \cdot \boldsymbol{\xi}^*)^2 \, \boldsymbol{n} \cdot \nabla \left(p_0 + \frac{1}{8 \, \pi} \left| \boldsymbol{B}_0 \right|^2 \right) + (\boldsymbol{n} \cdot \boldsymbol{\xi}^*)^2 \, \hat{\boldsymbol{n}} \cdot \nabla \left(\frac{1}{8 \, \pi} \left| \boldsymbol{B}_0 \right|^2 \right) \right\} \mathrm{d}S \tag{B.20a}$$

$$\delta W_{\mathrm{vac}} = -\frac{1}{16 \, \pi} \oiint \Re \left\{ (\hat{\boldsymbol{n}} \cdot \boldsymbol{\xi}^*) \, \hat{\boldsymbol{B}}_0 \cdot \nabla \times \boldsymbol{A} \right\} \mathrm{d}S. \tag{B.20b}$$

Here, $\hat{Q}$ labels a vacuum quantity outside the star. In particular, the surface normal pointing outwards is $\hat{\boldsymbol{n}} = -\boldsymbol{n}$. Furthermore, $\boldsymbol{A}$ denotes the vacuum vector potential, fulfilling the Maxwell equations $\hat{\boldsymbol{E}} = -\partial_t \boldsymbol{A}/c + \hat{\boldsymbol{E}}_0$ and $\hat{\boldsymbol{B}} = \nabla \times \boldsymbol{A} + \hat{\boldsymbol{B}}_0$ for the exterior.

Note that δW_{vac} given by (B.20b) can also be expressed by a volume integral over the stellar exterior. However, we will keep the surface integral form for drawing the conclusions.

Equation (B.19) with (B.20) implies that surface and vacuum contributions to δW vanish if either the displacement field itself vanishes at the stellar surface, or if it is purely parallel to the stellar surface:

$$\delta W = \delta W_{\mathrm{star}} \qquad \text{if} \qquad (\boldsymbol{\xi})_{\mathrm{surf}} = 0 \qquad \vee \qquad (\boldsymbol{n} \cdot \boldsymbol{\xi})_{\mathrm{surf}} = 0. \tag{B.21}$$

That means, surface contributions to δW are negligible in this work if condition (B.21) is fulfilled for the explicit form constructed for $\boldsymbol{\xi}$.

In particular, this can be achieved by localising the displacement field into a closed region A inside the star. All terms in the energy variation integral are proportional to the displacement field. Therefore, A is the only region inside the star that contributes to the integrand.

Stellar surface integrals can be replaced by surface integrals over the surface of A:

$$\oiint_{\partial V} \mathcal{E} \, \mathrm{d}S = \oiint_{\partial A} \mathcal{E} \, \mathrm{d}S. \tag{B.22}$$

Consequently, the condition for the construction of a localised displacement field is

$$\delta W = \delta W_{\text{star}} \qquad \text{if} \qquad (\boldsymbol{\xi})_{\partial A} = 0 \qquad \vee \qquad (\boldsymbol{n}\cdot\boldsymbol{\xi})_{\partial A} = 0. \tag{B.23}$$

In the case of stratified stars, the discussion given in this section holds as well. According to equation (4.6), the structure of the energy variation density (B.17) remains unchanged when the polytropic star is replaced by the stratified one. Only the polytropic index Γ_0 is replaced by Γ_1.

B.5. Dropping the Cowling-approximation

B.5.1. $\delta\Phi$ explicitly for $\boldsymbol{\xi}$ expressed by spherical harmonics

Chandrasekhar & Lebovitz (1964) derived an expression for the Euler perturbation of the gravitational potential in an axisymmetric system where the displacement field is expressed by spherical harmonics. This derivation will be outlined here in order to draw the analogy to the derivation made in section 4.2.3, where the displacement field was chosen according to the mixed field case (2.130).

According to equation (2.91), the Euler perturbation of the gravitational potential is formally given by

$$\delta\Phi = \pm G \iiint \rho_0(\boldsymbol{r}')\,\boldsymbol{\xi}(\boldsymbol{r}')\cdot\nabla_{\boldsymbol{r}'}\left(\frac{1}{|\boldsymbol{r}-\boldsymbol{r}'|}\right) r'^2 \sin\vartheta'\,\mathrm{d}r'\,\mathrm{d}\vartheta'\,\mathrm{d}\varphi' + \mathcal{O}(\boldsymbol{\xi}^2), \tag{B.24}$$

where spherical coordinates (2.4) have been chosen in order to allow for a straightforward analogy to the mixed field choice for $\boldsymbol{\xi}$. Nevertheless, the system is assumed to be axisymmetric rather than spherically symmetric. The integral extends over the total stellar volume.

The absolute value in (B.24) can be expanded in terms of spherical harmonics $Y_\lambda^\mu(\vartheta',\varphi')$, defined in equation (2.137):

$$\frac{1}{|\boldsymbol{r}-\boldsymbol{r}'|} = \sum_{\lambda=0}^{\infty} \frac{4\pi}{2\lambda+1}\, f_\lambda(r,r') \sum_{\mu=-\lambda}^{\lambda} Y_\lambda^\mu(\vartheta,\varphi)\, Y_\lambda^\mu(\vartheta',\varphi'), \tag{B.25}$$

with the radius-dependent component

$$f_\lambda(r,r') = \begin{cases} \frac{r'^\lambda}{r^{\lambda+1}} & \text{if } r' \le r \\ \frac{r^\lambda}{r'^{\lambda+1}} & \text{if } r' \ge r. \end{cases} \tag{B.26}$$

Alternatively, (B.26) can be written as

$$f_\lambda(r,r') = \frac{r_<^\lambda}{r_>^{\lambda+1}} \qquad \text{with} \qquad r_< \equiv \min(r,r') \qquad r_> \equiv \max(r,r'). \tag{B.27}$$

Note that our form of the expansion (B.25) slightly differs from the form given in Chandrasekhar & Lebovitz (1964), since we use normalised spherical harmonics as opposed to

Chandrasekhar and Lebovitz.

After the expansion (B.25) is inserted to (B.24), all $\boldsymbol{r}'$-independent quantities as well as the summations can be pulled out of the integral, making use of the gradient's linearity and the distributive property:

$$\delta\Phi(\boldsymbol{r}) = \pm \sum_{\lambda=0}^{\infty} \sum_{\mu=-\lambda}^{\lambda} \frac{4\,\pi\,G}{2\,\lambda+1}\, Y_\lambda^\mu(\vartheta,\varphi) \iiint \left\{ \rho_0(r')\, \boldsymbol{\xi}^*(\boldsymbol{r}') \cdot \nabla_{\boldsymbol{r}'} \left[f_\lambda(r,r')\, Y_\lambda^\mu(\vartheta',\varphi') \right] \right\} r'^2 \sin\vartheta'\, \mathrm{d}r'\, \mathrm{d}\vartheta'\, \mathrm{d}\varphi' + \mathcal{O}(\boldsymbol{\xi}^2). \tag{B.28}$$

Here, we took into account that $\boldsymbol{\xi}(\boldsymbol{r}')$ and $Y_\lambda^\mu(\vartheta',\varphi')$ are actual complex functions. As shown in the appendix section A.5.4, their product is solely real and thus maintains the physical meaningfulness of $\delta\Phi$. According to the particular form of their complex parts, $\boldsymbol{\xi}^* \sim \mathrm{e}^{-im\varphi}$ and $Y_\lambda^\mu(\vartheta',\varphi') \sim \mathrm{e}^{\mathrm{i}\mu\varphi}$, the result of the integral in (B.28) would be identical if only the real part of the integrand would be considered. In contrast to the integrand of δW, where the real part was taken over the total integrand, no additional factor appears here. The detailed explanation of this circumstance can be found in the appendix section A.5.4.

Further, the spherical symmetry of the background quantities has been applied in (B.28) by assuming $\rho_0(\boldsymbol{r}') = \rho_0(r')$.

Next, the displacement field is expressed by spherical harmonics according to (2.136). Then, the angular integration can be carried out. For radial functions $F(r)$, Chandrasekhar (1961) gives a relation which follows from the orthogonality properties (A.52) of the spherical harmonics' derivatives:

$$\iint \boldsymbol{\xi}_{lm}^*(\boldsymbol{r}') \cdot \nabla_{\boldsymbol{r}'} \left[F(r')\, Y_\lambda^\mu(\vartheta',\varphi') \right] \mathrm{d}S' = \left[g(r')\, \mathrm{d}_{r'} F(r') + F(r')\, \mathrm{d}_{r'} h(r') \right] \frac{\delta_{l\lambda}\, \delta_{m\mu}}{r'^2}. \tag{B.29}$$

The derivation of (B.29) is shown in the appendix section B.5.3.

In contrast to Chandrasekhar (1961), we used normalised spherical harmonics as defined in (2.137) with the normalisation constant (2.138). The prefactor in (B.29) thus differs from the form given by Chandrasekhar.

The angular surface element dS' can be expressed in spherical coordinates as $dS' = \sin\vartheta'\, \mathrm{d}\vartheta'\, \mathrm{d}\varphi'$, for instance. The integral extends over the total angle, i.e. $\vartheta = [0,\pi]$ and $\varphi = [0,2\,\pi]$.

Note that λ and μ are the mode indices characterising the spherical harmonics appearing inside the gradient in (B.29), whereas l and m denote the mode indices of the spherical harmonics representing $\boldsymbol{\xi}_{lm}$ according to (2.136).

Applying relation (B.29) on (B.28), the Euler perturbation becomes

$$\delta\Phi(\boldsymbol{r}) = \pm \sum_{\lambda=0}^{\infty} \sum_{\mu=-\lambda}^{\lambda} \frac{4\,\pi\,G}{2\,\lambda+1}\, Y_\lambda^\mu(\vartheta,\varphi)\,\delta_{l\lambda}\,\delta_{m\mu} \tag{B.30}$$

$$\int_0^R \rho_0(r')\left[g(r')\,\mathrm{d}_{r'} f_\lambda(r,r') + f_\lambda(r,r')\,\mathrm{d}_{r'} h(r')\right]\mathrm{d}r' + \mathcal{O}(\boldsymbol{\xi}^2)$$

$$= \pm \frac{4\,\pi\,G}{2\,l+1}\, Y_l^m(\vartheta,\varphi) \tag{B.31}$$

$$\int_0^R \rho_0(r')\left[g(r')\,\mathrm{d}_{r'} f_l(r,r') + f_l(r,r')\,\mathrm{d}_{r'} h(r')\right]\mathrm{d}r' + \mathcal{O}(\boldsymbol{\xi}^2),$$

where the Kronecker-deltas have been evaluated.

The derivative of $f_l(r,r')$, defined by (B.26) can be evaluated by splitting the radial integral into two integration areas with $r' \le r$ and $r' \ge r$:

$$\delta\Phi(\boldsymbol{r}) = \pm \frac{4\,\pi\,G}{2\,l+1}\, Y_l^m(\vartheta,\varphi)\left\{\int_0^r \rho_0(r')\left[g(r')\,l\,\frac{r'^{l-1}}{r^{l+1}} + \frac{r'^{l}}{r^{l+1}}\,\mathrm{d}_{r'} h(r')\right]\mathrm{d}r'\right. \tag{B.32}$$

$$\left. + \int_r^R \rho_0(r')\left[-g(r')\,(l+1)\,\frac{r^l}{r'^{l+2}} + \frac{r^l}{r'^{l+1}}\,\mathrm{d}_{r'} h(r')\right]\mathrm{d}r'\right\} + \mathcal{O}(\boldsymbol{\xi}^2)$$

$$= \pm \frac{4\,\pi\,G}{2\,l+1}\, Y_l^m(\vartheta,\varphi)\left\{\frac{1}{r^{l+1}}\int_0^r \rho_0(r')\,r'^{l}\left[l\,\frac{g(r')}{r'} + \mathrm{d}_{r'} h(r')\right]\mathrm{d}r'\right. \tag{B.33}$$

$$\left. - r^l \int_r^R \frac{\rho_0(r')}{r'^{l+1}}\left[(l+1)\,\frac{g(r')}{r'} - \mathrm{d}_{r'} h(r')\right]\mathrm{d}r'\right\} + \mathcal{O}(\boldsymbol{\xi}^2).$$

Finally, the Euler perturbation of the gravitational potential can be written as

$$\delta\Phi(\boldsymbol{r}) = \delta\Phi(r)\, Y_l^m(\vartheta,\varphi) + \mathcal{O}(\boldsymbol{\xi}^2), \tag{B.34}$$

where the angular part is expressed by spherical harmonics. The radial part is given by

$$\delta\Phi(r) = \pm\frac{4\,\pi\,G}{2\,l+1}\left[\frac{J_l(r)}{r^{l+1}} - r^l\,K_l(r)\right], \tag{B.35}$$

where we defined the radial functions

$$J_l(r) = \int_0^r \rho_0(r')\,r'^{l}\left[l\,\frac{g(r')}{r'} + \mathrm{d}_{r'} h(r')\right]\mathrm{d}r' \tag{B.36a}$$

$$K_l(r) = \int_r^R \frac{\rho_0(r')}{r'^{l+1}}\left[(l+1)\,\frac{g(r')}{r'} - \mathrm{d}_{r'} h(r')\right]\mathrm{d}r'. \tag{B.36b}$$

The expression for $\delta\Phi$ in (B.34) represents the form derived by Chandrasekhar & Lebovitz (1964), given in (4.11) with (4.12) and (4.13).

B.5.2. δW^{nC} explicitly for $\boldsymbol{\xi}$ expressed by spherical harmonics

In this section, the additional gravitational energy variation caused by the full non-Cowling treatment is derived, in the case where the displacement field is expressed by spherical harmonics.

This can be achieved by using the expression for the gravitational potential set up in the previous section. We follow the procedure outlined in Chandrasekhar & Lebovitz (1964).

According to (4.9) and (2.78), the additional term in the energy variation when dropping the Cowling approximation is

$$\delta W_{\text{grav}}^{\text{nC}} = \mp\frac{1}{4}\iiint \rho_0(r)\,\Re\left\{\boldsymbol{\xi}^*\cdot\nabla\delta\Phi(\boldsymbol{r})\right\}\,\mathrm{d}V. \tag{B.37}$$

If the volume element is expressed in spherical coordinates and the expression given for $\delta\Phi(\boldsymbol{r})$ by equations (4.11) and (4.12) is inserted, (B.37) becomes

$$\delta W_{\text{grav}}^{\text{nC}} = -\frac{\pi G}{2l+1}\iiint \rho_0(r)\,\Re\left\{\boldsymbol{\xi}^*_{l'm'}\cdot\nabla\left[\left(\frac{J_l(r)}{r^{l+1}}-r^l K_l(r)\right)Y_l^m(\vartheta,\varphi)\right]\right\} r^2\sin\vartheta\,\mathrm{d}r\,\mathrm{d}\vartheta\,\mathrm{d}\varphi. \tag{B.38}$$

We kept the first order terms in $\delta\Phi(\boldsymbol{r})$, ensuring that $\delta W_{\text{grav}}^{\text{nC}}$ is of second order in $\boldsymbol{\xi}$ as demanded. Here, we denote the mode indices of the spherical harmonics expressing $\boldsymbol{\xi}_{l'm'}$ by m' and l', keeping in mind that they can generally differ from the mode indices m and l of the spherical harmonics describing $\delta\Phi$.

Remember that we take into account that $\boldsymbol{\xi}$ and $\delta\Phi(\boldsymbol{r})$ are both generally complex functions, expressed by spherical harmonics. The real part of the product insures that the integral is real and physically reasonable, see appendix section A.5.4.

The integral extends over the total stellar volume.

Next, relation (B.29), used in the previous paragraph, can be applied to carry out the angular integration over the scalar product of $\boldsymbol{\xi}^*_{l'm'}$ with the gradient of the product of a radial function $F(r) = \left(\frac{J_l(r)}{r^{l+1}}-r^l K_l(r)\right)$ and a spherical harmonic. In this step, the displacement field is expressed by spherical harmonics as well, according to choice (2.136).

Relation (B.29) finally reveals that non-vanishing contributions only appear for $m = m'$ and $l = l'$:

$$\delta W_{\text{grav}}^{\text{nC}} = -\frac{2\pi G}{2l+1}\int_0^R \rho_0(r)\left\{g(r)\,\mathrm{d}_r\left(\frac{J_l(r)}{r^{l+1}}-r^l K_l(r)\right)+\mathrm{d}_r h(r)\left(\frac{J_l(r)}{r^{l+1}}-r^l K_l(r)\right)\right\}\,\mathrm{d}r. \tag{B.39}$$

The radial derivative of $F(r)$ is given by

$$\mathrm{d}_r\left(\frac{J_l(r)}{r^{l+1}}-r^l\,K_l(r)\right) = -\frac{l+1}{r^{l+2}}\,J_l(r)-l\,r^{l-1}\,K_l(r)+(2l+1)\,\frac{\rho_0(r)\,g(r)}{r^2}, \tag{B.40}$$

according to Chandrasekhar & Lebovitz (1964). A proof for this relation is given in section

B.5.4.

Inserting (B.40) and sorting the terms by the appearance of $J_l(r)$ and $K_l(r)$, (B.39) becomes

$$\delta W_{\text{grav}}^{\text{nC}} = -2\pi G \int_0^R \frac{\rho_0^2(r)\, g^2(r)}{r^2}\,\mathrm{d}r - \frac{2\pi G}{2l+1}\cdot \tag{B.41}$$
$$\int_0^R \rho_0(r) \left\{ -\left(\frac{l+1}{r^{l+2}}\, g(r) - \frac{\mathrm{d}_r h(r)}{r^{l+1}} \right) J_l(r) - \left(l\, r^{l-1} g(r) + r^l\, \mathrm{d}_r h(r) \right) K_l(r) \right\} \mathrm{d}r.$$

The derivatives of $J_l(r)$ and $K_l(r)$, following from their definition in (4.13), are given by

$$\mathrm{d}_r J_l(r) = \rho_0(r)\, r^l \left[\frac{l\, g(r)}{r} + \mathrm{d}_r h(r) \right] \tag{B.42a}$$

$$\mathrm{d}_r K_l(r) = -\frac{\rho_0(r)}{r^{l+1}} \left[(l+1)\, \frac{g(r)}{r} - \mathrm{d}_r h(r) \right], \tag{B.42b}$$

as calculated in the appendix section B.5.5. Note that $d_r K_l(r)$ equals the negative integrand in the definition of $K_l(r)$, due to its integration boundaries.

Identifying (B.42) in (B.41), the additional energy variation term can be expressed as

$$\delta W_{\text{grav}}^{\text{nC}} = -2\pi G \int_0^R \frac{\rho_0^2(r)\, g^2(r)}{r^2}\,\mathrm{d}r - \frac{2\pi G}{2l+1} \int_0^R \left\{ J_l(r)\, \mathrm{d}_r K_l(r) - K_l(r)\, \mathrm{d}_r J_l(r) \right\} \mathrm{d}r. \tag{B.43}$$

Chandrasekhar & Lebovitz (1964) further simplify the second integral by applying

$$\int_0^R \left\{ J_l(r')\, \mathrm{d}_{r'} K_l(r') - K_l(r')\, \mathrm{d}_{r'} J_l(r') \right\} \mathrm{d}r' = -2 \int_0^R \mathrm{d}_{r'} J_l(r')\, K_l(r')\, \mathrm{d}r'. \tag{B.44}$$

The derivation of relation (B.44) is outlined in the appendix section B.5.6.

Applying (B.44) to (B.43), the non-Cowling energy variation term can be written in the alternate form

$$\delta W_{\text{grav}}^{\text{nC}} = -2\pi G \int_0^R \frac{\rho_0^2(r)\, g^2(r)}{r^2}\,\mathrm{d}r + \frac{4\pi G}{2l+1} \int_0^R \mathrm{d}_r J_l(r)\, K_l(r)\, \mathrm{d}r. \tag{B.45}$$

Both forms, (B.43) and (B.45) represent the expressions given in equation (4.14).

B.5.3. Relation for the angular integration for displacement fields expressed by spherical harmonics

In the course of dropping the Cowling approximation, an expression for the angular part of the required integration comes in useful.

For displacement fields expressed by spherical harmonics, it can be derived from their

orthogonality properties. While the relation given by Chandrasekhar (1961) holds for unnormalised spherical harmonics, the derivation shown is this section applies for normalised spherical harmonics.

Both expressions, $\delta\Phi$ and $\delta W_{\mathrm{grav}}^{\mathrm{nC}}$, involve the real part of a scalar product, containing the displacement field and a gradient of the product of a radial function $F(r)$ with a spherical harmonic.

Working in spherical coordinates (2.4) with the gradient given by equation (A.11), the angular integral of this expression is

$$\iint \left\{ \boldsymbol{\xi}^*_{l'm'} \cdot \nabla \left[F(r)\, Y_l^m(\vartheta,\varphi) \right] \right\} \mathrm{d}S \tag{B.46}$$

$$= \iint \left\{ \xi_r^* \, \mathrm{d}_r F(r)\, Y_l^m(\vartheta,\varphi) + \xi_\vartheta^* \frac{F(r)}{r} \, \partial_\vartheta Y_l^m(\vartheta,\varphi) + \xi_\varphi^* \frac{F(r)}{r \sin\vartheta} \, \partial_\varphi Y_l^m(\vartheta,\varphi) \right\} \mathrm{d}S \tag{B.47}$$

$$= \iint \left\{ \frac{g(r)\, \mathrm{d}_r F(r)}{r^2} \, Y_{l'}^{m'\,*}(\vartheta,\varphi)\, Y_l^m(\vartheta,\varphi) + \frac{\mathrm{d}_r h(r)\, F(r)}{l(l+1)\, r^2} \, \partial_\vartheta Y_{l'}^{m'\,*}(\vartheta,\varphi)\, \partial_\vartheta Y_l^m(\vartheta,\varphi) \right. \tag{B.48}$$

$$\left. + \frac{\mathrm{d}_r h(r)\, F(r)}{l(l+1)\, r^2 \sin^2\vartheta} \, \partial_\varphi Y_{l'}^{m'\,*}(\vartheta,\varphi)\, \partial_\varphi Y_l^m(\vartheta,\varphi) \right\} \mathrm{d}S,$$

where assumption (2.136) has been applied for the displacement field. The mode indices of $\boldsymbol{\xi}_{l'm'}$ are named l' and m', as they generally differ from the mode indices l and m of $Y_l^m(\vartheta,\varphi)$ appearing in the integral (B.46).

Note that the azimuthal integral automatically provides a real number despite the complex scalar product involving $\boldsymbol{\xi}^*$ and Y_l^m. The reason is the particular form of the imaginary part for both functions. This will be seen below when the integral is traced back to the spherical harmonics orthogonality relations. Also compare appendix section A.5.4.

The integral (B.46) comprises the total angular area element. It can be evaluated for instance in spherical coordinates as $\mathrm{d}S = \sin\vartheta \, \mathrm{d}\vartheta \, \mathrm{d}\varphi$, with the integration boundaries $\vartheta = [0, \pi]$ and $\varphi = [0, 2\,\pi]$.

Next, the integrand can be split into two parts: one part containing the spherical harmonics and the other part containing their derivatives. All radial functions are real and can be factored out of the integrals:

$$\iint \left\{ \boldsymbol{\xi}^*_{l'm'} \cdot \nabla \left[F(r)\, Y_l^m(\vartheta,\varphi) \right] \right\} \mathrm{d}S \tag{B.49}$$

$$= \frac{g(r)\, \mathrm{d}_r F(r)}{r^2} \iint \left\{ Y_{l'}^{m'\,*}(\vartheta,\varphi)\, Y_l^m(\vartheta,\varphi) \right\} \mathrm{d}S + \frac{\mathrm{d}_r h(r)\, F(r)}{l(l+1)\, r^2} \cdot \tag{B.50}$$

$$\iint \frac{1}{\sin^2\vartheta} \left\{ \sin^2\vartheta \, \partial_\vartheta Y_{l'}^{m'\,*}(\vartheta,\varphi)\, \partial_\vartheta Y_l^m(\vartheta,\varphi) + \partial_\varphi Y_{l'}^{m'\,*}(\vartheta,\varphi)\, \partial_\varphi Y_l^m(\vartheta,\varphi) \right\} \mathrm{d}S.$$

Then, the orthogonality relations for normalised spherical harmonics (A.51) and their derivatives (A.52) are applied to yield the end result

$$\iint \left\{ \boldsymbol{\xi}^*_{l'm'} \cdot \nabla \left[F(r)\, Y_l^m(\vartheta,\varphi) \right] \right\} \mathrm{d}S = \left[g(r)\, \mathrm{d}_r F(r) + F(r)\, \mathrm{d}_r h(r) \right] \frac{\delta_{l'l}\, \delta_{m'm}}{r^2}. \tag{B.51}$$

B.5.4. Derivative of $F(r)$ describing the gravitational potential

In this section, the derivative of the radial function $F(r)$ containing $J(r)$ and $K(r)$ will be calculated, proving expressions (B.40) and (4.37).

We use a universal notation applicable for both choices we make for the displacement field, which are $\boldsymbol{\xi}$ expressed by spherical harmonics and $\boldsymbol{\xi}$ in the mixed field case.

First, the chain rule is applied to $d_r F(r) = \left[\frac{J(r)}{r^{l+1}} - r^l\, K(r)\right]$:

$$\mathrm{d}_r\left[\frac{J(r)}{r^{l+1}} - r^l\, K(r)\right] = -\frac{l+1}{r^{l+2}}\, J(r) - l\, r^{l-1}\, K(r) + \frac{d_r J(r)}{r^{l+1}} - r^l\, \mathrm{d}_r K(r). \tag{B.52}$$

Next, the derivatives of $J(r)$ and $K(r)$ are inserted according to (B.42) and (4.40), respectively.

In the case where the displacement field is expressed by spherical harmonics, with $J(r) = J_l(r)$ and $K(r) = K_l(r)$, the derivative is

$$\mathrm{d}_r\left[\frac{J_l(r)}{r^{l+1}} - r^l\, K_l(r)\right] = -\frac{l+1}{r^{l+2}}\, J_l(r) - l\, r^{l-1}\, K_l(r) + \frac{d_r J_l(r)}{r^{l+1}} - r^l\, \mathrm{d}_r K_l(r) \tag{B.53}$$

$$= -\frac{l+1}{r^{l+2}}\, J_l(r) - l\, r^{l-1}\, K_l(r) + \frac{\rho_0(r)\, r^l}{r^{l+1}}\left[\frac{l\, g(r)}{r} + \mathrm{d}_r h(r)\right] \tag{B.54}$$

$$+ \frac{\rho_0(r)\, r^l}{r^{l+1}}\left[\frac{(l+1)\, g(r)}{r} - \mathrm{d}_r h(r)\right]$$

$$= -\frac{l+1}{r^{l+2}}\, J_l(r) - l\, r^{l-1}\, K_l(r) + (2\,l+1)\, \frac{\rho_0(r)\, g(r)}{r^2}, \tag{B.55}$$

where arithmetic transformation finally led to the form given in (B.40).

In the mixed field case, with $J(r) = J_\lambda^m(r)$, $K(r) = K_\lambda^m(r)$ and $l = \lambda$, the derivative is

$$\mathrm{d}_r\left[\frac{J_\lambda^m(r)}{r^{\lambda+1}} - r^\lambda\, K_\lambda^m(r)\right] \tag{B.56}$$

$$= -\frac{\lambda+1}{r^{\lambda+2}}\, J_\lambda^m(r) - \lambda\, r^{\lambda-1}\, K_\lambda^m(r) \tag{B.57}$$

$$+ \int_0^\pi \rho_0(r)\, r\left[\left(\lambda \tilde{R}(r,\vartheta') + \frac{m\,\tilde{T}(r,\vartheta')}{\sin\vartheta'}\right)\Theta_\lambda^m(\vartheta') + \tilde{S}(r,\vartheta')\,\partial_{\vartheta'}\Theta_\lambda^m(\vartheta')\right]\sin^2\vartheta'\,\mathrm{d}\vartheta'$$

$$+ \int_0^\pi \rho_0(r)\, r\left[\left((\lambda+1)\tilde{R}(r,\vartheta') - \frac{m\,\tilde{T}(r,\vartheta')}{\sin\vartheta'}\right)\Theta_\lambda^m(\vartheta') - \tilde{S}(r,\vartheta')\,\partial_{\vartheta'}\Theta_\lambda^m(\vartheta')\right]\sin^2\vartheta'\,\mathrm{d}\vartheta'$$

$$= -\frac{\lambda+1}{r^{\lambda+2}}\, J_\lambda^m(r) - \lambda\, r^{\lambda-1}\, K_\lambda^m(r) + (2\,\lambda+1)\, r\, \rho_0(r) \int_0^\pi \tilde{R}(r,\vartheta')\,\Theta_\lambda^m(\vartheta')\,\sin^2\vartheta'\,\mathrm{d}\vartheta', \tag{B.58}$$

where arithmetic cancellation led to the form given in (4.37).

B.5.5. Derivatives of $J(r)$ and $K(r)$ describing the gravitational potential

In this section, we find expressions for the derivatives $d_r J(r)$ and $d_r K(r)$ of the radial functions

$$J(r) \equiv \int_0^r j(r')\,\mathrm{d}r' \qquad\qquad K(r) \equiv \int_r^R k(r')\,\mathrm{d}r' \tag{B.59}$$

describing $\delta\Phi$.

We use a universal notation applicable to both choices we make for the displacement field.

In the case where $\boldsymbol{\xi}$ is expressed by spherical harmonics, according to equation (4.13), the integrands are

$$j(r') = j_l(r') \equiv \rho_0(r')\, r'^l \left[\frac{l\, g(r')}{r'} + \mathrm{d}_{r'} h(r')\right] \tag{B.60a}$$

$$k(r') = k_l(r') \equiv \frac{\rho_0(r')}{r'^{l+1}} \left[(l+1)\,\frac{g(r')}{r'} - \mathrm{d}_{r'} h(r')\right]. \tag{B.60b}$$

In the mixed field case with choice (2.130) for $\boldsymbol{\xi}$, according to equation (4.29), the integrands are

$$\begin{aligned} j(r') = j_\lambda^m(r') \equiv \int_0^\pi \rho_0(r')\, r'^{\lambda+2} \Bigg[\Bigg(\lambda\,\tilde{R}(r',\vartheta') + \frac{m\,\tilde{T}(r',\vartheta')}{\sin\vartheta'}\Bigg)\Theta_\lambda^m(\vartheta') \\ + \tilde{S}(r',\vartheta')\,\partial_{\vartheta'}\Theta_\lambda^m(\vartheta')\Bigg] \sin^2\vartheta'\,\mathrm{d}r'\,\mathrm{d}\vartheta' \end{aligned} \tag{B.61a}$$

$$\begin{aligned} k(r') = k_\lambda^m(r') \equiv \int_0^\pi \frac{\rho_0(r')}{r'^{\lambda-1}} \Bigg[\Bigg((\lambda+1)\,\tilde{R}(r',\vartheta') - \frac{m\,\tilde{T}(r',\vartheta')}{\sin\vartheta'}\Bigg)\Theta_\lambda^m(\vartheta') \\ - \tilde{S}(r',\vartheta')\,\partial_{\vartheta'}\Theta_\lambda^m(\vartheta')\Bigg] \sin^2\vartheta'\,\mathrm{d}r'\,\mathrm{d}\vartheta'. \end{aligned} \tag{B.61b}$$

The antiderivatives of $j(r')$ and $k(r')$ are denoted as $\mathcal{J}(r')$ and $\mathcal{K}(r')$. Based on equation (B.59), the radial derivatives of $J(r)$ and $K(r)$ are

$$\mathrm{d}_r J(r) = \mathrm{d}_r\left(\int_0^r j(r')\,\mathrm{d}r'\right) = \mathrm{d}_r\left(\Big[\mathcal{J}(r')\Big]_0^r\right) = \mathrm{d}_r\Big(\mathcal{J}(r) - \underbrace{\mathcal{J}(0)}_{0}\Big) = +\mathrm{d}_r\mathcal{J}(r) \tag{B.62a}$$

$$\mathrm{d}_r K(r) = \mathrm{d}_r\left(\int_r^R k(r')\,\mathrm{d}r'\right) = \mathrm{d}_r\left(\Big[\mathcal{K}(r')\Big]_r^R\right) = \mathrm{d}_r\Big(\underbrace{\mathcal{K}(R)}_{0} - \mathcal{K}(r)\Big) = -\mathrm{d}_r\mathcal{K}(r). \tag{B.62b}$$

Here, we took into account that for both choices of $\boldsymbol{\xi}$ the integrand $j(r')$ vanishes at the stellar centre if $l > 1$ and that the integrand $k(r')$ vanishes at the stellar surface due to

$\rho_0(R) = 0$. The integration constants are set to zero without restriction.

We further consider that the derivative $d_r\mathcal{J}(r)$ or $d_r\mathcal{K}(r)$ of an antiderivative $\mathcal{J}(r)$ or $\mathcal{K}(r)$ of the function $j(r)$ or $k(r)$ is the function $j(r)$ or $k(r)$ itself.

Thus,

$$\mathrm{d}_r J(r) = +\mathrm{d}_r\mathcal{J}(r) = +j(r) \tag{B.63a}$$

$$\mathrm{d}_r K(r) = -\mathrm{d}_r\mathcal{K}(r) = -k(r). \tag{B.63b}$$

In the case where $\boldsymbol{\xi}$ is expressed by spherical harmonics, the final result follows from equation (B.63) with (B.60).

The radial derivatives of $J_l(r)$ and $K_l(r)$ are

$$\mathrm{d}_r J_l(r) = +j_l(r) = \rho_0(r)\, r^l \left[\frac{l\, g(r)}{r} + \mathrm{d}_r h(r)\right] \tag{B.64a}$$

$$\mathrm{d}_r K_l(r) = -k_l(r) = -\frac{\rho_0(r)}{r^{l+1}} \left[(l+1)\,\frac{g(r)}{r} - \mathrm{d}_r h(r)\right]. \tag{B.64b}$$

Analogously, in the mixed field case with choice (2.130) for $\boldsymbol{\xi}$, the result follows from equation (B.63) with (B.61).

The radial derivatives of $J_\lambda^m(r)$, $K_\lambda^m(r)$ are

$$\mathrm{d}_r J_\lambda^m(r) = +j_\lambda^m(r) = \int_0^\pi \rho_0(r)\, r^{\lambda+2} \left[\left(\lambda\,\tilde{R}(r,\vartheta') + \frac{m\,\tilde{T}(r,\vartheta')}{\sin\vartheta'}\right)\Theta_\lambda^m(\vartheta') + \tilde{S}(r,\vartheta')\,\partial_{\vartheta'}\Theta_\lambda^m(\vartheta')\right]\sin^2\vartheta'\,\mathrm{d}\vartheta' \tag{B.65a}$$

$$\mathrm{d}_r K_\lambda^m(r) = -k_\lambda^m(r) = -\int_0^\pi \frac{\rho_0(r)}{r^{\lambda-1}} \left[\left((\lambda+1)\,\tilde{R}(r,\vartheta') - \frac{m\,\tilde{T}(r,\vartheta')}{\sin\vartheta'}\right)\Theta_\lambda^m(\vartheta') - \tilde{S}(r,\vartheta')\,\partial_{\vartheta'}\Theta_\lambda^m(\vartheta')\right]\sin^2\vartheta'\,\mathrm{d}\vartheta'. \tag{B.65b}$$

Relations (B.64) and (B.65) are utilised in section B.5.2 and section 4.2.4 to simplify the expression for the non-Cowling contribution in the energy variation.

B.5.6. Integral of $J(r)\,\mathrm{d}_r K(r) - K(r)\,\mathrm{d}_r J(r)$ describing $\delta\Phi(r)$

In this section, the simplifying relation for the integral of $J(r)\,\mathrm{d}_r K(r) - K(r)\,\mathrm{d}_r J(r)$ shown in Chandrasekhar & Lebovitz (1964) will be derived.

We use a universal notation, applicable for both choices of the displacement field we make. If $\boldsymbol{\xi}$ is expressed by spherical harmonics, $J(r) = J_l(r)$ and $K(r) = K_l(r)$ holds. In the mixed field case where $\boldsymbol{\xi}$ is chosen according to equation (2.130), $J(r) = J_\lambda^m(r)$ and $K(r) = K_\lambda^m(r)$ holds.

First, we apply the chain rule to the product of $J(r)$ and $K(r)$:

$$\mathrm{d}_r\Big[J(r)\,K(r)\Big] = \mathrm{d}_r J(r)\,K(r) + J(r)\,\mathrm{d}_r K(r) \tag{B.66}$$

$$J(r)\,\mathrm{d}_r K(r) - K(r)\,\mathrm{d}_r J(r) = \mathrm{d}_r\Big[J(r)\,K(r)\Big] - 2\,\mathrm{d}_r J(r)\,K(r). \tag{B.67}$$

The second step follows by arithmetic rearrangements.

Next, the radial integration can be applied:

$$\int_0^R \Big[J(r)\,\mathrm{d}_r K(r) - K(r)\,\mathrm{d}_r J(r)\Big]\,\mathrm{d}r = \int_0^R \mathrm{d}_r\Big[J(r)\,K(r)\Big]\,\mathrm{d}r - 2\int_0^R \mathrm{d}_r J(r)\,K(r)\,\mathrm{d}r \tag{B.68}$$

$$= \Big[J(r)\,K(r)\Big]_0^R - 2\int_0^R \mathrm{d}_r J(r)\,K(r)\,\mathrm{d}r. \tag{B.69}$$

Here, we considered that the antiderivative of $\mathrm{d}_r\Big[J(r)\,K(r)\Big]$ is the product $\Big[J(r)\,K(r)\Big]$ itself.

According to their definition in (B.60) and (B.61), the integrand $j(r)$ vanishes at $r = 0$ and the integrand $k(r)$ vanishes at $r = R$.

Without restriction, we set the integration constants to zero and obtain

$$\int_0^R \Big[J(r)\,\mathrm{d}_r K(r) - K(r)\,\mathrm{d}_r J(r)\Big]\,\mathrm{d}r = J(R)\underbrace{K(R)}_{0} - \underbrace{J(0)}_{0}K(0) - 2\int_0^R \mathrm{d}_r J(r)K(r)\,\mathrm{d}r \tag{B.70}$$

$$= -2\int_0^R \mathrm{d}_r J(r)\,K(r)\,\mathrm{d}r. \tag{B.71}$$

Relation (B.71) holds for both choices, $\boldsymbol{\xi}$ expressed by spherical harmonics and $\boldsymbol{\xi}$ in the mixed field case. It is applied in sections B.5.2 and 4.2.4 to simplify the expression derived for $\delta W_{\mathrm{grav}}^{\mathrm{nC}}$.

B.5.7. Search for symmetries in $\delta\Phi(\boldsymbol{r})$ in the mixed field case

In section B.5.1, where $\boldsymbol{\xi}$ was expressed by spherical harmonics via (2.136), the expression for the gravitational Euler perturbation $\delta\Phi$ could be simplified by making use of the orthogonality properties of spherical harmonics. Based on relation (B.29), the λ-summation could be removed from $\delta\Phi$.

In the mixed field case where the displacement field (2.130) is chosen according to Akgün et al., we need to examine whether a similar relation can be applied in order to simplify the expression for $\delta\Phi$.

Starting from equation (4.27) with (4.28) and (4.29), an orthogonality relation needs to be found for the ϑ- and φ-dependent quantities that allows us to evaluate the angular

integral and remove the λ-summation in

$$\delta\Phi(\boldsymbol{r}) = \pm \sum_{\lambda=m}^{\infty} \frac{8\pi^2 G}{2\lambda+1} Y_\lambda^m(\vartheta,\varphi)\left[\frac{J_\lambda^m(r)}{r^{\lambda+1}} - r^\lambda K_\lambda^m(r)\right] + \mathcal{O}(\boldsymbol{\xi}^2), \tag{B.72}$$

with

$$J_\lambda^m(r) = \int_0^\pi \int_0^r \rho_0(r')\, r'^{\lambda+2}\left[\left(\lambda\,\tilde{R}(r',\vartheta') + \frac{m\,\tilde{T}(r',\vartheta')}{\sin\vartheta'}\right)\Theta_\lambda^m(\vartheta') + \tilde{S}(r',\vartheta')\,\partial_{\vartheta'}\Theta_\lambda^m(\vartheta')\right]\sin^2\vartheta'\,\mathrm{d}r'\,\mathrm{d}\vartheta' \tag{B.73a}$$

$$K_\lambda^m(r) = \int_0^\pi \int_r^R \frac{\rho_0(r')}{r'^{\lambda-1}}\left[\left((\lambda+1)\,\tilde{R}(r',\vartheta') - \frac{m\,\tilde{T}(r',\vartheta')}{\sin\vartheta'}\right)\Theta_\lambda^m(\vartheta') - \tilde{S}(r',\vartheta')\,\partial_{\vartheta'}\Theta_\lambda^m(\vartheta')\right]\sin^2\vartheta'\,\mathrm{d}r'\,\mathrm{d}\vartheta'. \tag{B.73b}$$

In the case where $\boldsymbol{\xi}$ is expressed by spherical harmonics, the simplifying relation (B.29) is

$$\iint \boldsymbol{\xi}_{lm}^*(\boldsymbol{r}')\cdot\nabla_{\boldsymbol{r}'}\left[F(r')\,Y_\lambda^\mu(\vartheta',\varphi')\right]\mathrm{d}S' = \left[g(r')\,\mathrm{d}_{r'}F(r') + F(r')\,\mathrm{d}_{r'}h(r')\right]\frac{\delta_{l\lambda}\,\delta_{m\mu}}{r'^2}, \tag{B.74}$$

with $\mathrm{d}S' = \sin\vartheta'\,\mathrm{d}\vartheta\,\mathrm{d}\varphi$. The integral extends over the full angle.

Remember that the symmetry in φ' has already been utilised in (B.72) to remove the μ-summation. Also note that the polar part $\Theta_\lambda^m(\vartheta')$ of the spherical harmonics in the searched relation would take the role of $Y_\lambda^\mu(\vartheta',\varphi')$ in relation (B.74).

The goal is to find an orthogonality based relation for (B.72) in analogy to (B.74).

For this purpose, the integrands of (B.73) need to be screened for a possible trigonometric dependence on ϑ' that might lead to a systematic cancellation of terms when the ϑ'-integral is performed in the interval $[0,\pi]$.

Similar to the case where $\boldsymbol{\xi}$ was expressed by spherical harmonics, the associated Legendre polynomials included in $\Theta_\lambda^m(\vartheta') = N_{\lambda m}P_{\lambda m}(\cos\vartheta')$ entail a periodic dependence on ϑ'. However, the displacement field dependence on ϑ' is unknown and needs to be investigated.

The explicit form of $\boldsymbol{\xi}$ is determined by the choices for $\tilde{R}$, $\tilde{S}$ and subsequently $\tilde{T}$ made in (5.46) and (5.47) according to Akgün et al. (2013). The $\boldsymbol{\xi}$-defining functions $\tilde{R}$ and $\tilde{S}$ do not depend on ϑ' in a periodic way, as can be seen from equation (5.46), with the definition of $\tilde{\chi}$ in (5.48):

$$\tilde{R}(r',\vartheta') = \begin{cases} -\frac{\xi_0}{r'}\,\tilde{\sigma}\left(1-\tilde{\chi}^2\right)^{\sigma-1}\,\partial_{\vartheta'}\tilde{\chi}^2, & \text{in A} \\ 0 & \text{else} \end{cases} \tag{B.75}$$

$$\tilde{S}(r',\vartheta') = \begin{cases} \frac{\xi_0}{R}\,\tilde{\sigma}\left(1-\tilde{\chi}^2\right)^{\sigma-1}\,\partial_{x'}\tilde{\chi}^2, & \text{in A} \\ 0 & \text{else,} \end{cases} \tag{B.76}$$

with $x' = \frac{r'}{R}$ and

$$\tilde{\chi}^2(r', \vartheta') = \left(\frac{x' - x_0}{\delta_r}\right)^2 + \left(\frac{\vartheta' - \vartheta_0}{\delta_\vartheta}\right)^2 \qquad \partial_{\vartheta'}\tilde{\chi}^2 = 2\,\frac{\vartheta' - \vartheta_0}{\delta_\vartheta^2} \qquad \partial_{x'}\tilde{\chi}^2 = 2\,\frac{x' - x_0}{\delta_r^2}. \tag{B.77}$$

The remaining $\boldsymbol{\xi}$-defining function $\tilde{T}$ partially depends on ϑ' in a periodic, but non-trivial way, as can be seen from equation (5.47) with the definition of E_1 in (5.55), (5.56) and (5.57):

$$\tilde{T}(\vartheta') \sim \frac{\beta(\vartheta')\,\Lambda(\beta(\vartheta'), \vartheta')}{4\pi\, r \sin\vartheta'} + 2\, r \sin\vartheta'\, \Gamma_1\, p_0\, D_0(\vartheta') + r \sin\vartheta'\, \Lambda(p_0) \pm r \sin\vartheta'\, \rho_0\, \Lambda(\Phi_0), \tag{B.78}$$

with

$$\beta(\vartheta') = B_0\, \eta_{\mathrm{tor}}\, R\left(f(x')\, \sin^2\vartheta' - 1\right)^2 \tag{B.79}$$

$$\Lambda(\beta(\vartheta'), \vartheta') = \tilde{R}(\vartheta')\, \partial_{r'}\beta + \frac{\tilde{S}(\vartheta')\, \partial_{\vartheta'}\beta(\vartheta')}{r'} \tag{B.80}$$

$$D_0(\vartheta') = \frac{3\tilde{R}(\vartheta')}{r'} + \partial_{r'}\tilde{R}(\vartheta') + \frac{2\tilde{S}(\vartheta')}{r'}\cot\vartheta' + \frac{\partial_{\vartheta'}\tilde{S}(\vartheta')}{r'} \tag{B.81}$$

$$\Lambda(p_0), \Lambda(\Phi_0) \sim \tilde{R}(\vartheta'), \tag{B.82}$$

cf. relations (5.51) and (5.52).

That means, according to the systematic trigonometric dependence of Θ_λ^m on ϑ', orthogonality relations might exist. However, in non-trivial cases their application is prohibited by the additional partially trigonometric dependence of $\tilde{T}$ on ϑ'.

The specific choice we make for $\tilde{R}$, $\tilde{S}$ and $\tilde{T}$ in section 5.3 represents a non-trivial case. It will thus not be possible to remove the λ-summation from $\delta\Phi$ as given by (B.72).

Instead, the expression can be written in a compact form. The λ-summation is approximated by neglecting higher order terms $\lambda \geq 3$, as shown in equation (4.30).

B.6. Eigenvalue problems

B.6.1. Magnetised neutron stars as an eigenvalue problem

The perturbed system of a stellar fluid considered in this work and described by the Euler equation of motion (2.16), can be understood as an eigenvalue problem (Unno et al., 1989; Tassoul, 2000).

The Euler equation reads

$$\rho\, \mathrm{D}_t \boldsymbol{v} = \mathrm{RHS}, \tag{B.83}$$

where for instance in the case of a magnetised self-gravitating fluid, the right hand side is given by

$$\mathrm{RHS} = -\nabla p \pm \rho\, \nabla\Phi + \frac{\boldsymbol{j} \times \boldsymbol{B}}{c}. \tag{B.84}$$

According to relation (2.68), the perturbed Euler equation can be written as

$$\rho \, \mathrm{D}_t^2 \boldsymbol{\xi} = \delta\mathrm{RHS}, \tag{B.85}$$

or

$$\mathrm{D}_t^2 \boldsymbol{\xi} = \frac{\delta\mathrm{RHS}(\boldsymbol{\xi})}{\rho(\boldsymbol{\xi})}, \tag{B.86}$$

where for (B.84), the perturbed right hand side is given by

$$\delta\mathrm{RHS} = -\nabla \left(p_0 + \delta p\right) \pm \left(\rho_0 + \delta\rho\right) \nabla \left(\Phi_0 + \delta\Phi\right) + \frac{1}{c} \left[\left(\boldsymbol{j}_0 + \delta\boldsymbol{j}\right) \times \left(\boldsymbol{B}_0 + \delta\boldsymbol{B}\right)\right]. \tag{B.87}$$

Applying ansatz (2.43), it is

$$\boldsymbol{\xi}_n(\boldsymbol{r}, t) = \boldsymbol{\xi}(\boldsymbol{r}) \, \mathrm{e}^{\mathrm{i}\omega_n t} \qquad \mathrm{D}_t \boldsymbol{\xi}_n = \mathrm{i}\omega_n \, \boldsymbol{\xi}_n \qquad \mathrm{D}_t^2 \boldsymbol{\xi}_n = -\omega_n^2 \, \boldsymbol{\xi}_n. \tag{B.88}$$

Inserting this into (B.86), the perturbed Euler equation

$$-\omega_n^2 \, \boldsymbol{\xi}_n = \frac{\delta\mathrm{RHS}(\boldsymbol{\xi}_n)}{\rho(\boldsymbol{\xi}_n)} \tag{B.89}$$

can be written in the form of an eigenvalue problem

$$\mathbf{L} \, \boldsymbol{\xi}_n = \omega_n^2 \, \boldsymbol{\xi}_n, \tag{B.90}$$

with the eigenvalue operator $\mathbf{L}$ and the eigenvalue ω_n^2 for the eigenmode $\boldsymbol{\xi}_n = \boldsymbol{u}_n$. For reasons of clarity, we write the mode index as a subscript in this section. The eigenvalue operator is defined by

$$\mathbf{L} \, \boldsymbol{\xi} = -\frac{\delta\mathrm{RHS}(\boldsymbol{\xi})}{\rho(\boldsymbol{\xi})}. \tag{B.91}$$

B.6.2. Perturbation theory on eigenvalue problems

The eigenvalues λ_n and eigenmodes $\boldsymbol{u}_n$ of an eigenvalue problem

$$\mathbf{L} \, \boldsymbol{u} = \lambda \, \boldsymbol{u} \tag{B.92}$$

can approximately be determined in a perturbative approach (Mathews & Walker, 1969; Seifert, 2007).

It is assumed that the system state can be described as a small deviation from a well-known equilibrium state.

Then, the operator $\mathbf{L}$ is expressible as the sum of the equilibrium operator $\mathbf{L}^{(0)}$ and a small correction $\delta\mathbf{L}$:

$$\mathbf{L} = \mathbf{L}^{(0)} + \delta\mathbf{L}. \tag{B.93}$$

The eigenvalues and eigenmodes can be expressed by the expansions

$$\lambda_n = \lambda_n^{(0)} + \lambda_n^{(1)} + \lambda_n^{(2)} + \mathcal{O}(\delta^3) \tag{B.94a}$$

$$\boldsymbol{u}_n = \boldsymbol{u}_n^{(0)} + \sum_m a_{mn}^{(1)}\, \boldsymbol{u}_m^{(0)} + \sum_m a_{mn}^{(2)}\, \boldsymbol{u}_m^{(0)} + \mathcal{O}(\delta^3), \tag{B.94b}$$

where the superscript denotes the perturbation order and a_{mn} are expansion coefficients. The order of the small perturbation is denoted by δ.

Ansatz (B.94) can now be inserted into the eigenvalue problem (B.92). With the use of the equilibrium eigenvalue equation,

$$\mathbf{L}^{(0)}\, \boldsymbol{u}_n^{(0)} = \lambda_n^{(0)}\, \boldsymbol{u}_n^{(0)}, \tag{B.95}$$

the correction of the eigenvalue in first perturbation order follows as

$$\lambda_n^{(1)} = {\boldsymbol{u}_n^{(0)}}^T\, \delta\mathbf{L}\, \boldsymbol{u}_n^{(0)}, \tag{B.96}$$

where T denotes the transpose of $\boldsymbol{u}_n^{(0)}$. Therefore, the eigenvalue of the perturbed system is given by

$$\lambda_n = \lambda_n^{(0)} + {\boldsymbol{u}_n^{(0)}}^T\, \delta\mathbf{L}\, \boldsymbol{u}_n^{(0)} + \mathcal{O}(\delta^2). \tag{B.97}$$

In the case of an undegenerated eigenvalue $\lambda_n^{(0)}$ of the unperturbed system, the first order correction of the eigenvector $\boldsymbol{u}_n$ can be derived as

$$\boldsymbol{u}_n^{(1)} = \sum_p \frac{{\boldsymbol{u}_p^{(0)}}^T\, \delta\mathbf{L}\, \boldsymbol{u}_n^{(0)}}{\lambda_n^{(0)} - \lambda_p^{(0)}}\, \boldsymbol{u}_p^{(0)}. \tag{B.98}$$

Therefore, the eigenvector of the perturbed system is given by

$$\boldsymbol{u}_n = \boldsymbol{u}_n^{(0)} + \sum_p \frac{{\boldsymbol{u}_p^{(0)}}^T\, \delta\mathbf{L}\, \boldsymbol{u}_n^{(0)}}{\lambda_n^{(0)} - \lambda_p^{(0)}}\, \boldsymbol{u}_p^{(0)} + \mathcal{O}(\delta^2) \qquad \forall \quad p \neq n. \tag{B.99}$$

B.6.3. Mathematical connection of eigenfrequency and energy variation

According to the perturbation theory outlined in the previous section, the eigenfrequency of a stellar fluid can be approximately expressed.

In basis free representation, and according to relation (B.97), the stellar eigenfrequency is given by

$$\omega_n^2 = {\omega_n^{(0)}}^2 + \frac{\langle u_n^{(0)} \,|\, \delta\mathbf{L}(\mathbf{r}) \,|\, u_n^{(0)} \rangle}{\langle u_n^{(0)} \,|\, u_n^{(0)} \rangle} + \mathcal{O}(\delta^2). \tag{B.100}$$

Here, we took into account that the eigenvalue of the star is given by $\lambda_n = \omega_n^2$, as can be seen by comparison of equations (B.92) and (B.90). Further, we apply the Dirac notation.

The stellar eigenfunctions $\boldsymbol{u}$ form a complete orthogonal basis,

$$\langle u_n^{(0)} \,|\, u_m^{(0)} \rangle = N\, \delta_{mn}. \tag{B.101}$$

The eigenvectors are generally not normalised and posses the norm

$$N = \langle u_n^{(0)} \,|\, u_n^{(0)} \rangle = \iiint \boldsymbol{u}_n^{(0)^*}(\boldsymbol{r}) \cdot \boldsymbol{u}_n^{(0)}(\boldsymbol{r}) \rho(\boldsymbol{r}) \,\mathrm{d}^3\boldsymbol{r}. \tag{B.102}$$

The equilibrium stellar eigenvalue problem reads

$$\mathbf{L}^{(0)} \,|u_n^{(0)}\rangle = {\omega_n^{(0)}}^2 \,|u_n^{(0)}\rangle \,, \tag{B.103}$$

where multiplication with $\langle u_n^{(0)}|$ gives

$${\omega_n^{(0)}}^2 = \frac{\langle u_n^{(0)} \,|\, \mathbf{L}^{(0)} \,|\, u_n^{(0)} \rangle}{N}. \tag{B.104}$$

Therefore, the eigenfrequency (B.100) can be expressed as

$$\omega_n^2 = \frac{\langle u_n^{(0)} \,|\, \mathbf{L}^{(0)} \,|\, u_n^{(0)} \rangle}{\langle u_n^{(0)} \,|\, u_n^{(0)} \rangle} + \frac{\langle u_n^{(0)} \,|\, \delta\mathbf{L}(\mathbf{r}) \,|\, u_n^{(0)} \rangle}{\langle u_n^{(0)} \,|\, u_n^{(0)} \rangle} + \mathcal{O}(\delta^2) \tag{B.105}$$

$$= \frac{\langle u_n^{(0)} \,|\, \mathbf{L}^{(0)} + \delta\mathbf{L}(\mathbf{r}) \,|\, u_n^{(0)} \rangle}{\langle u_n^{(0)} \,|\, u_n^{(0)} \rangle} + \mathcal{O}(\delta^2) \tag{B.106}$$

$$= \frac{\langle u_n^{(0)} \,|\, \mathbf{L} \,|\, u_n^{(0)} \rangle}{\langle u_n^{(0)} \,|\, u_n^{(0)} \rangle} + \mathcal{O}(\delta^2). \tag{B.107}$$

Analogously, in mass representation with

$$\langle m \,|\, u \rangle = \boldsymbol{u}(m) \qquad \text{and} \qquad \int |m\rangle \langle m| \,\mathrm{d}m = 1, \tag{B.108}$$

it is

$$\omega_n^2 = \frac{\int \boldsymbol{u}_n^{(0)^*}(m) \cdot \mathbf{L}(m) \,\boldsymbol{u}_n^{(0)}(m) \,\mathrm{d}m}{\int \boldsymbol{u}_n^{(0)^*}(m) \cdot \boldsymbol{u}_n^{(0)}(m) \,\mathrm{d}m} + \mathcal{O}(\delta^2). \tag{B.109}$$

This expression can be transformed into the positional representation applying $\mathrm{d}m = \rho(\boldsymbol{r}) \,\mathrm{d}V$:

$$\omega_n^2 = \frac{\iiint \boldsymbol{u}_n^{(0)^*}(\boldsymbol{r}) \cdot \mathbf{L}(\boldsymbol{r}) \,\boldsymbol{u}_n^{(0)}(\boldsymbol{r}) \,\rho(\boldsymbol{r}) \,\mathrm{d}V}{\iiint \boldsymbol{u}_n^{(0)^*}(\boldsymbol{r}) \cdot \boldsymbol{u}_n^{(0)}(\boldsymbol{r}) \,\rho(\boldsymbol{r}) \,\mathrm{d}V} + \mathcal{O}(\delta^2). \tag{B.110}$$

Remember the definition of $\mathbf{L}$ by equation (B.91). For polytropic stars in Cowling approximation, according to (B.87), it is

$$\mathbf{L}\,\boldsymbol{\xi} = \frac{\nabla\,(p_0 + \delta p) \mp (\rho_0 + \delta\rho)\,\nabla\,(\Phi_0 + \delta\Phi) - 1/c\;(\boldsymbol{j}_0 + \delta\boldsymbol{j}) \times (\boldsymbol{B}_0 + \delta\boldsymbol{B})}{\rho_0 + \delta\rho} + \mathcal{O}(\boldsymbol{\xi}^2) \tag{B.111a}$$

$$= \frac{\nabla\delta p \mp \delta\rho\nabla\Phi_0 \mp \rho_0\nabla\delta\Phi - 1/c\;(\boldsymbol{j}_0 \times \delta\boldsymbol{B}) - 1/c\;(\delta\boldsymbol{j} \times \boldsymbol{B}_0)}{\rho_0 + \delta\rho} + \mathcal{O}(\boldsymbol{\xi}^2). \tag{B.111b}$$

The last step follows with the equilibrium Euler equation (2.28).

On the other hand, the energy variation density for the polytropic star in Cowling approximation, given by equations (2.79), is

$$\mathcal{E} = \frac{1}{4}\,\Re\left\{\boldsymbol{\xi}^* \cdot \nabla\delta p \mp \rho_0\,(\boldsymbol{\xi}^* \cdot \nabla\delta\Phi) \mp \delta\rho\,(\boldsymbol{\xi}^* \cdot \nabla\Phi_0) - \boldsymbol{\xi}^* \cdot \frac{\boldsymbol{j}_0 \times \delta\boldsymbol{B}}{c} - \boldsymbol{\xi}^* \cdot \frac{\delta\boldsymbol{j} \times \boldsymbol{B}_0}{c}\right\}. \quad \text{(B.112)}$$

Comparison of (B.111b) and (B.112) yields

$$\mathcal{E}\left(\boldsymbol{\xi} = \boldsymbol{u}_n^{(0)}\right) = \frac{1}{4}\,\Re\left\{\boldsymbol{u}^* \cdot \mathbf{L}\,\boldsymbol{u}\,\rho\right\} + \mathcal{O}(\boldsymbol{\xi}^2). \quad \text{(B.113)}$$

Expressing equation (B.110) with real parts as well, it is

$$\omega_n^2 = \frac{1/2\;\Re\left\{\iiint \boldsymbol{u}_n^{(0)^*} \cdot \mathbf{L}\,\boldsymbol{u}_n^{(0)}\,\rho\,\mathrm{d}V\right\}}{1/2\;\Re\left\{\iiint \boldsymbol{u}_n^{(0)^*} \cdot \boldsymbol{u}_n^{(0)}\,\rho\,\mathrm{d}V\right\}} + \mathcal{O}(\boldsymbol{\xi}^2). \quad \text{(B.114)}$$

Therefore, with equation (2.78), the eigenfrequency can be expressed in terms of the energy variation for an eigenmode-type displacement field:

$$\omega_n^2 = \frac{4\,\delta W\left(\boldsymbol{\xi} = \boldsymbol{u}_n^{(0)}\right)}{\Re\left\{\iiint \boldsymbol{u}_n^{(0)^*} \cdot \boldsymbol{u}_n^{(0)}\,\rho\,\mathrm{d}V\right\}}. \quad \text{(B.115)}$$

The factor 4 appearing in this expression is caused by the following effects. First, the real part in the denominator has not been evaluated yet, proving the factor 1/2. Secondly, the definition of the energy variation provides a factor 1/2 as well, as shown in the derivation of δW in equation (2.75).

C. Supporting calculations for the applications of the semi-analytic method

In this chapter, derivations and explanations supporting the argumentations in the application chapter 5 will be presented.

C.1. Stars with purely toroidal magnetic fields

This section shows the mathematical background regarding the application of the semi-analytic method on toroidally magnetised neutron stars, presented in section 5.1.

C.1.1. Analytical criteria for the Tayler instability

In Tayler (1973), three stability criteria have been set up for the toroidally magnetised neutron star. If one of them is violated, a displacement field can always be found that leads to a negative energy variation, i.e. an instability.

In this section and the subsequent sections, this proof will be outlined and the impact of the additional terms appearing in the energy variation (5.11) compared to Tayler's form will be examined.

For the construction of the stability criteria, the integrand of the explicit energy variation form (5.11) is written as the sum of a positive definite term and a quadratic form in X and Z:

$$\delta W = \frac{\pi}{2} \iint \left\{ \bar{D} \left(\varpi \, \partial_\varpi \left(\frac{X}{\varpi} \right) + \partial_z Z \right)^2 + \bar{A} \, X^2 + \bar{B} \, X Z + \bar{C} \, Z^2 \right\} \varpi \, \mathrm{d}\varpi \, \mathrm{d}z. \tag{C.1}$$

The prefactors are

$$\bar{A} = B_\varphi^2 \frac{m^2-2}{\varpi^2} - \frac{2\,B_\varphi\,\partial_\varpi B_\varphi}{\varpi} \pm \partial_\varpi\Phi_0\,\partial_\varpi\rho_0 - \frac{\rho_0^2\,\partial_\varpi\Phi_0^2}{\Gamma_0\,p_0} - \frac{B_\varphi^2}{2\,\Gamma_0\,p_0}\left(\frac{\partial_\varpi\,(\varpi B_\varphi)}{\varpi}\right)^2 \tag{C.2a}$$
$$\mp \frac{\rho_0\,B_\varphi}{\Gamma_0\,p_0\,\varpi}\,\partial_\varpi\Phi_0\,\partial_\varpi\,(\varpi B_\varphi)$$

$$\bar{B} = -\frac{2\,B_\varphi\,\partial_z B_\varphi}{\varpi} \pm \partial_\varpi\Phi_0\,\partial_z\rho_0 \pm \partial_z\Phi_0\,\partial_\varpi\rho_0 - \frac{2\rho_0^2}{\Gamma_0\,p_0}\,\partial_\varpi\Phi_0\,\partial_z\Phi_0 - \frac{B_\varphi^2}{\Gamma_0\,p_0\,\varpi}\,\partial_\varpi\,(\varpi B_\varphi)\,\partial_z B_\varphi \tag{C.2b}$$
$$\mp \frac{\rho_0\,B_\varphi}{\Gamma_0\,p_0}\left(\frac{\partial_\varpi\,(\varpi B_\varphi)}{\varpi}\,\partial_z\Phi_0 + \partial_z B_\varphi\,\partial_\varpi\Phi_0\right)$$

$$\bar{C} = B_\varphi^2\frac{m^2}{\varpi^2} \pm \partial_z\Phi_0\,\partial_z\rho_0 - \frac{\rho_0^2\,\partial_\varpi\Phi_0^2}{\Gamma_0\,p_0} - \frac{B_\varphi^2}{2\,\Gamma_0\,p_0}\,(\partial_z B_\varphi)^2 \mp \frac{\rho_0\,B_\varphi}{\Gamma_0\,p_0}\,\partial_z\Phi_0\,\partial_z B_z \tag{C.2c}$$

$$\bar{D} = B_\varphi^2, \tag{C.2d}$$

where the last two terms in $\bar{A}$, $\bar{B}$ and $\bar{C}$ represent additional terms compared to Tayler's form, resulting from the negligence of the magnetic field in the equilibrium equation.

The particular form of (C.2) will be derived below when the energy variation is set up explicitly in section C.1.5 for the toroidal field application.

According to equation (C.1), the stability criteria for the neutron star are

$$\bar{A} \overset{!}{>} 0 \qquad\qquad \bar{C} \overset{!}{>} 0 \qquad\qquad \bar{B}^2 \overset{!}{<} 4\,\bar{A}\,\bar{C}. \tag{C.3}$$

The first and second criterion ensure that the quadratic terms $\bar{A}\,X^2$ and $\bar{C}\,Z^2$ provide positive contributions to the integrand. The third criterion follows from the requirement $\bar{B}\,XZ \overset{!}{<} \bar{A}\,X^2 + \bar{C}\,Z^2$, which guarantees that the potentially negative mixed term $\bar{B}\,XZ$ will be compensated by the positive definite terms. The equivalence of both expressions, $\bar{B}\,XZ \overset{!}{<} \bar{A}\,X^2 + \bar{C}\,Z^2$ and $\bar{B}^2 \overset{!}{<} 4\,\bar{A}\,\bar{C}$, is shown in section C.1.3.

The only remaining term $\bar{D}$ is positive and therefore the three criteria (C.3) are sufficient for stability.

Tayler remarks that these criteria are not only sufficient, but also "necessary" for stability. This statement must be understood in the sense that as soon as one of the criteria is violated, it is always possible to find a displacement field that creates a negative energy variation. If this is the case, the equilibrium state is unstable per definition, cf. equation (2.45).

However, the fact that criteria (C.3) are "necessary" for stability does not imply that any arbitrary combination of $\boldsymbol{\xi}$-defining functions will facilitate $\delta W < 0$ as soon as one of the criteria is violated.

Based on the analytic stability criteria (C.3), a displacement field that reveals the Tayler instability can be constructed. This will be done in section C.1.4.

C.1.2. Stability criterion violation in the toroidally magnetised neutron star

A simple estimate shows that the first stability criterion given in (C.3) is violated close to the stellar symmetry axis if $B_\varphi \neq 0$.

For the purpose of validating this statement, the system quantities can be expanded around $\varpi = 0$.

For small ϖ, the system quantities and their derivatives are adequately described by

$$B_\varphi = (B_\varphi)_1 \frac{\varpi}{\varpi_0} + (B_\varphi)_2 \frac{\varpi^2}{\varpi_0^2} + \mathcal{O}\left(\varpi^3\right) \qquad \partial_\varpi B_\varphi = \frac{(B_\varphi)_1}{\varpi_0} + \mathcal{O}\left(\varpi\right) \tag{C.4}$$

$$\rho_0 \sim \varpi^2 + \mathcal{O}(\varpi^3) \qquad \partial_\varpi \rho_0 \sim \varpi + \mathcal{O}(\varpi^2)$$

$$\Phi_0 \sim \varpi^2 + \mathcal{O}(\varpi^3) \qquad \partial_\varpi \Phi_0 \sim \varpi + \mathcal{O}(\varpi^2) \tag{C.5}$$

Here, $(B_\varphi)_i$ denote expansion coefficients independent of ϖ, and ϖ_0 is the constant that de-dimensionalises the cylindrical coordinate.

Applying expansion (C.4), we can find the lowest ϖ-order contribution of each term appearing in $\bar{A}$ in equation (C.2):

$$\bar{A} = \underbrace{B_\varphi^2 \frac{m^2-2}{\varpi^2}}_{\sim 1+\mathcal{O}(\varpi)} \underbrace{- \frac{2\, B_\varphi\, \partial_\varpi B_\varphi}{\varpi}}_{\sim 1+\mathcal{O}(\varpi)} \underbrace{\pm\, \partial_\varpi \Phi_0\, \partial_\varpi \rho_0}_{\sim \varpi^2+\mathcal{O}(\varpi^3)} \underbrace{- \frac{\rho_0^2\, \partial_\varpi \Phi_0^2}{\Gamma_0\, p_0}}_{\varpi^6+\mathcal{O}(\varpi^7)} \tag{C.6}$$

$$\underbrace{- \frac{B_\varphi^2}{2\,\Gamma_0\, p_0} \left(\partial_\varpi B_\varphi + \frac{B_\varphi}{\varpi}\right)^2}_{\sim \varpi^2+\mathcal{O}(\varpi^3)} \underbrace{\mp \frac{\rho_0\, B_\varphi}{\Gamma_0\, p_0\, \varpi}\, \partial_\varpi \Phi_0 \left(\varpi\, \partial_\varpi B_\varphi + B_\varphi\right)}_{\sim \varpi^4+\mathcal{O}(\varpi^5)}.$$

For small ϖ, the first and second term dominate, independently of the existence of the last two additional terms.

For a mode index of $m = 1$, both dominant terms are negative if $B_\varphi \neq 0$. The stability criterion $\bar{A} \overset{!}{>} 0$ is thus violated.

Note that for mode indices $m > 1$, the first dominant term is positive and might compensate the negative contribution from the second term. The stability criterion might still be violated but it is not an obvious implication anymore.

Therefore, we constrain on the case $m = 1$ in this application.

C.1.3. Algebraic transformation of the stability criterion for the mixed terms

From equation (C.1), the stability criterion for the prefactor $\bar{B}$ of the mixed terms in the quadratic form is

$$\bar{B}\, X Z \overset{!}{<} \bar{A}\, X^2 + \bar{C}\, Z^2. \tag{C.7}$$

This inequality can be rewritten, under the assumption made in section C.1.5 that the functions X and Z are real, which implies $X^2 > 0$ and $Z^2 > 0$:

$$\bar{B}^2 X^2 Z^2 \overset{!}{<} \left(\bar{A} X^2 + \bar{C} Z^2\right)^2 \tag{C.8}$$

$$\bar{B}^2 \overset{!}{<} \bar{A}^2 \frac{X^2}{Z^2} + 2\bar{A}\bar{C} + \bar{C}^2 \frac{Z^2}{X^2}. \tag{C.9}$$

Arbitrary real numbers U fulfil

$$(U-1)^2 \geq 0 \tag{C.10}$$

$$U^2 - 2U + 1 \geq 0. \tag{C.11}$$

Thus, for $U = \dfrac{\bar{C}}{\bar{A}} \dfrac{Z^2}{X^2}$, it is

$$\frac{\bar{C}^2}{\bar{A}^2} \frac{Z^4}{X^4} - 2 \frac{\bar{C}}{\bar{A}} \frac{Z^2}{X^2} + 1 \geq 0. \tag{C.12}$$

Multiplication with $\bar{A}^2 \dfrac{X^2}{Z^2}$ yields

$$\bar{A}^2 \frac{X^2}{Z^2} - 2\bar{A}\bar{C} + \bar{C}^2 \frac{Z^2}{X^2} \geq 0. \tag{C.13}$$

For criterion (C.9) this implies

$$\bar{B}^2 \overset{!}{<} \underbrace{\bar{A}^2 \frac{X^2}{Z^2} + \bar{C}^2 \frac{Z^2}{X^2}}_{\geq 2\bar{A}\bar{C}} + 2\bar{A}\bar{C}. \tag{C.14}$$

That means, a sufficient condition for the validity of criterion (C.9) can be formulated: The demanded inequality is always fulfilled if

$$\bar{B}^2 \overset{!}{<} 4\bar{A}\bar{C}. \tag{C.15}$$

This form is the criterion given in equation (C.3).

C.1.4. Construction of the explicit displacement field

According to section C.1.2, one of the stability criteria (C.3) for toroidally magnetised neutron stars is violated close to the symmetry axis.

Following Tayler (1973), we choose a position (ϖ_0, z_0) inside the integration area of the δW-calculation where the first criterion shall be violated. Then, the $\boldsymbol{\xi}$-defining functions X and Z from ansatz (2.121) need to be chosen in such a way that the energy variation becomes negative due to the violation in (ϖ_0, z_0).

We follow Tayler's steps while keeping track of the additional terms in (C.2).

The derivation of the explicit form for $\boldsymbol{\xi}$ shown here is based on expression (5.11) which has been derived on the basis of ansatz (2.121) alone, without further assumptions for X or Z.

Displacement field ansatz

Tayler introduces new variables $X'' \equiv \dfrac{X}{\varpi}$ and $Z'' \equiv \dfrac{Z}{\varpi}$ that simplify the quadratic term in the energy variation density given by equation (5.11) to

$$B_\varphi^2\, \varpi^2 \left(\partial_\varpi \left(X''\right) + \partial_z \left(Z''\right)\right)^2 . \tag{C.16}$$

For an appropriate construction of the $\boldsymbol{\xi}$-defining functions, a coordinate transformation is applied afterwards. Locally, the cylindrical coordinates (ϖ, z) can approximately be considered as cartesian. A transformation to new coordinates (ϖ', z') with the origin (ϖ_0, z_0) diagonalises the quadratic form in the integrand of expression (5.11):

$$\delta W = \frac{\pi}{2} \iint \left\{ \bar{D}' \left(\partial_{\varpi'} X' + \partial_{z'} Z'\right)^2 + \bar{A}'\, X'^2 + \bar{B}'\, X' Z' + \bar{C}'\, Z'^2 \right\} \mathrm{d}\varpi'\, \mathrm{d}z' \tag{C.17}$$

$$= \frac{\pi}{2} \iint \left\{ \bar{D}' \left(\partial_{\varpi'} X' + \partial_{z'} Z'\right)^2 + \left(X', Z'\right) \begin{pmatrix} \bar{A}' & \bar{B}'/2 \\ \bar{B}'/2 & \bar{C}' \end{pmatrix} \begin{pmatrix} X' \\ Z' \end{pmatrix} \right\} \mathrm{d}\varpi'\, \mathrm{d}z', \tag{C.18}$$

where the quadratic form has been expressed in matrix notation. The prefactors A', B', C' and D' have been redefined in such a way that the factor ϖ vanishes in the integrand. At the origin, the mixed term vanishes: $B'(\varpi_0, z_0) = 0$.

This procedure shown in Tayler (1973) equally holds for the altered form of the energy variation here, including the additional terms.

For convenience, we place the instability position in this work in the equatorial plane. The distance from the symmetry axis is described by the small value ϵ_A: $(\varpi_0, z_0) = (\epsilon_A, 0)$. With this choice, the particular coordinate transformation from (ϖ, z) to (ϖ', z') simplifies to

$$\varpi' = \varpi - \epsilon_A \qquad z' = z \qquad X' = X'' = \frac{X}{\varpi} \qquad Z' = Z'' = \frac{Z}{\varpi}. \tag{C.19}$$

For an illustration compare figure 2.15.

Next, the ansatz

$$X' = X_0 \sin\left(k_A\, \varpi'\right) \cos\left(l_A\, z'\right) \qquad Z' = Z_0 \cos\left(k_A\, \varpi'\right) \sin\left(l_A\, z'\right) \tag{C.20}$$

$$X = \varpi\, X_0 \sin\left(k_A\, (\varpi - \epsilon_A)\right) \cos\left(l_A\, z\right) \qquad Z = \varpi\, Z_0 \cos\left(k_A\, (\varpi - \epsilon_A)\right) \sin\left(l_A\, z\right) \tag{C.21}$$

is chosen for the $\boldsymbol{\xi}$-defining functions with

$$k_A\, X_0 + l_A\, Z_0 = 0. \tag{C.22}$$

That way, the positive term in equation (C.1) vanishes globally and does not need to be compensated in order to achieve a negative energy variation:

$$\bar{D}' \left(\partial_\varpi \left(\frac{X}{\varpi} \right) + \partial_z \left(\frac{Z}{\varpi} \right) \right)^2 = \bar{D}' \underbrace{\left(k_A X_0 + l_A Z_0 \right)}_{0} \cos\left(k_A \, \varpi' \right) \cos\left(l_A \, z' \right) = 0. \tag{C.23}$$

Note that the positive term remained unchanged by the additional terms in the energy variation. Therefore, Tayler's ansatz (C.20) is applicable here as well.

Furthermore, the assumptions

$$|X_0| \gg |Z_0| \qquad\qquad |l_A| \gg |k_A| \gg \frac{1}{h} \tag{C.24}$$

are made. That way, terms including X dominate over terms including Z. The second requirement guarantees that equation (C.22) can still be fulfilled.

Beyond that, the second requirement ensures that the spatial variation of X and Z happens on a length scale which is short compared to the one of the system quantities with the scale height h.

Displacement field localisation

The displacement field must be defined in a small region around the instability only.

The localisation area is thus chosen as

$$A = \left\{ \varpi \in \mathbb{R} \left| \epsilon_A - \frac{\pi}{k_A} < \varpi < \epsilon_A + \frac{\pi}{k_A} \right. , z \in \mathbb{R} \left| -\frac{\pi}{l_A} < z < \frac{\pi}{l_A} \right. \right\}, \tag{C.25}$$

with

$$\epsilon_A \overset{!}{>} \frac{\pi}{k_A}. \tag{C.26}$$

For the purpose of keeping the localisation region in the physically meaningful range of $\varpi \geq 0$, it would be sufficient to require $\epsilon_A \overset{!}{\geq} \frac{\pi}{k_A}$. By demanding the strict inequality instead, we simultaneously exclude the stellar symmetry axis from A in order to avoid possible singularities at $\varpi = 0$.

The localisation region is visualised in figure 2.15.

Note that according to the second requirement in (C.24), $|\pi/k_A| \gg |\pi/l_A|$ holds. That means, the extent of the localisation area in ϖ-direction is larger than the extension of the localisation area in z-direction.

Beyond that, the localisation area is oriented in such a way that on its boundaries, the displacement field is parallel to the boundary.

At the left and right hand side boundaries, $\varpi' = -\pi/k_A$ and $\varpi' = \pi/k_A$, the ϖ'-component of the displacement field vanishes:

$$X' \sim \sin\left(k_A \, \varpi' \right) = \sin\left(\pm\pi \right) = 0, \tag{C.27a}$$

while $Z' \neq 0$ in general.

At the lower and upper boundaries, $z' = -\frac{\pi}{l_A}$ and $z' = \frac{\pi}{l_A}$, the z'-component of the displacement field vanishes:

$$Z' \sim \sin\left(l_A\, z'\right) = \sin\left(\pm\pi\right) = 0, \tag{C.27b}$$

while $X' \neq 0$ in general.

This definition ensures that the surface integral contribution to the energy variation which is proportional to $\boldsymbol{n}\cdot\boldsymbol{\xi}$ does not need to be taken into account, cf. appendix section B.4.

Instability proof capability of the displacement field

Next, we need to show that the assumptions made above for $\boldsymbol{\xi}$ facilitate the proof of the Tayler instability, independent of the additional terms in equation (C.2).

Applying the assumptions, the energy variation given by equation (5.11) can be estimated inside the localisation area:

$$\delta W = \frac{\pi}{2} \iint \left\{ \underbrace{\bar{D}' \left(\partial_{\varpi'} X' + \partial_{z'} Z'\right)^2}_{0} + \underbrace{\bar{A}'\, X'^2}_{<0} + \underbrace{\bar{B}'\, X' Z'}_{\ll \bar{A}'\, X'^2} + \underbrace{\bar{C}'\, Z'^2}_{\ll \bar{A}'\, X'^2} \right\} \mathrm{d}\varpi'\, \mathrm{d}z' \tag{C.28}$$

$$\delta W_{\text{ in } A} \approx \frac{\pi}{2} \iint \bar{A}'\, X'^2\, \mathrm{d}\varpi'\, \mathrm{d}z' < 0, \tag{C.29}$$

cf. equation (C.17).

Inside A, the first term vanishes according to equation (C.23).

The second term is negative at the origin (ϖ_0, z_0), as reasoned in and below equation (C.6). According to the second requirement in (C.24), the system quantity dependent expression $\bar{A}'$ varies spatially slowly with (ϖ, z), compared to X' and Z'. It is thus a valid assumption that the second term is also negative everywhere inside the localisation region.

The third term vanishes at the origin (ϖ_0, z_0), caused by the diagonalisation described below equation (C.18). According to the slow spatial variation of $\bar{B}'$ caused by the second requirement in (C.24), this term is negligible compared to the other contributions everywhere inside the constrained localisation area.

The last term in (C.28) is small compared to the second one because of the first requirement in (C.24).

According to the above discussion, equation (C.28) proves that the displacement field constructed here creates a negative energy variation. It is thus suitable for the verification of the Tayler instability.

The constructed form is applicable in both cases, with and without the additional terms caused by the negligence of the magnetic field in the equilibrium equation. It will be used in the code in section 5.1 in order to prove the Tayler instability with the semi-analytic method.

Displacement field parameter choice

Once an appropriate structure for $\boldsymbol{\xi}$ has been found, convenient values for the parameters X_0, Z_0, l and k need to be chosen.

The parameters must portray a system with a positive energy variation for $B_\varphi = 0$, which especially implies $\delta W_{\text{grav}} > 0$, in order to make the Tayler instability $\delta W(B_\varphi \neq 0) < 0$ detectable.

The system needs to represent a realistic neutron star model with typical values for mass, radius and compactness. In this work, different models will be tested in order to show the universality of the Tayler instability verification.

For the choice of l and k, we need to consider that the instability region covers the area close to the z-axis. The localisation area (C.25), however, is more extended in ϖ-direction than in z-direction according to the second requirement in (C.24).

That means, we need to ensure that the localisation area is large enough to contain a sufficient amount of integration grid points along z. At the same time, it must not be too wide to extend too far from the stellar axis.

It would be convenient to modify A from an "oblate" to a "prolate" shape by interchanging l and k. However, this is not possible in a straightforward manner. We would need to ensure again that the surface integral contribution is negligible, since equations (C.27) are not valid anymore when l and k are interchanged.

Therefore, we keep the extent of A as small as possible along ϖ, and by that even smaller along z, with a still acceptable number of grid points in z-direction.

Based on these considerations, the parameter sets used in the computation are shown in and below table 5.1.

C.1.5. Derivation of the explicit form for the energy variation

The energy variation for polytropes in Cowling approximation, given by equation (2.116) with (2.117), can be rewritten and simplified for the particular toroidal field case investigated in this work.

For this purpose, the assumptions made by Tayler (1973) and shown in section 5.1 for the toroidally magnetised neutron star will be applied.

In this section, the derivation of the final explicit form is presented.

It slightly differs from the derivation shown by Tayler (1973). In contrast to Tayler, we neglect the magnetic contribution to the hydrostatic equilibrium equation (2.29) for the sake of consistency. We assume that the magnetic field is superimposed to the unmagnetised background, which was built by the system equations (2.26). In contrast, Tayler (1973) includes the impact of the magnetic field on the equilibrium in (2.29), because this allows for the cancellation of several terms in the subsequent derivation. Consequently, the energy variation density derived here will contain additional terms compared to Tayler's form.

Beyond that, the real part ensuring the energy variation to be physically meaningful will be taken in the integrand $\mathcal{E}$ rather than immediately inside the displacement field choice $\boldsymbol{\xi}$, as explained in section 2.3.3 and in the appendix section A.5.4.

Finally, we will derive the explicit forms for the different energy variational contributions $\mathcal{E}_{\mathrm{magn}}$, $\mathcal{E}_{\mathrm{fluid}}$ and $\mathcal{E}_{\mathrm{grav}}$ separately first, in order to keep track of the origin of the particular terms. In the end, these contributions will be added, and after some cancellations, the analogue to Tayler's result follows.

Starting from equations (2.117) for the energy variation density, we first insert the assumption (2.31) of a toroidal magnetic field, $\boldsymbol{B} = (0, B_\varphi, 0)$, depicted in cylindrical coordinates. According to equations (2.14d) and (2.101d), it is further

$$\boldsymbol{j}_0 = \frac{c}{4\pi}\begin{pmatrix} -\partial_z B_\varphi \\ 0 \\ \frac{\partial_\varpi(\varpi B_\varphi)}{\varpi} \end{pmatrix} \qquad \delta\boldsymbol{B} = \begin{pmatrix} \frac{B_\varphi}{\varpi}\,\partial_\varphi \xi_\varpi \\ -\partial_z(\xi_z B_\varphi) - \partial_\varpi(\xi_\varpi B_\varphi) \\ \frac{B_\varphi}{\varpi}\,\partial_\varphi \xi_z \end{pmatrix}. \tag{C.30}$$

Finally, we use relation (A.1) for the gradient of the product and take into account the axisymmetry of the equilibrium quantities. Minor rearrangement yields

$$\begin{aligned}
\mathcal{E}_{\mathrm{magn}} = \; & \frac{1}{4}\,\Re\Bigg\{ \frac{B_\varphi^2}{\varpi^2}\left(\partial_\varphi \xi_\varpi^* \,\partial_\varphi \xi_\varpi + \partial_\varphi \xi_z^* \,\partial_\varphi \xi_z\right) \\
& + \Big(\partial_\varpi\left(\xi_\varpi^* B_\varphi\right) + \partial_z\left(\xi_z^* B_\varphi\right)\Big)\Big(\partial_\varpi\left(\xi_\varpi B_\varphi\right) + \partial_z\left(\xi_z B_\varphi\right)\Big) \\
& - \left(\frac{\partial_\varpi(\varpi B_\varphi)}{\varpi}\xi_\varpi^* + \partial_z B_\varphi\, \xi_z^*\right)\Big(\partial_\varpi\left(\xi_\varpi B_\varphi\right) + \partial_z\left(\xi_z B_\varphi\right)\Big) \\
& - \frac{B_\varphi}{\varpi^2}\,\partial_\varpi\left(\varpi B_\varphi\right)\xi_\varphi^*\,\partial_\varphi \xi_\varpi - \frac{B_\varphi}{\varpi}\,\partial_z B_\varphi\, \xi_\varphi^*\,\partial_\varphi \xi_z \Bigg\}
\end{aligned} \tag{C.31a}$$

$$\mathcal{E}_{\mathrm{fluid}}^{\mathrm{poly}} = \frac{1}{4}\,\Re\left\{\Gamma_0\, p_0\,(\nabla\cdot\boldsymbol{\xi}^*)\,(\nabla\cdot\boldsymbol{\xi}) + \left(\xi_\varpi\,\partial_\varpi p_0 + \xi_z\,\partial_z p_0\right)(\nabla\cdot\boldsymbol{\xi}^*)\right\} \tag{C.31b}$$

$$\mathcal{E}_{\mathrm{grav}}^{\mathrm{Cowl}} = \pm\frac{1}{4}\,\Re\left\{\left(\xi_\varpi\,\partial_\varpi\Phi_0 + \xi_z\,\partial_z\Phi_0\right)\left(\rho_0\,(\nabla\cdot\boldsymbol{\xi}^*) + \xi_\varpi^*\,\partial_\varpi\rho_0 + \xi_z^*\,\partial_z\rho_0\right)\right\}. \tag{C.31c}$$

Note that compared to relation (2.117a) expressed in non-rationalised units, we now switched to geometrised rationalised units for the sake of consistency with Tayler's work. According to equation (2.117a), $\mathcal{E}_{\mathrm{magn}}$ would contain an additional prefactor of $1/(4\pi)$ that stems from the non-rationalised formulation (2.14) of the Maxwell equations and that is consequently neglected here.

Next, the toroidal field choice (2.121) for the displacement field will be inserted under the assumption of $m \neq 0$. The case $m = 0$ needs to be treated separately, due to the singularity that arises when dividing by m. Since we assume $m = 1$ in this work, this case is not relevant here.

With the divergence in cylindrical coordinates given by equation (A.13),

$$\nabla \cdot \boldsymbol{\xi} = \frac{\partial_\varpi (\varpi\, \xi_\varpi)}{\varpi} + \frac{\partial_\varphi \xi_\varphi}{\varpi} + \partial_z \xi_z \tag{C.32}$$

$$= \left(\frac{X}{\varpi} + \partial_\varpi X \right) \mathrm{e}^{\,im\varphi} - Y\ \mathrm{e}^{\,im\varphi} + \partial_z Z\ \mathrm{e}^{\,im\varphi} \tag{C.33}$$

$$\nabla \cdot \boldsymbol{\xi}^* = \left(\frac{X^*}{\varpi} + \partial_\varpi X^* \right) \mathrm{e}^{-im\varphi} - Y^*\, \mathrm{e}^{-im\varphi} + \partial_z Z^*\, \mathrm{e}^{-im\varphi}, \tag{C.34}$$

the energy variation density contributions can be expressed as

$$\begin{aligned} \mathcal{E}_{\mathrm{magn}} = \ & \frac{1}{4}\, \Re \left\{ \frac{B_\varphi^2 m^2}{\varpi^2} \left(X^* X + Z^* Z \right) + \left(\partial_\varpi \left(X\, B_\varphi \right) + \partial_z \left(Z\, B_\varphi \right) \right) \right. \\ & \cdot \left(\partial_\varpi \left(X^*\, B_\varphi \right) + \partial_z \left(Z^*\, B_\varphi \right) - \frac{\partial_\varpi (\varpi B_\varphi)}{\varpi}\, X^* - \partial_z B_\varphi\, Z^* \right) \\ & \left. - \frac{B_\varphi}{\varpi^2}\, \partial_\varpi (\varpi B_\varphi)\, Y^* X - \frac{B_\varphi}{\varpi}\, \partial_z B_\varphi\, Y^* Z \right\} \end{aligned} \tag{C.35a}$$

$$\begin{aligned} \mathcal{E}_{\mathrm{fluid}}^{\mathrm{poly}} = \ & \frac{1}{4}\, \Re \left\{ \Gamma_0\, p_0 \left(\frac{\partial_\varpi (\varpi X^*)}{\varpi} - \frac{Y^*}{\varpi} + \partial_z Z^* \right) \right. \\ & \left. \cdot \left(\frac{\partial_\varpi (\varpi X)}{\varpi} - \frac{Y}{\varpi} + \partial_z Z + X\, \partial_\varpi p_0 + Z\, \partial_z p_0 \right) \right\} \end{aligned} \tag{C.35b}$$

$$\begin{aligned} \mathcal{E}_{\mathrm{grav}}^{\mathrm{Cowl}} = \pm \frac{1}{4}\, \Re \ & \left\{ \left(X\, \partial_\varpi \Phi_0 + Z\, \partial_z \Phi_0 \right) \right. \\ & \left. \cdot \left[\rho_0 \left(\frac{\partial_\varpi (\varpi X^*)}{\varpi} - \frac{Y^*}{\varpi} + \partial_z Z^* \right) + X^*\, \partial_\varpi \rho_0 + Z^*\, \partial_z \rho_0 \right] \right\}. \end{aligned} \tag{C.35c}$$

The exponential functions cancelled out completely, for equations (C.31) involved products of $\boldsymbol{\xi}$-components of opposite conjugation only.

For comparison of (C.35) with Tayler (1973), note that products of complex functions obey the relation $\Re\{a^* b\} = \Re\{a\, b^*\}$, according to equation (A.29).

The generally complex $\boldsymbol{\xi}$-defining functions can now be split into real and imaginary parts, denoted by the indices R and I:

$$X = X_R + iX_I \qquad Y = Y_R + iY_I \qquad Z = Z_R + iZ_I. \tag{C.36}$$

Expressions (C.35) can then be simplified considering relations (A.29) and (A.30) for the product of complex conjugated numbers.

In doing so, we take into account that all other quantities B_φ, m, Γ_0 and Q_0 appearing in the integrand as well as the coordinate ϖ are real numbers. Finally, the calculation rules for complex conjugation, $(a_R\, b)^* = a_R\, b^*$ and $(a + b)^* = a^* + b^*$, can be applied.

After these steps, the integrand contributions are

$$\begin{aligned}\mathcal{E}_{\text{magn}} = \frac{1}{4}\Bigg\{ & \frac{B_\varphi^2 m^2}{\varpi^2}\left(X_R^2 + Z_R^2\right) + \left(\partial_\varpi\left(X_R B_\varphi\right) + \partial_z\left(Z_R B_\varphi\right)\right)^2 \\ & - \left(\partial_\varpi\left(X_R B_\varphi\right) + \partial_z\left(Z_R B_\varphi\right)\right)\left(\frac{\partial_\varpi\left(\varpi B_\varphi\right)}{\varpi} X_R + \partial_z B_\varphi Z_R\right) \\ & - \frac{B_\varphi}{\varpi^2}\partial_\varpi\left(\varpi B_\varpi\right) Y_R X_R - \frac{B_\varphi}{\varpi}\partial_z B_\varphi Y_R Z_R \\ & + \frac{B_\varphi^2 m^2}{\varpi^2}\left(X_I^2 + Z_I^2\right) + \left(\partial_\varpi\left(X_I B_\varphi\right) + \partial_z\left(Z_I B_\varphi\right)\right)^2 \\ & - \left(\partial_\varpi\left(X_I B_\varphi\right) + \partial_z\left(Z_I B_\varphi\right)\right)\left(\frac{\partial_\varpi\left(\varpi B_\varphi\right)}{\varpi} X_I + \partial_z B_\varphi Z_I\right) \\ & - \frac{B_\varphi}{\varpi^2}\partial_\varpi\left(\varpi B_\varpi\right) Y_I X_I - \frac{B_\varphi}{\varpi}\partial_z B_\varphi Y_I Z_I\Bigg\}\end{aligned} \tag{C.37a}$$

$$\begin{aligned}\mathcal{E}^{\text{poly}}_{\text{fluid}} = \frac{\Gamma_0 p_0}{4}\Bigg\{ & \left(\frac{\partial_\varpi\left(\varpi X_R\right)}{\varpi} - \frac{Y_R}{\varpi} + \partial_z Z_R\right)^2 + \left(\frac{\partial_\varpi\left(\varpi X_R\right)}{\varpi} - \frac{Y_R}{\varpi} + \partial_z Z_R\right) \\ & \cdot \left(X_R\,\partial_\varpi p_0 + Z_R\,\partial_z p_0\right) + \left(\frac{\partial_\varpi\left(\varpi X_I\right)}{\varpi} - \frac{Y_I}{\varpi} + \partial_z Z_I\right)^2 \\ & + \left(\frac{\partial_\varpi\left(\varpi X_I\right)}{\varpi} - \frac{Y_I}{\varpi} + \partial_z Z_I\right)\left(X_I\,\partial_\varpi p_0 + Z_I\,\partial_z p_0\right)\Bigg\}\end{aligned} \tag{C.37b}$$

$$\begin{aligned}\mathcal{E}^{\text{Cowl}}_{\text{grav}} = \pm\frac{1}{4}\Bigg\{ & \left(X_R\,\partial_\varpi\Phi_0 + Z_R\,\partial_z\Phi_0\right)\left[\rho_0\left(\frac{\partial_\varpi\left(\varpi X_R\right)}{\varpi} - \frac{Y_R}{\varpi} + \partial_z Z_R\right) + X_R\,\partial_\varpi\rho_0 + Z_R\,\partial_z\rho_0\right] \\ & \left(X_I\,\partial_\varpi\Phi_0 + Z_I\,\partial_z\Phi_0\right)\left[\rho_0\left(\frac{\partial_\varpi\left(\varpi X_I\right)}{\varpi} - \frac{Y_I}{\varpi} + \partial_z Z_I\right) + X_I\,\partial_\varpi\rho_0 + Z_I\,\partial_z\rho_0\right]\Bigg\}.\end{aligned} \tag{C.37c}$$

In equations (C.37), it becomes obvious that real and imaginary parts of X, Y and Z contribute equivalent parts to $\mathcal{E}$.

The energy variation density can then be written as

$$\mathcal{E} = \bar{\mathcal{E}}(X_R, Y_R, Z_R) + \bar{\mathcal{E}}(X_I, Y_I, Z_I) \tag{C.38a}$$

with

$$\bar{\mathcal{E}}(\mathcal{X}, \mathcal{Y}, \mathcal{Z}) = \bar{\mathcal{E}}_{\text{magn}}(\mathcal{X}, \mathcal{Y}, \mathcal{Z}) + \bar{\mathcal{E}}^{\text{poly}}_{\text{fluid}}(\mathcal{X}, \mathcal{Y}, \mathcal{Z}) + \bar{\mathcal{E}}^{\text{Cowl}}_{\text{grav}}(\mathcal{X}, \mathcal{Y}, \mathcal{Z}) \tag{C.38b}$$

for

$$\mathcal{X} = \{X_R, X_I\} \qquad \mathcal{Y} = \{Y_R, Y_I\} \qquad \mathcal{Z} = \{Z_R, Z_I\} \tag{C.38c}$$

and

$$\bar{\mathcal{E}}_{\mathrm{magn}}(\mathcal{X},\mathcal{Y},\mathcal{Z}) = \frac{1}{4}\left\{\frac{B_\varphi^2 m^2}{\varpi^2}\left(\mathcal{X}^2+\mathcal{Z}^2\right)+\left(\partial_\varpi\left(\mathcal{X}B_\varphi\right)+\partial_z\left(\mathcal{Z}B_\varphi\right)\right)^2\right. \tag{C.39a}$$
$$-\left(\partial_\varpi\left(\mathcal{X}B_\varphi\right)+\partial_z\left(\mathcal{Z}B_\varphi\right)\right)\left(\frac{\partial_\varpi\left(\varpi B_\varphi\right)}{\varpi}\mathcal{X}+\partial_z B_\varphi\,\mathcal{Z}\right)$$
$$\left.-\frac{B_\varphi}{\varpi^2}\partial_\varpi\left(\varpi B_\varphi\right)\mathcal{Y}\,\mathcal{X}-\frac{B_\varphi}{\varpi}\partial_z B_\varphi\,\mathcal{Y}\,\mathcal{Z}\right\}$$

$$\bar{\mathcal{E}}^{\mathrm{poly}}_{\mathrm{fluid}}(\mathcal{X},\mathcal{Y},\mathcal{Z}) = \frac{\Gamma_0\,p_0}{4}\left\{\left(\frac{\partial_\varpi\left(\varpi\mathcal{X}\right)}{\varpi}-\frac{\mathcal{Y}}{\varpi}+\partial_z\mathcal{Z}\right)^2\right. \tag{C.39b}$$
$$\left.+\left(\frac{\partial_\varpi\left(\varpi\mathcal{X}\right)}{\varpi}-\frac{\mathcal{Y}}{\varpi}+\partial_z\mathcal{Z}\right)\left(\mathcal{X}\,\partial_\varpi p_0+\mathcal{Z}\,\partial_z p_0\right)\right\}$$

$$\bar{\mathcal{E}}^{\mathrm{Cowl}}_{\mathrm{grav}}(\mathcal{X},\mathcal{Y},\mathcal{Z}) = \pm\frac{1}{4}\left\{\left(\mathcal{X}\,\partial_\varpi\Phi_0+\mathcal{Z}\,\partial_z\Phi_0\right)\left[\rho_0\left(\frac{\partial_\varpi\left(\varpi\mathcal{X}\right)}{\varpi}-\frac{\mathcal{Y}}{\varpi}+\partial_z\mathcal{Z}\right)\right.\right. \tag{C.39c}$$
$$\left.\left.+\mathcal{X}\,\partial_\varpi\rho_0+\mathcal{Z}\,\partial_z\rho_0\right]\right\}.$$

Next, the integrand will be minimised with respect to the ξ_φ-component $\mathcal{Y}$, in accordance with Tayler (1973).

The integrand is extremal when the first derivative vanishes:

$$\partial_{\mathcal{Y}}\,\bar{\mathcal{E}} \stackrel{!}{=} 0, \tag{C.40}$$

which gives

$$-\frac{B_\varphi}{\varpi}\left(\frac{\partial_\varpi\left(\varpi B_\varphi\right)}{\varpi}\mathcal{X}+\partial_z B_\varphi\,\mathcal{Z}\right)-\frac{2\,\Gamma_0\,p_0}{\varpi}\left(\frac{\partial_\varpi\left(\varpi\mathcal{X}\right)}{\varpi}-\frac{\mathcal{Y}}{\varpi}+\partial_z\mathcal{Z}\right) \tag{C.41}$$
$$-\frac{1}{\varpi}\left(\mathcal{X}\,\partial_\varpi p_0+\mathcal{Z}\,\partial_z p_0\right)\mp\frac{\rho_0}{\varpi}\left(\mathcal{X}\,\partial_\varpi\Phi_0+\mathcal{Z}\,\partial_z\Phi_0\right)\stackrel{!}{=}0.$$

Note that the second derivative,

$$\partial^2_{\mathcal{Y}}\,\bar{\mathcal{E}} = \frac{2\,\Gamma_0\,p_0}{\varpi^2} > 0, \tag{C.42}$$

is positive which implies that the extremum determined by requirement (C.41) represents in fact a minimum of the energy variation.

Equation (C.41) can be solved for $\mathcal{Y}$, using the hydrostatic equilibrium equation (2.29).

We receive the $\mathcal{Y}_{\min}$-value which minimises the integrand:

$$\mathcal{Y}_{\min} = \left(\partial_\varpi\left(\varpi\mathcal{X}\right) + \varpi\,\partial_z\mathcal{Z}\right) \pm \frac{\rho_0\varpi}{\Gamma_0\,p_0}\left(\mathcal{X}\,\partial_\varpi\Phi_0 + \mathcal{Z}\,\partial_z\mathcal{Z}\right) + \frac{\varpi B_\varphi}{2\,\Gamma_0\,p_0}\left(\frac{\partial_\varpi\left(\varpi B_\varphi\right)}{\varpi}\mathcal{X} + \partial_z B_\varphi\mathcal{Z}\right). \tag{C.43}$$

Note that the final term in expression (C.43) represents an additional term in comparison to Tayler's result. The consideration of the magnetic field in the hydrostatic equilibrium equation equation (2.29) allows Tayler (1973) to cancel the magnetic field terms in expression (C.43).

Inserting $\mathcal{Y}_{\min}$ into $\mathcal{E}$, the minimised energy variation density contributions (C.39) can be calculated.

The magnetic contribution is

$$\begin{aligned}\bar{\mathcal{E}}_{\mathrm{magn}}(\mathcal{X},\mathcal{Y}_{\min},\mathcal{Z}) = \frac{1}{4}\Bigg\{&\frac{B_\varphi^2\,m^2}{\varpi^2}\left(\mathcal{X}^2+\mathcal{Z}^2\right) + \left(\partial_\varpi\left(\mathcal{X}\,B_\varphi\right) + \partial_z\left(\mathcal{Z}\,B_\varphi\right)\right)^2\\ &- \left(\partial_\varpi\left(\mathcal{X}\,B_\varphi\right) + \partial_z\left(\mathcal{Z}\,B_\varphi\right)\right)\left(\frac{\partial_\varpi\left(\varpi B_\varphi\right)}{\varpi}\,\mathcal{X} + \partial_z B_\varphi\,\mathcal{Z}\right)\\ &- \frac{B_\varphi}{\varpi}\left(\frac{\partial_\varpi\left(\varpi B_\varphi\right)}{\varpi}\,\mathcal{X} + \partial_z B_\varphi\,\mathcal{Z}\right)\mathcal{Y}\Bigg\},\end{aligned} \tag{C.44}$$

where the $\mathcal{Y}$-independent terms as well as the first of the linear $\mathcal{Y}$-terms can be multiplied out. Numerous terms add up to zero. The remaining terms can be rearranged in the following form:

$$\begin{aligned}\bar{\mathcal{E}}_{\mathrm{magn}}(\mathcal{X},\mathcal{Y}_{\min},\mathcal{Z}) = \frac{1}{4}\Bigg\{&B_\varphi^2\left(\varpi\,\partial_\varpi\left(\frac{\mathcal{X}}{\varpi}\right) + \partial_z\mathcal{Z}\right)^2 + B_\varphi^2\,m^2\,\frac{\mathcal{X}^2+\mathcal{Z}^2}{\varpi^2} - \frac{2\,B_\varphi^2\,\mathcal{X}^2}{\varpi^2}\\ &- \frac{2\,B_\varphi\,\mathcal{X}}{\varpi}\left(\partial_\varpi B_\varphi\,\mathcal{X} + \partial_z B_\varphi\,\mathcal{Z}\right) \mp \frac{\rho_0\,B_\varphi}{\Gamma_0\,p_0}\left(\frac{\partial_\varpi\left(\varpi B_\varphi\right)}{\varpi}\,\mathcal{X} + \partial_z B_\varphi\mathcal{Z}\right)\\ &\cdot\left(\mathcal{X}\,\partial_\varpi\Phi_0 + \mathcal{Z}\,\partial_z\Phi_0\right) - \frac{B_\varphi^2}{2\,\Gamma_0\,p_0}\left(\frac{\partial_\varpi\left(\varpi B_\varphi\right)}{\varpi}\,\mathcal{X} + \partial_z B_\varphi\mathcal{Z}\right)^2\Bigg\},\end{aligned} \tag{C.45}$$

where the first term has been written as a squared binomial.

While equation (C.45) holds for arbitrary mode indices $m \neq 0$, the expression simplifies

under the assumption of $m = 1$ to

$$\begin{aligned}\bar{\mathcal{E}}_{\mathrm{magn}}(\mathcal{X},\mathcal{Y}_{\min},\mathcal{Z}) = \frac{1}{4}\Bigg\{ & B_\varphi^2\left(\varpi\,\partial_\varpi\left(\frac{\mathcal{X}}{\varpi}\right)+\partial_z\mathcal{Z}\right)^2 + B_\varphi^2\,\frac{\mathcal{Z}^2-\mathcal{X}^2}{\varpi^2} \\ & - \frac{2\,B_\varphi\,\mathcal{X}}{\varpi}\left(\partial_\varpi B_\varphi\,\mathcal{X}+\partial_z B_\varphi\,\mathcal{Z}\right) \mp \frac{\rho_0\,B_\varphi}{\Gamma_0\,p_0}\left(\frac{\partial_\varpi\left(\varpi B_\varphi\right)}{\varpi}\,\mathcal{X}+\partial_z B_\varphi\mathcal{Z}\right) \\ & \cdot\left(\mathcal{X}\,\partial_\varpi\Phi_0+\mathcal{Z}\,\partial_z\Phi_0\right) - \frac{B_\varphi^2}{2\,\Gamma_0\,p_0}\left(\frac{\partial_\varpi\left(\varpi B_\varphi\right)}{\varpi}\,\mathcal{X}+\partial_z B_\varphi\mathcal{Z}\right)^2\Bigg\}.\end{aligned} \tag{C.46}$$

Before setting up the fluid contribution, we apply $\mathcal{Y}_{\min}$ given by equation (C.43) to simplify the following expression:

$$\frac{\partial_\varpi\left(\varpi\mathcal{X}\right)}{\varpi} - \frac{\mathcal{Y}_{\min}}{\varpi} + \partial_z\mathcal{Z} = \mp\frac{\rho_0}{\Gamma_0\,p_0}\left(\mathcal{X}\,\partial_\varpi\Phi_0+\mathcal{Z}\,\partial_z\Phi_0\right) - \frac{B_\varphi}{2\,\Gamma_0\,p_0}\left(\frac{\partial_\varpi\left(\varpi B_\varphi\right)}{\varpi}\,\mathcal{X}+\partial_z B_\varphi\,\mathcal{Z}\right). \tag{C.47}$$

Applying relation (C.47) and the hydrostatic equilibrium equation $\nabla p = \pm\rho_0\nabla\Phi_0$, the fluid contribution (C.39b) becomes

$$\begin{aligned}\bar{\mathcal{E}}^{\mathrm{poly}}_{\mathrm{fluid}}(\mathcal{X},\mathcal{Y}_{\min},\mathcal{Z}) = \frac{1}{4}\Bigg\{ & \frac{\rho_0^2}{\Gamma_0\,p_0}\left(\mathcal{X}\,\partial_\varpi\Phi_0+\mathcal{Z}\,\partial_z\Phi_0\right)^2 \\ & \pm\frac{2\rho_0\,B_\varphi}{2\,\Gamma_0\,p_0}\left(\frac{\partial_\varpi\left(\varpi B_\varphi\right)}{\varpi}\,\mathcal{X}+\partial_z B_\varphi\,\mathcal{Z}\right)\left(\mathcal{X}\,\partial_\varpi\Phi_0+\mathcal{Z}\,\partial_z\Phi_0\right) \\ & + \frac{B_\varphi^2}{4\,\Gamma_0\,p_0}\left(\frac{\partial_\varpi\left(\varpi B_\varphi\right)}{\varpi}\,\mathcal{X}+\partial_z B_\varphi\,\mathcal{Z}\right)^2 - \frac{\rho_0^2}{\Gamma_0\,p_0}\left(\mathcal{X}\,\partial_\varpi\Phi_0+\mathcal{Z}\,\partial_z\Phi_0\right)^2 \\ & \mp\frac{\rho_0\,B_\varphi}{2\,\Gamma_0\,p_0}\left(\frac{\partial_\varpi\left(\varpi B_\varphi\right)}{\varpi}\,\mathcal{X}+\partial_z B_\varphi\,\mathcal{Z}\right)\left(\mathcal{X}\,\partial_\varpi\Phi_0+\mathcal{Z}\,\partial_z\Phi_0\right)\Bigg\}\end{aligned} \tag{C.48}$$

$$\begin{aligned} = \frac{1}{4}\Bigg\{ & \pm\frac{\rho_0\,B_\varphi}{2\,\Gamma_0\,p_0}\left(\frac{\partial_\varpi\left(\varpi B_\varphi\right)}{\varpi}\,\mathcal{X}+\partial_z B_\varphi\,\mathcal{Z}\right)\left(\mathcal{X}\,\partial_\varpi\Phi_0+\mathcal{Z}\,\partial_z\Phi_0\right) \\ & + \frac{B_\varphi^2}{4\,\Gamma_0\,p_0}\left(\frac{\partial_\varpi\left(\varpi B_\varphi\right)}{\varpi}\,\mathcal{X}+\partial_z B_\varphi\,\mathcal{Z}\right)^2\Bigg\}.\end{aligned} \tag{C.49}$$

Applying relation (C.47) once more, the gravitational contribution (C.39c) can be written as

$$\begin{aligned}\bar{\mathcal{E}}^{\mathrm{Cowl}}_{\mathrm{grav}}(\mathcal{X},\mathcal{Y}_{\min},\mathcal{Z}) &= \frac{1}{4}\left\{\pm\left(\mathcal{X}\,\partial_\varpi\Phi_0+\mathcal{Z}\,\partial_z\Phi_0\right)\left(\mathcal{X}\,\partial_\varpi\rho_0+\mathcal{Z}\,\partial_z\rho_0\right)-\frac{\rho_0^2}{\Gamma_0\,p_0}\left(\partial_\varpi\Phi_0+\mathcal{Z}\,\partial_z\Phi_0\right)^2\right.\\ &\qquad\left.\mp\frac{\rho_0 B_\varphi}{2\Gamma_0\,p_0}\left(\mathcal{X}\,\partial_\varpi\Phi_0+\mathcal{Z}\,\partial_z\Phi_0\right)\left(\frac{\partial_\varpi\left(\varpi B_\varphi\right)}{\varpi}\,\mathcal{X}+\partial_z B_\varphi\,\mathcal{Z}\right)\right\}.\end{aligned} \tag{C.50}$$

Finally, the separate contributions (C.45), (C.49) and (C.50) can be added.

The energy variation density does not depend on the azimuthal angle and it can be integrated over φ. According to the fact that real and imaginary parts of X and Z contribute equivalent terms, the $\boldsymbol{\xi}$-defining functions can be chosen real without restriction, $X = X_R$, $Z = Z_R$.

Thus, from equations (2.116) and (C.38),

$$\delta W = \iiint \Re\left\{\bar{\mathcal{E}}(X_R,Y_R,Z_R)+\bar{\mathcal{E}}(X_I,Y_I,Z_I)\right\}\mathrm{d}V \tag{C.51}$$

$$\begin{aligned}&= \frac{\pi}{2}\iint\left\{B_\varphi^2\left(\varpi\,\partial_\varpi\left(\frac{X}{\varpi}\right)+\partial_z Z\right)^2+B_\varphi^2\,\frac{(m^2-2)\,X^2+m^2\,Z^2}{\varpi^2}\right.\\ &\quad-\frac{2\,B_\varphi\,X}{\varpi}\left(\partial_\varpi B_\varphi\,X+\partial_z B_\varphi\,Z\right)\pm\left(X\,\partial_\varpi\Phi_0+Z\,\partial_z\Phi_0\right)\left(X\,\partial_\varpi\rho_0+Z\,\partial_z\rho_0\right)\\ &\quad-\frac{\rho_0^2}{\Gamma_0\,p_0}\left(X\,\partial_\varpi\Phi_0+Z\,\partial_z\Phi_0\right)^2-\frac{B_\varphi^2}{4\Gamma_0\,p_0}\left(\frac{\partial_\varpi\left(\varpi B_\varphi\right)}{\varpi}\,X+\partial_z B_\varphi Z\right)^2\\ &\quad\left.\mp\frac{\rho_0 B_\varphi}{\Gamma_0\,p_0}\left(X\,\partial_\varpi\Phi_0+Z\,\partial_z\Phi_0\right)\left(\frac{\partial_\varpi\left(\varpi B_\varphi\right)}{\varpi}\,X+\partial_z B_\varphi\,Z\right)\right\}\varpi\,\mathrm{d}\varpi\,\mathrm{d}z.\end{aligned} \tag{C.52}$$

This form matches the energy variation density given by Tayler (1973), remembering that the last two additional terms cancelled out in Tayler's approach.

The first additional term was caused by the extra terms appearing in $\mathcal{Y}_{\min}$ in equation (C.43) compared to Tayler's form. The second additional term arose directly from using the equilibrium equation of the unmagnetised system while inserting $\mathcal{Y}_{\min}$ into $\bar{\mathcal{E}}$.

Note that in Herbrik & Kokkotas (2017), the extra terms that appear in $\mathcal{Y}_{\min}$ when the magnetic field is not considered in the equilibrium equation, were not taken into account. Therefore, the analogue to equation (C.52) in Herbrik & Kokkotas (2017) only contained the second additional term, but not the first one.

C.2. Stars with purely poloidal magnetic fields

C.2.1. Construction of the toroidal coordinate system

The concrete structure of the poloidal magnetic field applied in Markey & Tayler (1973) is determined by the toroidal coordinate system given in equation (2.8). Its construction

is shown here.

The ansatz for the toroidal coordinate system are orthogonal curvilinear coordinates with the line and volume elements

$$\mathrm{d}s^2 = h_\psi^2\,\mathrm{d}\psi^2 + h_\varphi^2\,\mathrm{d}\varphi^2 + h_\chi^2\,\mathrm{d}\chi^2 \qquad \mathrm{d}V = J\,\mathrm{d}\psi\,\mathrm{d}\varphi\,\mathrm{d}\chi, \tag{C.53}$$

where the scale factors h_i and the Jacobi determinant J need to be determined. Cf. section A.3. Two of the coordinates are the stream function ψ as well as the azimuthal angle φ. Together with χ, the coordinate set $\{\psi, \varphi, \chi\}$ forms a right-handed system.

Geometrical reasons, cf. figure 2.4, and the definition of cylindrical coordinates (2.6), suggest the transformation equations

$$x = \varpi\cos\varphi \qquad y = \varpi\sin\varphi \qquad z = \bar{r}\sin\chi, \tag{C.54}$$

with

$$\varpi = R_\mathrm{tor} - \bar{r}\cos\chi \qquad \bar{r} = \bar{r}(\psi). \tag{C.55}$$

The scale factors are given by the general form (A.16) for orthogonal curvilinear coordinates. With equations (C.54) and (C.55) they are

$$h_\varphi = \left|\partial_\varphi \boldsymbol{r}\right| = \sqrt{(\partial_\varphi x)^2 + (\partial_\varphi y)^2 + (\partial_\varphi z)^2} = \varpi \tag{C.56a}$$

$$h_\chi = \left|\partial_\chi \boldsymbol{r}\right| = \sqrt{(\partial_\chi x)^2 + (\partial_\chi y)^2 + (\partial_\chi z)^2} = \bar{r}, \tag{C.56b}$$

where relation (A.25) has been applied.

The determination of h_ψ requires an assumption for the magnetic field: The magnetic flux through the torus spun by the toroidal coordinates is set to a specific value. The surface S be enclosed by the torus, as can be seen from figure 2.9a. It is located in the (ϖ, φ)-plane.

The magnetic flux through S along the stellar symmetry axis is

$$\Phi_\mathrm{magn} = \int \boldsymbol{B}\,\mathrm{d}\boldsymbol{S} = \iint \boldsymbol{B}\cdot\boldsymbol{n}\,\mathrm{d}S = \int_0^{2\pi}\int_0^{R_\mathrm{tor}-\bar{r}} B_\chi^{\chi=0}\,\varpi\,\mathrm{d}\varpi\,\mathrm{d}\varphi = 2\pi\int_0^{R_\mathrm{tor}-\bar{r}} B_\chi^{\chi=0}\,\varpi\,\mathrm{d}\varpi, \tag{C.57}$$

where $\boldsymbol{n}$ denotes the surface normal to S, and $B_\chi^{\chi=0}$ is the magnetic field strength in S, i.e. for $\chi = 0$. Here, we took into account the axisymmetry of the magnetic field, $\boldsymbol{B} = \boldsymbol{B}(\varpi, z)$ from equation (5.25).

Markey and Tayler set the magnetic flux to

$$\Phi_\mathrm{magn} \overset{!}{=} 2\pi\psi. \tag{C.58}$$

Thus, from equation (C.57),

$$\psi = \int B_\chi^{\chi=0}\, \varpi \,\mathrm{d}\varpi \qquad\qquad \mathrm{d}\psi = B_\chi^{\chi=0}\, \varpi \,\mathrm{d}\varpi = -B_\chi^{\chi=0}\,(R_\mathrm{tor} - \bar{r})\,\mathrm{d}\bar{r}. \tag{C.59}$$

Here, we applied relation (C.55) to receive for $\chi = 0$:

$$\mathrm{d}_{\bar{r}}\varpi\Big|_{\chi=0} = -\cos\chi\Big|_{\chi=0} = -1 \qquad\qquad \mathrm{d}\varpi\Big|_{\chi=0} = -\,\mathrm{d}\bar{r}. \tag{C.60}$$

Equation (C.59) provides a relation for the stream function at the position $\chi = 0$. However, in order to determine h_ψ, the dependence of $B_\chi(\bar{r})$ must be known. According to the flux conservation along each magnetic flux tube, Markey and Tayler choose the magnetic field as $B_\chi \sim 1/\varpi$.

With the assumption

$$B_\chi = \frac{B_\mathrm{pol}\,\bar{r}}{\varpi} = \frac{B_\mathrm{pol}\,\bar{r}}{R_\mathrm{tor} - \bar{r}\cos\chi}, \tag{C.61}$$

relation (C.59) can be evaluated for $\chi = 0$. Applying (C.55), it becomes

$$\mathrm{d}\psi = -B_\mathrm{pol}\,\frac{\bar{r}}{\varpi}\,(R_\mathrm{tor} - \bar{r})\,\mathrm{d}\bar{r} = -B_\mathrm{pol}\,\bar{r}\,\mathrm{d}\bar{r}. \tag{C.62}$$

Integration finally yields

$$\psi = -\int B_\mathrm{pol}\,\bar{r}\,\mathrm{d}\bar{r} = -\frac{1}{2}\,B_\mathrm{pol}\,\bar{r}^2 + C \qquad\qquad \bar{r} = \pm\sqrt{-\frac{2\psi}{B_\mathrm{pol}}}, \tag{C.63}$$

where the integration constant was set to zero.

Note that $\psi \le 0$, i.e. $\bar{r}$ is real everywhere. Further, the positive sign of the square root is chosen in order to achieve $\bar{r} > 0$. Then,

$$\partial_\psi \bar{r} = -\frac{1}{\bar{r}\,B_\mathrm{pol}} \tag{C.64}$$

follows from equation (C.63).

With this relation, the remaining scale factor h_ψ can be calculated, applying its definition (A.16), equations (C.54) and relation (A.25):

$$h_\psi = \sqrt{\left(\partial_\psi x\right)^2 + \left(\partial_\psi y\right)^2 + \left(\partial_\psi z\right)^2} \tag{C.65}$$

$$= \sqrt{\left(\partial_{\bar{r}} x\,\partial_\psi \bar{r}\right)^2 + \left(\partial_{\bar{r}} y\,\partial_\psi \bar{r}\right)^2 + \left(\partial_{\bar{r}} z\,\partial_\psi \bar{r}\right)^2} = \frac{1}{\bar{r}\,B_\mathrm{pol}} = \frac{1}{\varpi\,B_\chi}, \tag{C.66}$$

where the final step follows from choice (C.61) for the magnetic field.

Finally, the Jacobi determinant follows according to its definition in (A.16):

$$J = \det \begin{pmatrix} \frac{\cos\chi\cos\varphi}{B_{\mathrm{pol}}\,\bar{r}} & \frac{\cos\chi\sin\varphi}{B_{\mathrm{pol}}\,\bar{r}} & -\frac{\sin\chi}{B_{\mathrm{pol}}\,\bar{r}} \\ -(R_{\mathrm{tor}} - \bar{r}\cos\chi)\sin\varphi & (R_{\mathrm{tor}} - \bar{r}\cos\chi)\cos\varphi & 0 \\ \bar{r}\cos\varphi\,\sin\chi & \bar{r}\sin\varphi\,\sin\chi & \bar{r}\cos\chi \end{pmatrix} \tag{C.67}$$

$$= \frac{R_{\mathrm{tor}} - \bar{r}\cos\chi}{B_{\mathrm{pol}}} = \frac{\varpi}{B_{\mathrm{pol}}} = \frac{\bar{r}}{B_\chi}, \tag{C.68}$$

where relation (A.25) has been applied.

Choice (C.61) for the magnetic field ensures that the current density is uniform close to the neutral line.

According to Ampère's law (2.14d), applying relation (A.19) for the curl in curvilinear coordinates and with $\boldsymbol{B} = B_\chi\,\boldsymbol{e}_\chi$, the current density is

$$\boldsymbol{j} = \nabla \times \boldsymbol{B} = \begin{pmatrix} 0 \\ j_\varphi \\ 0 \end{pmatrix}, \tag{C.69}$$

with

$$j_\varphi = \frac{1}{h_\psi\,h_\chi}\left[\partial_\chi\left(h_\psi\,B_\psi\right) - \partial_\psi\left(h_\chi\,B_\chi\right)\right] = -\frac{\partial_\psi\left(h_\chi\,B_\chi\right)}{h_\psi\,h_\chi} = -\frac{\varpi}{J}\,\partial_\psi\left(JB_\chi^2\right). \tag{C.70}$$

For the last step, the scale factors (C.56) and (C.66) as well as the magnetic field choice (C.61) have been inserted.

Finally, according to the chain rule and with (C.64), (C.68) as well as

$$\partial_\psi\varpi = \partial_{\bar{r}}\varpi\,\partial_\psi\bar{r} = \frac{\cos\chi}{\bar{r}\,B_{\mathrm{pol}}}, \tag{C.71}$$

the current density becomes

$$j_\varphi = -B_{\mathrm{pol}}^2\,\partial_\psi\left(\frac{\bar{r}^2}{\varpi}\right) = -B_{\mathrm{pol}}^2\left(\frac{2\,\bar{r}}{\varpi}\,\partial_\psi\bar{r} - \frac{\bar{r}^2}{\varpi^2}\,\partial_\psi\varpi\right) = \frac{B_{\mathrm{pol}}}{\varpi}\left(\frac{\bar{r}\,\cos\chi}{\varpi} + 2\right). \tag{C.72}$$

At the neutral line,

$$j_\varphi\left(\varpi = R_{\mathrm{tor}}, \bar{r} = 0\right) = \frac{2\,B_{\mathrm{tor}}}{R_{\mathrm{tor}}}. \tag{C.73}$$

The current density is constant, i.e. it is consistent as demanded above.

C.2.2. Construction of the explicit displacement field

Geometrical analogy to the toroidal field case

In section 2.3.3, it was briefly mentioned that the displacement field choice (2.125) for the poloidally magnetised star is geometrically equivalent to choice (2.121) of the toroidal field case. This circumstance will be discussed here in greater detail.

The Tayler instability for both magnetic field components is expected to be located close to the magnetic field's symmetry axis.

This symmetry axis also represents the axis of reference for a displacement field which is appropriate for a Tayler instability investigation. In the case of the toroidal field, the symmetry axis of the magnetic field corresponds to the stellar symmetry axis. For the poloidal field, the magnetic field is symmetrical with respect to the neutral line.

That means, the displacement field reference axis in the toroidal, respectively poloidal field case, is the stellar symmetry axis, respectively the neutral line.

With this analogy, the correspondence of the displacement field components between both cases can be understood.

The displacement field component parallel to the reference axis is ξ_z in cylindrical coordinates for the toroidal case, and ξ_φ in toroidal coordinates for the poloidal case.

The component tangential to the right-handed circle around the reference axis is ξ_φ in cylindrical coordinates for the toroidal case, and ξ_χ in toroidal coordinates for the poloidal case.

The absolute value of the final component describes the distance to the reference axis. It is ξ_ϖ in cylindrical coordinates for the toroidal case, and $\xi_{\bar{r}}$ in toroidal coordinates for the poloidal case.

The dependency on the exponential function persists in both cases, as chosen by (2.43), cf. figure 2.14. Furthermore, the prefactor for the azimuthal component is proportional to i/m for both cases, in order to keep the expression real when ξ_φ is derived with respect to φ.

Incompressible class of perturbations

The constraints (5.28) Markey and Tayler impose on the displacement field imply an incompressible character of the applied perturbation mode, which can be shown as follows.

The Eulerian density perturbation caused by the displacement field is given by equation (2.101a), and can be split into two terms by relation (A.1). For polytropes, the equation of state (2.22) and the hydrostatic equilibrium equation (2.29) yield relation (C.125) for the connection of the density gradient and the gravitational field vector (2.17).

Thus,

$$\delta\rho = -\nabla(\rho_0\boldsymbol{\xi}) + \mathcal{O}(\boldsymbol{\xi}^2) = -\rho_0\,(\nabla\cdot\boldsymbol{\xi}) - \boldsymbol{\xi}\cdot(\nabla\rho_0) + \mathcal{O}(\boldsymbol{\xi}^2) = -\rho_0\,(\nabla\cdot\boldsymbol{\xi}) - \frac{\rho_0^2}{\Gamma_0\, p_0}\,\boldsymbol{\xi}\cdot\boldsymbol{g} + \mathcal{O}(\boldsymbol{\xi}^2) = 0, \tag{C.74}$$

where the final step follows with the conditions $\boldsymbol{\xi}\cdot\boldsymbol{g} = 0$ and $\nabla\cdot\boldsymbol{\xi} = 0$ from (5.28).

The imposed displacement field is divergence free and the density gradient in the polytropic star is purely radial and points towards the stellar centre. It is therefore parallel to the gravitational field vector.

With the assumption that the displacement field is perpendicular to $\boldsymbol{g}$, i.e. $\boldsymbol{\xi} \perp \boldsymbol{e}_r$, the Euler perturbation $\delta\rho$ vanishes for the applied displacement field. The imposed perturbation does not change the fluid density at a fixed local position.

Therefore, $\boldsymbol{\xi}$ as chosen by assumptions (5.28), purely shifts fluid elements and does not compress them.

Displacement field ansatz

The conditions (5.28) discussed in the previous section translate into relations between the $\boldsymbol{\xi}$-defining functions when choice (2.125) for the displacement field is inserted.

The requirement $\boldsymbol{\xi} \cdot \boldsymbol{g} \stackrel{!}{=} 0$ gives

$$X\,\partial_\psi \Phi_0 + \varpi\, B_\chi^2 Z\,\partial_\chi \Phi_0 \stackrel{!}{=} 0. \tag{C.75}$$

Applying formula (A.18) for the divergence in orthogonal coordinates, as well as relations (C.56), (C.66) and (A.25), the divergence of the displacement field is

$$\nabla \cdot \boldsymbol{\xi} = B_{\mathrm{pol}} \frac{\partial_\psi \left(\varpi\, \bar{r}\, \xi_\psi\right)}{\varpi} + \frac{\partial_\varphi\, \xi_\varphi}{\varpi} + \frac{\partial_\chi \left(\varpi\, \xi_\chi\right)}{\varpi\, \bar{r}} \tag{C.76}$$

$$= \left\{ \frac{B_{\mathrm{pol}}}{\varpi}\, \partial_\psi \left(J\, X\right) - Y + \frac{B_{\mathrm{pol}}}{\varpi}\, \partial_\chi Z \right\} \mathrm{e}^{\mathrm{i}m\varphi}, \tag{C.77}$$

where the poloidal field choice (C.61) and the Jacobi determinant (C.68) have been used. Beyond that, we took into account that $\bar{r} = \bar{r}(\psi)$ and that X, Y and Z are independent of φ.

Finally, the requirement for the divergence-free displacement field gives

$$\partial_\psi \left(J\, X\right) - J\, Y + \partial_\chi Z \stackrel{!}{=} 0. \tag{C.78}$$

Conditions (C.75) and (C.78) allow it to express the $\boldsymbol{\xi}$-defining functions Y and Z in terms of X.

For geometrical reasons, illustrated in figure C.1, the gravitational field vector components obey the following relation

$$\frac{g_\psi}{g_\chi} = \frac{R_{\mathrm{tor}}\, \cos\chi - \bar{r}}{R_{\mathrm{tor}}\, \sin\chi}. \tag{C.79}$$

This relation holds for arbitrary displacement field choices under the assumption that the gravitational field vector is purely radial, i.e. $\boldsymbol{g} = (g_r, 0, 0)$ in spherical coordinates.

Applying the magnetic field choice (C.61), Z follows from condition (C.75):

$$Z = -X\, \frac{\varpi\, \left(R_{\mathrm{tor}}\, \cos\chi - \bar{r}\right)}{\bar{r}^2\, B_{\mathrm{pol}}^2\, R_{\mathrm{tor}}\, \sin\chi}. \tag{C.80}$$

From that, the derivative

$$\partial_\chi Z = \frac{1}{\bar{r}^2\, B_{\mathrm{pol}}^2\, R_{\mathrm{tor}}} \left[\varpi\, \left(R_{\mathrm{tor}}\, \cos\chi - \bar{r}\right) \left(\frac{X\, \cos\chi}{\sin^2\chi} - \frac{\partial_\chi X}{\sin\chi} \right) - X \left(R_{\mathrm{tor}} \left(\bar{r}\, \cos\chi - \varpi\right) - \bar{r}^2 \right) \right] \tag{C.81}$$

can be calculated.

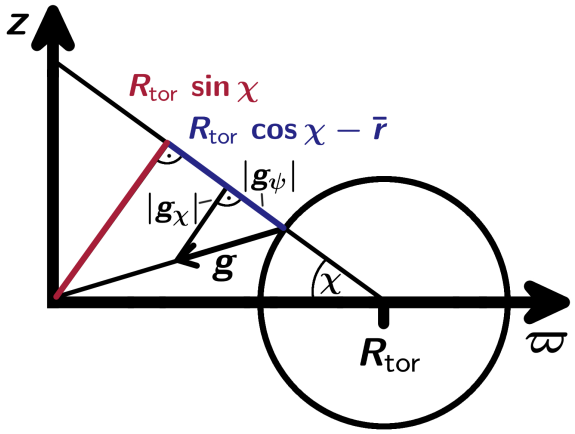

Figure C.1.: Geometrical consideration of gravitational field vector components, see equation (C.79).

Besides this, from equation (C.67),

$$\partial_\psi J = \frac{\cos\chi}{\bar{r}\, B_{\mathrm{pol}}^2} \tag{C.82}$$

follows.

With the use of relations (C.81) and (C.82), Y is explicitly given by condition (C.78):

$$Y = \partial_\psi X + \frac{1}{J}\left(X\,\partial_\psi J + \partial_\chi Z\right). \tag{C.83}$$

According to relations (C.80) and (C.83), Y and Z are completely determined by the choice of X.

Displacement field localisation

The displacement field needs to be localised in order to avoid surface integral contributions to the energy variation, cf. appendix section B.4.

Due to the system geometry, the most straightforward way is to localise the displacement field to a torus including the neutral line, cf. figure 2.16. For an effective localisation, the displacement field must vanish naturally at the torus surface ψ_{tor}, or it must be orthogonal to the torus surface normal, as shown in equation (B.21).

Relations (C.80), (C.81) and (C.83) imply that $Y = Y(X)$ and $Z = Z(X)$. More precisely, Y and Z vanish for all (ψ,χ) where $X = 0$ and $\partial_\psi X = 0$. Therefore, the localisation can be achieved with an appropriate choice for X.

We choose the ansatz

$$X = f(\psi,\chi)\,(\psi - \psi_{\mathrm{tor}})^2, \tag{C.84}$$

with

$$\partial_\psi X = \partial_\psi f(\psi,\chi)\,(\psi - \psi_{\mathrm{tor}})^2 + 2\,f(\psi,\chi)\,(\psi - \psi_{\mathrm{tor}}). \tag{C.85}$$

The square ensures that both X as well as $\partial_\psi X$, and by that also Y and Z, vanish at the torus surface.

The remaining function $f(\psi,\chi) \neq 0$ can generally depend on ψ and χ. It needs to be chosen in such a way that it does not compensate the proportionality of $X \sim (\psi - \psi_{\mathrm{tor}})^2$, nor cause any kind of singularity.

Displacement field parameter choice

Once ansatz (C.84) has been chosen in order to localise the displacement field, an appropriate choice for function $f(\psi,\chi)$ is required.

Besides fulfilling the conditions mentioned above, it needs to guarantee that the Tayler instability is detectable.

In the subsequent section it will be seen that with displacement field choice (2.125), there are particular choices of X, Y and Z for which the energy variation δW does not depend on the magnetic field strength B_{pol}. In this case, the magnetic field amplitude can be factored out of the integrand and the structural character of the Tayler instability becomes obvious. Our choice of function $f(\psi,\chi)$ shall enable this scenario.

From equation (5.39), the magnetic field dependence of the $\boldsymbol{\xi}$-defining functions and their derivatives required for an instability proof can be deduced:

$$\delta W = \frac{\pi}{2} \iint \Bigg\{ \underbrace{\frac{(\partial_\chi X)^2}{\varpi\, \bar{r}^2}}_{\mathrm{I}} + \underbrace{\frac{\varpi\, B_{\mathrm{pol}}^2}{m^2}\,(\partial_\chi Y)^2}_{\mathrm{II}} + \frac{\bar{r}^2\, B_{\mathrm{pol}}^2}{\varpi}\,(\underbrace{\partial_\psi X}_{\mathrm{III}} \underbrace{-Y}_{\mathrm{IV}})^2 + B_{\mathrm{pol}}\,\frac{2\,R_{\mathrm{tor}} - \bar{r}\,\cos\chi}{\varpi^2} \Bigg(\underbrace{X\,\partial_\psi X}_{\mathrm{V}} \underbrace{-X\,Y}_{\mathrm{VI}} + \underbrace{\frac{B_{\mathrm{pol}}}{\varpi}\,Z\,\partial_\chi X}_{\mathrm{VII}} \Bigg) \Bigg\}\, \mathrm{d}\varpi\, \mathrm{d}z. \tag{C.86}$$

Note that this form of the energy variation has been derived with the displacement field assumptions made in this section so far. It is presented here only to motivate the choice of $f(\psi,\chi)$. Its derivation will be shown in section C.2.3.

Expression (C.86) provides the following conditions for the magnetic field to cancel out of the integrand:

$$\begin{aligned} \mathrm{I} &\Rightarrow \partial_\chi X \overset{!}{\sim} 1 & \qquad \mathrm{V} &\overset{\mathrm{III}}{\Rightarrow} X \overset{!}{\sim} 1 \\ \mathrm{II} &\Rightarrow \partial_\chi Y \overset{!}{\sim} B_{\mathrm{pol}}^{-1} & \qquad \mathrm{VI} &\overset{\mathrm{IV}}{\Rightarrow} X \overset{!}{\sim} 1 \\ \mathrm{III} &\Rightarrow \partial_\psi X \overset{!}{\sim} B_{\mathrm{pol}}^{-1} & \qquad \mathrm{VII} &\overset{\mathrm{I}}{\Rightarrow} Z \overset{!}{\sim} B_{\mathrm{pol}}^{-2}. \\ \mathrm{IV} &\Rightarrow Y \overset{!}{\sim} B_{\mathrm{pol}}^{-1} \end{aligned} \tag{C.87}$$

For the requirements following from terms V, VI and VII, the conditions derived from terms III, IV and I have been used. Note that the mixed binomial term of III and IV also

requires $\partial_\psi X\, Y \overset{!}{\sim} B_{\rm pol}^{-2}$. However, this condition is already covered by conditions III and IV.

For the purpose of deriving conditions for $f(\psi,\chi)$ from relations (C.87), the $B_{\rm pol}$- and $f(\psi,\chi)$-dependency of X, Y, Z and their derivatives needs to be known.

Applying ansatz (C.84), we must consider the implicit dependency of ψ on the field strength $B_{\rm pol}$. The radial distance $\bar{r}$, on the contrary, is a pure geometrical quantity. Therefore, ψ is expressed in terms of $\bar{r}$, according to (2.8).

Then,

$$(\psi-\psi_{\rm tor})^2 = \frac{B_{\rm pol}^2}{4}\left(\bar{r}^2-\bar{r}_{\rm tor}^2\right)^2 \qquad\qquad \bar{r}_{\rm tor} = \sqrt{-\frac{2\,\psi_{\rm tor}}{B_{\rm pol}}}. \tag{C.88}$$

We insert ansatz (C.84) into the formulas (C.80) and (C.83) for the $\boldsymbol{\xi}$-defining functions. With relation (C.88), this provides the explicit dependencies of X, Y, Z and their derivatives on $B_{\rm pol}$ and $f(\psi,\chi)$:

$$\begin{aligned}
X &= \frac{B_{\rm pol}^2}{4} f\left(\bar{r}^2-\bar{r}_{\rm tor}^2\right)^2\\
\partial_\psi X &= \frac{B_{\rm pol}^2}{4}\partial_\psi f\left(\bar{r}^2-\bar{r}_{\rm tor}^2\right)^2 - B_{\rm pol} f\left(\bar{r}^2-\bar{r}_{\rm tor}^2\right)\\
\partial_\chi X &= \frac{B_{\rm pol}^2}{4}\partial_\chi f\left(\bar{r}^2-\bar{r}_{\rm tor}^2\right)^2\\
\partial_{\chi\psi} X &= \frac{B_{\rm pol}^2}{4}\partial_{\chi\psi} f\left(\bar{r}^2-\bar{r}_{\rm tor}^2\right)^2 - B_{\rm pol}\,\partial_\chi f\left(\bar{r}^2-\bar{r}_{\rm tor}^2\right)\\
Y &= \frac{1}{\varpi\, B_{\rm pol}}\left(X\,\frac{\cos\chi}{\bar{r}} + B_{\rm pol}^2\,\partial_\chi Z\right) + \partial_\psi X\\
\partial_\chi Y &= -\frac{X}{B_{\rm pol}}\frac{\sin\chi}{\varpi}\left(\frac{\cos\chi}{\varpi}+\frac{1}{\bar{r}}\right) + \frac{\partial_\chi X}{B_{\rm pol}}\frac{\cos\chi}{\varpi\,\bar{r}} + \partial_\chi\partial_\psi X - B_{\rm pol}\,\partial_\chi Z\,\frac{\bar{r}\sin\chi}{\varpi^2} + B_{\rm pol}\,\frac{\partial_\chi^2 Z}{\varpi}\\
Z &= -f\left(\bar{r}^2-\bar{r}_{\rm tor}^2\right)^2\,\frac{\varpi\,(R_{\rm tor}\cos\chi-\bar{r})}{4\,\bar{r}^2\,R_{\rm tor}\sin\chi}\\
\partial_\chi Z &= \frac{\left(\bar{r}^2-\bar{r}_{\rm tor}^2\right)^2}{4\,\bar{r}^2\,R_{\rm tor}}\left[f\,\frac{R_{\rm tor}^2+\bar{r}^2-\bar{r}\,R_{\rm tor}\cos\chi\left(\sin^2\chi+2\right)}{\sin^2\chi} - \partial_\chi f\,\frac{\varpi\,(R_{\rm tor}\cos\chi-\bar{r})}{\sin\chi}\right]\\
\partial_\chi^2 Z &= \frac{\left(\bar{r}^2-\bar{r}_{\rm tor}^2\right)^2}{4\,\bar{r}^2\,R_{\rm tor}}\left[f\,\frac{\bar{r}\,R_{\rm tor}\left(\cos^4\chi+3\right)-2\,\cos\chi\left(\bar{r}^2+R_{\rm tor}^2\right)}{\sin^3\chi}\right.\\
&\qquad \left. +\partial_\chi f\,\frac{2\left(\bar{r}^2+R_{\rm tor}^2\right)-2\,\bar{r}\,R_{\rm tor}\cos\chi\left(2+\sin^2\chi\right)}{\sin^2\chi} - \partial_\chi^2 f\,\frac{\varpi\,(R_{\rm tor}\cos\chi-\bar{r})}{\sin\chi}\right],
\end{aligned} \tag{C.89}$$

where the second derivatives are denoted by $\partial_{ij}\equiv\partial_i\partial_j$ and $\partial_i^2=\partial_i\partial_i$.

With expressions (C.89), the requirements (C.87) for the $\boldsymbol{\xi}$-defining functions translate into conditions for $f(\psi, \chi)$:

$$
\begin{array}{lllll}
\text{I} & \Rightarrow & & \partial_\chi f \overset{!}{\sim} B_{\text{pol}}^{-2} & \\
\text{II} & \Rightarrow & X \overset{!}{\sim} 1 \quad \rightarrow & f \overset{!}{\sim} B_{\text{pol}}^{-2} & \\
 & \Rightarrow & \partial_\chi X \overset{!}{\sim} 1 \quad \rightarrow & \partial_\chi f \overset{!}{\sim} B_{\text{pol}}^{-2} & \\
 & \Rightarrow & \partial_{\chi,\psi} X \overset{!}{\sim} B_{\text{pol}}^{-1} \quad \rightarrow & \partial_{\chi\psi} f \overset{!}{\sim} B_{\text{pol}}^{-3}, \quad \partial_\chi f \overset{!}{\sim} B_{\text{pol}}^{-2} & \\
 & \Rightarrow & \partial_\chi Z \overset{!}{\sim} B_{\text{pol}}^{-2} \quad \rightarrow & f \overset{!}{\sim} B_{\text{pol}}^{-2}, \quad \partial_\chi f \overset{!}{\sim} B_{\text{pol}}^{-2} & \\
 & \Rightarrow & \partial_\chi^2 Z \overset{!}{\sim} B_{\text{pol}}^{-2} \quad \rightarrow & f \overset{!}{\sim} B_{\text{pol}}^{-2}, \quad \partial_\chi f \overset{!}{\sim} B_{\text{pol}}^{-2}, & \partial_\chi^2 f \overset{!}{\sim} B_{\text{pol}}^{-2} \\
\text{III} & \Rightarrow & & \partial_\psi f \overset{!}{\sim} B_{\text{pol}}^{-3}, \quad f \overset{!}{\sim} B_{\text{pol}}^{-2} & \\
\text{IV} & \Rightarrow & X \overset{!}{\sim} 1 \quad \rightarrow & f \overset{!}{\sim} B_{\text{pol}}^{-2} & \\
 & \Rightarrow & \partial_\chi Z \overset{!}{\sim} B_{\text{pol}}^{-2} \quad \rightarrow & f \overset{!}{\sim} B_{\text{pol}}^{-2}, \quad \partial_\chi f \overset{!}{\sim} B_{\text{pol}}^{-2} & \\
 & \Rightarrow & \partial_\psi X \overset{!}{\sim} B_{\text{pol}}^{-1} \quad \rightarrow & \partial_\psi f \overset{!}{\sim} B_{\text{pol}}^{-3}, \quad f \overset{!}{\sim} B_{\text{pol}}^{-2} & \\
\text{V} & \Rightarrow & & f \overset{!}{\sim} B_{\text{pol}}^{-2} & \\
\text{VI} & \Rightarrow & & f \overset{!}{\sim} B_{\text{pol}}^{-2} & \\
\text{VII} & \Rightarrow & & f \overset{!}{\sim} B_{\text{pol}}^{-2}. &
\end{array}
\tag{C.90}
$$

As can be seen, all conditions from different terms are consistent.

Summarising, function $f(\psi, \chi)$ must be chosen under the conditions

$$
f \overset{!}{\sim} B_{\text{pol}}^{-2} \qquad \partial_\psi f \overset{!}{\sim} B_{\text{pol}}^{-3} \qquad \partial_\chi f \overset{!}{\sim} B_{\text{pol}}^{-2} \qquad \partial_{\chi\psi} f \overset{!}{\sim} B_{\text{pol}}^{-3} \qquad \partial_\chi^2 f \overset{!}{\sim} B_{\text{pol}}^{-2}. \tag{C.91}
$$

For the sake of comparability of this work with Markey & Tayler (1973), we choose

$$
f(\psi, \chi) = \frac{X_0 \sin\chi}{B_{\text{pol}}^2}. \tag{C.92}
$$

That way, our choice of X is equivalent to the form in Markey and Tayler, with the additional localisation factor $(\psi - \psi_{\text{tor}})^2$ and the poloidal field dependency B_{pol}^{-2}.

Thus,

$$
\partial_\psi f = 0 \qquad \partial_\chi f = \frac{X_0 \cos\chi}{B_{\text{pol}}^2} \qquad \partial_{\chi\psi} f = 0. \tag{C.93}
$$

Applying choice (C.92) with (C.93) to (C.89), the explicit form of X, Y and Z presented in equation (5.31) follows.

Finally, according to equations (C.86), (C.87) and (C.90), the $\boldsymbol{\xi}$-defining functions can be redefined in such a way that the magnetic field cancels out of the integrand:

$$\begin{aligned} f_{\mathrm{B}} &\equiv B_{\mathrm{pol}}^2 f & \left(\partial_\psi X\right)_{\mathrm{B}} &\equiv B_{\mathrm{pol}}\, \partial_\psi X \\ X_{\mathrm{B}} &\equiv X & \left(\partial_\chi X\right)_{\mathrm{B}} &\equiv \partial_\chi X \\ Y_{\mathrm{B}} &\equiv B_{\mathrm{pol}}\, Y & \left(\partial_\chi Y\right)_{\mathrm{B}} &\equiv B_{\mathrm{pol}}\, \partial_\chi Y \\ Z_{\mathrm{B}} &\equiv B_{\mathrm{pol}}^2 Z & \left(\partial_\chi \partial_\psi X\right)_{\mathrm{B}} &\equiv B_{\mathrm{pol}}\, \partial_\chi \partial_\psi X. \end{aligned} \tag{C.94}$$

The form of the energy variation following from that will be shown in the subsequent section.

C.2.3. Derivation of the explicit form for the energy variation

In this section, the energy variation (2.116) with (2.117), describing polytropes in Cowling approximation, is simplified for the specific case of poloidally magnetised stars. The assumptions used for the poloidal field case are made by Markey & Tayler (1973) and they are presented in section 5.2.

The derivation of the final form slightly differs from the procedure presented in Markey & Tayler (1973).

As for the toroidal field case, we will use an actually complex displacement field, in contrast to Markey and Tayler, and take the real part ensuring the physical meaningfulness of δW over the total integrand. The appearance of an additional factor in the integrand caused by this procedure is explained in the appendix section A.5.4.

Further, the definition of ξ_φ given in (5.27b) factorises the imaginary unit. This ansatz will facilitate a straightforward and consistent description of X, Y and Z concerning their real and imaginary parts. In contrast, Markey and Tayler utilise an imaginary $\boldsymbol{\xi}$-defining function $Y^{\mathrm{MT}} = iY_I^{\mathrm{MT}}$ with $\xi_\varphi^{\mathrm{MT}} = \frac{\varpi Y}{m}\, \mathrm{e}^{\mathrm{i}m\varphi}$.

Applying assumptions (5.28), the general form of the energy variation reduces to its magnetic part (2.117a).

In toroidal coordinates (2.8), set up in section C.2.1, we first apply the poloidal magnetic field choice (5.25) to receive

$$\boldsymbol{\xi} \times \boldsymbol{B} = \begin{pmatrix} \xi_\varphi B_\chi \\ -\xi_\psi B_\chi \\ 0 \end{pmatrix}. \tag{C.95}$$

With the scale factors, given in (C.56) and (C.66), and the expression of the curl in toroidal coordinates from equation (A.19), it is

$$\delta B_\psi = \frac{1}{h_\varphi h_\chi}\left[\partial_\varphi\left(h_\chi \left(\boldsymbol{\xi}\times\boldsymbol{B}\right)_\chi\right) - \partial_\chi\left(h_\varphi \left(\boldsymbol{\xi}\times\boldsymbol{B}\right)_\varphi\right)\right] = \frac{1}{\varpi B_\chi J}\,\partial_\chi\left(\varpi B_\chi \xi_\psi\right) \tag{C.96a}$$

$$\delta B_\varphi = \frac{1}{h_\psi h_\chi}\left[\partial_\chi\left(h_\psi \left(\boldsymbol{\xi}\times\boldsymbol{B}\right)_\psi\right) - \partial_\psi\left(h_\chi \left(\boldsymbol{\xi}\times\boldsymbol{B}\right)_\chi\right)\right] = \frac{\varpi}{J}\,\partial_\chi\left(\frac{\xi_\varphi}{\varpi}\right) \tag{C.96b}$$

$$\delta B_\chi = \frac{1}{h_\psi h_\varphi}\left[\partial_\psi\left(h_\varphi \left(\boldsymbol{\xi}\times\boldsymbol{B}\right)_\varphi\right) - \partial_\varphi\left(h_\psi \left(\boldsymbol{\xi}\times\boldsymbol{B}\right)_\psi\right)\right] = -B_\chi\left[\partial_\chi\left(\varpi B_\chi \xi_\psi\right) - \partial_\varphi\left(\frac{\xi_\varphi}{\varpi}\right)\right]. \tag{C.96c}$$

In the last step, relations $J = \varpi/B_{\mathrm{pol}}$ and $\bar{r}\,B_{\mathrm{pol}} = \varpi\,B_\chi$ from equations (C.68) and (C.66) have been applied. Inserting the magnetic field perturbation (C.96) and the current density given by equations (C.69) and (C.72), the energy variation density becomes

$$\begin{aligned}\mathcal{E} = \frac{1}{4}\,\Re\Bigg\{ & \frac{\partial_\chi\left(\varpi\,B_\chi\,\xi_\psi^*\right)\,\partial_\chi\left(\varpi\,B_\chi\,\xi_\psi\right)}{\varpi^2\,B_\chi^2\,J^2} + \frac{\varpi^2}{J^2}\,\partial_\chi\left(\frac{\xi_\varphi^*}{\varpi}\right)\partial_\chi\left(\frac{\xi_\varphi}{\varpi}\right) \\ & + B_\chi^2\left[\partial_\psi\left(\varpi\,B_\chi\,\xi_\psi^*\right) + \partial_\varphi\left(\frac{\xi_\varphi^*}{\varpi}\right)\right]\left[\partial_\psi\left(\varpi\,B_\chi\,\xi_\psi^*\right) + \partial_\varphi\left(\frac{\xi_\varphi^*}{\varpi}\right)\right] \\ & - \frac{\partial_\psi\left(B_\chi^2\,J\right)}{J}\left[\varpi\,B_\chi\,\xi_\psi^*\left[\partial_\psi\left(\varpi\,B_\chi\,\xi_\psi\right) + \partial_\varphi\left(\frac{\xi_\varphi}{\varpi}\right)\right] + \frac{\xi_\chi^*}{B_\chi}\,\partial_\chi\left(\varpi\,B_\chi\,\xi_\psi\right)\right]\Bigg\}.\end{aligned} \tag{C.97}$$

Compared to Markey & Tayler (1973), this expression contains the additional factor 1/2 because the real part has not been evaluated yet, cf. appendix section A.5.4.

Compared to the original general expression (2.117a), the prefactor $1/(4\,\pi)$ is neglected here because it stemmed from the non-rationalised form of the Maxwell equations (2.14). Here, we switched to rationalised units in accordance with Markey and Tayler's approach.

Once the poloidal field choice (2.125) for the displacement field has been inserted, the exponential functions cancel out and the φ-integral can be evaluated to give

$$\begin{aligned}\delta W = \frac{\pi}{2}\iint \Re\Bigg\{ & \frac{\partial_\chi X^*\,\partial_\chi X}{\varpi^2\,B_\chi^2\,J} + \frac{\varpi^2\,\partial_\chi Y^*\,\partial_\chi X}{m^2\,J} + B_\chi^2\,J\left(\partial_\psi X - Y\right)\left(\partial_\psi X^* - Y^*\right) \\ & - \partial_\psi\left(B_\chi^2\,J\right)\left(X\,\partial_\psi X^* - X\,Y^* + \frac{Z}{J}\,\partial_\chi X^*\right)\Bigg\}\,\mathrm{d}\psi\,\mathrm{d}\chi,\end{aligned} \tag{C.98}$$

where relation (2.116) has been used.

According to relation (A.29), this integrand can be split into two complex conjugated parts with

$$\delta W = \frac{\pi}{4}\iint \Re\left\{M + M^*\right\}\,\mathrm{d}\psi\,\mathrm{d}\chi \tag{C.99}$$

and

$$\begin{aligned}M = & \frac{\partial_\chi X^*\,\partial_\chi X}{\varpi^2\,B_\chi^2\,J} + \frac{\varpi^2\,\partial_\chi Y^*\,\partial_\chi X}{m^2 J} + B_\chi^2\,J\left(\partial_\psi X - Y\right)\left(\partial_\psi X^* - Y^*\right) \\ & - \partial_\psi\left(B_\chi^2\,J\right)\left(X\,\partial_\psi X^* - X\,Y^* + \frac{Z}{J}\,\partial_\chi X^*\right).\end{aligned} \tag{C.100}$$

Applying relation (A.31), it becomes obvious that the integrand can be expressed in terms of the real part only:

$$\delta W = \frac{\pi}{2}\iint M_R\,\mathrm{d}\psi\,\mathrm{d}\chi \tag{C.101}$$

with

$$M_R = \frac{(\partial_\chi X_R)^2}{\varpi^2 B_\chi^2 J} + \frac{\varpi^2}{m^2 J} (\partial_\chi Y_R)^2 + B_\chi^2 J \left(\partial_\psi X_R - Y_R\right)^2 \\ - \partial_\psi \left(B_\chi^2 J\right) \left(X_R \partial_\psi X_R - X_R Y_R + \frac{Z_R \partial_\chi X_R}{J}\right). \tag{C.102}$$

In this step, the complex scalar products have been evaluated with the use of expression (A.29).

Next, the magnetic field choice (C.61) is inserted and the integral is expressed in cylindrical coordinates, using the volume elements (2.7) and (2.10):

$$\delta W = \frac{\pi}{2} \iint \left\{ \frac{(\partial_\chi X)^2}{\varpi \bar{r}^2} + \frac{\varpi B_{\mathrm{pol}}^2}{m^2} (\partial_\chi Y)^2 + \frac{\bar{r}^2 B_{\mathrm{pol}}^2}{\varpi} \left(\partial_\psi X - Y\right)^2 \right. \\ \left. + B_{\mathrm{pol}} \frac{2 R_{\mathrm{tor}} - \bar{r} \cos\chi}{\varpi^2} \left(X \partial_\psi X - X Y + \frac{B_{\mathrm{pol}}}{\varpi} Z \partial_\chi X\right) \right\} \mathrm{d}\varpi \, \mathrm{d}z. \tag{C.103}$$

Here, we transformed the expression back to cylindrical coordinates because we will perform the numerical integration in ϖ and z.

Afterwards, the explicit choices (C.89), (C.92) and (C.93) for the $\boldsymbol{\xi}$-defining functions constructed in the previous section are applied. Expression (C.103) motivates the redefinition of the $\boldsymbol{\xi}$-defining functions shown in equation (C.94), that aims on the cancellation of the magnetic field amplitude B_{pol} in all integrand terms.

Thus, the energy variation finally becomes

$$\delta W = \frac{\pi}{2} \iint \left\{ \frac{(\partial_\chi X)_B^2}{\varpi \bar{r}^2} + \frac{\varpi}{m^2} (\partial_\chi Y)_B^2 + \frac{\bar{r}^2}{\varpi} \left(\left(\partial_\psi X\right)_B - Y_B\right)^2 \right. \\ \left. + \frac{2 R_{\mathrm{tor}} - \bar{r} \cos\chi}{\varpi^2} \left(X_B \left(\partial_\psi X\right)_B - X_B Y_B + \frac{Z_B \left(\partial_\chi X\right)_B}{\varpi}\right) \right\} \mathrm{d}\varpi \, \mathrm{d}z. \tag{C.104}$$

C.2.4. Analytical stability consideration

The analytic instability consideration presented in Markey & Tayler (1973) proves that the system is unstable in the limit of infinitely high mode indices m.

The integrand expression is subsequently simplified, where term II in expression (C.86) vanishes due to its proportionality $\mathcal{E}_{II} \sim 1/m^2$. With the assumption $X^{\mathrm{MT}} = X_0^{\mathrm{MT}} \sin\chi$, the ψ- and χ-integrals in (C.103) are evaluated analytically to receive a simple expression for δW:

$$\delta W^{\mathrm{MT}} = -\frac{2\pi \left(X_0^{\mathrm{MT}}\right)^2}{a^2 B_{\mathrm{pol}} R_{\mathrm{tor}}^3} \left(2 - \frac{2 - a^2}{2\sqrt{1 - a^2}}\right) \qquad a \equiv \frac{\bar{r}}{R_{\mathrm{tor}}}. \tag{C.105}$$

According to

$$\frac{2\,\pi\,\left(X_0^{\mathrm{MT}}\right)^2}{a^2\,B_{\mathrm{pol}}\,R_{\mathrm{tor}}^3} > 0, \tag{C.106}$$

the onset of the instability for $\delta W^{\mathrm{MT}} < 0$ is given by

$$2 - \frac{2-a^2}{2\sqrt{1-a^2}} > 0 \qquad \Rightarrow \qquad a^4 + 12a^2 - 12 < 0 \qquad \Rightarrow \qquad a < \sqrt{0.928} = 0.963. \tag{C.107}$$

Therefore, in the limit of $m \to \infty$, the instability occurs in the neighbourhood of the neutral line.

The infinite mode index corresponds to displacement fields with an infinitesimally small perturbation length scale in φ-direction compared to the length of the neutral line.

In this case, the curvature of the torus including the neutral line is negligible and the system is equivalent to the toroidal field case with the straight cylindrical fluid discharge.

This result has been derived for each magnetic surface ψ = const separately. For finite m, the positive definite term

$$\mathcal{E}_{II} = \frac{\varpi\,B_{\mathrm{pol}}^2}{m^2}\,(\partial_\chi Y)^2 \tag{C.108}$$

increases the energy variation. Single magnetic surfaces do not provide unstable modes.

C.3. Stars with mixed magnetic fields and stratification

C.3.1. Construction of the displacement field

This section outlines the construction of the displacement field shown by Akgün et al. (2013).

Analogy to the toroidal field perturbation

The magnetic field component that is tested for stability in the mixed field system is the toroidal one. The utilised displacement field (2.130) is therefore equivalent to the displacement field applied in the toroidal field case (2.121).

This can be seen by transforming the vector components of the mixed field displacement field choice into cylindrical coordinates via (A.26). The mixed field choice becomes

$$\xi_\varpi = \tilde{R}(r,\vartheta)\,r\sin^2\vartheta\,\mathrm{e}^{\mathrm{i}m\varphi} + \tilde{S}\,r\sin\vartheta\,\cos\vartheta\,\mathrm{e}^{\mathrm{i}m\varphi} \tag{C.109a}$$

$$\xi_\varphi = \mathrm{i}\,\tilde{T}(r,\vartheta)\,r\sin\vartheta\,\mathrm{e}^{\mathrm{i}m\varphi} \tag{C.109b}$$

$$\xi_z = \tilde{R}(r,\vartheta)\,r\sin\vartheta\,\cos\vartheta\,\mathrm{e}^{\mathrm{i}m\varphi} - \tilde{S}\,r\sin^2\vartheta\,\mathrm{e}^{\mathrm{i}m\varphi}\,. \tag{C.109c}$$

According to the transformation equations (2.4) and (2.6) of spherical and cylindrical coordinates, it is

$$\varpi = r\,\sin\vartheta \qquad\qquad z = r\,\cos\vartheta. \tag{C.110}$$

Therefore, comparison of the coefficients between the toroidal field choice (2.121) and (C.109) provides a relation between the $\boldsymbol{\xi}$-defining functions X, Y, Z and $\tilde{R}$, $\tilde{S}$, $\tilde{T}$.

Choices (2.121) and (2.130) are identical if

$$X = \left(\varpi\,\tilde{R} + z\,\tilde{S}\right)\frac{\varpi}{r} \tag{C.111}$$

$$Y = m\,\varpi\,\tilde{T} \tag{C.112}$$

$$Z = \left(z\,\tilde{R} - \varpi\,\tilde{S}\right)\frac{\varpi}{r}. \tag{C.113}$$

Displacement field ansatz and localisation

As explained in section 5.3, the $\boldsymbol{\xi}$-defining functions $\tilde{R}$, $\tilde{S}$ and $\tilde{T}$ are chosen in such a way that the Tayler instability of the toroidal magnetic field is detectable in the absence of the poloidal field component, $\eta_{\mathrm{pol}} = 0$.

For their construction, the sum of the toroidal and hydrostatic energy variation density contributions (C.120a) and (C.120c) must be negative. These expressions are briefly derived in the subsequent section C.3.2. However, note that they have been derived by applying the general displacement field ansatz (2.130) only, without further assumptions on $\tilde{R}$, $\tilde{S}$ or $\tilde{T}$.

First, the energy variation integrand (C.122) for the purely toroidally magnetised star is minimised with respect to the ξ_φ-defining function $\tilde{T}$, analogously to the $\mathcal{E}(Y)$-minimisation in section 5.1.

Second, the condition

$$\partial_r\left(r\,\tilde{R}\right) + \partial_\vartheta \tilde{S} = 0 \tag{C.114}$$

for $\tilde{R}$ and $\tilde{S}$ ensures that the positive definite term in the energy variation density vanishes. It is fulfilled by the ansatz

$$\tilde{R} = \frac{\partial_\vartheta \Pi}{x} \qquad\qquad \tilde{S} = -\partial_x \Pi, \tag{C.115}$$

with a scalar function $\Pi(x,\vartheta)$. Remember the definition of the dimensionless radial coordinate $x \equiv r/R$.

Finally, the displacement field is localised.

According to equation (B.21), the surface integral contributions are negligible if $\boldsymbol{\xi}$ smoothly goes to zero at the boundary of the localisation region. However, Akgün et al. argue that Tayler's localisation choice (5.6) of the toroidal field case is not applicable here. The superimposed poloidal magnetic field component requires a continuous behaviour of the displacement field at the boundaries of the localisation area in order to avoid singularities. Therefore, $\Pi(x,\vartheta)$ is chosen in such a way that the displacement field vanishes at the boundary, while its derivatives remain finite:

$$\Pi(x,\vartheta) = \frac{\xi_0}{R}\left(1 - \bar{\chi}^2(x,\vartheta)\right)^\sigma \qquad \bar{\chi}^2(x,\vartheta) = \left(\frac{x - x_0}{\delta_r}\right)^2 + \left(\frac{\vartheta - \vartheta_0}{\delta_\vartheta}\right)^2. \tag{C.116}$$

Combining assumptions (C.115) and (C.116), the explicit choice for $\boldsymbol{\xi}$ given in equation (5.46) follows.

C.3.2. Derivation of the explicit form for the energy variation

In the mixed field case, we express the energy variation by the compact form (5.54) of Akgün et al. (2013).

The derivation of this expression starting from the general form (4.47) with (4.48) for the energy variation and the energy variation densities is outlined here.

As explained in section 3, Akgün et al. redefine the energy variation density contributions to a toroidal, poloidal, mixed magnetic and hydrostatic part, cf. equations (5.49) and (5.50). Their form is given by expressions (4.48).

The magnetic contribution (4.48a) can be rearranged applying identity (A.4). With relation (2.14d) and the mixed magnetic field ansatz $\boldsymbol{B} = \boldsymbol{B}_{\mathrm{tor}} + \boldsymbol{B}_{\mathrm{pol}}$, the separate magnetic contributions are

$$\mathcal{E}_{\mathrm{tor}} = \frac{1}{16\,\pi}\,\Re\left\{\delta\boldsymbol{B}^*_{\mathrm{tor}}\cdot\delta\boldsymbol{B}_{\mathrm{tor}} - \boldsymbol{\xi}^*\times\left(\nabla\times\boldsymbol{B}_{\mathrm{tor}}\right)\cdot\delta\boldsymbol{B}_{\mathrm{tor}}\right\} \tag{C.117}$$

$$\mathcal{E}_{\mathrm{pol}} = \frac{1}{16\,\pi}\,\Re\left\{\delta\boldsymbol{B}^*_{\mathrm{pol}}\cdot\delta\boldsymbol{B}_{\mathrm{pol}} - \boldsymbol{\xi}^*\times\left(\nabla\times\boldsymbol{B}_{\mathrm{pol}}\right)\cdot\delta\boldsymbol{B}_{\mathrm{pol}}\right\} \tag{C.118}$$

$$\begin{aligned}\mathcal{E}_{\mathrm{cross}} = \frac{1}{16\,\pi}\,\Re\Big\{&\delta\boldsymbol{B}^*_{\mathrm{tor}}\cdot\delta\boldsymbol{B}_{\mathrm{pol}} + \delta\boldsymbol{B}^*_{\mathrm{pol}}\cdot\delta\boldsymbol{B}_{\mathrm{tor}} - \boldsymbol{\xi}^*\times\left(\nabla\times\boldsymbol{B}_{\mathrm{tor}}\right)\cdot\delta\boldsymbol{B}_{\mathrm{pol}}\\ &- \boldsymbol{\xi}^*\times\left(\nabla\times\boldsymbol{B}_{\mathrm{pol}}\right)\cdot\delta\boldsymbol{B}_{\mathrm{tor}}\Big\}.\end{aligned} \tag{C.119}$$

Note that according to the definition of $\delta W^{\mathrm{A}} = 1/2\iiint \mathcal{E}^{\mathrm{A}}\,\mathrm{d}V$ in Akgün et al. (2013), the energy variation we defined in equation (2.116) contains an additional factor of 1/2: $\mathcal{E} = \mathcal{E}^{\mathrm{A}}/2$.

The hydrostatic part follows from the fluid and Cowling gravitational contribution (4.48b) and (4.48c). The transformation from $\delta W_{\mathrm{fluid}}$ and $\delta W^{\mathrm{Cowl}}_{\mathrm{grav}}$ to the form used by Akgün et al. is shown in the appendix section C.3.3.

With the usage of the mixed magnetic field choice (2.33) and some notational definitions given by equations (5.51) and (5.52), the newly defined energy variation contributions become

$$\begin{aligned}\mathcal{E}_{\mathrm{tor}} = \frac{1}{16\,\pi}\,\Re\Bigg\{&\left(\frac{\beta\left(\partial_r\left(r\,\tilde{R}\right)+\partial_\vartheta\tilde{S}\right)}{r}+\frac{\Lambda(\beta)}{2}\right)^2 - \left(\frac{m\,\beta\,\tilde{T}}{\varpi}+\frac{\Lambda(\beta)}{2}\right)^2\\ &+\frac{m^2\,\beta^2}{\varpi^2}\left(\tilde{R}^2+\tilde{S}^2+\tilde{T}^2\right)\Bigg\}\end{aligned} \tag{C.120a}$$

$$\begin{aligned}\mathcal{E}_{\mathrm{pol}} = \frac{1}{16\,\pi}\,\Re\Bigg\{&\left(\frac{m\,\partial_r\alpha\,\tilde{T}-\partial_r\left(\varpi\,\Lambda(\alpha)\right)}{\varpi}+\frac{\Delta^*\alpha\,\tilde{R}}{2}\right)^2 + \left(\frac{m\,\partial_\vartheta\alpha\,\tilde{T}-\partial_\vartheta\left(\varpi\,\Lambda(\alpha)\right)}{\varpi\,r}\right.\\ &\left.+\frac{\Delta^*\alpha\,\tilde{S}}{2}\right)^2 + \left(\frac{\partial_\vartheta\alpha\,\partial_r\tilde{T}-\partial_r\alpha\,\partial_\vartheta\tilde{T}}{r}\right)^2 - \frac{\left(\Delta^*\alpha\right)^2}{4}\left(\tilde{R}^2+\tilde{S}^2\right)\Bigg\}\end{aligned} \tag{C.120b}$$

$$\mathcal{E}_{\mathrm{hyd}} = \frac{\varpi^2}{4}\,\Re\left\{\Gamma_1\,p_0\,D_m^2 + \left(\Lambda(p_0)-\rho_0\,\Lambda(\Phi_0)\right)\,D_m - \Lambda(\rho_0)\,\Lambda(\Phi_0)\right\} \tag{C.120c}$$

and

$$\mathcal{E}_{\text{cross}} = 0. \tag{C.121}$$

Analogously to the previous applications, the $\boldsymbol{\xi}$-defining functions can be chosen real without restriction, which causes the mixed magnetic term (C.121) to vanish. Also, quantities D_m and Λ that depend on the $\boldsymbol{\xi}$-defining functions are real with this choice and the complex scalar products in (C.120a), (C.120b) and (C.120c) can be replaced by products of the real parts of the functions. Since all remaining functions are fully real, no prefactors arise when the real parts are evaluated.

With (C.120), the energy variation density for the purely toroidally magnetised star can be expressed as

$$\mathcal{E}_{\text{tor}} + \mathcal{E}_{\text{hyd}} = \frac{1}{4}\left\{E_0 + E_1\, m\,\tilde{T} + E_2\,\left(m\,\tilde{T}\right)^2\right\}, \tag{C.122}$$

where the prefactors E_0, E_1 and E_2 are defined in equation (5.55) with (5.56) and (5.57).

Next, the minimising value (5.47) for $\tilde{T}$ is inserted to receive the energy variation density of the toroidally magnetised neutron star that has been minimised with respect to ξ_φ:

$$\mathcal{E}_{\text{tor}}(\tilde{R},\tilde{S},\tilde{T}_{\min}) + \mathcal{E}_{\text{hyd}}(\tilde{R},\tilde{S},\tilde{T}_{\min}) = \frac{E_0}{4} - \frac{E_1^2}{16\,E_2}, \tag{C.123}$$

for $m \neq 0$.

Note that in accordance to section 5.1, the integrand has been minimised for the toroidally magnetised star only, and not for the mixed field case.

Finally, the poloidal field contribution (C.120b) is added to receive the explicit form of the energy variation for the mixed field case, given by equation (5.54).

C.3.3. Verification of the energy variation considering stratification

According to equation (2.78) with expressions (4.6) and (2.115), the total energy variation of an unmagnetised stratified star in Cowling approximation is

$$\mathcal{E}_{\text{fluid}} + \mathcal{E}_{\text{grav}}^{\text{Cowl}} = \frac{1}{4}\,\Re\left\{\Gamma_1\, p_0\,(\nabla\cdot\boldsymbol{\xi}^*)\,(\nabla\cdot\boldsymbol{\xi}) + \boldsymbol{\xi}\cdot\nabla p_0\,(\nabla\cdot\boldsymbol{\xi}^*) \pm \boldsymbol{\xi}\cdot\nabla\Phi_0\,(\nabla\cdot(\rho_0\,\boldsymbol{\xi}^*))\right\}. \tag{C.124}$$

The gradients of fluid pressure and gravitational potential can be rewritten according to relation (A.24) and the hydrostatic equilibrium equation (2.29):

$$\nabla p_0 = \frac{\Gamma_0\, p_0}{\rho_0}\,\nabla\rho_0 \qquad\qquad \nabla\Phi_0 = \pm\frac{\nabla p_0}{\rho_0} = \pm\frac{\Gamma_0\, p_0}{\rho_0^2}\,\nabla\rho_0. \tag{C.125}$$

Thus,

$$\mathcal{E}_{\text{fluid}} + \mathcal{E}_{\text{grav}}^{\text{Cowl}} = \frac{1}{4}\,\Re\left\{\Gamma_1\, p_0\,(\nabla\cdot\boldsymbol{\xi}^*)\,(\nabla\cdot\boldsymbol{\xi}) + \frac{\Gamma_0\, p_0}{\rho_0}\,\boldsymbol{\xi}\cdot\nabla\rho_0\left(\nabla\cdot\boldsymbol{\xi}^* + \frac{\nabla\cdot(\rho_0\,\boldsymbol{\xi}^*)}{\rho_0}\right)\right\}. \tag{C.126}$$

Applying identity (A.1) on $\boldsymbol{\xi}\cdot\nabla\rho_0 = \nabla\cdot(\rho_0\,\boldsymbol{\xi}) - \rho_0\,(\nabla\cdot\boldsymbol{\xi})$, finally gives

$$\begin{aligned}\mathcal{E}_{\text{fluid}} + \mathcal{E}^{\text{Cowl}}_{\text{grav}} = \frac{1}{4}\,\Re\Big\{&\Gamma_1\,p_0\,(\nabla\cdot\boldsymbol{\xi}^*)\;(\nabla\cdot\boldsymbol{\xi}) + \frac{\Gamma_0\,p_0}{\rho_0}\;(\nabla\cdot\boldsymbol{\xi}^*)\;(\nabla\cdot(\rho_0\,\boldsymbol{\xi})) \\ &- \Gamma_0\,p_0\,(\nabla\cdot\boldsymbol{\xi}^*)\;(\nabla\cdot\boldsymbol{\xi}) + \frac{\Gamma_0\,p_0}{\rho_0^2}\;(\nabla\cdot(\rho_0\,\boldsymbol{\xi}^*))\;(\nabla\cdot(\rho_0\,\boldsymbol{\xi})) \\ &- \frac{\Gamma_0\,p_0}{\rho_0}\,(\nabla\cdot\boldsymbol{\xi})\,(\nabla\cdot(\rho_0\,\boldsymbol{\xi}^*))\Big\}\end{aligned} \tag{C.127}$$

$$= \frac{1}{4}\,\Re\left\{(\Gamma_1-\Gamma_0)\;p_0\,(\nabla\cdot\boldsymbol{\xi}^*)\;(\nabla\cdot\boldsymbol{\xi}) + \frac{\Gamma_0\,p_0}{\rho_0^2}\;(\nabla\cdot(\rho_0\,\boldsymbol{\xi}^*))\;(\nabla\cdot(\rho_0\,\boldsymbol{\xi}))\right\}. \tag{C.128}$$

Note that in the last step, the terms cancelled out according to relation (A.29). The terms are identical independent of which factor is complex conjugated.

Equation (C.128) is equivalent to the expression given by Akgün et al. (2013) for the energy variation of a non-magnetised star with stratification in Cowling approximation. For comparison, consider the differing notation for the polytropic indices used by Akgün et al. shown in table E.3. Further remember $\mathcal{E} = \mathcal{E}^{\text{A}}/2$. Applying the magnetic field assumption (5.43) as well as notations (5.51) and (5.52), the explicit expression (C.120c) for the hydrostatic contribution follows from (C.128).

C.3.4. Analytical stability consideration

The analytic stability consideration Akgün et al. (2013) provide for the purely toroidally magnetised star is equivalent to the one given by Tayler (1973) and shown in section C.1.1.

The minimised energy variation density for the toroidally magnetised star (C.123) with $m \neq 0$ can be rewritten in the following form:

$$\mathcal{E}_{\text{tor}} + \mathcal{E}_{\text{fluid}} + \mathcal{E}^{\text{Cowl}}_{\text{grav}} = \frac{\beta^2}{16\,\pi}\left(D_0 - \frac{2\,\Lambda(\varpi)}{\varpi}\right)^2 + \frac{\varpi^2}{4}\left(\bar{A}_m\,\tilde{R}^2 + \bar{B}_m\,\tilde{R}\,\tilde{S} + \bar{C}_m\,\tilde{S}^2\right). \tag{C.129}$$

In analogy to expression (C.1), the first term is positive definite, while the remaining formula can be expressed in a quadratic form, where the prefactors $\bar{A}_m$, $\bar{B}_m$ and $\bar{C}_m$ are equivalent to the prefactors given in (C.2). The derived stability criterion is thus identical to (C.3).

The analytical stability consideration Akgün et al. give for the neutron star with the mixed magnetic field is based on approximations of the energy variation densities (C.120). Their explicit forms (5.60a), (5.60b) and (5.58) with (5.56) and (5.57) are first approximated similar to the poloidal contribution (5.61).

Afterwards, the separate contributions to the energy variation are estimated under the assumption of a vanishing extent of the localisation region. That way, the integrals can be calculated analytically.

The general stability criterion for the mixed field star,

$$\delta W = \delta W_{\text{tor}} + \delta W_{\text{pol}} + \delta W_{\text{hyd}} \overset{!}{>} 0, \tag{C.130}$$

translates into a critical poloidal field strength which is necessary to stabilise the toroidal field instability that is present for the applied displacement field mode:

$$\left(\frac{b_{\mathrm{pol}}}{b_{\mathrm{tor}}}\right)^2 > \delta_\vartheta^2 \, \frac{I_\sigma}{J_\sigma} \left[\frac{k_{\mathrm{tor}}}{k_{\mathrm{pol}}} \left(\frac{\delta_r}{\delta_\vartheta}\right)^2 - \frac{k_{\mathrm{hyd}}}{k_{\mathrm{pol}}} \, \frac{\Gamma_1 - \Gamma_0}{\Gamma_0} \, \frac{8\,\pi\,p_c}{B_0^2\, b_{\mathrm{tor}}^2} \left(\frac{\delta_r}{\delta_\vartheta}\right)^4 \right], \tag{C.131}$$

where

$$b_{\mathrm{tor}} \equiv 0.0254\,\eta_{\mathrm{tor}} \qquad\qquad b_{\mathrm{pol}} \equiv \frac{35}{4}\,\eta_{\mathrm{pol}} \tag{C.132}$$

and

$$I_\sigma \equiv \frac{\pi\,\sigma}{2} \left(\sigma - \frac{1}{2}\right)^{-1} \qquad J_\sigma \equiv \frac{\pi\,\sigma^2}{6}\,(\sigma - 1) \left(\sigma - \frac{1}{2}\right)^{-1} \left(\sigma - \frac{3}{2}\right)^{-1}. \tag{C.133}$$

The numerical constants k_{tor}, k_{pol} and k_{hyd} were defined as proportionality factors of the approximated energy variation contributions δW_{tor}, δW_{pol} and δW_{hyd}. According to Akgün et al. (2013), they are given by

$$k_{\mathrm{tor}} = -\frac{\pi\,R^2}{2}\,\bar{C}_m(x_0, \vartheta_0)\, x_0^4 \sin^3\vartheta_0\, \frac{8\,\pi}{B_0^2\, b_{\mathrm{tor}}^2} \tag{C.134a}$$

$$k_{\mathrm{pol}} = \frac{\pi\,R^2}{2}\,\bar{D}_m(x_0, \vartheta_0)\, x_0^6 \sin^3\vartheta_0\, \frac{8\,\pi}{B_0^2\, b_{\mathrm{pol}}^2} \tag{C.134b}$$

$$k_{\mathrm{hyd}} = \frac{\pi\,R^2}{2}\,\bar{A}_m(x_0, \vartheta_0)\, x_0^2 \sin^3\vartheta_0\, \frac{1}{p_c}\, \frac{\Gamma_0}{\Gamma_1 - \Gamma_0}. \tag{C.134c}$$

Note that p_c is the central pressure in the star. The function $\bar{D}_m(x, \vartheta)$ has been defined for $\mathcal{E}_{\mathrm{pol}}$ in analogy to the quadratic form coefficients $\bar{A}_m$, $\bar{B}_m$ and $\bar{C}_m$ in $\mathcal{E}_{\mathrm{tor}}$ and $\mathcal{E}_{\mathrm{hyd}}$.

As it can be seen from (C.134), the numerical constants k_{tor}, k_{pol} and k_{hyd} solely depend on constants, such as the localisation parameters, the stellar radius, the central pressure and – via $\bar{A}_m$, $\bar{B}_m$, $\bar{C}_m$ and $\bar{D}_m$ – on values of the equilibrium quantities $Q_0(x_0, \vartheta_0)$ at the localisation position of the displacement field. These values $Q_0(x_0, \vartheta_0)$ are given by the analytical relations Akgün et al. choose for the density, mass and pressure distribution and the gravitational potential.

Note that in contrast to k_{tor} and k_{pol}, k_{hyd} additionally depends on the polytropic index Γ_1 of the perturbations.

The stability criterion (C.131) contains system parameters on the right hand side. In order to find the absolute minimum field strength η_{pol} for which the toroidal field Tayler instability can be stabilised, Akgün et al. next maximise this right hand side with respect to the appearing parameters σ and $\delta_r/\delta_\vartheta$.

The maximising values are

$$\sigma = \frac{3+\sqrt{3}}{2} \approx 2.37 \tag{C.135}$$

$$\left(\frac{\delta_r}{\delta_\vartheta}\right)^2 = \frac{k_{\mathrm{tor}}}{2\,k_{\mathrm{hyd}}(\Gamma_1)}\,\frac{b_{\mathrm{tor}}^2\,B_0^2}{8\,\pi\,p_c}\,\frac{\Gamma_0}{\Gamma_1-\Gamma_0}, \tag{C.136}$$

where we keep in mind that k_{hyd} in expression (C.136) depends on Γ_1 itself.

Applying the maximising parameter choices, the stability criterion (C.131) becomes for the extremal case

$$\left(\frac{b_{\mathrm{pol}}}{b_{\mathrm{tor}}}\right)^2 > \delta_\vartheta^2\,\frac{I_\sigma}{J_\sigma}\,\frac{k_{\mathrm{tor}}^2}{4\,k_{\mathrm{pol}}\,k_{\mathrm{hyd}}(\Gamma_1)}\,\frac{B_0^2\,b_{\mathrm{tor}}^2}{8\,\pi\,p_c}\,\frac{\Gamma_0}{\Gamma_1-\Gamma_0}. \tag{C.137}$$

With relation (C.132), the critical minimum poloidal field strength for arbitrary choices of Γ_1 is thus given by

$$\eta_{\mathrm{pol}}^{\mathrm{crit}} = \frac{4}{35}\,\delta_\vartheta\,\frac{k_{\mathrm{tor}}}{\sqrt{4\,k_{\mathrm{pol}}\,k_{\mathrm{hyd}}(\Gamma_1)}}\,\sqrt{\frac{I_\sigma}{J_\sigma}\,\frac{B_0^2\,b_{\mathrm{tor}}^2}{8\,\pi\,p_c}\,\frac{\Gamma_0}{\Gamma_1-\Gamma_0}}. \tag{C.138}$$

Finally, applying the explicit parameters chosen by Akgün et al. and presented in section 5.3, the stability criterion reads

$$\eta_{\mathrm{pol}} > \eta_{\mathrm{pol}}^{\mathrm{crit}} = 6.759\times10^{-5}\,\delta_\vartheta\,\sqrt{\frac{\Gamma_0\,\Gamma_1}{\Gamma_1-\Gamma_0}}. \tag{C.139}$$

Note that Akgün et al. assume relations (C.135) and (C.136) for deriving the stability criterion (C.139). If the results produced with the semi-analytic method shall be comparable to this analytic stability criterion, assumptions (C.135) and (C.136) must be used in this work as well.

This implies that the localisation area needs to be adjusted each time the polytropic index Γ_1 of the perturbations is varied. The detailed discussion on this fact is given in the computation section of 5.3.

For the sake of completeness, with the parameter choices made by Akgün et al. and shown in section 5.3, the numerical constants (C.134) become

$$k_{\mathrm{tor}} = 1.057\,199 \qquad k_{\mathrm{pol}} = 0.083\,23 \qquad k_{\mathrm{hyd}} = \frac{7.715\,55}{\Gamma_1}. \tag{C.140}$$

The central pressure can be expressed as

$$p_c = 10^6\,\frac{B_0^2}{8\,\pi}. \tag{C.141}$$

D. Illustration of numerical routines

In this chapter, numerical methods applied in this work are illustrated.

D.1. Cubic spline interpolation in one dimension

In this section, the interpolation method shown in section 4.3.2 is explained.

Cubic spline interpolation approximates a required function locally using different third degree polynomials inside different intervals. The interval boundaries correspond to the grid points of given values and are labelled by the index $s = 0, ..., n$. The polynomials of neighbouring intervals as well as their first and second derivatives are matched at these grid points, achieving high accuracy with comparably low effort. In certain cases, the interpolation can even be exact.

Generally, a system quantity $Q(r)$ in the interval $[r_s, r_{s+1}]$ is approximated by

$$Q(r) = a_s(r - r_s)^3 + b_s(r - r_s)^2 + c_s(r - r_s) + d_s \qquad h_s = r_{s+1} - r_s, \tag{D.1}$$

where h_s denotes the interval width. The derivatives are

$$\mathrm{d}_r Q(r) = 3\,a_s(r - r_s)^2 + 2\,b_s(r - r_s) + c_s \tag{D.2}$$

$$d_r^2 Q(r) = 6\,a_s(r - r_s) + 2\,b_s. \tag{D.3}$$

The function values at the grid points, their first and second derivatives are denoted as

$$Q_s \equiv Q(r_s) \qquad F_s \equiv \mathrm{d}_r Q(r)\Big|_{r_s} \qquad S_s \equiv d_r^2 Q(r)\Big|_{r_s}. \tag{D.4}$$

The interpolation coefficients for the interval $[r_s, r_{s+1}]$ can be determined by evaluating the interpolation formula (D.1) for Q and S at the grid points r_s and r_{s+1}:

$$Q_s = d_s \quad \Rightarrow \quad d_s = Q_s \tag{D.5a}$$

$$Q_{s+1} = h_s^3\,a_s + h_s^2\,b_s + h_s\,c_s + d_s \quad \Rightarrow \quad c_s = \frac{Q_{s+1} - Q_s}{h_s} - \frac{2\,h_s\,S_s + h_s\,S_{s+1}}{6} \tag{D.5b}$$

$$S_s = 2\,b_s \quad \Rightarrow \quad b_s = \frac{S_s}{2} \tag{D.5c}$$

$$S_{s+1} = 6\,h_s\,a_s + 2\,b_s \quad \Rightarrow \quad a_s = \frac{S_{s+1} - S_s}{6\,h_s}. \tag{D.5d}$$

The coefficients are thus implicitly given by the function values Q_s, Q_{s+1} and their second derivatives S_s, S_{s+1}.

The second derivatives can be calculated matching F_s given by (D.2) at the boundary

point r_s of the intervals $[s-1, s]$ and $[s, s+1]$:

$$c_s = 3\,a_{s-1}\,(r_s - r_{s-1})^2 + 2\,b_{s-1}\,(r_s - r_{s-1}) + c_{s-1}. \tag{D.6}$$

Inserting (D.5) and the definition of h_s from (D.1) provides a relation between S_i and Q_i:

$$h_{s-1}\,S_{s-1} \;+\; 2\,(h_{s-1} + h_s)\,S_s \;+\; h_{s+1}\,S_{s+1} = 6\left(\frac{Q_{s+1} - Q_s}{h_s} - \frac{Q_s - Q_{s-1}}{h_{s-1}}\right), \quad s = 1, ..., n-1. \tag{D.7}$$

Equation (D.7) represents a linear system of equations for $S_1, ..., S_{n-1}$.

Due to the lack of outer neighbours, the outermost intervals require a special treatment at $s = 0$ and $s = n$. Reasonable values S_0 and S_n where the polynomials can be matched to need to be found.

In the neutron star, S_0 and S_n are not explicitly known for all system quantities. We thus use a linear interpolation to calculate S_0 and S_n from their next and second-next neighbours S_1, and S_2, as well as S_{n-1} and S_{n-2}:

$$\frac{S_1 - S_0}{h_0} = \frac{S_2 - S_1}{h_1} \qquad\qquad \frac{S_n - S_{n-1}}{h_{n-1}} = \frac{S_{n-1} - S_{n-2}}{h_{n-2}}. \tag{D.8}$$

Thus,

$$S_0 = \frac{(h_0 + h_1)\,S_1 - h_0\,S_2}{h_1} \qquad S_n = \frac{(h_{n-2} + h_{n-1})\,S_{n-1} - h_{n-1}\,S_{n-2}}{h_{n-2}}. \tag{D.9}$$

In total, the cubic splines method requires the solution of a linear system of equations with $n+1$ equations for $n+1$ unknowns $S_0, ..., S_n$.

The total cubic spline interpolation procedure using linear extrapolation can then be summarised by equations (D.1), (D.5), the boundary conditions

$$\frac{(h_0 + h_1)\,(h_0 + 2h_1)}{h_1}\,S_1 + \frac{h_1^2 - h_0^2}{h_1}\,S_2 = 6\left(\frac{Q_2 - Q_1}{h_1} - \frac{Q_1 - Q_0}{h_0}\right) \tag{D.10a}$$

$$\frac{h_{n-2}^2 - h_{n-1}^2}{h_{n-2}}\,S_{n-2} + \frac{(h_{n-1} + h_{n-2})\,(h_{n-1} + 2\,h_{n-2})}{h_{n-2}}\,S_{n-1} = 6\left(\frac{Q_n - Q_{n-1}}{h_{n-1}} - \frac{Q_{n-1} - Q_{n-2}}{h_{n-2}}\right) \tag{D.10b}$$

and the linear system of equations for $S_1, ..., S_{n-1}$:

$$\left(\begin{array}{cccccc|c} h_1 & 2\,(h_1 + h_2) & h_2 & 0 & ... & 0 & 6\left(\frac{Q_3 - Q_2}{h_2} - \frac{Q_2 - Q_1}{h_1}\right) \\ 0 & h_2 & 2\,(h_2 + h_3) & h_3 & ... & 0 & 6\left(\frac{Q_4 - Q_3}{h_3} - \frac{Q_3 - Q_2}{h_2}\right) \\ ... & ... & ... & ... & ... & ... & ... \\ 0 & 0 & 0 & 0 & ... & h_{n-2} & 6\left(\frac{Q_{n-1} - Q_{n-2}}{h_{n-2}} - \frac{Q_{n-2} - Q_{n-3}}{h_{n-3}}\right) \end{array}\right). \tag{D.10c}$$

E. List of notations

Physical scalar quantities

A	Displacement field localisation area where $\boldsymbol{\xi} \neq 0$
$\bar{A}$	Quadratic form prefactor of $\mathcal{E}$ in the toroidal field case
$\bar{A}_m$	Quadratic form prefactor of $\mathcal{E}$ in the mixed field case
a_s	Cubic splines interpolation coefficient
B_{pol}	Poloidal magnetic field amplitude
B_{tor}	Toroidal magnetic field amplitude
$B_{\mathrm{tor}}^{\mathrm{crit}}$	Critical toroidal magnetic field strength for instability in the toroidal field case
$B_{\mathrm{pol}}^{\mathrm{max}}$	Maximum of the poloidal magnetic field amplitude
$B_{\mathrm{tor}}^{\mathrm{max}}$	Maximum of the toroidal magnetic field amplitude
B_0	Overall magnetic field amplitude in the mixed field case
$\bar{B}$	Quadratic form prefactor of $\mathcal{E}$ in the toroidal field case
$\bar{B}_m$	Quadratic form prefactor of $\mathcal{E}$ in the mixed field case
b_j	Prefactors Runge-Kutta method
b_s	Cubic splines interpolation coefficient
$\bar{C}$	Quadratic form prefactor of $\mathcal{E}$ in the toroidal field case
$\bar{C}_m$	Quadratic form prefactor of $\mathcal{E}$ in the mixed field case
$c_{n,l,m}$	Expansion coefficients for an expansion in stellar eigenfunctions
c_s	Cubic splines interpolation coefficient
c^p	Specific heat capacity for isobaric processes
c^V	Specific heat capacity for isochoric processes
D_m	Abbreviatory notation in the mixed field case
$\bar{D}$	Prefactor of a contribution to $\mathcal{E}$ in the toroidal field case
$\bar{D}_m$	Prefactor of a contribution to $\mathcal{E}$ in the mixed field case
d_s	Cubic splines interpolation coefficient
E	Energy
E_{grav}	Gravitational potential energy
E_{int}	Internal energy
E_{kin}	Kinetic energy
E_{pol}	Energy variation density contribution in the mixed field case, cf. (5.58)
E_0	Energy variation density contribution in the mixed field case, cf. (5.55)
E_1	Energy variation density contribution in the mixed field case, cf. (5.55)
E_2	Energy variation density contribution in the mixed field case, cf. (5.55)
e^-	Electron
$F(r)$	Abbreviatory function for $J(r)/r^{l+1} - r^l\, K(r)$
$f(x)$	$\boldsymbol{B}$-defining dimensionless function in the mixed field case
$f(\psi, \chi)$	$\boldsymbol{\xi}$-defining function in the poloidal field case
f_k^q	2D-Simpson approximated inner integrand

$f_\lambda(r, r')$	Radial part of the $1/\lvert\boldsymbol{r} - \boldsymbol{r}'\rvert$-expansion
G_k	2D-Simpson approximated outer integrand
$g(r)$	$\boldsymbol{\xi}$-defining function for the expression by spherical harmonics
h	Typical scale height of stellar physical quantities
h_r	Runge-Kutta step width
h_z	Simpson interval width along z
h_ϑ	Simpson interval width along ϑ
h_ϖ	Simpson interval width along ϖ
$h(r)$	$\boldsymbol{\xi}$-defining function for the expression by spherical harmonics
$I(r)$	Radial function describing $\delta W_{\text{grav}}^{\text{nC}}$ in the mixed field case
I_σ	Abbreviatory notation in the mixed field case, cf. equation (C.133)
$J(r)$	Radial function describing $\delta\Phi$
J_σ	Abbreviatory notation in the mixed field case, cf. equation (C.133)
$K(r)$	Radial function describing $\delta\Phi$
k	Simpson grid point index for ϖ
k_A	A-defining constant in the toroidal field case
k_{br}	Proportionality constant stellar spin-down
k_{hyd}	Proportionality constant of δW_{hyd} in the mixed field case
k_j	Intermediate values Runge-Kutta method
k_{pol}	Proportionality constant of δW_{pol} in the mixed field case
k_{tor}	Proportionality constant of δW_{tor} in the mixed field case
L	Luminosity
l	Polar angular mode index
l_A	A-defining constant in the toroidal field case
M	Stellar mass
m	Azimuthal angular mode index
$m(r)$	Mass enclosed by a sphere with radius r
m^{crit}	Critical angular mode index for instability in the poloidal field case
m_n	Neutron mass
n	Neutron
n	Temporal mode index
n_r	Number of Simpson intervals for the $J(r)$-, $K(r)$-calculation
n_z	Number of Simpson intervals along z
n_ϑ	Number of Simpson intervals along ϑ
n_ϖ	Number of Simpson intervals along ϖ
n_{br}	Braking index
p	Fluid pressure
p_ε	Vacuum pressure level for numerical computations
p^+	Proton
Q	Generally perturbed system quantity
Q^{A}	Quantity Q as defined by Akgün et al. (2013)
Q_{B}	$\boldsymbol{\xi}$-defining quantity independent of B_{pol} in the poloidal field case
Q_c	Quantity at the stellar centre $Q_c = Q_0(r = 0)$
Q^{E}	Euler perturbed quantity
Q_I	Imaginary part of quantity Q
Q^{L}	Lagrange perturbed quantity

Q^{MT}	Quantity Q as defined by Markey & Tayler (1973)
Q_R	Real part of quantity Q
Q_0	Equilibrium quantity
$\tilde{Q}$	Dimensionless quantity
$\tilde{Q}^*$	Dimensionless geometrised quantity
q	Simpson grid point index for z
q_e	Electric charge
R	Stellar radius
R_S	Schwarzschild radius
R_{tor}	Distance between the torus centre and the stellar symmetry axis, 'major radius'
R_∞	Radiation radius
$\tilde{R}$	$\boldsymbol{\xi}$-defining function in the mixed field case
r_c	Central radial coordinate for numerical computations
r_0	A-defining constant in the mixed field case
$\bar{r}$	Torus radius, 'minor radius'
$S(\mathrm{star})$	Two dimensional stellar integration area for constant φ
$\tilde{S}$	$\boldsymbol{\xi}$-defining function in the mixed field case
s	Runge-Kutta/Simpson grid point index for r
$\bar{s}$	$J(r)$-, $K(r)$-Simpson grid point index
$s(\mathrm{max})$	Number of Runge-Kutta intervals
T	Temperature
T_{eff}	Effective blackbody temperature of a neutron star
$\tilde{T}$	$\boldsymbol{\xi}$-defining function in the mixed field case
$\tilde{T}_{\mathrm{min}}$	$\mathcal{E}$-minimising value of $\tilde{T}$
t	Simpson grid point index for ϑ
t	Time
u	Axisymmetric system quantity $\in \{m_0, \rho_0, p_0, \Phi_0, \alpha, \beta\}$ in the mixed field case
u_k	A-defining numerical parameter in the toroidal field case
u_l	A-defining numerical parameter in the toroidal field case
u_z	n_z-defining factor
u_ϖ	n_ϖ-defining factor
$u_h(r)$	Radial part of the angular stellar eigenfunction component
$u_r(r)$	Radial part of the radial stellar eigenfunction component
V	System volume
W	Total system energy
X	$\boldsymbol{\xi}$-defining function in the toroidal and poloidal field case
X_0	Constant amplitude of the $\boldsymbol{\xi}$-defining function X
x	Dimensionless radial coordinate
x^f	Final integration bound for an integration over x
x^i	Initial integration bound for an integration over x
x^p	Proton to neutron density fraction
Y	$\boldsymbol{\xi}$-defining function in the toroidal and poloidal field case
Y_{min}	$\mathcal{E}$-minimising value of Y
Z	$\boldsymbol{\xi}$-defining function in the toroidal and poloidal field case

Z_0	Constant amplitude of the $\boldsymbol{\xi}$-defining function Z
$\hat{\alpha}$	Dimensionless $\boldsymbol{B}$-defining function in the mixed field case
$\hat{\beta}$	Dimensionless $\boldsymbol{B}$-defining function in the mixed field case
Γ_0	Polytropic index of the equilibrium system
Γ_1	Polytropic index for a fixed proton fraction
ΔQ	Lagrangian perturbation of quantity Q
Δp^{poly}	Lagrangian fluid pressure perturbation in a polytropic star
$\Delta\Gamma$	Difference between the polytropic indices Γ_1 and Γ_0
δQ	Eulerian perturbation of quantity Q
δp^{poly}	Eulerian fluid pressure perturbation in a polytropic star
$\delta Q \equiv \delta Q^{(1)}$	First variation of quantity Q, $\forall Q \neq W$
$\delta W \equiv \delta W^{(2)}$	Second energy variation
$\delta W_{\mathrm{fluid}}$	Fluid contribution to the energy variation
δW_{grav}	Gravitational contribution to the energy variation
$\delta W_{\mathrm{grav}}^{\mathrm{Cowl}}$	Gravitational contribution to the energy variation in Cowling approximation
$\delta W_{\mathrm{grav}}^{\mathrm{nC}}$	Additional non-Cowling gravitational contribution to the energy variation
δW_{hyd}	Hydrostatic contribution to the energy variation
δW_i	i-th contribution to the energy variation
δW_{magn}	Magnetic contribution to the energy variation
δW_{star}	Stellar volume contribution to the energy variation
δW_{surf}	Stellar surface contribution to the energy variation
δW_{vac}	Vacuum exterior volume contribution to the energy variation
$\delta\widetilde{W}^{\max}$	Maximal computed energy variation according to numerical accuracy
$\delta\widetilde{W}^{\min}$	Minimal computed energy variation according to numerical accuracy
δ_r	A-defining constant in the mixed field case
δ_ϑ	A-defining constant in the mixed field case
ϵ_A	A-defining constant in the toroidal field case
η_{pol}	Poloidal field strength parameter in the mixed field case
$\eta_{\mathrm{pol}}^{\mathrm{crit}}$	Critical poloidal field strength for stability in the mixed field case
η_{tor}	Toroidal field strength parameter in the mixed field case
ϑ_0	A-defining constant in the mixed field case
κ	Polytropic constant
$\Lambda(u)$	Abbreviatory notation in the mixed field case
λ	Summation index
λ_C	Compton wave length
μ	Summation index
ν_e	Electron neutrino
$\bar{\nu}_e$	Electron antineutrino
ξ_0	Displacement field amplitude in the mixed field case
ρ	Mass density
ρ_e	Electric charge density
ρ^n	Neutron mass density
ρ^p	Proton mass density

σ	$\boldsymbol{\xi}$-defining function in the mixed field case
Φ	Gravitational potential
Φ_{ext}	Gravitational potential at the stellar surface
Φ_{magn}	Magnetic flux
$\bar{\chi}$	$\boldsymbol{\xi}$-defining function in the mixed field case
ψ_{tor}	A-defining constant in the poloidal field case
Ω	Stellar angular velocity
ω_n	Stellar eigenfrequency of the eigenmode n
$\mathcal{E}$	Energy variation density
$\mathcal{E}_{\text{cross}}$	Mixed magnetic field contribution to the energy variation density in the mixed field case
$\mathcal{E}_{\text{fluid}}$	Fluid contribution to the energy variation density
$\mathcal{E}_{\text{fluid}}^{\text{poly}}$	Fluid contribution to the energy variation density in a polytropic star
$\mathcal{E}_{\text{grav}}$	Gravitational contribution to the energy variation density
$\mathcal{E}_{\text{grav}}^{\text{Cowl}}$	Gravitational contribution to the energy variation density in Cowling approximation
$\mathcal{E}_{\text{grav}}^{\text{nC}}$	Additional non-Cowling gravitational contribution to the energy variation density
$\mathcal{E}_{\text{hyd}}$	Hydrostatic contribution to the energy variation density
$\mathcal{E}_{\text{magn}}$	Magnetic contribution to the energy variation density
$\mathcal{E}_{\text{pol}}$	Poloidal magnetic field contribution to the energy variation density in the mixed field case
$\mathcal{E}_{\text{tor}}$	Toroidal magnetic field contribution to the energy variation density in the mixed field case

Physical vector quantities

$\boldsymbol{A}$	Vacuum vector potential
$\boldsymbol{B}$	Magnetic field vector
$\boldsymbol{B}_{\text{pol}}$	Magnetic field vector of the poloidal field
$\boldsymbol{B}_{\text{tor}}$	Magnetic field vector of the toroidal field
$\boldsymbol{D}$	Electric displacement field vector
$\boldsymbol{E}$	Electric field vector
$\boldsymbol{e}$	Unit vector
$\boldsymbol{g}$	Gravitational field vector
$\boldsymbol{j}$	Electric current density
$\boldsymbol{n}$	Normal unit vector
$\boldsymbol{p}$	Momentum
$\boldsymbol{p}_n$	Neutron momentum
$\boldsymbol{r}$	Position vector
$\boldsymbol{S}$	Surface vector
$\boldsymbol{S}^{(m)}$	Solution vector Gauss-Seidel method
$\boldsymbol{u}_{n,l,m}$	Stellar eigenfunctions
$\boldsymbol{v}$	Fluid velocity

$\boldsymbol{\xi}$	Displacement field vector, time-independent amplitude
$\boldsymbol{\xi}^n(\boldsymbol{r},t)$	Displacement field vector of mode n, including time-dependence
$\boldsymbol{\Omega}$	Vectorial stellar angular velocity

Mathematical notations, operators, coordinates

D_t	Material time derivative
d_i	Total derivative
e	Euler's number
i	Imaginary unit
J	Jacobi determinant
N_{lm}	Spherical harmonics normalisation constant
$P_{lm}(\cos\vartheta)$	Associated Legendre polynomials
$P^s(r)$	Polynomial defined in the interval $[s, s+1]$
Q^*	Complex conjugate of Q
r	Radial distance
$\bar{r}$	Toroidal radial distance
$Y_l^m(\vartheta,\varphi)$	Spherical harmonics
x	Cartesian coordinate
y	Cartesian coordinate
z	Cartesian coordinate, cylindrical height
δ_{ij}	Kronecker delta
$\Theta_l^m(\vartheta)$	Polar angular part of the spherical harmonics $Y_l^m(\vartheta,\varphi)$
θ	Polar angle
ϖ	Cylindrical radial distance
φ	Azimuthal angle
χ	Poloidal angle
ψ	Stream function
$\mathbb{C}$	Set of complex numbers
∂_i	Partial derivative
∂_{ij}	Second partial derivative $\partial_i\partial_j$
∂_i^2	Second partial derivative $\partial_i\partial_i$
$\mathbb{R}^+$	Set of positive real numbers
$\mathfrak{R}$	Real part
$\mathfrak{I}$	Imaginary part
$\mathcal{O}(x^k)$	Orders of magnitude k or higher in x
$\boldsymbol{\nabla}$	Nabla operator
$\boldsymbol{\nabla}_{\boldsymbol{r}}$	Nabla operator with respect to $\{r,\vartheta,\varphi\}$
$Q\vert_x$	Quantity Q evaluated at x

Physical constants (Constants and Units, 2017)

c	$= 2.997\,924\,58 \times 10^{10}\,\mathrm{cm\ s^{-1}}$	Speed of light
G	$= 6.673\,84 \times 10^{-8}\,\mathrm{cm^3\ g^{-1}\ s^{-2}}$	Gravitational constant
h_P	$= 6.626\,07 \times 10^{-27}\,\mathrm{cm^2\ g\ s^{-1}}$	Planck constant
$M_\odot$	$= 1.9884 \times 10^{33}\,\mathrm{g}$	Solar mass
σ_{SB}	$= 5.670\,367 \times 10^{-5}\,\mathrm{g\ s^{-3}\ K^{-4}}$	Stefan-Boltzmann constant

Abbreviations

CFS instability	Chandrasekhar-Friedman-Schutz instability
LHS	Left hand side
MHD	Magnetohydrodynamics
QCD	Quantum chromo dynamics
QPO	Quasi periodic oscillation
TOV equations	Tolman-Oppenheimer-Volkoff equations

Table E.3.: Legend of polytropic indices and sign conventions used by different authors.

	Polytropic index for the background quantities	Polytropic index for a fixed proton fraction	Sign convention
This work	Γ_0	Γ_1	$\boldsymbol{g} = \pm\nabla\Phi$
Akgün et al. (2013)*	γ	Γ	$\boldsymbol{g} = -\nabla\Phi$
Bernstein et al. (1958)	γ	-	$\boldsymbol{g} = -\nabla\Phi$
Chandrasekhar & Lebovitz (1964)	γ	-	$\boldsymbol{g} = +\nabla\Phi$
Passamonti et al. (2009)	Γ_β	Γ_f	-
Robe (1968)	$1 + \frac{1}{n}$	γ	-
Shapiro & Teukolsky (1983)	Γ	Γ_1	$\boldsymbol{g} = -\nabla\Phi$
Tayler (1973)	γ	-	$\boldsymbol{g} = +\nabla\Phi$

* Note that Akgün et al. (2013) use the index 1 for quantities in the presence of the magnetic field.

F. Acknowledgements

Great scientific contributions to this work have been made by several persons, who provided ideas and inspired new thoughts in numerous discussions: Prof. Kostas Kokkotas, who suggested the idea of the semi-analytic method, Dr. Samuel Lander and Prof. Andreas Reisenegger, who provided helpful comments and suggestions during the realisation process, as well as many others. Prof. Wilhelm Kley very kindly agreed to become the second supervisor of this project.

This work was kindly partially funded by the CARL-ZEISS foundation.

Ich danke Gott und dem Trampolinspringen.

Bibliography

Aerts, C., Christensen-Dalsgaard, J., & Kurtz, D. W. (2010). *Asteroseismology*. Dordrecht, Heidelberg, London, New York: Springer.

Akgün, T., Miralles, J. A., Pons, J. A., & Cerda-Duran, P. (2016). The force-free twisted magnetosphere of a neutron star. *MNRAS*, *462*, 1894–1909.

Akgün, T., Reisenegger, A., Mastrano, A., & Marchant, P. (2013). Stability of magnetic fields in non-barotropic stars: an analytic treatment. *MNRAS*, *433*, 2445–2466.

Alpar, A., & Baykal, A. (2006). Pulsar braking indices, glitches and energy dissipation in neutron stars. *MNRAS*, *372*, 489–496.

Baiotti, L., & Rezzolla, L. (2017). Binary neutron star mergers: a review of Einstein's richest laboratory. *Reports on Progress in Physics*, *80*, 096901.

Bernstein, I. B., Frieman, E. A., Kruskal, M. D., & Kulsrud, R. M. (1958). An energy principle for hydromagnetic stability problems. *Proceedings of the Royal Society, A*, *244*, 17–40.

Bose, S., Chakravarti, K., Rezzolla, L., Sathyaprakash, B. S., & Takami, K. (2017). Neutron star radius from a population of binary neutron star mergers. arXiv: 1705.10850. 2017-08-21.

Braithwaite, J. (2004). *Stable and unstable magnetic fields in stars*. Dissertation, University of Amsterdam.

Braithwaite, J. (2006a). A differential rotation driven dynamo in a stably stratified star. *A&A*, *449*, 451–460.

Braithwaite, J. (2006b). The stability of toroidal fields in stars. *A&A*, *453*, 687–698.

Braithwaite, J., & Spruit, H. C. (2006). Evolution of the magnetic field in magnetars. *A&A*, *450*, 1097–1106.

Bronstein, I. N., Semendjajew, K. A., Musiol, G., & Mühlig, H. (2008). *Taschenbuch der Mathematik*. Verlag Harri Deutsch.

Chandrasekhar, S. (1961). *Hydrodynamic and Hydromagnetic Stability*. New York: Oxford University Press.

Chandrasekhar, S. (1964). A general variational principle governing the radial and the non-radial oscillations of gaseous masses. *ApJ*, *139*, 664–674.

Chandrasekhar, S. (1965). The stability of gaseous masses for radial and non-radial oscillations in the post-newtonian approximation of general relativity. *ApJ*, *142*, 1519–1540.

Chandrasekhar, S., & Lebovitz, N. R. (1964). Non-radial oscillations of gaseous masses. *ApJ*, *140*, 1517–1528.

Ciolfi, R., Ferrari, V., Gualtieri, L., & Pons, J. A. (2009). Relativistic models of magnetars: the twisted torus magnetic field configuration. *MNRAS*, *397*, 913–924.

Colaiuda, A., Ferrari, V., Gualtieri, L., & Pons, J. A. (2008). Relativistic models of magnetars: structure and deformations. *MNRAS*, *385*, 2080–2096.

Colaiuda, A., & Kokkotas, K. D. (2011). Magnetar oscillations in the presence of a crust. *MNRAS*, *414*, 3014–3022.

Constants and Units (2017). The NIST Reference on Constants, Units, and Uncertainty. 2017-09-14.
URL `https://physics.nist.gov/cuu/index.html`

Finn, L. S. (1987). g-modes in zero-temperature neutron stars. *MNRAS*, *227*, 265–293.

Flügge, S. (1958). *Astrophysik II: Sternaufbau*, vol. LI of *Handbuch der Physik*. Berlin, Göttingen, Heidelberg: Springer-Verlag.

Friedman, J. L., Lindblom, L., Rezzolla, L., & Chugunov, A. I. (2017). Limits on magnetic field amplification from the r-mode instability.

Gabler, M., Cerda-Duran, P., Stergioulas, N., Font, J. A., & Müller, E. (2012). Magnetoelastic oscillations of neutron stars with dipolar magnetic fields. *MNRAS*, *421*, 2054–2078.

Gold, T. (1968). Rotating neutron stars as the origin of the pulsating radio sources. *Nature*, *218*, 731–732.

Goldreich, P., & Julian, W. H. (1969). Pulsar electrodynamics. *ApJ*, *157*, 869–880.

Goldreich, P., & Reisenegger, A. (1992). Magnetic field decay in isolated neutron stars. *ApJ*, *395*, 250–258.

Graber, V., Andersson, N., Glampedakis, K., & Lander, S. K. (2015). Magnetic field evolution in superconducting neutron stars. *MNRAS*, *453*, 671–681.

Grad, H., & Rubin, H. (1958). Hydromagnetic equilibria and force-free fields. In *Proceedings of the Second United Nations International Conference on the Peaceful Uses of Atomic Energy*, vol. 31, (pp. 190–197).

Haskell, B., Priymak, M., Patruno, A., Oppenoorth, M., Melatos, A., & Lasky, P. D. (2015). Detecting gravitational waves from mountains on neutron stars in the Advanced Detector Era. *MNRAS*, *450*, 2393–2403.

Herbrik, M., & Kokkotas, K. D. (2017). Stability analysis of magnetized neutron stars - a semi-analytic approach. *MNRAS*, *466*, 1330–1347.

Hewish, A., Bell, S. J., Pilkongton, J., Scott, P. F., & Collins, R. A. (1968). Observation of a rapidly pulsating radio source. *Nature*, *217*, 709–713.

Kargaltsev, O., Kouveliotou, C., Pavlov, G. G., Gögüs, E., Lin, L., Wachter, S., Griffith, R. L., Kaneko, Y., & Younes, G. (2012). X-ray observations of the new unusual magnetar swift J1834.9–0846. *ApJ*, *748*.

Kawamura, T., Giacomazzo, B., Kastaun, W., Ciolfi, R., Endrizzi, A., Baiotti, L., & Perna, R. (2016). Binary neutron star mergers and short gamma-ray bursts: Effects of magnetic field orientation, equation of state, and mass ratio. *Phys. Rev. Lett.*, *94*, 064012.

Kokkotas, K. D. (2011). Neutron stars: Rotational and magnetic field instabilities. In *The multidisciplinary universe – A conference in honor of Jorge Dias de Deus*.

Lander, S. K., Andersson, N., Anatonopoulou, D., & Watts, A. L. (2015). Magnetically driven crustquakes in neutron stars. *MNRAS*, *449*, 2047–2058.

Lander, S. K., Andersson, N., & Glampedakis, K. (2011). Magnetic neutron star equilibria with stratification and type II superconductivity. *MNRAS*, *419*, 732–747.

Lander, S. K., & Jones, D. I. (2009). Magnetic fields in axisymmetric neutron stars. *MNRAS*, *395*, 2162–2176.

Lander, S. K., & Jones, D. I. (2010). Oscillations and instabilities in neutron stars with poloidal magnetic fields. *MNRAS*, *412*, 1730–1740.

Lander, S. K., & Jones, D. I. (2011). Instabilities in neutron stars with toroidal magnetic fields. *MNRAS*, *412*, 1394–1400.

Lander, S. K., & Jones, D. I. (2012). Are there any stable magnetic fields in barotropic stars? *MNRAS*, *424*, 482–494.

Lasky, P. D., Zink, B., Kokkotas, K. D., & Glampedakis, K. (2011). Hydromagnetic instabilities in relativistic neutron stars. *ApJ*, *735*, L20 (5pp).

Lattimer, J. (2016). Observed neutron star masses. 2017-06-13.
URL `https://stellarcollapse.org/nsmasses`

Lattimer, J. M., & Prakash, M. (2001). Neutron star structure and the equation of state. *ApJ*, *550*, 426–442.

Lattimer, J. M., & Prakash, M. (2004). The physics of neutron stars. *Science*, *304*, 536–542.

Lattimer, J. M., & Prakash, M. (2005). Ultimate energy density of observable cold baryonic matter. *Phys. Rev. Lett.*, *94*, 111101.

Lazzati, D., Perna, R., & Begelman, M. C. (2008). X-ray flares, neutrino cooled disks, and the dynamics of late accretion in GRB engines. *MNRAS*, *388*, L15–L19.

Lorre, C., & Aronsohn, L. (2009). The Guitarist Amplification, The Big Bang Theory, Season 3 Episode 7, CBS, USA, TV show episode.

Magnetar Catalog (2016). McGill Online Magnetar Catalog. 2017-07-15.
URL `http://www.physics.mcgill.ca/~pulsar/magnetar/main.html`

Manchester, R. N., Hobbs, G. B., Teoh, A., & Hobbs, M. (2005). The australia telescope national facility pulsar catalogue. *AJ*, *129*, 1993–2006.

Markey, P., & Tayler, R. J. (1973). The adiabatic stability of stars containing magnetic fields – II Poloidal fields. *MNRAS*, *163*, 77–91.

Markey, P., & Tayler, R. J. (1974). The adiabatic stability of stars containing magnetic fields – III Additional results for poloidal fields. *MNRAS*, *168*, 505–514.

Mastrano, A., & Melatos, A. (2011). Instability-driven interfacial dynamo in protoneutron stars. *MNRAS*, *417*, 508–516.

Mastrano, A., Melatos, A., Reisenegger, A., & Akgün, T. (2011). Gravitational wave emission from a magnetically deformed non-barotropic neutron star. *MNRAS*, *417*, 2288–2299.

Mathews, J., & Walker, R. L. (1969). *Mathematical Methods of Physics*. Addison-Wesley Publishing Company, Inc.

Melatos, A., & Payne, D. J. B. (2005). Gravitational radiation from an accreting millisecond pulsar with a magnetically confined mountain. *ApJ*, *623*, 1044–1050.

Mestel, L. (1999). *Stellar Magnetism*. No. 99 in International Series of Monographs on Physics. Oxford: Oxford University Press.

Olausen, S. A., & Kaspi, V. M. (2014). The McGill Magnetar Caralog. *ApJ*, *212*.

Özel, F., & Freire, P. (2016). Masses, radii and the equation of state of neutron stars. *ARA&A*, *54*, 401–440.

Passamonti, A. (2009). Time evolution of rapidly rotating stratified neutron stars. *Journal of Physics: Conference Series*, *189*.

Passamonti, A., Haskell, B., Andersson, N., Jones, D. I., & Hawke, I. (2009). Oscillations of rapidly rotating stratified neutron stars. *MNRAS*, *394*, 730–741.

Passamonti, A., & Lander, S. K. (2014). Quasi-periodic oscillations in superfluid magnetars. *MNRAS*, *438*, 156–168.

Perego, A., Rosswog, S., Cabezon, R. M., Korobkin, O., Käppeli, R., Arcones, A., & Liebendörfer, M. (2014). Neutrino-driven winds from neutron star merger remnants. *MNRAS*, *443*, 3134–3156.

Perna, R., & Pons, J. A. (2011). A unified model of the magnetar and radio pulsar bursting phenomenology. *ApJ*, *727*, L51.

Perna, R., Pons, J. A., Vigano, D., & Rea, N. (2014). The many lives of magnetized neutron stars. *Astronomical Notes*, *335*, 715–720.

Pitts, E., & Tayler, R. J. (1985). The adiabatic stability of stars containing magnetic fields – VI The influence of rotation. *MNRAS*, *216*, 139–154.

Pizzochero, P. M., Antonelli, M., Haskell, B., & Seveso, S. (2017). Constraints on pulsar masses from the maximum observed glitch. *Nature Astronomy*, *1*, 0134.

Pons, J. A., Link, B., Miralles, J. A., & Geppert, U. (2007). Evidence for heating of neutron stars by magnetic-field decay. *Phys. Rev. Lett.*, *98*, 071101.

Potekhin, A. Y., Pons, J. A., & Page, D. (2016). Neutron stars - cooling and transport. In *The Strongest Magnetic Fields in the Universe*, vol. 54 of *Space Sciences Series of ISSI*, (pp. 245–297).

Pulsar Catalogue (2017). ATNF Pulsar Catalogue. 2017-07-15.
URL `http://www.atnf.csiro.au/people/pulsar/psrcat/`

Rembiasz, T., Obergaulinger, M., Guilet, J., Cerda-Duran, P., Aloy, M. A., & Müller, E. (2017). Magnetorotational instability in core-collapse supernovae. arXiv: 1707.00983. 2017-07-16.

Robe, H. (1968). Les oscillations non radiales des polytropes. *Annales d'Astrophysique*, *31*, 475–482.

Ruderman, M., Zhu, T., & Chen, K. (1998). Neutron star magnetic field evolution, crust movement, and glitches. *ApJ*, *492*, 267–280.

Scholz, P., Camilo, F., Sarkissian, J., Reynolds, J. E., Levin, L., Bailes, M., Burgay, M., Johnston, S., Kramer, M., & Possenti, A. (2017). Spin-down evolution and radio disappearance of the magnetar PSR J1622-4950. *ApJ*, *841*, 126.

Schwenzer, K. (2015). Compact stars – lecture notes.

Sedrakian, D. M., Sedrakian, A. D., & Zharkov, G. F. (1997). Type I superconductivity of protons in neutron stars. *MNRAS*, *290*, 203–207.

Seifert, U. (2007). Quantenmechanik – lecture notes.

Shapiro, S. L., & Teukolsky, S. A. (1983). *Black Holes, White Dwarfs and Neutron Stars - The Physics of Compact Objects*. WILEY-VCH Verlag GmbH & Co. KGaA.

Smeyers, P., & van Hoolst, T. (2010). *Linear Isentropic Oscillations of Stars*. No. 371 in Astrophysics and Space Science Library. Berlin: Springer.

Sotani, H., Kokkotas, K. D., & Stergioulas, N. (2007). Torsional oscillations of relativistic stars with dipole magnetic fields. *MNRAS*, *375*, 261–277.

Tassoul, J.-L. (2000). *Stellar Rotation*. Cambridge: Cambridge University Press.

Tauris, T. M., Kramer, M., Freire, P. C. C., Wex, N., Janka, H.-T., Langer, N., Podsiadlowski, P., Bozzo, E., Chaty, S., Kruckow, M. U., van den Heuvel, E. P. J., Antoniadis, J., Breton, R. P., & Champion, D. J. (2017). Formation of double neutron star systems. arXiv:1706.09438. 2017-08-21.

Tayler, R. J. (1973). The adiabatic stability of stars containing magnetic fields – I Toroidal fields. *MNRAS*, *161*, 365–380.

Tayler, R. J. (1980). The adiabatic stability of stars containing magnetic fields – IV Mixed poloidal and toroidal fields. *MNRAS*, *191*, 151–163.

Tayler, R. J. (1981). The adiabatic stability of stars containing magnetic fields – V Effect of ohmic diffusion on stable fields. *MNRAS*, *198*, 811–815.

Thompson, C., & Duncan, R. C. (1993). Neutron star dynamos and the origins of pulsar magnetism. *ApJ*, *408*, 194–217.

Thompson, C., & Duncan, R. C. (1995). The soft gamma repeaters as very strongly magnetized neutron stars. I. radiative mechanism for outbursts. *MNRAS*, *275*, 255–300.

Thompson, M. J. (2006). *An Introduction to Astrophysical Fluid Dynamics*. London: Imperial College Press.

Unno, W., Osaki, Y., Ando, H., Saio, H., & Shibahashi, H. (1989). *Nonradial Oscillations of Stars*. University of Tokyo Press.

Wessel, S. (2009). Astronomie und Astrophysik I und II – lecture notes.

Wright, G. A. E. (1973). Pinch instabilities in magnetic stars. *MNRAS*, *162*, 339–358.